Vol. 60 APRIL, 1956 No. 4

THE JOURNAL OF PHYSICAL CHEMISTRY

(Registered in U. S. Patent Office)

THE JOURNAL OF PHYSICAL CHEMISTRY

(Registered in U. S. Patent Office)

Published monthly by the American Chemical Society at 20th and Northampton Sts., Easton, Pa.

Entered as second-class matter at the Post Office at Easton, Pennsylvania.

The *Journal of Physical Chemistry* is devoted to the publication of selected symposia in the broad field of physical chemistry and to other contributed papers.

Manuscripts originating in the British Isles, Europe and Africa should be sent to F. C. Tompkins, The Faraday Society, 6 Gray's Inn Square, London W. C. 1, England.

Manuscripts originating elsewhere should be sent to W. Albert Noyes, Jr., Department of Chemistry, University of Rochester, Rochester 20, N. Y.

Correspondence regarding accepted copy, proofs and reprints should be directed to Assistant Editor, Allen D. Bliss, Department of Chemistry, Simmons College, 300 The Fenway, Boston 15, Mass.

Business Office: Alden H. Emery, Executive Secretary, American Chemical Society, 1155 Sixteenth St., N. W., Washington 6, D. C.

Advertising Office: Reinhold Publishing Corporation, 430 Park Avenue, New York 22, N. Y.

Articles must be submitted in duplicate, typed and double spaced. They should have at the beginning a brief Abstract, in no case exceeding 300 words. Original drawings should accompany the manuscript. Lettering at the sides of graphs (black on white or blue) may be pencilled in and will be typeset. Figures and tables should be held to a minimum consistent with adequate presentation of information. Photographs will not be printed on glossy paper except by special arrangement. All footnotes and references to the literature should be numbered consecutively and placed in the manuscript at the proper places. Initials of authors referred to in citations should be given. Nomenclature should conform to that used in *Chemical Abstracts*, mathematical characters marked for italic, Greek letters carefully made or annotated, and subscripts and superscripts clearly shown. Articles should be written as briefly as possible consistent with clarity and should avoid historical background unnecessary for specialists.

Symposium papers should be sent in all cases to Secretaries of Divisions sponsoring the symposium, who will be responsible for their transmittal to the Editor. The Secretary of the Division by agreement with the Editor will specify a time after which symposium papers cannot be accepted. The Editor reserves the right to refuse to publish symposium articles, for valid scientific reasons. Each symposium paper may not exceed four printed pages (about sixteen double spaced typewritten pages) in length except by prior arrangement with the Editor.

Remittances and orders for subscriptions and for single copies, notices of changes of address and new professional connections, and claims for missing numbers should be sent to the American Chemical Society, 1155 Sixteenth St., N. W., Washington 6, D. C. Changes of address for the *Journal of Physical Chemistry* must be received on or before the 30th of the preceding month.

Claims for missing numbers will not be allowed (1) if received more than sixty days from date of issue (because of delivery hazards, no claims can be honored from subscribers in Central Europe, Asia, or Pacific Islands other than Hawaii), (2) if loss was due to failure of notice of change of address to be received before the date specified in the preceding paragraph, or (3) if the reason for the claim is "missing from files."

Subscription Rates (1956): members of American Chemical Society, $8.00 for 1 year; to non-members, $16.00 for 1 year. Postage free to countries in the Pan American Union; Canada, $0.40; all other countries, $1.20. $12.50 per volume, foreign postage $1.20, Canadian postage $0.40; special rates for A.C.S. members supplied on request. Single copies, current volume, $1.35; foreign postage, $0.15; Canadian postage $0.05. Back issue rates (starting with Vol. 56): $15.00 per volume, foreign postage $1.20, Canadian, $0.40; $1.50 per issue, foreign postage $0.15, Canadian postage $0.05.

The American Chemical Society and the Editors of the *Journal of Physical Chemistry* assume no responsibility for the statements and opinions advanced by contributors to This Journal.

The American Chemical Society also publishes *Journal of the American Chemical Society*, *Chemical Abstracts*, *Industrial and Engineering Chemistry*, *Chemical and Engineering News*, *Analytical Chemistry*, *Journal of Agricultural and Food Chemistry* and *Journal of Organic Chemistry*. Rates on request.

THE JOURNAL OF
PHYSICAL CHEMISTRY

(Registered in U. S. Patent Office)

VOLUME 60 APRIL 16, 1956 NUMBER 4

POROSITY OF ANODIC OXIDE COATINGS ON ALUMINUM. COMPARISON OF *n*-BUTANE AND KRYPTON SORPTION

BY LEE A. COSGROVE

Aluminum Research Laboratories, Aluminum Company of America, New Kensington, Pa.

Received May 21, 1955

The surface area, pore volume and diameter of the porous type of anodic oxide coating applied to aluminum have been investigated by sorption techniques with krypton at −195.8° and *n*-butane at 0°. Surface areas are greater for films formed in sulfuric than in chromic or oxalic acid electrolytes. At constant temperature, forming voltage and electrolyte concentration, areas increase with increasing coating time. Areas, calculated for constant coating thickness, decrease with increasing forming voltage and constant electrolyte concentration and temperature. Pore diameters are greatest in films formed in chromic acid electrolyte. For oxide films with pore diameters greater than 160 Å., krypton sorption gives results inconsistent with *n*-butane sorption and metallographic examination. The use of solid rather than extrapolated liquid vapor pressures for krypton calculations gives better agreement with *n*-butane and electron microscope calculations.

Burwell, Smudski and May[1] reported relative areas (ratio of total area to geometric area) varying from 6 to 619 from ethylene and nitrogen sorption isotherms for 99.5% aluminum (designated 1050) anodically coated in several electrolytes. The value for uncoated, solvent-cleaned material was 1.5. More recently, Keller, Hunter and Robinson,[2] through the use of the electron microscope, demonstrated that the porous type of oxide coating formed on aluminum in sulfuric acid, oxalic acid or chromic acid electrolytes consists of closely packed cells predominantly hexagonal in shape. Each cell has a pore extending from the surface of the oxide to the thin non-porous barrier layer at the base of the pore. The diameter of the pore at its base has been calculated to range from 120 Å. for a 15% sulfuric acid electrolyte to 240 Å. for a 3% chromic acid electrolyte. Hunter and Fowle[3] have shown the rate at which electrolytes that produce a porous type of coating dissolve the oxide coating. Thus, the pores in the oxide film are considered to be tapered and should have a larger diameter at the film surface than at their base.

By analysis of sorption–desorption isotherms, it is possible, in addition to determining the relative area of a porous surface, to derive the total pore volume and, in the case of tapered pores of uniform size, to make reasonable approximations of their taper. A series of anodic oxide films formed in various electrolytes has been investigated using *n*-butane at 0° as sorbate in a quartz balance system and krypton at −195.8° as sorbate in a low pressure volumetric system. Because of their agreement with electron microscope data, the results obtained from *n*-butane sorption are used as a basis for evaluation of the krypton sorption data.

Experimental

High purity (99.99%) aluminum foil with a geometric area of 720 cm.² was made the anode in a well-stirred electrolytic bath with inert cathode under the specified conditions of temperature, voltage, time and electrolyte composition. A sample of this foil 24 cm.² in geometric area was used in the krypton measurements, the remainder with *n*-butane.

Immediately after coating, the samples were evacuated in the sorption system. In the krypton low pressure system, helium (spectroscopically pure, Linde Air Products Co.) was used to measure the free space. The sample bulb was immersed in a liquid nitrogen-bath whose temperature, measured with a nitrogen vapor pressure thermometer, determined the saturation pressure of krypton.[4-6] Krypton (spectroscopically pure, Linde Air Products Co.) gas pressures were measured with a McLeod gage to ±0.001 mm. Chemically pure *n*-butane gas (Ohio Chemical Co.) was used as a sorbate in the quartz balance system. The elongation of the quartz spring was measured with a cathetom-

(1) R. L. Burwell, Jr., P. A. Smudski and T. P. May, *J. Am. Chem. Soc.*, **69**, 1525 (1947).

(2) F. Keller, M. S. Hunter and D. L. Robinson, *J. Electrochem. Soc.*, **100**, 411 (1953).

(3) M. S. Hunter and P. Fowle, *ibid.*, **101**, 514 (1954).

(4) A. S. Friedman and David White, *J. Am. Chem. Soc.*, **72**, 3931 (1950).

(5) J. J. Meihuizen and C. A. Crommelin, *Physica*, **IV**, 1 (1937).

(6) W. H. Keesom, J. Mazur and J. J. Meihuizen, *ibid.*, **II**, 669 (1935).

TABLE I

PROPERTIES OF ANODIC OXIDE FILMS

BET relative surface area, cm.²/cm.²		Porosity, %			Av. Kelvin		Pore diameter, Å. 4 × pore vol. surface area		
Krypton	n-Butane	Krypton	n-Butane	Estimated[d]	Krypton	n-Butane	Krypton	n-Butane	Estimated[e]
30-min., 70°F., 10-v., 0.00016″ thick, 15% sulfuric acid electrolyte									
300	200	16.8	15.7	..	80	78	87	126	141
30-min., 70°F., 15-v., 0.00035″ thick, 15% sulfuric acid electrolyte									
480	320	15.2	14.9	12.6	91	95	113	166	141
60-min., 70°F., 15-v., 0.00060″ thick, 15% sulfuric acid electrolyte									
900	680	14.2	17.9	17.5	111	101	97	161	162
30-min., 80°F., 30-v., 0.00012″ thick, 2% oxalic acid electrolyte									
57	49	7.1	8.2	5.5	146	126	153	203	200[f]
60-min., 100°F., 40-v., 0.00017″ thick, 3% chromic acid electrolyte									
92	97	..	16.3	3.6	..	309	..	290	270[f]
70°F., 15-v., 15% sulfuric acid electrolyte									
490[a]	..	14.0	..	12.6	91	..	106	..	141
560[b]	..	14.8	..	14.2	96	..	125	..	148
820[c]	..	15.0	..	15.9	117	..	112	..	155

[a] 30-minute, 0.000365″. [b] 40-minute, 0.000465″. [c] 50-minute, 0.00060″. [d] Based on electron microscope data.[2] [e] Based on electron microscope data[2] and solution rate determinations.[3] [f] Unpublished data on solution rate.

eter equipped with a vernier scale which could be read to ±0.001 mm. Gas pressures in this system were measured with a mercury manometer to ±0.1 mm.

Surface areas were calculated by the Brunauer, Emmett, Teller[7] (BET) equation. In some cases with both the krypton and the *n*-butane system, the values derived from this equation did not fall on a straight line. A smooth curve was drawn through these points, and a straight line intersecting this curve at 0.065 and 0.130 relative pressure was extrapolated to zero relative pressure. Russell and Cochran[8] found that this method of treating the data gave surface areas comparable to those determined by nitrogen sorption for several aluminum oxides. Molecular areas of krypton and *n*-butane were taken as 20.8[9] and 39 Å.²[,8] respectively.

The porosity from sorption data is the volume of gas absorbed at saturation pressure expressed as per cent. of the total volume of the oxide. The porosity from metallographic examination is estimated from the number and average diameter of the pores per unit area, the average pore diameter being derived from the cell base pattern and solution rate of the oxide film in the electrolyte.[2]

The average Kelvin pore diameter is calculated from a point on the desorption curve chosen half way between the horizontal portion of the desorption curve and a line equal to $2V_m$. The equation (assuming complete wetting) is[10]

$$\ln p/p_0 = -2V\sigma/rRT$$

In this relationship, p is equilibrium pressure, p_0 saturation pressure, σ surface tension of krypton (15 dynes per cm.)[11] or *n*-butane (15.2 dynes/cm.),[12] V molar volume of krypton (31 ml. at 77.3°K.)[13] or *n*-butane (93.9 ml. at 0°),[14] r the capillary radius, R the gas constant (8.314 × 10⁷ erg./deg. mole) and T the absolute temperature. With the proper values substituted, the equation for krypton becomes

$$r(\text{Å.}) = -6.30/\log p/p_0$$

and for *n*-butane

$$r(\text{Å.}) = -5.42/\log p/p_0$$

To compensate for the layers of gas still absorbed on the walls of the pores during the hysteresis measurements, a correction amounting to two layers or 5 Å. for krypton sorption and 8 Å. for the *n*-butane sorption is added.

One common method for calculating pore radius from sorption data is to assume the pores are all identical cylinders. Using this assumption and neglecting the area of the bottom of the pore, the average pore diameter is: av. pore diameter cm. = 4 × total pore vol. cm.³/surface area cm.².

Discussion of Results

The surface area, porosity and pore diameter of the different types of coatings as determined by *n*-butane and krypton sorption and estimated from metallographic examination are compared in Table I.

Surface Area.—All the coatings discussed in this paper show a high ratio of true surface area to geometric area. The first coating in Table I shows a relative area of 300 by krypton sorption and 200 by *n*-butane sorption. The poor agreement is ascribed to the uncertainty in the knowledge of krypton and *n*-butane molecular areas on this material and mechanical difficulties in the *n*-butane system. Relative areas increase with increasing coating time when temperature, forming voltage and electrolyte concentration are constant. When calculated to constant coating thickness, areas decrease with increasing formation voltage for a given electrolyte at constant temperature. For example, the first two coatings in Table I show areas of 300 and 480, respectively, for the coatings formed at 10 and 15 volts. However, the coating formed at 15 volts is over twice as thick. While it is realized that area is not an exact linear function of coating thickness, increasing the thickness of the coating formed at 10 volts to 0.00035″ would approximately double the area, giving a calculated value of 600 to compare to the 480 for the coating formed at 15 volts.

The relative areas of films formed in oxalic acid

(7) S. Brunauer, P. H. Emmett and E. Teller, *J. Am. Chem. Soc.*, **60**, 309 (1938).

(8) A. S. Russell and C. N. Cochran, *Ind. Eng. Chem.*, **42**, 1332 (1950).

(9) R. T. Davis, Jr., T. W. DeWitt and P. H. Emmett, THIS JOURNAL, **51**, 1232 (1947).

(10) S. Brunauer, "The Adsorption of Gases and Vapors," Princeton University Press, Princeton, N. J., 1943, p. 120.

(11) "Gmelins Handbuch der Anorganischen Chemie—Inert Gases," Berlin, 1926, p. 176.

(12) D. L. Katz and W. Saltman, *Ind. Eng. Chem.*, **31**, 91 (1939).

(13) E. Mathias, C. A. Crommelin and J. J. Meihuizen, *Compt. rend.*, **204**, 630 (1937).

(14) Anon., *Ind. Eng. Chem.*, **34**, 1240 (1942).

and chromic acid electrolytes are much less than those formed in sulfuric acid electrolytes. While the relative areas of coatings formed in sulfuric acid are measured to be 50% higher with krypton than with *n*-butane, with oxalic acid electrolyte the difference is much less, and with chromic acid electrolyte the *n*-butane area exceeds that of the krypton. This is additional proof that the effective molecular areas of the sorbates vary with the nature of the surface.

Porosity.—While there is good agreement between the porosities as measured by krypton and *n*-butane for the 30-minute, 10-volt and 15-volt coatings formed in sulfuric acid electrolyte, there is an obvious discrepancy for the 60-minute coating (Table I). With the coating formed in 15% sulfuric acid electrolyte, assuming the pores are approximately truncated cones, solution during coating formation is calculated to increase the % porosity from 12.6 for the 30-minute to 17.5 for the 60-minute coating. Therefore, the apparent decrease in porosity as measured by krypton sorption with increased coating time in this electrolyte is laid to a fundamental error in interpreting the sorption data. To maintain constant all variables except time, three specimens were removed from a single large sample being coated at 15 volts, 70°F. in 15% sulfuric acid, at intervals of 30, 40 and 50 minutes. Figure 1 is a composite

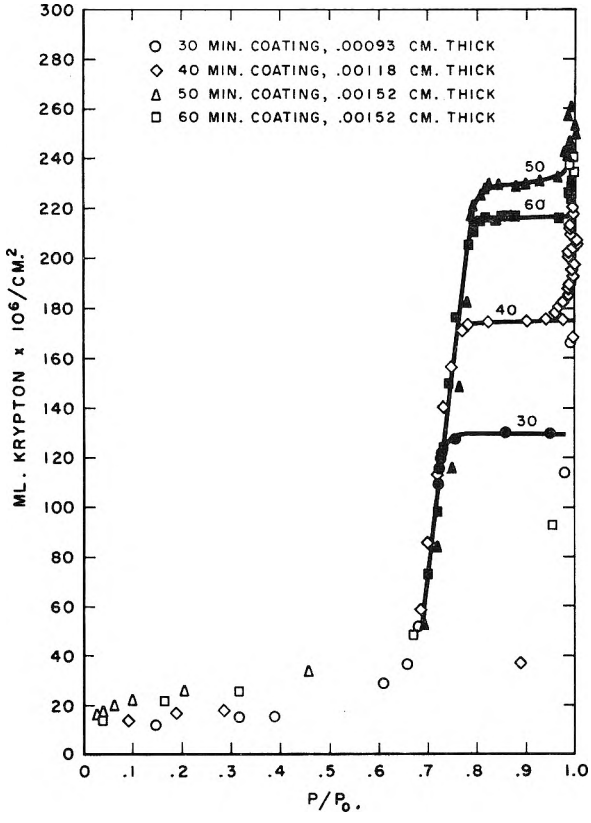

Fig. 1.—Oxide film formed in 15% sulfuric acid at 70°F. and 15 volts.

of the isotherms. The adsorption portions of the isotherms have been omitted since they are quite similar. The porosities for the 30- and 40-minute specimens increase in a normal manner, 14.0 and 14.8%, respectively, and although the pore volume of the 50-minute coating shows a marked increase over that of the 40-minute, the porosity increases only to 15%.

It appears then that an anomalous behavior of krypton sorption begins to show for samples coated between 40 and 50 minutes in sulfuric acid electrolyte. A further example of this anomaly can be had by comparing the total pore volume of the 50- and 60-minute coatings also shown in Fig. 1. The coating thickness was identical for both specimens, but as a result of the longer solvent action of the electrolyte, the 60-minute coating should have had a slightly greater pore volume. The opposite was found experimentally with krypton sorption. It is postulated, therefore, that the krypton hysteresis loop with these 50- and 60-minute coatings begins upon desorption with the pores not completely filled with condensate.

Other examples that the pores may not be completely filled with krypton can be had by comparing the pore volumes of the coating formed in oxalic acid electrolyte (pores slightly larger than those formed in sulfuric acid), the krypton value being lower than that found with the *n*-butane. With the coating formed in 3% chromic acid electrolyte with substantially larger pores, the krypton sorption isotherm gave no indication of a hysteresis loop, although a well-defined loop was found with *n*-butane (Fig. 2). The estimated porosity of this

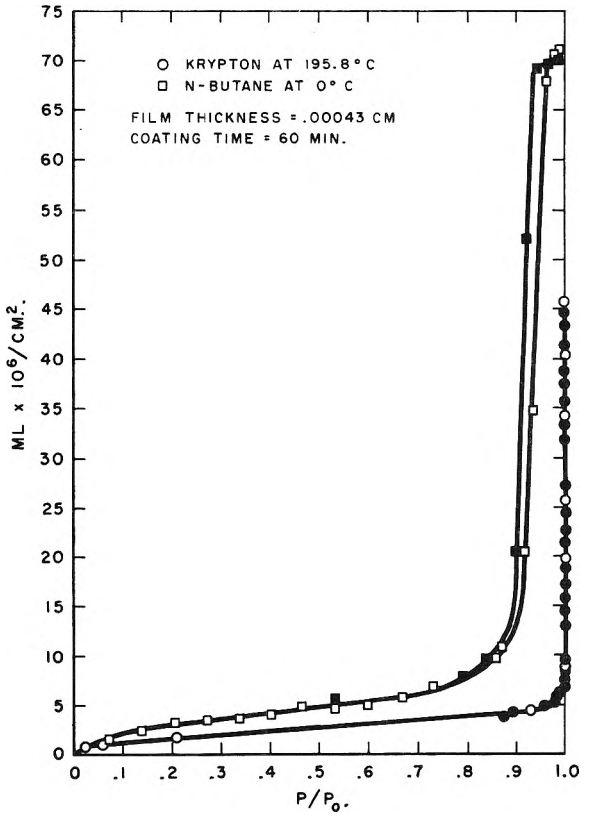

Fig. 2.—Oxide film formed in 3% chromic acid at 100°F. and 40 volts.

coating is only 25% of that found experimentally with *n*-butane.

Pore Diameter.—For pores less than 100 Å. in diameter, the agreement between krypton and *n*-butane calculations of average Kelvin pore diameter is good. Above this pore diameter, these values with krypton exceed those with *n*-butane. With the (4 × pore volume)/(surface area) type of calculation for pore diameter, the krypton values agree fairly well with those from the average Kelvin equation. The *n*-butane values are high, presumably because of inaccuracies in these surface areas. Diameters of the pores at their midpoints were calculated from data from metallographic examination,[2] and solution rate experiments.[3] These estimates are in every case higher than those previously discussed, except for the values based on the inaccurate *n*-butane surface area data.

The constant value of pore diameter, as calculated on the assumptions of Keller, Hunter and Robinson[2] that pore size is independent of forming voltage (other conditions equal), is not confirmed by the sorption measurements for the 10-volt and 15-volt coatings made in a sulfuric acid electrolyte. It might be noted that the solution rates calculated from the slope of the desorption curve are approximately half of those of Hunter and Fowle.[3]

Evaluation of Krypton Data.—Most determinations of porosity have been carried out with sorbates that would normally be liquid at the temperatures employed. For the case of krypton which condenses as a solid, there is little information on the best method for treating sorption data. Davis, DeWitt and Emmett[9] thought it best to calculate relative pressures as though the krypton condensed as the liquid. Surface areas of the present samples were essentially the same whether the vapor pressure of the solid or liquid was used. However, pore diameters, as calculated using liquid vapor pressures, were absurdly small while the diameters calculated using solid vapor pressures check the *n*-butane and electron microscope data for certain samples.

It has been observed on these and other equivalent specimens not reported that the sharp break in the desorption portion of the krypton isotherm for specimens coated longer than 40 minutes in 15% sulfuric acid electrolyte at 15 volts and 70°F. occurs at a relative pressure of about 0.82. Using the previously mentioned Kelvin equation, the pore diameter when corrected for two layers of sorbent gas is 160 Å. Assuming that (for coatings formed in sulfuric acid electrolyte under conditions of temperature, voltage and concentration just listed) the maximum diameter of the pores which will give hysteresis with krypton at −193.8° is about 160 Å., there is a logical explanation for the apparent decrease in porosity with increased coating time. For coating times of 30 to 40 minutes, solvent action by the electrolyte does not increase the diameter of the outer end of the pores enough to exceed this 160 Å. maximum, and porosities as measured by krypton sorption are reasonable. For all longer coating times, the 160 Å. maximum is exceeded at the outer end of the pore, and results are anomalous. Since at saturation sufficient krypton is condensed to completely fill the pores and cover the sample, it must be assumed that upon desorption no hysteresis occurs until the pores have been emptied down to this 160 Å. maximum.

The 160 Å. maximum diameter apparently holds only for the sulfuric acid electrolyte under the conditions previously mentioned. With a 2% oxalic acid coating at 30 volts and 80°F., a 30-minute coating shows a break in the krypton desorption isotherm at 200 Å.

THE KINETICS OF THE HOMOGENEOUS PRECIPITATION OF BARIUM SULFATE[1]

BY F. C. COLLINS

Polytechnic Institute of Brooklyn, Brooklyn, N. Y., and

J. P. LEINEWEBER

American Cyanamid Company, Bound Brook, N. J.

Received August 15, 1955

The nucleation and growth of barium sulfate crystallites in homogeneous precipitations has been investigated using both electrical conductivity and light scattering measurements. The sulfate ion was generated by the LaMer–Dinegar method of the persulfate–thiosulfate reaction. On the basis of the Becker–Döring nucleation theory, it is assumed that the precipitation involves nucleation which occurs in a single burst and which is followed by the diffusion-controlled growth of the crystallites in the supersaturated solution. The observed supersaturation ratio at the time of nucleation is strongly dependent on the purity of the reagents. With repeated recrystallizations and filtrations, a maximum supersaturation ratio of 32/1 in water in terms of mean ionic activities was reached. Water–glycerol mixtures gave higher supersaturation ratios when corrected for the variation of the solubility product in the mixtures. The growth of the crystallites was found to agree closely with the equation of Frisch and Collins wherein the radius is at first proportional to the time and then converges to the law according to which the radius squared is proportional to the time. The Frisch–Collins equation enables the calculation of the fraction of fruitful encounters of the ions with the growing crystallites. This fraction is small, being of the order of 5×10^{-5} in both water and water–glycerol mixtures. The growth rates of the crystallites follows the predicted dependence on the viscosity of the medium.

Introduction

The mechanism of the precipitation of crystals from supersaturated liquid solutions has been fairly well established by previous studies, among which several may be cited,[2–5] to consist in the production of critical nuclei in the supersaturated solution followed by the diffusion-controlled growth of these nuclei into crystallites. The theoretical treatment of the latter process is complicated by the moving boundary of the growing crystallites, the competition of the multiplicity of the crystallites for the diffusing molecules or ions in the supersaturated medium, and by the fact that every molecule or ion diffusing up to the surface of the growing crystallite need not become part of the crystal but may diffuse away again. The effects of the moving boundary and the competition of the multiple sinks has been considered in papers by Reiss and LaMer[6a] and Reiss.[6b] More recently Frisch and Collins[7] have derived a relation between the radius of the growing crystallites and the time taking into account all three of these effects. The principal purpose of the present investigation was to determine whether the predictions of the Frisch–Collins growth equation were in quantitative agreement with experiment.

The theory of Becker and Döring[8] for the spontaneous generation of nuclei of the new phase in supersaturated media gives the dependence of the nucleation rate upon the interfacial tension, the supersaturation ratio and the temperature. In the nucleation of liquid aerosols in supersaturated vapor, the Becker–Döring theory leads to nearly quantitative agreement with experiment. In the precipitation of crystals from liquid solution, the interpretation is made questionable by the paucity of interfacial tension data and by the doubt, in any particular case, whether self-nucleation or nucleation by foreign substances was involved. The present investigation included a study of the effect of very careful freeing of the system of dust particles upon the maximum supersaturation ratio attained.

The barium sulfate system was selected for study because of its interest in analytical chemistry and experimentally convenient time for crystallite growth. The system turned out to have other advantages in the nearly spherical form of the growing particles for ease in theoretical analysis and the relatively small difference in the refractive indices of the crystalline barium sulfate which simplified the interpretation of the light scattering data.

Homogeneous precipitations have the obvious advantage in kinetic studies of precipitation in that the complications due to random local excess concentrations unavoidable in the mixing of reagent solutions are obviated. The LaMer–Dinegar[2] method of homogeneously generating sulfate ion by the persulfate–thiosulfate reaction was used in the present investigation.

The course of the precipitation was followed both by conductance and by light scattering measurements. With the particular apparatus used, conductance measurements appeared to give the more precise results. The studies were carried out both in aqueous and in water–glycerol solutions. The latter solutions were used to determine the effect of the viscosity variation upon the diffusion-controlled growth process. The effect of temperature variation was not investigated, all measurements being made at 25°.

The employment of water–glycerol solutions made necessary the determination of the solubility

(1) The material presented in this paper was taken from the dissertation submitted by James P. Leineweber in partial fulfillment of the requirements for the degree of Doctor of Philosophy at the Polytechnic Institute of Brooklyn, Brooklyn, N. Y. Presented at the 128th National ACS Meeting at Minneapolis, September, 1955, Division of Colloid Chemistry.

(2) V. K. LaMer and R. H. Dinegar, *J. Am. Chem. Soc.*, **73**, 380 (1951).

(3) J. A. Christiansen and A. Nielson, *Acta Chem. Scand.*, **5**, 673 (1951).

(4) D. Turnbull, *Acta Metall.*, **1**, 684 (1953).

(5) R. A. Johnson and J. D. O'Rourke, *J. Am. Chem. Soc.*, **76**, 2124 (1954).

(6) (a) H. Reiss and V. K. LaMer, *J. Chem. Phys.*, **18**, 1 (1950); (b) H. Reiss, *ibid.*, **18**, 840 (1950).

(7) H. L. Frisch and F. C. Collins, *ibid.*, **21**, 2158 (1953).

(8) R. Becker and W. Döring, *Ann. Physik*, [5] **24**, 719 (1935).

of barium sulfate and a kinetic study of the persulfate–thiosulfate reaction rate in these solutions. The activity coefficients of the various electrolytes involved were corrected for the change in the dielectric constant of the medium.

Preliminary Theoretical Discussion

The conventional solution to Fick's differential diffusion law[9] as ordinarily applied in diffusion-controlled reaction processes assumes the existence of a single spherical sink with fixed boundaries in a medium of infinite extent. The concentration of the diffusing at the boundary is taken to be zero which is equivalent to the assumption that every molecule or ion diffusing up to the surface of the sink is destroyed. These assumptions do not take into account (1) the effect of the moving sink boundary on the diffusion flow rate, (2) the fact that molecules which would be otherwise available for diffusion to any given crystallite are being used up in the growth of other crystallities, or (3) the possibility that a molecule may diffuse up to a given crystallite and diffuse away again without adding to it.

The solution developed by Frisch and Collins[7] made use of an earlier proposal by Collins and Kimball[10] for the boundary condition to be used in the solution of Fick's law

$$\frac{\partial c}{\partial t} = \bar{D}\left(\frac{\partial^2 c}{\partial r^2} + \frac{2}{r}\frac{\partial c}{\partial r}\right) \qquad (1)$$

where c is the concentration of the diffusing species, r the distance from a central reference point and t the time. The proposed boundary condition is

$$\gamma\left(\frac{\partial c}{\partial r}\right)_R = c(R) \qquad (2)$$

where $\gamma = D/k$. Here k has the significance of a specific reaction rate for a molecule within one diffusional displacement $\bar{s}$ from the boundary R of the central sink. If the diffusion process is interpreted in terms of a random walk[11] then

$$D = \frac{1}{6}\nu\overline{s^2}$$

where ν is the displacement frequency and $\overline{s^2}$ is the mean square displacement. The equation for γ may then be given as the ratio of the mean diffusional displacement and reaction or absorption probability α.

$$\gamma = \frac{1}{6}\nu\overline{s^2}\Big/\frac{1}{6}\alpha\nu\bar{s} \simeq \bar{s}/\alpha$$

The effect of the moving boundary $R(t)$ is handled by a perturbation method which leads to the following approximate solution of eq. 1 for a single sink and the boundary condition (2)

$$c(r,t) = a - \frac{a[R(t)-\beta]}{r}\left\{\operatorname{erfc}\frac{r-R(t)}{2(Dt)^{1/2}} - \left[\frac{Dt}{\beta^2} + \frac{r-R(t)}{\beta}\right]\operatorname{erfc}\left[\frac{r-R(t)}{2(Dt)^{1/2}} + \frac{(Dt)^{1/2}}{\beta}\right]\right\} \qquad (3)$$

where a is the initial concentration which is assumed to be uniform throughout the diffusion field and $\beta = \gamma R(t)/[R(t) + \gamma]$. The function erfc x has the usual significance

$$\operatorname{erfc} x = \frac{2}{\sqrt{\pi}}\int_x^\infty e^{-y^2}\mathrm{d}y \qquad (4)$$

The flux $\Phi_1(t)$ to the single sink is

$$\Phi_1(t) = 4\pi R^2(t)\left(\frac{\partial c}{\partial r}\right)_{R(t)} \qquad (5)$$

and is related to the rate of advance of the moving boundary by

$$K\Phi_1(t) = \frac{\mathrm{d}V}{\mathrm{d}t} = 4\pi R^2(t) \qquad (6)$$

where V is the volume of the crystallite and the specific growth constant K depends on the units of concentration and length. The differential equation for the moving boundary is now readily obtained from eq. 3, 5, 6, and is

$$\frac{\mathrm{d}R}{\mathrm{d}t} = \frac{\alpha K D\beta}{\gamma R}\left\{1 - \exp\left(\frac{Dt}{\beta^2}\right)\operatorname{erfc}\left[\frac{(Dt)^{1/2}}{\beta}\right]\right\} \qquad (7)$$

The depletion of the concentration of the diffusing species by the presence of the competing sinks is taken account of by adding the term

$$-m\Phi_m(t)c(r,t)/[a - m\int_0^t \Phi_m(\tau)\mathrm{d}\tau]$$

to eq. 1, where m is the number density of growing crystallites. The equation for the flux then can be readily shown to have the form

$$\Phi_m(t) = \Phi_1 \exp\left[-\frac{m}{a}\int_0^t \Phi_1(\tau)\,\mathrm{d}\tau\right] \qquad (8)$$

From eq. 8 it is shown readily that the radius of any given crystallite is given by

$$\frac{KDat}{R_\infty(\gamma + R_\infty)} = \frac{1}{6}\ln\frac{R^2/R_\infty^2 + R/R_\infty + 1}{(1 - R/R_\infty)^2} + \frac{1}{\sqrt{3}}\left(\frac{1 - R_\infty/\gamma}{1 + R_\infty/\gamma}\right)\left[\tan^{-1}\left(\frac{2R + R_\infty}{R_\infty\sqrt{3}}\right) - \tan^{-1}\frac{1}{\sqrt{3}}\right] \qquad (9)$$

where R_∞ is the radius attained by the crystallites when the supersaturation is exhausted.

In homogeneous precipitations, eq. 6 of Frisch and Collins[7] will not give satisfactory results because of the continued generation of a diffusing species by the homogeneous chemical reaction. The straightforward mathematical handling of the uniform source function by introducing an appropriate correction, represented by the chemical reaction, into eq. 1 and then proceeding to derive an equation analogous to eq. 9 turns out to be intractable. As an alternative, an approximate solution of paralleling eq. 9 is obtained by a perturbation method.

The reaction generating the sulfate ion is slow compared to the growth process and the concentrations of persulfate and thiosulfate ions change but little from their initial values. Hence the concentration of the sulfate produced after nucleation can be represented as pt where p is constant to a good approximation. Let us now define R_T which represents the limiting radius that the crystallites would obtain if no more of the diffusing species were generated after the time $t = T$

$$\frac{a + pt}{m} = \frac{4}{3}\pi R_T^3 K \qquad (10)$$

(9) M. v. Smoluchowski, *Z. physik. Chem.*, **92**, 192 (1917).
(10) F. C. Collins and G. E. Kimball, *J. Colloid Sci.*, **4**, 425 (1949).
(11) S. Chandrasekhar, *Rev. Mod. Phys.*, **15**, 1 (1943).

The approximate growth equation is then

$$\frac{KD(a + pt)t}{R_T(\gamma + R_T)} = \frac{1}{6}\ln\frac{R^2/R_T^2 + R/R_T + 1}{(1 - R/R_T)^2} + \frac{1}{\sqrt{3}}\left[\frac{1 - R_T/\gamma}{1 + R_T/\gamma}\right]\left[\tan^{-1}\left(\frac{2R + R_T}{R_T\sqrt{3}}\right) - \tan^{-1}\frac{1}{\sqrt{3}}\right] \quad (11)$$

Eq. 10 has two limiting forms, $R_T \gg \gamma$ and $R_T \ll \gamma$ which are shown in Fig. 1a as plots of the reduced radius R/R_T *vs.* the reduced time $\theta = KD(a + pt)t/R_T(\gamma + R_T)$. These plots are suitable for the interpretation of data from light scattering measurements. For comparison with conductivity measurements, the plots of the reduced volume $(V/V_T) = (R/R_T)^3$ *vs.* the reduced time are more appropriate, and are shown in Fig. 1b.

It is to be noted that eq. 11 does not expressly take account of the fact that the crystallites grow by the diffusion of two different ionic species. The development of the theory implicitly assumes that only the diffusion of the scarce species (here the sulfate ion) need be followed. This assumption appears to be sufficiently valid for the present purpose as the concentration of the more abundant species (the barium ion) is sufficiently large to be practically unaffected by the relatively small diffusion gradients.

Experimental

Preparation of Reagents and Cleansing of Apparatus.—Because of the large effects on the observed supersaturation ratio due to very minor amounts of impurities, considerable care was exercised in the purification of the reagents and the elimination of dust from the experimental system. The latter proved to be particularly important in the case of the sodium thiosulfate and the distilled water.

The water used for all solutions was prepared in an all-glass distillation apparatus similar to that described by Ballentine[12] except that a bubble cap column was used in place of the packed column described by Ballentine. The still remained in continuous operation throughout the present investigation to avoid contamination by dust during shut-downs.

The glycerol was reagent grade material and was used without further purification. It had a specific conductance of 1.5×10^{-6} ohm^{-1}.

The salts used were all analytical grade and were freed from dust particles by repeated filtration of their solutions followed by recrystallization. Except for a few filtrations where a fine sintered glass filter was used, the filtrations were carried out with a filter mat prepared from "Microfine" glass fibers having an average diameter of 0.05 μ. The glass fibers were furnished through the courtesy of Glass Fibers, Inc., New York, N. Y.

The barium sulfate and the potassium persulfate were prepared by four successive glass fiber mat filtrations followed by recrystallization from the supercooled solution.

The impurities present in the sodium thiosulfate as received from the manufacturer proved to be very effective in lowering the supersaturation required for nucleation. Accordingly, precipitation runs were made with the thiosulfate filtered in three different ways: (method A) four times through a "fine grade" sintered glass filter, (method B) four times through the glass fiber filter, and (method C) twelve times through the glass fiber filter. After filtration, the thiosulfate was recrystallized from the supercooled solution.

The glassware and the conductivity cell used in the experiments were cleaned with chromic acid solution and, after careful rinsing with the dust-free distilled water, allowed to stand at least one hour before use. Ordinary distilled water used in the cleansing operation was found to affect the supersaturation ratio attained in the precipitation. The conductivity of a fresh portion of the dust-free distilled water was measured as a final check of the cleanliness of the conductivity cell and, if above 1.5×10^{-6} ohm^{-1}, the cleansing was repeated.

(12) R. Ballentine, *Anal. Chem.*, **26**, 549 (1954).

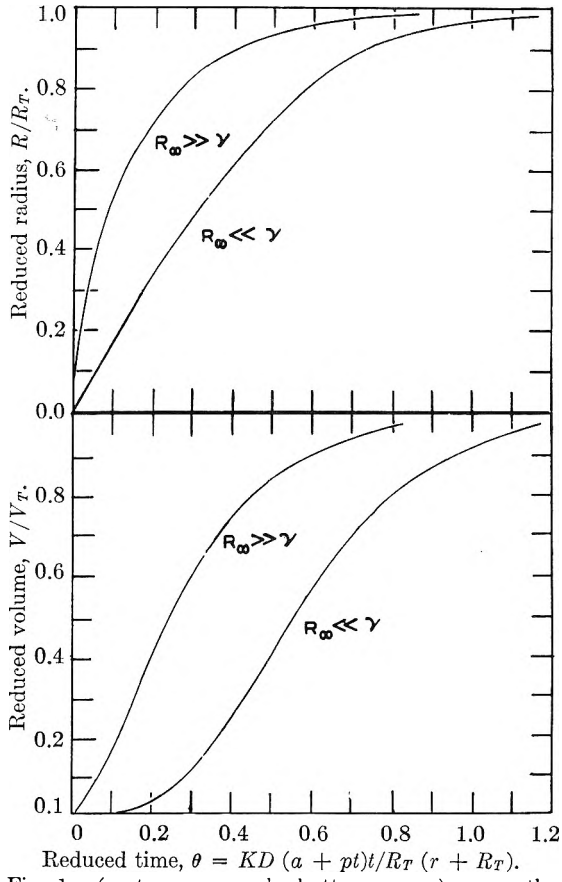

Fig. 1.—(a, top curve; b, bottom curve): growth of crystallite particles from eq. 11 for pure diffusion-controlled growth ($R_T >> \gamma$) and surface activation energy controlled growth ($R_T << \gamma$).

Apparatus.—The conductivity bridge and its accessories were constructed from precision components at the laboratories of the American Cyanamid Company according to the design of Shedlovsky.[13] It had a precision of ±0.1%. The conductance cell was of the type designed by Jones and Bollinger and had a constant of 4.337.

The light scattering measurements were made with a Brice–Phoenix Light Scattering Photometer manufactured by the Phoenix Instrument Company, Philadelphia, Pa. Monochromatic light of 5461 Å. wave length was obtained from a mercury arc by the use of Wratten filters. Measurements were made in a dissymmetry cell with faces at 45, 90 and 135°. The instrument is capable of measuring scattered light at 10^{-6} of the intensity of the incident beam.

Kinetics of the Persulfate–Thiosulfate Reaction.—The kinetics of the reaction

$$2S_2O_3^{=} + S_2O_8^{=} \longrightarrow 2SO_4^{=} + S_4O_6^{=} \quad (12)$$

were studied at 25° in the presence and absence of barium nitrate and glycerol. The barium nitrate was found to promote the reaction and glycerol had no observable effect on the rate of the reaction.

The reaction system was prepared by mixing the sodium thiosulfate solution (containing barium nitrate in some of the runs) with the potassium persulfate solution. The reaction was carried out at 25.0°. Aliquots were withdrawn at 30-minute intervals and rapidly titrated with previously standardized iodine solution. Rapid titration was necessary because of the slow reaction between iodine and persulfate ions.

The reaction was found to be first order in thiosulfate and independent of the concentration of the persulfate in agreement with the results of King and Steinbach.[14] As the kinetics work was only incidental to the main purpose of the in-

(13) T. Shedlovsky, *J. Am. Chem. Soc.*, **52**, 1793 (1930).

(14) C. V. King and L. Steinbach, *ibid.*, **52**, 4779 (1930).

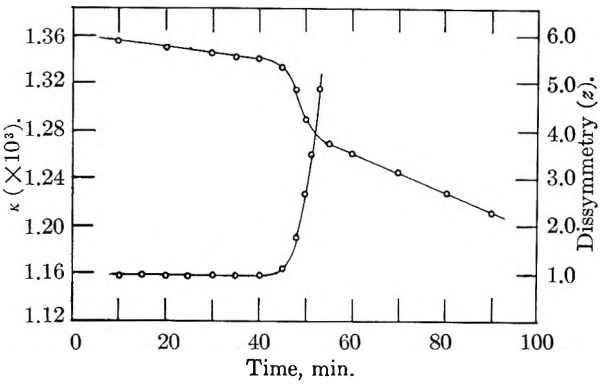

Fig. 2.—Conductance and scattering dissymmetry *vs.* time for a typical run.

vestigation, the detailed rate data will not be presented here. The over-all expression for the first-order rate constant, in units of min.$^{-1}$ and moles/liter for the second term, is

$$k = 2.00 \times 10^{-4} + 0.132[Ba(NO_3)_2] \qquad (12)$$

The estimated precision of the constants is ±2%. The first-order constant compares with the value of 1.87×10^{-4} reported by King and Steinbach.

Activity Coefficient of Barium Sulfate.—In order to calculate solubility product and hence the supersaturation of barium sulfate in water and water–glycerol solutions, the mean ionic activity of the di-divalent electrolyte was required. Fortunately, the total ionic strength changed but little in the course of the precipitation and hence can be considered constant.

The mean activity coefficient of $f_\pm$ of zinc sulfate in water up to ionic strengths $\mu = 0.06$ is given by semi-empirical modification of the Debye–Hückel equation[15]

$$\log_{10} f_\pm = \frac{AZ_+Z_-\mu^{1/2}}{1 + aB\mu^{1/2}} - C\mu^{1/2} \qquad (13)$$

At 25° the constants assume the following values, $A = 354.3/\mathfrak{D}^{3/2}$, $B = 2.91 \times 10^8/\mathfrak{D}^{1/2}$, and $C = 0.373$ for zinc sulfate, $\mathfrak{D}$ being the dielectric constant of the medium. The distance of the closest approach of the ions was here taken to be 3.6×10^{-8} cm. in agreement with LaMer and Dinegar.[21] The values for the dielectric constants of the water–glycerol solutions at 25° were taken from the data of Albright[16] and are given in Table I.

TABLE I

VARIOUS PROPERTIES OF WATER–GLYCEROL MIXTURES AND OF BARIUM SULFATE DISSOLVED THEREIN

Wt. % Glycerol	Dielectric constant	Viscosity, cp.	Calcd. equiv. conductance $BaSO_4$, moles/eq.	Solubility $BaSO_4$ (moles/l.) $\times 10^5$	Calcd. diffusion coeff. $BaSO_4$, cm.^{2}/sec. $\times 10^6$
0.0	(78.54)	(0.894)	(144.4)	(1.09)	(0.5)
.25	72.7	1.81	71.0	0.97	.25
.50	65.8	5.04	26.8	.84	.09
.75	56.2	27.7	4.5	.65	.02

Solubility of Barium Sulfate.—The solubility of barium sulfate in the water–glycerol solutions was determined conductometrically. The low solubility of barium sulfate of course precludes direct measurement of its equivalent conductance in the water–glycerol solutions. The several measurements required for its direct determination were avoided by the use of zinc sulfate as a model system. Appropriate corrections were introduced to compensate for the lower equivalent conductance of the zinc ion. The calculated equivalent conductances at infinite dilution are given in Table I. The solubility values also are given in Table I and are each the mean of three determinations which agree to a precision of 1%.

(15) S. Glasstone, "Introduction to Electrochemistry," D. Van Nostrand Co., Inc., New York, N. Y., 1942, pp. 145–147.

(16) P. S. Albright, *J. Am. Chem. Soc.*, **59**, 2101 (1937).

Viscosity of the Water–Glycerol Mixtures.—The viscosities of the water–glycerol mixtures at 25.00 ± 0.005° were determined in the usual manner with Ostwald capillary viscometer using water as the reference liquid and are shown in Table I.

Barium Sulfate Precipitation.—The persulfate–thiosulfate reaction was initiated by mixing the sodium thiosulfate–barium nitrate solution with the potassium persulfate solution, both of which previously had been equilibrated to 25.0°. In the experiments which were followed by conductivity measurements, the mixing was done in the conductivity cell and the measurements were taken at one-minute intervals. The data for a typical run are presented in Fig. 2 while a summary of the experimental conditions for the 18 precipitation experiments are given in Table II.

The light scattering experiments were carried out as follows:

After mixing the components in the same manner as described for the conductance measurements, the solution was transferred to the light scattering cell. The relative intensities of the scattered light at 45 and 135° from the incident beam were measured at five-minute intervals. These data were then used to calculate the dissymmetry ratio and finally the particle size of the crystallites. The dissymmetry tables of Doty and Steiner[17] were used to interpret the data.

The light scattering data for a typical run are also presented in Fig. 2. Both sets of data represent the same run.

Discussion of the Precipitation Results

The initial linear portion of the conductivity *vs.* time curves as in Fig. 2 corresponds to the difference in the conductivities of the sulfate and tetrathionate ions compared with the persulfate–thiosulfate ions. The point of deviation from linearity is taken as the time of nucleation and the commencement of the growth of the crystallites. It was determined graphically from an enlarged plot of the data.

The difference in conductivity $\Delta\kappa$ between the extrapolation of the initial linear portion of the conductivity–time curves and the actual curves may be taken as proportional to the volume V of the crystallites at the time $t = T$. The final linear portion of the conductance time curves corresponds to the precipitation of all of the barium sulfate present beyond the equilibrium solubility. Hence the interval $\Delta\kappa$ between the two linear curves is proportional to the volume V_T that the crystallites would have at $t = T$ if complete precipitation had taken place. It is found that the two experimental linear curves intersect at zero time as required by this interpretation. This fact further indicates that the rate of the persulfate–thiosulfate reaction is not affected by the formation of the precipitate. The experimental values of the ratio $V/V_T = \Delta\kappa/\Delta\kappa_T$ are given as points *vs.* the time in Fig. 3 while the theoretical curve from eq. 11 appears as a solid line. The zero of time is here taken as the time of nucleation. The observed close agreement between the theoretical curve and the experimental points depends upon a proper choice being made for the units of reduced time $\theta = KD(a + pt)t/R_T(\gamma + R_T)$. However, the general form of the experimental curve is in excellent agreement with the theoretical equation.

It will be seen that if the volume ratio V/V_T is plotted as a function of log t as in Fig. 4, the experimental curves for all the runs under the various experimental conditions should differ only by displacement on the log t axis. This facilitates the evaluation of the units of reduced

(17) P. Doty and R. F. Steiner, *J. Chem. Phys.*, **18**, 1211 (1950).

TABLE II

DATA FROM BARIUM SULFATE PRECIPITATION EXPERIMENTS

Concn. of $Na_2S_2O_3$[d] ($\times 10^3$)	Concn. of $Ba(NO_3)_2$[d] ($\times 10^3$)	Reaction rate ($\times 10^6$)	Nucleation time (min.)	Concn. of SO_4^- at t_0 ($\times 10^5$)	f^+	Super-satn. ratio	Crystallite radius at $\Delta K/\Delta K_T$ = 0.5 ($\times 10^4$), cm.	Adsorption probability ($\times 10^5$)
1.0 (A)	5.0	0.86	38	3.26	0.509	18.7	...	...
3.0 (A)	5.0	2.58	17	4.39	.448	19.2	...	...
2.0 (A)	3.0	1.20	44	5.28	.523	19.0	...	...
1.0 (B)	5.0	0.86	67	5.76	.509	24.8	0.126	5.7
2.0 (B)	5.0	1.73	37	6.40	.476	24.6	.100	4.7
1.0 (B)	9.0	1.40	32	4.48	.431	25.2	.126	6.5
1.0 (C)	5.0	0.86	107	9.20	.509	31.5	...	...
3.0 (C)	5.0	2.58	47	12.1	.448	31.8	...	...
4.0 (C)	3.0	2.40	81	19.5	.457	31.9	...	...
1.0 (B)	5.0	0.86	68	5.84	.509	25.0	.126	5.7
3.0 (B)	5.0	2.58	29	7.47	.448	25.1	.087	7.1
4.0 (B)	3.0	2.40	51	12.2	.457	25.2	.079	5.0
4.0 (B)[a]	5.0	3.44	58	19.8	.392	40.2	.079	4.9
8.0 (B)[a]	5.0	6.88	43	29.6	.324	40.5	.063	6.9
4.0 (B)[b]	5.0	3.44	93	31.9	.344	51.7	.079	8.1
6.0 (B)[b]	7.0	6.78	46	31.2	.291	51.0	.069	5.3
4.0 (B)[c]	5.0	3.44	108	37.2	.270	58.0	.079	7.1
8.0 (B)[c]	5.0	6.88	91	62.6	.217	57.9	.063	4.5

[a] Solvent, 25% glycerol. [b] Solvent, 50% glycerol. [c] Solvent, 75% glycerol. [d] (A), (B), (C) indicate method of purification of $Na_2S_2O_3$.

time log $[R_T(\gamma + R_T)/KD(a + pt)]$. As $a \gg pt$ during the growth time of the crystallites and further $R_T \ll \gamma$, the determination of the magnitude of the units of the reduced time enables γ to be calculated readily. The diffusion constant D of barium sulfate in water was taken to be 0.5×10^{-5} cm.^{2}/0 cc. while the specific growth constant K was taken as 52 cm.^{2}/mole, from the molar

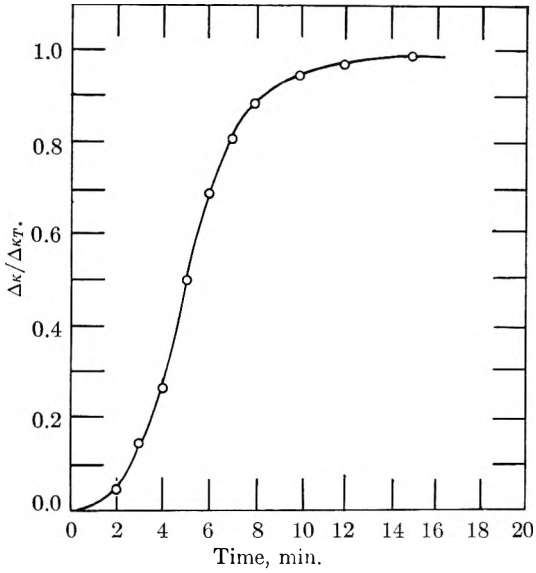

Fig. 3.—$\Delta\kappa/\Delta\kappa_T$ *vs.* time for a typical run. (The solid curve is theoretical. The points are experimental data.)

density of crystalline barium sulfate. The diffusion constant D in the water-glycerol solutions was assumed to be inversely proportional to the viscosity of the medium. The evaluation of the absorption probability α from γ requires an *ad hoc* assumption as to the mean length $\bar{s}$ of a displacement in the diffusional random walk. For convenience, $\bar{s}$ is taken to be equal to 10^{-8} cm. Its precise value will not significantly affect the order of magnitude of the absorption coefficient, which turns out to be very small, being approximately 5×10^{-5}.

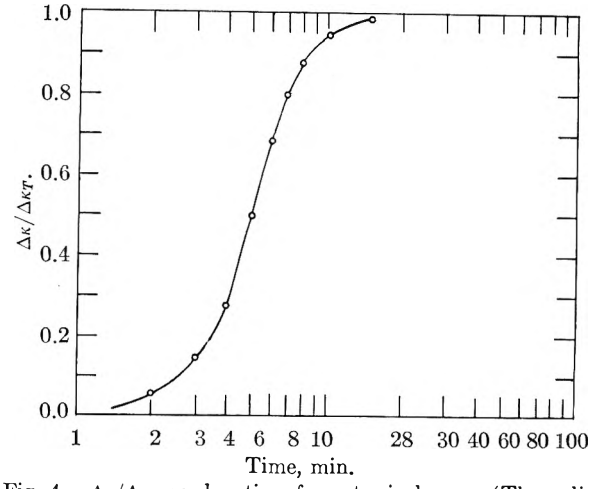

Fig. 4.—$\Delta\kappa/\Delta\kappa_T$ *vs.* log time for a typical run. (The solid curve is theoretical. The points are experimental data.)

The close agreement with the experimental results with eq. 11 seems to confirm the present assumptions as to the mechanism of the precipitation process and the details of the diffusion-controlled growth of the crystallites. The low value of the absorption probability α and its lack of dependence on the composition in water–glycerol mixtures is of particular interest.

Among the factors which might influence the value of α would be the mobile layer of absorbed solvent and ions postulated by Volmer.[18] The lack of dependence of α on the fraction of glycerol in the solvent tends to argue against this hypothesis. Another reason for the smallness of α might be a

(18) M. Volmer, *Z. physik. Chem.*, **102**, 267 (1922).

non-stoichiometric ratio of $SO_4^{=}$ to Ba^{++} at the surface of the growing crystallite which would lead to electrostatic repulsion of the sulfate.

The data make clear that the supersaturation ratio depends on the degree of purification of reagents, particularly that of the thiosulfate. The increase of the supersaturation ratio in the aqueous solutions by *ca.* 70% depending only on the method of filtration of the thiosulfate solutions in the preparation of this reagent infers that spontaneous self-nucleation did not occur in the present precipitations. It is suggested that the nucleation was heterogeneous, possibly taking place on a pre-existing embryo of elemental sulfur, so that the critical nucleus consists of an agglomerate of the foreign substance and barium sulfate. The marked dependence of the supersaturation ratio upon the fraction of glycerol in the solvent may be due to the variation of the interfacial tension between the critical nucleus and the solvent.

Summary and Conclusion

In the observed growth behavior of barium sulfate crystallites, the dependence of size upon the time and the diffusion coefficient are in satisfactory agreement with the Frisch–Collins equation. The observed small absorption coefficient indicates the existence of a free energy barrier at the surface of the crystallites. Growth experiments at other temperatures to determine the temperature coefficient of α and hence the magnitude of the free energy barrier would be of considerable interest. The dependence of α on the barium sulfate ratio and on the presence of surface active agents is likewise of interest.

It appears probable that the nucleation process in all of the present experiments was heterogeneous. The effect on the supersaturation ratio of further purification of the materials used in the system would be necessary for a firm conclusion regarding this point.

Acknowledgment.—The authors wish to acknowledge their indebtedness to the American Cyanamid Company for the use of their laboratory facilities in the experimental phases of the work and, in particular, for the friendly interest of Dr. R. H. Kienle.

HEATS OF ADSORPTION FROM SOLUTION FROM HEAT OF IMMERSION DATA

BY G. J. YOUNG, J. J. CHESSICK AND F. H. HEALEY

Contribution from the Surface Chemistry Laboratory, Lehigh University, Bethlehem, Penna.

Received August 29, 1955

The energetics of adsorption of *n*-butyl alcohol from aqueous solution by Graphon was studied. The adsorption isotherm, heats of solution of butanol in water and heats of immersion of Graphon in butyl alcohol solutions were determined. From these data heats of wetting of the Graphon surface by alcohol solutions of various concentrations could be evaluated. The heats of wetting were also calculated from an equation derived from a simple model and these calculated heats compared to the experimental values. The agreement was excellent and lent support to basic assumptions involved in the model of adsorption from solution.

Introduction

A quantitative measure of the interaction of a solid or a viscous, low vapor pressure liquid with an adsorbent is often desired. Since it is not possible to measure directly the heats of adsorption in such systems, an indirect method must be used. For example, if an index of the interaction of a solid resin or polymer with a filler surface is required, the most direct approach would be to dissolve the resin in a suitable solvent, measure the interaction of the solution with the filler surface, and then subtract out all effects due to the solvent to give the interaction of the resin with the adsorbent. This in effect would give the heat of adsorption of the resin from the solution.

Heats of adsorption for solid–gas systems have been investigated extensively; however, few attempts have been made to evaluate the heats of adsorption of a single component from solution. The temperature dependency of adsorption from solution has been studied, but these data do not lead directly to heats of adsorption[1] as is the case in solid–gas systems. Bartell[1] has estimated an enthalpy value for adsorption from solution from approximate equilibrium constant data and Ewing[2] has made use of the BET constant, c, to give a rough approximation of an energy of adsorption. Direct calorimetric measurements of the immersion of a solid into a solution also have been made; however, the heat of adsorption of a single component was not evaluated.

The present paper outlines an approach for the determination of heats of adsorption of a single component from solution by use of heat of immersion data. Equations are developed and evaluated for the system Graphon–butanol–water.

Experimental

Graphon, the adsorbent used in this investigation, is a graphitized carbon black characterized by a homogeneous surface.[3] The heat of immersion of Graphon in water has been determined as well as adsorption isotherms for water vapor.[4] The Graphon sample[5] had a surface area of 95

(1) F. E. Bartell, T. L. Thomas and Y. Fu, THIS JOURNAL, **55**, 1456 (1951).

(2) W. W. Ewing and F. W. J. Liu, *J. Colloid Sci.*, **8**, 204 (1953).

(3) T. L. Hill, P. H. Emmett and L. G. Joyner, *J. Am. Chem. Soc.*, **73**, 5102 (1951).

(4) G. J. Young, J. J. Chessick, F. H. Healey and A. C. Zettlemoyer, THIS JOURNAL, **58**, 313 (1954).

(5) This sample was furnished by W. D. Schaeffer of Godfrey L. Cabot Co., Boston, Mass.

m.²/g. as determined by nitrogen adsorption. The adsorbate, *n*-butyl alcohol, was obtained by purification and fractional distillation of a good laboratory grade reagent.

The adsorption isotherm for *n*-butyl alcohol on Graphon from aqueous solution was determined by interferometric analysis with a precision of *ca.* 2%. One hundred ml. of alcohol–water solutions of known concentrations were agitated at 25° in a closed flask with 5 g. of Graphon. The equilibrium solution was analyzed to obtain the amount of *n*-butyl alcohol adsorbed. Corrections in concentration arising from the adsorption of water and from changes in the molar volumes were negligible. The rate of adsorption was extremely rapid provided that there was sufficient agitation. Equilibrium concentrations obtained after 10 minutes showed no further change over a period of 24 hours.

The heats of immersion of Graphon in butanol–water solutions of various concentrations and heats of solution of butanol in water were obtained calorimetrically in an apparatus previously described.[6] The heat of immersion effects for this system were complete after a few minutes; the rapidity of the heat evolution again indicated rapid adsorption equilibrium.

Results and Discussion

When a solid surface is immersed in a solution which exerts no chemical or solvent action upon it, some of the solute is usually adsorbed onto the surface thus diluting the solution. Generally, the solute is not adsorbed to the complete exclusion of the solvent, hence adsorption of the solvent also occurs. The surface enthalpy of the solid is thus replaced by the interfacial enthalpies arising from adsorption of solvent and solute. In addition, interfaces are established between these new adsorbed phases and the remaining solution. These concepts can be formulated into a general equation to express the heat of immersion of a solid in a solution.

Development of an Equation to Express the Heat of Immersion of Graphon in Butanol–Water Solutions.—In a previous paper[7] it was suggested that for single component liquids, the interaction between molecules in the liquid state is generally a close approximation of the intermolecular interaction when the vapor is adsorbed onto a solid surface at monolayer coverage or greater. This implies that the heat of immersion is essentially a measure of the interaction energy of the adsorbed molecules with the surface since the energy of vaporization term for the liquid will be nearly equivalent to the interaction energy between adsorbed species.

For the butanol–water adsorbate system it will also be assumed, as in the previous paper, that interactions between molecules in the bulk solution are the same as for the adsorbed layer and thus are not included in the heat of immersion.

If nearest neighbor interactions are not included in the heat of immersion, then the only enthalpy changes to be considered are those for surface and interfacial changes. If θ is the fraction of the Graphon surface covered with adsorbed first layer molecules, the enthalpy contribution for covering this portion of the surface will be $\theta(h_s - h_{s1})$ where h_s is the surface enthalpy of the Graphon and h_{s1} is the surface enthalpy of the Graphon with adsorbed first layer butanol molecules. The enthalpy change for the formation of the interface between the adsorbed butanol and the solution is $\theta(h_{s1} - h_{1\sigma})$ where $h_{1\sigma}$ is the enthalpy of the adsorbed layer in contact with the solution. Similarly $(1 - \theta)(h_s - h_{s2})$ and $(1 - \theta)(h_{s2} - h_{2\sigma})$ are the enthalpy changes for the adsorption of first layer water molecules and the formation of the interface between these molecules and the solution. Here the subscript 2 refers to the water. Since the surface of Graphon is quite homogeneous, θ merely denotes a fraction of the surface and does not represent any particular site energy requirement.

The total enthalpy change for this wetting process is therefore

$$\Delta H_w = \{\theta(h_s - h_{s1}) + (1 - \theta)(h_s - h_{s2}) + \theta(h_{s1} - h_{1\sigma}) + (1 - \theta)(h_{s2} - h_{2\sigma})\} \quad (1)$$

In addition to the heat change for the wetting process, there is also an enthalpy change due to dilution of the solution, ΔH_D, with respect to one of the components. Thus the total heat effect measured, ΔH_I, on immersing the solid surface into the solution is

$$\Delta H_I = \Delta H_w + \Delta H_D$$

or

$$\Delta H_w = \Delta H_I - \Delta H_D = \{\theta\Delta h_{s1} + (1 - \theta)\Delta h_{s2} + \theta\Delta h_{1\sigma} + (1 - \theta)\Delta h_{2\sigma}\} \quad (2)$$

The terms Δh_{s1} and Δh_{s2} are directly the net integral energies of adsorption,[8,9] $N_1(E_{s1} - E_1)$ and $N_2(E_{s2} - E_2)$ where E_1 and E_2 are the energies of the pure solute and solvent, respectively, N is the number of molecules of these components adsorbed, and E_s is the energy of the adsorbed phase.

Evaluation of Terms in Equation 4 for Graphon in Butanol–Water Solutions.—The adsorption isotherm for *n*-butyl alcohol on Graphon from aqueous solutions at 25° is given in Fig. 1. The data agree essentially with those of Hansen[10]; the adsorption is monomolecular in the relative concentration region from approximately $c/c_0 = 0.12$ to $c/c_0 = 0.50$.

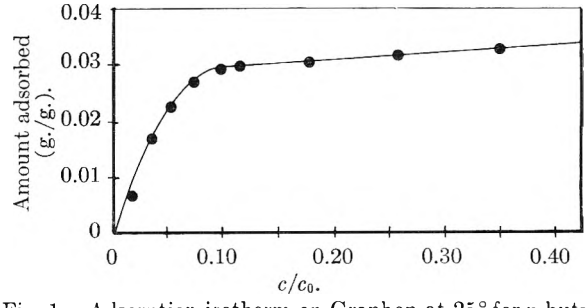

Fig. 1.—Adsorption isotherm on Graphon at 25° for *n*-butyl alcohol from aqueous solution.

The advancing contact angle of water on Graphon is 82 ± 2° while *n*-butyl alcohol spontaneously wets the Graphon surface. Thus the free energy change for the wetting of the Graphon surface by water at 25° is $(\gamma_S - \gamma_{SL}) = \pi_e + \gamma_L \cos\theta = 15.7 + 8.2 = 23.9$ ergs/cm.². The spreading pressure value at saturation, π_e, was evaluated by integration of isotherm data previously determined.[4] In the case of wetting of Graphon by *n*-butyl alcohol at

(6) A. C. Zettlemoyer, G. J. Young, J. J. Chessick and F. H. Healey, THIS JOURNAL, **57**, 43 (1953).

(7) J. J. Chessick, A. C. Zettlemoyer, F. H. Healey and G. J. Young, *Can. J. Chem.*, **33**, 251 (1955).

(8) T. L. Hill, *J. Chem. Phys.*, **17**, 520 (1949).

(9) G. Jura and T. L. Hill, *J. Am. Chem. Soc.*, **74**, 1498 (1952).

(10) R. S. Hansen and R. P. Craig, THIS JOURNAL, **58**, 211 (1954).

25°, the free energy change is $(\gamma_s - \gamma_{sL}) > \gamma_L = 24.5$ ergs/cm.^{2}. The heats of immersion of Graphon in water and *n*-butyl alcohol reflect the free energy changes in that the values are 32.2 and 114 ergs/cm.^{2}, respectively. From these considerations it appears certain that at V_m the hydrophobic Graphon surface is nearly completely covered by adsorbed alcohol molecules. This conclusion is further supported by the agreement in surface areas calculated from nitrogen adsorption data and from the butanol adsorption isotherm.

The B point of the adsorption isotherm given in Fig. 1 was taken as the V_m value. It was assumed that the *n*-butyl alcohol molecules adsorbed on the Graphon surface would orient with the hydrocarbon portion of the molecule lying flat on the surface and the polar hydroxyl group directed toward the liquid. Thus the area occupied by the butanol molecule should be closely approximated by the effective area occupied by a butane molecule lying flat on a surface. The effective area of the butane molecule thus oriented has been given as *ca.* 40 Å.^{2} from gas adsorption measurements.[11] The surface area calculated from these considerations is 98 m.^{2}/g., in excellent agreement with the surface area of 95 m.^{2}/g. calculated from nitrogen adsorption data.

Heats of solution of *n*-butyl alcohol in water are given as a function of concentration in Fig. 2. The values of ΔH_D were calculated from this graph.

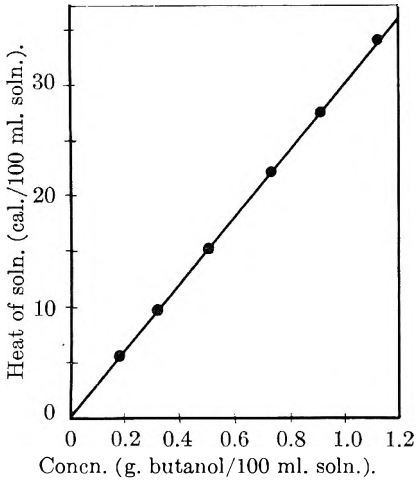

Fig. 2.—Heat of solution of *n*-butyl alcohol in water at 25°.

For the homogeneous Graphon surface, the terms Δh_{s1} and Δh_{s2} are linear functions of the amount adsorbed. In other words the interaction with the surface is the same for all portions of the surface. Values for these terms and others in equation 3 are tabulated in Table I together with the methods by which they were obtained.

Comparison of Heats of Wetting Calculated from Equation 4 and Determined Directly by Experiment.—Since all of the terms in equation 2 could be evaluated exactly or closely approximated, it was possible to compare values for heats of wetting of the Graphon in aqueous *n*-butyl alcohol solutions calculated from this equation to those determined directly by subtracting the heat of dilution from the total heat effect on immersing the Graphon. A comparison of these two methods of obtaining heats of wetting for the system is given in Fig. 3. The solid line represents values calculated from equation 2 and the points were obtained directly from the total heat effects and heats of dilution. Excellent agreement is shown between the calculated and experimental values. This verification of the validity of equation 2 for the system Graphon–butanol–water thus supports the important assumption that interactions between adsorbate molecules are approximately the same in the bulk liquid as in the adsorbed state for this system. In other words, the heat of immersion in this case essentially contains only the energy effect due to interactions between the surface and adsorbed molecules and not any appreciable contribution for interactions between the adsorbed molecules themselves.

(11) R. N. Smith, C. Pierce and H. Cordes, *J. Am. Chem. Soc.*, **72**, 5595 (1950).

TABLE I

VALUES OF TERMS IN EQUATION 2

Term	Value	Expt. method of evaluation
θ	Variable	Adsorption isotherm, Fig. 1
Δh_{s1}	65 ergs/cm.^{2}	Difference between heat of immersion of a clean Graphon surface and one covered with a monolayer of butanol
$\Delta h_{s2} + \Delta h_{2\sigma}$	32 ergs/cm.^{2}	Heat of immersion of Graphon in water. Assumed that $\Delta h_{2\sigma}$ does not vary appreciably with concn.
$\Delta h_{1\sigma}$	46 ergs/cm.^{2}	Heat of immersion of a Graphon surface covered with a monolayer of absorbed butanol molecules into a soln. in equil. with this surface. Assumed that $\Delta h_{1\sigma}$ does not vary appreciably with concn.
ΔH_D	Variable	Heats of soln. (Fig. 2)
ΔH_I	Variable	Measured directly by immersing Graphon in aqueous soln. of *n*-butanol

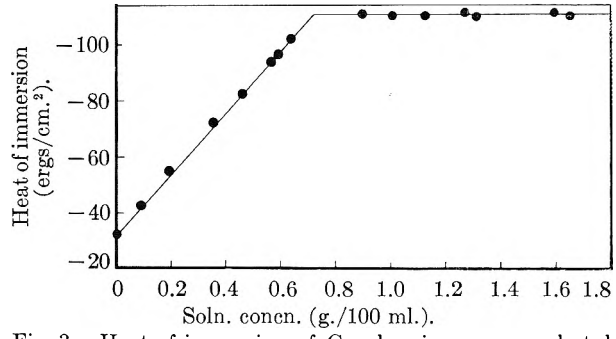

Fig. 3.—Heat of immersion of Graphon in aqueous *n*-butyl alcohol solutions.

It must be emphasized that the assumptions used in developing and evaluating equation 2 are specific for the system under consideration. However, similar, if more complex, equations may be developed for other systems (heterogeneous or homopolar adsorbents, polar or non-polar solutes and solvents, etc.). In practice, if an equation similar to

equation 2 can be established for a system, then this equation would be used to approximate the net energy of adsorption of the solute, $N_1(E_{s1} - E_1)$. Values of the net energy of adsorption in conjunction with isotherm data from solution at the same temperature are sufficient to calculate the integral heat of adsorption, isosteric heat of adsorption and other thermodynamic functions which are important in interpreting the behavior of the solute. For viscous or solid solutes these thermodynamic functions cannot be directly determined.

Acknowledgment.—The authors gratefully acknowledge the financial support of the Armstrong Cork Company, Lancaster, Penna.

HYDROTHERMAL REACTIONS BETWEEN CALCIUM HYDROXIDE AND AMORPHOUS SILICA

By Gunnar O. Assarsson and Erik Rydberg

Chemical Laboratory of the Geological Survey of Sweden, Stockholm 50, Sweden

Received August 31, 1955

The hydrothermal reactions between calcium hydroxide and amorphous silica were studied under carefully controlled experimental conditions within the time and temperature range of 2–48 hours and 120–220°. Reactions of two types take place, depending on the temperature, the boundary between them lying at 160–180°. The formation of the low temperature products (<160°) is dependent to a limited degree on the molar ratio of the reaction mixture; it is formed almost completely within one or two hours. The composition changes with the molar ratio of the mixture; the mixtures poor in lime contain a calcium silicate which probably has the composition of a monosilicate, while mixtures rich in lime give rise to a compound containing up to about 1.5 mole CaO per mole SiO_2 varying lime content being previously known. The X-ray patterns of this low temperature compound vary systematically, but slightly, according to the composition, probably due to the presence of two phases. At temperatures higher than 180° the low temperature silicate is first formed and then later transformed into other phases, the composition of which depends on the molar ratio of the mixtures. The preparation of molar ratio $CaO:SiO_2 = 0.67:1$ yields mixtures of compounds resembling gyrolite and tobermorite, the molar ratio 1:1 yields mixtures of gyrolite and xonotlite, the molar ratio 1.5:1 yields mixtures of xonotlite and β-dicalcium silicate hydrate, and the molar ratio 2:1 yields pure β-dicalcium silicate. The complete transformation of the low temperature phase into the high-temperature compounds requires a considerable time; more than 48 hours at 180° and more than 16 hours at 200°.

Introduction

In earlier works[1] we have examined the suitability of extraction methods for the determination of uncombined calcium hydroxide in silicate masses. Such methods seem at present to be the only ones applicable where a rapid investigation of pozzolanas and steam-cured lime-silica bricks is required. During the steam treatment of lime–silica masses some reactions take place which have hitherto not been fully elucidated. Though these reactions seem to be chiefly connected with technical procedures, the formation of the compounds in the hydrothermal system calcium hydroxide–amorphous silica is of certain chemical and mineralogical interest. The present paper will deal with the reactions occurring chiefly during the first period of formation of the calcium silicate hydrates, *i.e.*, from 2 to about 48 hours after the initial heating up period, within the temperature range 120–220°, those reactions being of greatest importance for estimation of the formation conditions of the silicate hydrates. Papers dealing with the properties of calcium silicate hydrates have been published in considerable numbers, and they cannot be reviewed here. For a general survey, however, reference is made to the summarizing works of some authors.[2]

(1) G. O. Assarsson and J. Bokström, *Anal. Chem.*, **25**, 1844 (1953); G. O. Assarsson, *Zement-Kalk-Gips*, **7**, 167 (1954).

(2) G. L. Kalousek, Third Intern. Symp. on the Chem. of Cement, London, 1954, p. 334; R. H. Bogue, Magazine of Concrete Res. No. 14, Dec. 1953, p. 87; R. H. Bogue, "The Chemistry of Portland Cement," Reinhold Publ. Corp., New York, N. Y., 1947; for the most recent years see also S. A. Greenberg, THIS JOURNAL, **58**, 362 (1954).

Experimental

The best practical method for preparation of the calcium silicate hydrates is that used earlier of allowing calcium hydroxide to react with amorphous silica, the reacting masses being as homogeneous as possible. The properties of the calcium silicate hydrates formed by synthesis in autoclaves depend to a certain extent on the details of the method used for their preparation.[3] Discrepancies between our results and earlier experiments appear to be due to incomplete control of the autoclaving.

Silica.—A commercial preparation, a slightly desiccated silica gel with 14% ignition loss was used. A residue of 0.2% remained after removal of the silica with hydrofluoric acid in the usual manner. For control, the silica was exposed in an X-ray camera; only a broad, very diffuse, and weak ring could be observed on the film between the *d*-values of 4–5 Å. The same result was obtained for preparations of the silica autoclaved 10 hours at 120° and at 200°.

Calcium Oxide.—This was prepared by burning the purest calcium carbonate for 24 hours at 1100°.

Procedure.—Calculated amounts of calcium oxide and silica were ground together in a mortar and sieved through a 0.1 mm. mesh three or four times in order to ensure thorough mixing. Only an insignificant amount of carbon dioxide (less than 0.1%) was taken up by the calcium oxide during the mixing procedure. The preparation was transferred to a platinum crucible and distilled water was cautiously added to produce a rather thick paste. The crucible was suspended without the cover from a silver support wire within the autoclave.

The autoclave used for the final experiments was made of stainless steel. It had a volume of about 150 ml. and was equipped with a valve which allowed evacuation or lowering of the steam pressure. The pressure was controlled with a precision manometer. Sufficient water was introduced to ensure the presence of saturated steam during the heating and some glass capillaries and small pieces of pumice were placed in the water in order to accelerate the attainment of equilibrium conditions.

(3) G. L. Kalousek, J. S. Logiudice and V. H. Dodson, *J. Am. Ceram. Soc.*, **37**, 7 (1954).

The autoclave was then closed and the pressure was reduced to about 7 mm. in order to avoid any eventual influence of the air in the autoclave. As it was important to reach the reaction temperature intended for the synthesis as rapidly as possible, the autoclave was placed in the furnace when this was at a temperature about 30° higher than the temperature required, and the temperature was afterwards lowered. In this way it was possible to shorten the heating-up period to about 20 minutes, which is important for the short time reactions. The temperature of the furnace was regulated automatically to within two degrees. After heating for the intended time the autoclave was cooled down by quenching in water.

The contents of the crucible were immediately mixed with acetone, pulverized and washed, three times with acetone and once with ethyl ether. The preparation was then dried at room temperature for two hours over calcium chloride at about 2 mm. The calcium silicate hydrate preparations were analyzed immediately in order to avoid any aging process which might possibly take place. Uncombined calcium hydroxide, ignition loss and carbon dioxide were determined.

The analyses for uncombined calcium hydroxide were performed according to the extraction method described earlier,[1] using glycerol–alcohol as the solvent and barium chloride as accelerator. In some cases it might have been expedient to determine unreacted silica present in the preparations. The most usual method for such determinations is Jander and Hoffmann's method,[4] based on a selective extraction with dilute acids. Some modifications of this method are described in the literature,[3,5] but the limited fitness for analytical purposes has also been emphasized.[3,4] Experiments performed on the present preparations according to this method gave results showing an imperfect reproducibility. Unreacted silica should, therefore, be determined in some other manner.

For the identification of the silicate hydrates by X-ray the samples were exposed in cameras of two diameters (57.3 and 114.7 mm.). The interferences of very small Bragg-angles could not be observed, but the angles larger than about $2\vartheta = 5°$ were measured with reasonably good accuracy. Samples containing free calcium hydroxide were treated with acetoacetic ester, according to the method of Franke,[6] in order to remove this hydroxide. Experiments for studying the effect of extraction on the silicate hydrates showed that it was not possible to establish any change in the structure of the silicate hydrates. A large number of X-ray exposures were performed in connection with the present investigation; the measurements of the diffraction can only be given here in the form of diagrams.

Results and Discussion

Earlier works on the hydrothermal syntheses of calcium silicate hydrates have been intended mainly to give an interpretation of the compounds formed at equilibrium at fixed temperatures, or to produce preparations of well-grown crystals suitable for optical and X-ray examinations. The present investigation is concerned with the rates of the reactions and, principally, establishment of which calcium silicate hydrates are formed under varying conditions. Results from earlier works will be used for comparison in identification of the products from the autoclaving. It is obvious that some metastable products are more or less rapidly transformed into more stable products. In no case, therefore, can it be assumed that the reactions here discussed always reached equilibrium, as the time of reaction has generally been rather short.

It is desirable to discuss the analytical methods used. The extraction method for determination of the uncombined calcium hydroxide due to Emley might have been undervalued. It is, however, evident from re-examinations,[1] that the silicate hydrates of low lime ratio (calcium oxide:silica < 1:1), autoclaved for more than four hours at a temperature higher than 140°, are decomposed only slightly by the solvent glycerol–alcohol. During preparation by treatment at a lower temperature for a shorter time the solvent obviously attacks the silicate to a certain degree, but not to such an extent that it is impossible to calculate the lime ratio of the silicate hydrates. At higher lime ratio (1.5:1 and 2:1) the determination is slightly more difficult. It is further evident that the silicates prepared at lower temperature (<180°) and for short periods of time are decomposed to a certain extent by the solvent. This influence may be estimated by repeated extractions and a correction factor applied. Some earlier extraction experiments showed that greater accuracy was attained in this way. The analytical error could amount to about 0.05 mole calcium oxide with a lime quotient 1.5:1 and about 0.07 mole at lime quotient 2:1; this accuracy is sufficient for an estimation of the mole ratio of the silicate hydrates. At high temperature (> 180°) with a long reaction time the silicates formed are very resistant toward the solvent.

The calculation of the hydrate water of the silicates is more difficult, as several factors interfere. The reaction mixtures having a low lime–silica ratio must contain significant amounts of uncombined silica, the absorbed water of which it should be possible to estimate indirectly, but the water absorbed by the minute crystals of the silicate is more uncertain. The total water content, however, was determined; the calculation of the hydrate water under certain assumptions will be discussed below.

In all preparations there occurs a small amount of carbon dioxide, which has, in spite of all precautions, been absorbed by the calcium hydroxide during the preparation. The strongest X-ray lines of calcium carbonate, formed in this way in the preparations, could not be discerned in the X-ray photographs. The correction of the molar ratio because of the carbon dioxide is about 0.01–0.04 mole per mole calcium oxide.

Lime Silica Ratio 0.67:1 and 1:1.—These two preparations give results which are in good agreement with one another (Table I). The analyses show that the calcium hydroxide in the mixtures generally reacts completely and rather rapidly with the silica during the autoclaving, forming a phase which will be assigned here as the low temperature phase B. Only in those experiments performed at low temperatures and rather short time is a small amount of calcium hydroxide left unreacted (Table I, 120°, 2 and 24 hours, 160 and 180°, 2 and 4 hours). In the other preparations all of the calcium hydroxide has been consumed in the silicate formation. Thus, calcium hydroxide reacts with amorphous silica up to a lime ratio of 1:1 rapidly when heated to a temperature of 160° or higher. The content of the hydrate water in the silicates is more difficult to estimate. As is shown below a certain amount of uncombined silica must be present in the preparations, but it is not possible to determine its real amount.

(4) W. Jander and E. Hoffmann, *Ang. Chem.*, **46**, 76 (1933).
(5) A. Steopoe, *Zement*, **29**, 193 (1940).
(6) B. Franke, *Z. anorg. allgem. Chem.*, **247**, 180 (1941).

TABLE I

TREATMENT IN AUTOCLAVE OF MIXTURES OF MOLAR RATIO $CaO:SiO_2$ = 0.67:1 AND 1:1 AT 120–220°

Phases: B (low temperature phase) = 1.5–1.0 $CaO{\cdot}SiO_2{\cdot}nH_2O$; T, G, X and H, synthetic phases resembling the minerals: tobermorite ($CaO{\cdot}SiO_2{\cdot}H_2O$) (T); gyrolite ($2CaO{\cdot}3SiO_2{\cdot}2H_2O$) (G); xonotlite ($3CaO{\cdot}3SiO_2{\cdot}H_2O$) (X); hillebrandite (or β-dicalcium silicate hydrate) ($2CaO{\cdot}SiO_2{\cdot}H_2O$) (H).

Autoclave		Mixture, molar ratio 0.67:1			Mixture, molar ratio 1:1		
Temp., °C.	Time, hr.	Per ign. subst. free lime, %[a]	Silicate; molar ratio $CaO:SiO_2:H_2O$	Phase	Per ign. subst. free lime, %[a]	Silicate; molar ratio $CaO:SiO_2:H_2O$	Phase
120	2	0.2	0.65:1:1.55	B	5.0	0.88:1:1.55	B
	24	*	0.66:1:1.50	B	0.3	0.97:1:1.90	B
160	2	*	0.66:1:1.50	B	1.1	0.94:1:1.85	B
	4	*	0.66:1:1.40	B	0.5	0.96:1:1.50	B
	8	...	...	...	*	0.98:1:1.45	B
	16	...	...	...	*	0.98:1:1.45	B
	24	*	0.66:1:1.30	B	*	0.99:1:1.30	B
	48	*	0.66:1:1.30	B	*	0.99:1:1.50	B
180	2	*	0.66:1:1.20	B	0.9	0.94:1:1.90	B
	4	...	0.67:1:1.20	B	0.3	0.97:1:1.20	B
	8	...	...	...	*	0.98:1:1.20	B
	16	...	...	...	*	0.98:1:1.55	B
	24	...	0.67:1:1.20	B	*	0.98:1:1.50	B
	48	...	0.67:1:1.10	B, G, T	*	0.98:1:0.60	B, G, X
200	2	...	0.67:1:1.10	B	*	0.99:1:1.15	B
	24	...	0.67:1:0.95	G, T	*	0.99:1:0.40	G, X
220	16	...	0.67:1:0.75	G, T	*	0.99:1:0.40	G, X

[a], * Deviation of molar ratio from the correct value is caused by small amounts of carbonate.

Some experiments with pure silica, autoclaved at 120–200° during 2–24 hours, showed, however, almost constant water content (6–8%). The molar ratio of the preparations at 160 and 180° seems to approach a constant final value of the hydrate water, which is lowered definitely only when a recrystallization sets in during formation of new phases (180°, 48 hours). Taylor[7] has shown that the low temperature phase B (Table I) has at least three states of hydration (2.5, 1.0, 0.5 moles H_2O). On account of this and the results recorded above and other properties of the silicates a re-examination of the compounds under lowered pressure is in progress.

The ratio, calcium oxide:silica, in the silicate formed at lower temperatures seems to indicate a monosilicate (phase B, Table I); the experiments with mixtures with a higher content of lime, however, give a compound with an excess of lime which increases with increasing lime ratio, as shown below (Table II, *cf.* also ref. 7). It is therefore most probable that the phase B might be even in the mixtures of low lime ratio where an excess of silica is present (0.67:1), of a very nearly monosilicate composition and at the lime ratio 1:1 of a monosilicate composition with a slight excess of lime. Thus, the silicate phase B, formed at low temperatures, has an average composition of 1–1.2 $CaO{\cdot}SiO_2{\cdot}2.5–1.5H_2O$. This leads to the conclusion that an excess of silica must be present in the autoclaved products of the mixtures of the ratio 0.67:1 and 1:1.

To identify the silicates formed the X-ray patterns were compared with those published earlier. The low temperature silicate preparations (phase B in Table I) showed generally the same pattern. The interferences are identical with those described by Heller and Taylor[8] as silicate CSH (I), by Bogue, assigned CSH (B).[9] The compound was later reinvestigated by Claringbull and Hey,[10] and showed very good agreement with the pattern of the mineral tobermorite, a monosilicate $CaO{\cdot}SiO_2{\cdot}H_2O$. The relationship leads these authors to the assumption that the "calcium silicate hydrate" (I) of Taylor may be regarded as synthetic tobermorite. The X-ray patterns of the preparations of the low temperature phase in the present investigation agree well with the previous work, but there is some small distinction worthy of mention. The reflection line at 5.5 Å. occurs in all the patterns but it is stronger and more distinct in the mixtures 0.67:1 than in the mixtures 1:1; these qualities are not dependent on the reaction temperature or time. Thus, it can be concluded that the difference in properties of the preparations must be connected with the lime content of the mixtures. There is also a broad, diffuse, weak band in the 1:1 mixtures between 6 and 7 Å. which does not occur in the pattern of the 0.67:1 mixtures, and which might be similarly explained.

Certain conclusions may be drawn from the above observations. Objections must be raised to the conception that the compound is formed having a stoichiometric composition and very easily takes up an excess of lime by absorption. It is also suggested in earlier works[11] dealing with this silicate, that definite compounds exist having the molar lime–silica ratios of about 4:5 and 5:4. The difference in the X-ray patterns shown above is sufficiently great to be taken into consideration. The molar ratio, unexpected from

(7) H. F. W. Taylor, *J. Chem. Soc.* 3683 (1950); 163 (1953).

(8) L. Heller and H. F. W. Taylor, *ibid.*, 2397 (1951).

(9) R. H. Bogue, Magazine of Concrete Res. No. 14, 1953, p. 87.

(10) G. F. Claringbull and M. H. Hey, *Min. Mag.*, **29**, 960 (1952).

(11) G. L. Kalousek, *J. Am. Concrete Inst.*, **25**, 365 (1954); see also ref. 2 (Kalousek).

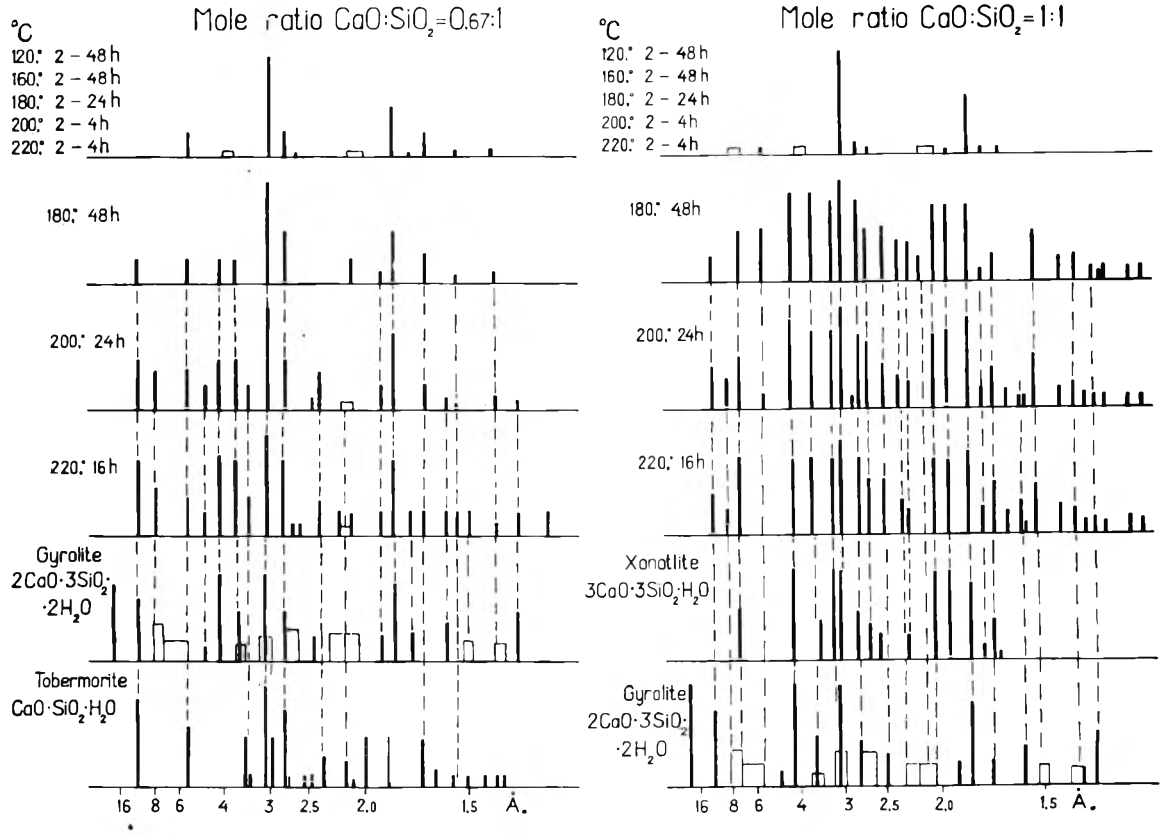

Fig. 1.—X-Ray interferences of the autoclaved mixtures of the molar ratio $CaO:SiO_2 = 0.67:1$ and 1:1, compared with those of tobermorite,[10] gyrolite[15] and xonotlite.[16, 17]

chemical points of view, may have another explanation. When the calcium hydroxide reacts rapidly with the silica, two products could be formed, one stable and one metastable, one of them being a monosilicate, the other a silicate with another molar ratio, *e.g.*, 3:2, as the low temperature phase probably contains more lime than a monocalcium silicate. If these are produced at about the same rate of formation and have nearly the same entropy under the reaction conditions involved, they must be formed at the same time in certain mutual proportions. One of the essential experimental conditions might be the diffusion surfaces, which are supersaturated with respect to the calcium silicate hydrates. In the present case the unavoidable lack of homogeneity in the reaction mixture favors such reactions. The stable and the metastable compounds can exist in the reaction mixture without reaching a real equilibrium within a reasonable time. The very slow transformation of the metastable monosilicate compounds into the stable ones is well established.[8] Similar circumstances may also prevail when the silicate hydrate is prepared from solutions. Metastable reaction products of similar character are known from other substances, *e.g.*, calcium aluminate solutions.[12]

It could be possible that the patterns of the two calcium silicate hydrates supposed to be mixed in the reaction products could be clearly discerned in the X-ray photographs. A certain difference between the X-ray patterns of the preparations poor and rich in lime was pointed out above, indicating that a difference in the X-ray patterns does occur. However, if the patterns of the two calcium silicate hydrates have an equal repeat unit, as pointed out by Bernal in connection with other calcium silicate hydrates,[13] the phases in the mixture will be difficult to distinguish conclusively by X-ray investigations only.

In a publication by Flint, McMurdie and Wells[14] a monosilicate hydrate ($CaO·SiO_2·H_2O$) is mentioned. According to the general survey of the formation conditions of the calcium silicate hydrates given by Bernal,[13] this silicate should be formed between 140 and 180°, the low temperature range. As far as it is possible to conclude from the X-ray photographs the silicate in question is not formed within the first 48 hours of the reactions.

The analyses (Table I) and the X-ray patterns (Fig. 1) show that the reaction products formed at higher temperatures and/or during a longer time contain new phases. Analytically it can only be established that a lowering of the hydrate water takes place with increasing temperature (> 180°) and time. The reflection lines of the substances formed at 180°, 24 hours, show only faint indications of the presence of new phases. The lines

(12) G. Assarsson, *Z. anorg. allgem. Chem.*, **222**, 321 (1935); Geological Survey of Sweden, Årsb. 30, No. 6 (1936) (in German) and literature cited there.

(13) J. D. Bernal, "Third Intern. Symp. on the Chem. of Cement," Cement and Concrete Assoc., London, 1954, p. 216.

(14) E. P. Flint, H. F. McMurdie and L. S. Wells, *J. Research Natl. Bur. Standards*, **21**, 617 (1938).

are distinct when the substance is prepared at 200°, 24 hours and at 220°, 16 hours, these two preparations showing almost identical patterns. When these patterns of the high temperature mixture 0.67:1 are compared with those of the low temperature preparations, it is, however, not possible to establish whether the compound formed at lower temperature is more or less transformed into the new phases, as the few interferences of the low temperature silicate coincide with the numerous lines of the high temperature phases. On the other hand, the 1:1 mixture changes its pattern in one respect with the temperature. The line at d = 5.5 Å. is very weak in the low temperature preparations, it is medium strong in the preparation 180°, 24 hours, and has disappeared in the 220° 16 hours product, thus showing a systematic recrystallization. When the patterns of the two mixtures, 0.67:1 and 1:1, prepared at 200°, 24 hours and 220°, 16 hours, are compared it is evident that the crystallized silicates of the two mixtures are different. It is also evident that a higher lime content of the mixture considerably favors the recrystallization at a temperature of 180° and higher.

The identification of the high temperature products raises some problems. The mixture calcium oxide:silica 0.67:1 corresponds in composition to the mineral gyrolite ($2CaO \cdot 3SiO_2 \cdot 2H_2O$) which could therefore be expected to be formed at higher temperatures. Some measurements of the X-ray pattern of the mineral have been published; those of Mackay and Taylor[15] will be used here for the identification. Most of the diffractions measured by these authors on the mineral are identical with those measured on the high temperature 0.67:1 mixture, but some of them are changed with respect to their intensity (d = 8.02, 5.53, 3.65, 2.79 Å.), and two lines which seem to be lacking among the reflexes of the mineral (d = 3.42, 1.68 Å.) are found to occur among those of the high temperature mixture. Those discrepancies can be explained by the presence of the compound corresponding to the mineral tobermorite, mentioned above, which shows all these lines in the intensity measured. The conclusion may therefore be drawn that the hydrothermal product formed when the mixture 0.67:1 is autoclaved at 200° for 24 hours comprises mainly a compound corresponding to gyrolite together with another compound, which corresponds to tobermorite.

The 1:1 mixture autoclaved at 180° for 48 hours has a medium-strong line at 5.5 Å., which disappears with more intensive treatment (220°, 16 hours, Fig. 1). As this line obviously belongs to the reflexes of tobermorite, its presence must be explained by the formation of well-grown crystals of this compound which at higher temperatures recrystallizes and is transformed into another compound. The new product shows the characteristic reflexion line of gyrolite (d = 11.0, 1.57 Å.), but most of its reflexes correspond to those of the mineral xonotlite ($3CaO \cdot 3SiO_2 \cdot H_2O$) described earlier.[14,16,17] The reflexes of the products formed on autoclaving at 180° for 48 hours, at 200° for 24 hours, and at 220° for 16 hours agree very well in other respects. The low temperature product (phase B) therefore recrystallizes in the following manner: the compound resembling tobermorite crystallizes at 180° together with those resembling xonotlite and gyrolite and disappears at higher temperature, probably transformed into the xonotlite compound; at 220° and 16 hours the reaction product contains the compound resembling gyrolite and xonotlite, with the latter in excess.

As a control to show that no recrystallization of the amorphous silica takes place, some preparations of the 0.67:1 and 1:1 mixtures were extracted with dilute hydrochloric acid, the remaining silica was dried cautiously and exposed in the X-ray camera. The intensity of the band (d = 4–5 Å.) observed in the X-ray photographs of the initial material mentioned above had increased, but there were no lines showing the presence of crystallized silica which could distort the results.

Molar Ratio Mixture CaO : SiO_2 = 1.5 : 1 and 2 : 1. —These two mixtures, when autoclaved at lower temperatures and/or during a short period of time at higher temperatures, show chemical properties which are due to the excess of lime present in the preparations. The lime reacts almost immediately with silica, as described above, but the magnitude of the excess of free lime present determines the extent to which the molar ratio 1:1 is exceeded in the calcium silicate formed. This molar ratio, calcium oxide:silica, is 1.25–1.30:1 for the lime mixture, 1.5:1 and 1.35–1.50:1 for the mixture 2:1 (Table II, phase B). The explanation given above for the formation of the silicates may also be applied to these reactions, and it is, of course, probable that the mixtures initially containing a larger excess of lime will contain, after treatment, more of the lime-rich phase. The initial reaction is therefore a rather rapid saturation of the silica immediately available. After this saturation the compounds formed are relatively stable in relation to the remaining excess of lime and the calcium hydroxide and phase B only react slowly. The analyses of the low temperature phase B reported in Table II show further that the water contents of the silicates formed vary from about 1.4 to 1.7 moles per mole of silica, as was found concerning the corresponding silicates of the mixtures with lower lime ratios.

The X-ray investigation of the low temperature substances shows that the patterns are chiefly the same as those reported above for the lower lime ratios, in spite of the excess of lime present in the silicate hydrates formed (Fig. 2). The reflection line at 5.5 Å., which could result from the silicate phase B poor in lime, could be discerned in the 1.5:1 mixtures as a very weak reflex, but not at all in the mixtures 2:1. This behavior further confirms the conclusion previously reached concerning the composition of the silicates and consequently also confirms the supposition that two calcium

(15) A. L. Mackay and H. F. W. Taylor, *Min. Mag.*, **30**, 80 (1953).

(16) W. Jander and B. Franke, *Z. anorg. allgem. Chem.*, **247**, 161 (1941).

(17) E. Thilo, H. Funk and E. M. Wichmann, *Abhandl. Deut. Akad. Wiss. Berlin*, **1950**, No. 4 (1951).

TABLE II

TREATMENT IN AUTOCLAVE OF MIXTURES OF MOLAR RATIO $CaO:SiO_2$ = 1.5:1 AND 2:1 AT 120–200°

Autoclave Temp., °C.	Time, hr.	Mixture, molar ratio 1.5:1 Per ign. subst. free lime, %	Silicate formed molar ratio $CaO:SiO_2:H_2O$	Phase (See Table I)	Mixture, molar ratio 2:1 Per ign. subst. free lime, %	Silicate formed molar ratio $CaO:SiO_2:H_2O$	Phase (See Table I)
120	2	18.0	0.95:1:1.85	B	27.0	1.10:1:1.65	B
	24	9.5	1.20:1:1.85	B	19.0	1.35:1:1.60	B
140	2	15.0	1.05:1:1.60	B	24.0	1.20:1:1.80	B
	4	13.0	1.10:1:1.50	B	23.5	1.20:1:1.75	B
	8	9.5	1.15:1:1.55	B	19.0	1.30:1:1.65	B
	24	9.0	1.20:1:1.65	B	19.0	1.30:1:1.75	B
160	2	13.0	1.10:1:1.75	B	22.5	1.25:1:1.95	B
	8	8.5	1.20:1:1.50	B	19.0	1.30:1:1.55	B
	24	7.0	1.25:1:1.45	B	15.0	1.45:1:1.50	B
	48	6.0	1.30:1:1.40	B	13.0	1.50:1:1.70	B
180	2	9.0	1.20:1:1.35	B	18.0	1.40:1:1.60	B
	8	6.5	1.25:1:1.55	B	13.0	1.50:1:1.50	B
	24	3.0	1.30:1:1.30	B, H, X	10.0	1.60:1:1.35	B, H
	48	1.0	1.45:1:1.20	(B), H, X	4.0	1.80:1:1.25	(B), H
200	2	8.0	1.20:1:1.40	B	18.5	1.35:1:1.60	B
	8	3.0	1.35:1:1.30	B, H	11.5	1.55:1:1.35	B, H
	16	0.5	1.45:1:0.80	(B), H, X	1.0	1.95:1:1.15	(BX), H

silicate phases are present in the low temperature mixtures. There are some other diffraction lines which occur in the X-ray pattern from the low temperature preparations of the mixtures 1.5:1 and 2:1, which are not shown by the low temperature preparations 0.67:1 and 1:1. These lines have very weak intensities in the lower temperature preparations (120°, 140°), but are slightly discernible in the higher temperature compounds (160°, 24 hours and 180°, 16 hours). It is plausible to connect these lines with the low temperature phase, rich in lime, assumed to be present.

At about 180° the reaction products change their character after about 24 hours in the autoclave, or if the temperature is higher, after a shorter period of time. The new compounds formed successively consume the excess of lime present, forming phases richer in lime than the low temperature phase. In the mixture with a lime ratio of 1.5:1 all lime is fixed after 48 hours at 180°,

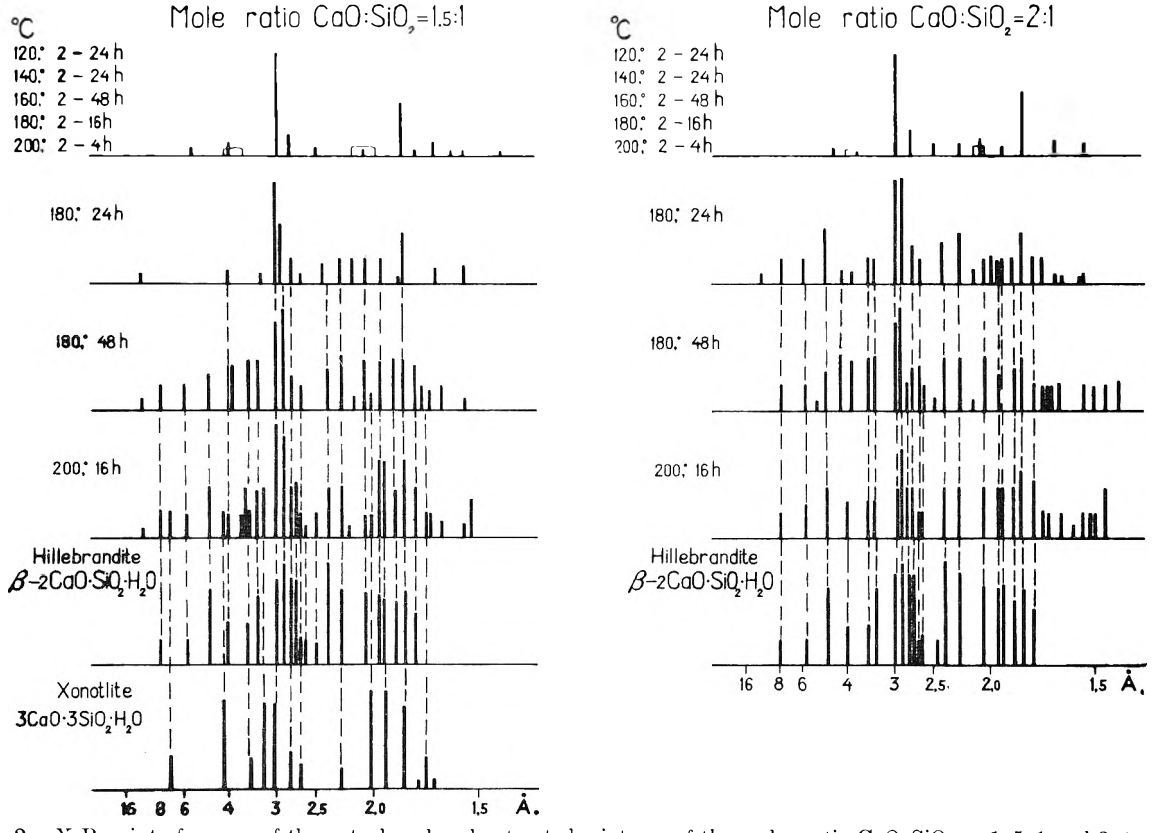

Fig. 2.—X-Ray interferences of the autoclaved and extracted mixtures of the molar ratio $CaO:SiO_2$ = 1.5:1 and 2:1 compared with those of hillebrandite (β-dicalcium silicate hydrate)[18, 19] and xonotlite.[16, 17]

or after 16 hours at 200° (Table II); the average molar ratio of the products formed has a value approaching $CaO:SiO_2:H_2O = 1.5:1:0.75$. The mixtures with the lime ratio 2:1, on the other hand, yield, under the same conditions, a reaction product of the composition 2:1:1. The lime ratio 1.5:1, however, presupposes that the reaction products also contain compounds with lower lime content than a disilicate. It is possible that uncombined silica could also occur, but crystalline silica (cristobalite, quartz) cannot be discerned on X-ray investigation of either of the preparations or of the silica residue obtained by treatment of the autoclaved products with dilute acid. Uncombined amorphous silica could also occur, but there is no reliable method known for its determination. However, mixtures of the molar ratio 1.5:1 and 2:1 can be autoclaved at 160° for more than 48 hours without changing the proportion of lime:silica in the silicate products formed. As the free lime present in the mixtures should react easily with any possible residue of amorphous silica, it is most probable that no substantial amount of amorphous silica occurs and that therefore all silica has reacted forming silicates of the phase B. Afterwards the reaction between the remaining free lime and the phase B sets in, running slowly in comparison with the formation of the phase B. The temperature at which the reaction changes its character is between 160 and 180°, and this boundary of the phase formation seems to be identical for the two mixtures 1.5:1 and 2:1.

The X-ray patterns of the high temperature products from the mixtures of lime ratio 1.5:1 and 2:1 also show a successive formation of some new phases. In the preparation from autoclaving of the 1.5:1 mixture at 180° for 24 hours some of the weak lines of the low temperature phases become stronger, indicating the formation of more well-crystallized compounds. Some new lines appear successively and after treatment at 180° for 48 hours and 200° for 16 hours the reaction products consist chiefly of β-disilicate (β-$2CaO\cdot SiO_2\cdot H_2O$) described by Heller and Taylor[18] and found by Heller[19] to be identical with the mineral hillebrandite. The pattern of this compound, as given by these authors, is in very good agreement with those of the present preparations (Fig. 2).

The autoclaved mixture of the molar ratio 1.5:1 must also contain compounds other than disilicate hydrate. Some of the diffractions which do not coincide with those of the β-disilicate, indicate that the reaction products (180°, 48 hours) contain substantially β-disilicate but also a certain amount of the xonotlite-like substance. The product formed on autoclaving at 200° for 16 hours also shows some lines of the compound resembling xonotlite. The crystallization of the compound of xonotlite-type seems to take place after the formation of the β-disilicate hydrate as the xonotlite lines occur in the 200°, 16 hours, preparation but not in the 180°, 48 hours, preparation.

One of the lines (d = 3.96 Å.) shown by the reaction products from treatment at 180° for 48 hours is worth some attention. It does not occur in the reaction products of the preparations autoclaved at 200° for 16 hours. The α-dicalcium silicate line 3.90 Å. nearly coincides with this line, but other strong lines of this compound are lacking. Possibly it belongs to a compound with low content of lime which is transformed at 200°.

The high temperature products of the mixtures with lime ratio 2:1 also show the beginning of the crystallization of β-disilicate hydrate at an autoclaving at 180° for 24 hours, which is more pro-

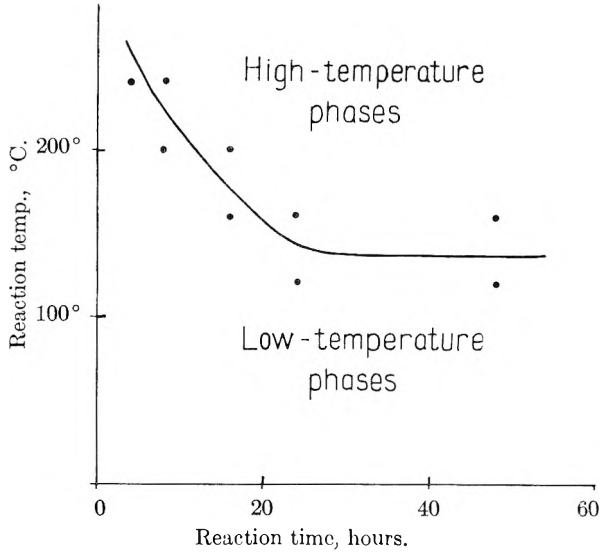

Fig. 3.—Relation between time, temperature and formation of the calcium silicate hydrates during autoclaving.

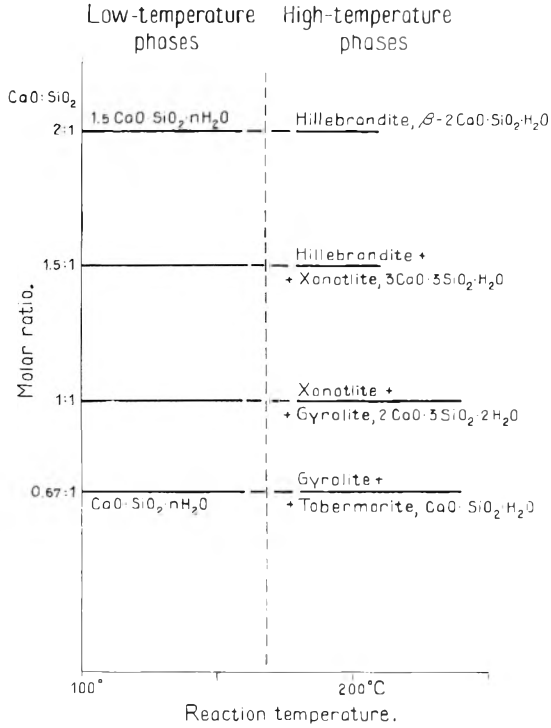

Fig. 4.—Relation between the molar ratio of the mixtures, the temperature and the phases formed at the autoclaving within about 48 hours. The mineral names refer only to the hydrothermal, synthetic phases resembling these minerals.

(18) L. Heller and H. F. W. Taylor, *J. Chem. Soc.*, 2535 (1952).

(19) L. Heller, *Min. Mag.*, **30**, 150 (1953); *Acta Cryst.*, **5**, 724 (1952).

nounced in this preparation than in the corresponding preparation with the lime ratio 1.5:1. The molar ratio of the calcium silicate formed, however, indicates that only a part of the calcium hydroxide present in the initial mixture (80% in the product after autoclaving at 180° for 24 hours) has been combined as silicate. As most of the combined lime has been bound by the formation of the β-disilicate hydrate, a certain quantity must be present as a silicate poor in lime. In the X-ray pattern of the preparations formed by treatment at 180° for 24 hours or for 48 hours the unidentified line d = 3.96 A., mentioned above, occurs, but this has disappeared from the pattern of the preparations formed by treatment at 200° for 16 hours. The latter preparation shows an X-ray pattern in complete agreement with that of the β-disilicate hydrate. It is also worthy of mention that two lines (4.17 and 2.07 Å.) obviously belonging to xonotlite are to be observed in the preparations (180°, 24 hours) and disappear at more intensive treatment (200°, 16 hours) showing that this substance is a metastable compound formed during the reaction.

The results above may be compared with those in the survey of the equilibria given by Bernal.[13] The phases in equilibrium in the low temperature range would comprise the compound of afwillite-type and in the mixture with the lime ratio 2:1 above 150° also that of hillebrandite-type (β-disilicate) according to Heller and Taylor.[18,19] None of these compounds could be discerned, in the X-ray photographs nor in the polarization microscope. The compounds in equilibrium at the temperatures 180° and higher would be γ-dicalcium silicate (γ-$2CaO \cdot SiO_2 \cdot H_2O$) in the mixtures of the lime ratio 2:1,[19] but here again the characteristic X-ray pattern of this compound was lacking in the 200°, 16 hours preparations.

The reactions described above are presented in diagram form in Figs. 3 and 4. Figure 3 shows the formation of the phases in relation to reaction time and temperature. The boundary between the two areas of the low and the high temperature phases cannot be drawn more exactly, as the identification must chiefly be based on X-ray observations, the accuracy of which is very limited. The diagram, however, gives a good conception of the reactions. Figure 4 shows the calcium silicate hydrate formed when the preparations were autoclaved for the longest time (48 hours); with extended reaction time the residues of the low temperature phase remaining among the high temperature compounds would be transformed completely. Between the low and high temperature areas there is a range of very uncertain observations, and the correct position of the boundary is therefore open to question.

Acknowledgment.—The authors wish to express their gratitude to the International Ytong Co. of Stockholm for a grant which made possible a wider investigation of the present topic in connection with the technical research of the hydrothermal reactions of the pozzolanas.

SODIUM TRANSPORT IN ISOLATED FROG SKIN[1]

BY HARUTO P. KATO,[2] BRUNO J. ZWOLINSKI, AND HENRY EYRING

Contribution from Graduate School, University of Utah, Salt Lake City, Utah

Received September 2, 1955

Tracer and e.m.f. measurements show that sodium influx follows a pattern similar to a Langmuir adsorption isotherm. On the assumption that the influx is chiefly due to a sodium complex, an equation is derived which fits the experimental data closely. A similar set of studies on the outflux shows a rather anomalous flux pattern. The measured and calculated flux values, using the experimentally determined transmembrane potentials in the equation for outflux, agree quite well. Temperature coefficients of flux on both the influx and outflux are described. None of the flux patterns could be fitted by a simple Arrhenius plot. This is in agreement with the equations derived for both influx and outflux of sodium ions which exhibit a complex temperature dependence. The effects of ATP and histamine on the transmembrane potential are described. ATP applied to the outside of the skin increases the transmembrane potential. Applied to the inside, ATP decreases the potential. Histamine applied inside, in certain concentrations, destroys the potential. The quantity required varies from skin to skin. Similar concentrations of histamine applied to the outside of the skin are without effect.

Introduction

The experiments performed on frog skin to date indicate the uniquely important role played by sodium in maintaining the skin potential. In isolated frog skin a net transport of sodium ion occurs. Ussing[3] has systematically studied both sodium influx and outflux. A suitably modified procedure provides the necessary data for our analysis. Absolute rate theory is used in the analysis of the diffusion of both charged and uncharged particles.

(1) This material is taken in part from a thesis submitted by H. P. Kato to the faculty of the Graduate School, University of Utah, in partial fulfillment of the requirements for the Ph.D. degree.

(2) Public Health Service Research Fellow of the National Institutes of Health and the National Institute of Arthritis and Metabolic Diseases; 1953 and 1954.

(3) H. H. Ussing, *Cold Spring Harbor Symposia Quant. Biol.*, **13**, 193 (1948).

Description of Experiment

Materials.—The experiments were carried out on the isolated abdominal skins of male grass frogs, *Rana Pipiens*. The General Biological Supply House of Chicago, Illinois, supplied the frogs.

Early experiments on frogs left in a cold room thermostated at 2° gave unsatisfactory results—the transmembrane potential decaying to zero in only two to three hours. The rate of oxygen consumption as measured in a Warburg apparatus also decreased with time. Changing the composition of the bathing solutions did not correct the decaying in the potential or respiration patterns. For example, Ringer solution was used with and without phosphate buffer. The calcium ion was omitted from the Ringer formula. Sodium chloride was used alone. Substrates such as glu-

cose, succinate, lactate and pyruvate were added. In addition, some of the solutions were equilibrated with oxygen. None of these procedures resolved the difficulties of maintaining constant or reproducible membrane potential readings. It was found, however, that keeping the frogs in an inclined tank containing water at temperatures closer to the experimental ones remedied earlier difficulties. During the summer the tank was partially buried in the ground, and in winter it was left indoors. The excised skin remained at a constant value for about 12 to 20 hours. A typical time–potential curve is shown in Fig. 1. The potential rises initially and becomes nearly constant with time. As other workers have discovered the transmembrane potential is a sensitive indicator of normal membrane stability.

The Ringer formula finally used was a modification of formulas from a variety of sources and is given in Table I. The concentrations of all ions other than the sodium ion were kept constant in all of the bathing solutions used in studying the active transport phenomena. In a few cases the quantity of sodium bicarbonate was reduced when sodium concentrations lower than 2.38 mM were needed. To attain equilibration with atmospheric CO_2, the solutions were exposed in open beakers overnight, reaching final pH values in the range of 8.1 to 8.3 units. The variation in pH readings was less than ± 0.2 during each flux measurement as well as for the duration of an experiment.

TABLE I

COMPOSITION OF RINGER SOLUTION USED

6.50 g. NaCl	= 111 mM
0.0750 g. KCl	= 1.00 mM
0.200 g. $CaCl_2$	= 1.80 mM
0.200 g. $NaHCO_3$	= 2.38 mM
(Na^+)	= 114 mM

Radioactive sodium-22 was used to determine the sodium fluxes which were computed from time–interval, count differences. The error involved in the pipetting times was generally 0.5–1.0%. Interval samples were counted in aluminum planchettes 1 mm. deep and about one inch in diameter. Because of the low energies of the β-rays, the specific activity depended on the thickness of the sample only; thus, the sample thicknesses needed to be reproduced accurately. Two factors helped in promoting a uniform sample layer. The low planchette walls minimized creeping, and the small amount of calcium in the Ringer formula precipitated, providing substance around which sodium chloride could in turn deposit. The measured β-absorption curve indicated that only a few of the flux values had to be corrected. The change in specific activity was in most cases within the over-all experimental error.

Apparatus.—An efficient air thermostat constructed to specifications given by Vernon[4] was used. Temperature control to better than 0.1° was attained over the temperature range of 10 to 40° which was available for measurement of temperature coefficients. The majority of the experiments were carried out at a standard temperature of 20.0°. The diffusion cell system in the thermostat was accessible through a large front door equipped with a small sliding glass window for extracting sample solutions.

The excised frog skin was mounted in Lucite cells somewhat similar to those described by Ussing.[3] A pair of improvised Lucite screens were used for mounting the skin and maintaining a constant flux area by counteracting the bulging pressure of the circulating solutions. The entire cell assembly was held together by a set of three brass screws.

The diffusion cells were connected by 2-mm. rubber tubing to two aerating bulbs which served as cell reservoirs for the calomel and glass electrodes. The spherical glass bulbs, 25 ml. in volume, were equipped with a pair of glass filter sticks for aerating the solutions with wet oxygen gas. Except for a small opening to equalize the oxygen pressure, the circulatory cell system was essentially closed. Evaporation was found to be negligible. The radioactive samples were conveniently removed from these bulbs.

A typical external mechanical eccentric pump was used for circulating the cell solutions at average rates of 500 ml./min. in each cell compartment. The total volume of solution on each side of the frog skin was about 15 ml.

(4) W. H. J. Vernon, *Trans. Faraday Soc.*, **27**, 241 (1931).

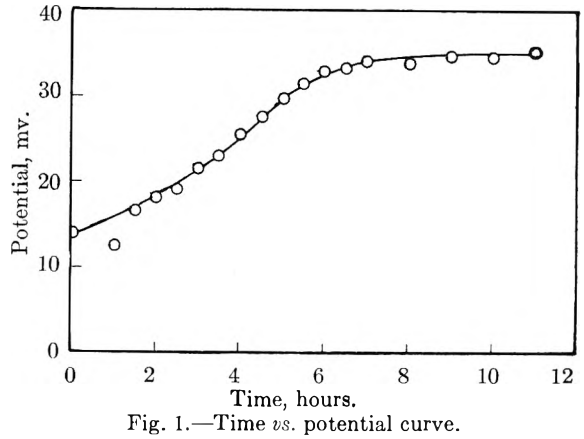

Fig. 1.—Time *vs.* potential curve.

The radioactive samples generally 0.5 to 1.0 ml. were withdrawn with calibrated micropipets. The interval samples were dried in the aluminum planchettes under infrared bulbs and counted with an end-window, Geiger–Mueller tube. Relative geometry was determined for the various shelf positions. When the samples were of high activity, a lower shelf was used in order to avoid dead-time corrections. The uncertainties of the individual counts were kept well under 1%. Counts were generally taken for at least one hour. The standard deviation in the count differences was held to 1 or 2%.

The transmembrane potentials were measured on a Leeds and Northrup, K-2 potentiometer with a pair of Beckman calomel microelectrodes. A very sensitive pointer–mirror type galvanometer was used as the null device. The electrode potential differences were taken, the electrodes being dipped in saturated KCl solution immediately before the transmembrane potentials were taken each time. The drift in the electrode potential difference was often quite large.

The pH of the solutions was determined with a Cambridge Research model pH meter. All levels and switches to the glass electrode were electrically shielded.

Experimental Procedure

1. **Influx *vs.* Outside Sodium Concentration.**—In the influx studies two series of Ringer solutions were prepared with the sodium ion concentrations varying from 2.38 to 125 mM. One set was radioactive. The non-radioactive solutions were used for washing out the cells prior to adding the radioactive solutions. The various radioactive solutions were used in a given experiment to determine the flux at a given outside sodium ion concentration. These radioactive solutions were reused for all of the experiments on influx. The solution bathing the inside was a full Ringer solution with a sodium ion concentration 114 mM. The equilibration period was one hour. The pipetting interval was also one hour. The drift in the transmembrane potential was about 0.5 mv. at most during the one-hour flux period following a one-hour equilibration period. One-milliliter samples were pipetted from the inside, and 0.1-ml. samples were pipetted from the outside at a convenient point in the flux interval. The inside solution was replenished with fresh bicarbonate Ringer solution at the close of each flux interval. This helped to keep the inside activity sufficiently low so that radioactive back diffusion could be neglected in making the calculations.

In some experiments as many as five solutions of different sodium ion concentrations bathed the outside. The flux values obtained during the final hours of the experiment fell off as a result of excessive deterioration of the skin. As the skin deteriorated the transmembrane potentials also decayed. When the transmembrane potentials decayed as much as 3 mv. during the one-hour flux period, the drop in flux was excessive. The number of different concentrations of sodium ion bathing the outside of the skin was in many cases limited to three. This procedure ensured that the points on the extreme limits of the curve would be accurate responses of a living skin. In some cases the lower concentrations were first used followed by a sequence of the higher concentrations of the sodium ion. In other cases the sequence of bathing solutions was just reversed. No hysteresis effects were observed, indicating that true flux patterns were being measured.

In calculating the sodium influx, it is necessary to know the volume of the inside solution within the over-all experimental error plus the concentrations of the Na ion in the outside solution.

2. **Outflux *vs.* Outside Sodium Concentration.**—Earlier experiments of Ussing indicated that the order of magnitude of outflux is roughly 10% of the influx. Initial theoretical calculations based on observed transmembrane potentials indicated a rather striking maximum in the outflux, near an outside sodium concentration of 5 m*M*. The specific activity of the complete Ringer on the inside was made large in order to permit extraction of flux samples at shorter intervals. Twenty-five milliliters of Ringer contained 0.4 millicuries of sodium-22. The relative activity amounted to about 10^5 counts per min. per ml. on the first shelf of the counting castle. The higher radioactive fluxes permitted a larger number of flux points to be obtained over the life of the skin, which helped to define more precisely the flux pattern. In all, about nine points were obtained, resulting in a smooth flux pattern.

The outflux was studied under conditions similar to the influx experiments. Inside was a full Ringer solution, and the outside sodium ion concentrations were again varied. The equilibration period was one-half hour as was also the flux interval.

The outflux calculations required a knowledge of the volume of the outside but not of the inside solutions. The outside solutions could never be completely drained, and hence the volume remaining on the walls of the apparatus had to be determined. A standard draining procedure was followed. With the aid of a rubber air bulb, the volume of the solution remaining was made reproducible, and amounted to 0.6 ml. This correction was used at each flux calculation.

Pipetting from the inside solution was less frequent. Usually three samples of 0.01 ml. were taken, and all three samples agreed very closely in their counting rates. Corrections have not been applied on the flux values at different outside sodium ion concentrations for the changes in specific activity. Calculations show the only value which is changed significantly is at 114 m*M* outside sodium ion concentration, and this value is low only by approximately 2.5%.

3. **Temperature Coefficient of Flux.**—Temperature effects on sodium fluxes and transmembrane potentials were studied between 12 and 35°. The thermostat capacity determined the lower temperature limit. The deterioration of the skin precluded any studies at temperatures beyond 35°. According to Barnes, cooling to 0° effects a rather marked drop in transmembrane potential.[6]

The constancy of the transmembrane potential was an excellent criteria for indicating the health of the skin. Flux values obtained, while the transmembrane potentials remained fairly constant, followed a smooth pattern. When the potentials decayed markedly over the flux period, the flux values were irregular.

An outside sodium ion concentration of 25 m*M* was used in these experiments. The inside was bathed by a full Ringer solution. The skin potential, as read between two calomel electrodes, was approximately 40 mv. With the reversible electrode-potential corrections applied, the junction potential becomes 76.5 mv. The flux period was one hour as was the period of equilibration.

4. **Effects of ATP and Histamine on the Skin Potential.**—The effect of these substances on the transmembrane potential was also studied at an outside sodium ion concentration of 25 m*M*. The inside solution was again a full Ringer solution. Adjustments were made on the *p*H values of the inside solution most of the time but not on the *p*H of the outside solutions. The inside *p*H never dropped below about 6.8. Flux and transmembrane potential are optimal between an inside *p*H of 6.8 and 8.6, whereas these variables are quite insensitive to outside *p*H within much broader limits of *p*H 5 to 9. Adenosine triphosphate (ATP) was used in the form of the disodium salt. Histamine was used in the form of histamine phosphate.

Theory and Results

The theory of sodium ion transport due to complex formation is widely accepted. A theoretical demonstration of sodium ion transport for the case of isolated cells has provided convincing proof of its plausibility.[5] Ussing has advocated the theory in connection with his work on frog skin.

For the case of isolated single cells we apply the term *passive* to ions which obey the Nernst equation for the potential, and the term *active* to those ions that do not. Transcellular sodium transport as it occurs in frog skin, for example, becomes a specialization of the single cell. In isolated frog skin a net inward transport of sodium chloride is observed. An equation applicable to frog skin for passive ions has been developed by Ussing which is based on flux ratios.

$$\frac{Q_1}{Q_2} = \frac{\gamma_1 c_1}{\gamma_2 c_2} e^{[z\mathfrak{F}/RT](\epsilon_1 - \epsilon_2)}$$

Here the two solutions in contact with the membrane are labeled 1 and 2. The flux of a given ion from solution 1 to solution 2 is given by Q_1; the simultaneous flux from 2 to 1 is given by Q_2. The γ's and c's are, respectively, the activity coefficients and concentrations of a given ion in the solutions as designated by the subscripts. Finally, $(\epsilon_1 - \epsilon_2)$ is the electrical potential difference between the two solutions, z is the charge of a given ion with sign $\mathfrak{F}$, the Faraday constant, R, the gas constant and T, the absolute temperature.

Some ions, notably potassium, chloride, bromide and iodide are very nearly passive.[7a,b] Sodium does not obey the Nernst equation, indicating active transport.[8] Theory must accordingly account for the specific nature of a transport mechanism which discriminates between potassium ions and sodium ions.

Among the various salts which have been tried, only sodium and lithium salts sustain the frog skin potential.[9] Lithium salts sustain a potential for a limited time of about 1.5 hours. Sodium and potassium differ in ionic radii. The tendency to complex is known to depend on the ionic radius.

A number of experimental facts point to the lipoid nature of membrane walls. Davson and Danielli quote a number of sources of evidence.[10] It is proposed that sodium complexes with a substance which results in an increased permeation of sodium ions through the membrane. Such a complexing substance, which we shall call pump substance, when combined with sodium ions facilitates the passage of the complex over the rate limiting barrier. The rate limiting barriers might be in the membrane phase itself. In such a case the pump substance should confer an added fat solubility to the sodium complex. An outward sodium concentration gradient (in the cell) can be maintained, providing the complexing agent is produced inside the cell and the sodium complex is destroyed or removed on the outside. A transmembrane potential will be sustained which is given by

$$\epsilon(\text{mv.}) = 59 \log (\text{NaP}^+)_i/(\text{NaP}^+)_o$$

(5) R. B. Parlin and H. Eyring, "Ion Transport Across Membranes," Columbia Univ. Press, New York, N. Y., 1953, pp. 103–108.

(6) T. C. Barnes, *J. Cellular Comp. Physiol.*, **13**, 39 (1939).

(7) (a) H. H. Ussing, *Acta Physiol. Scand.*, **19**, 43 (1949); (b) H. Linderholm, *ibid.*, **27**, Supp. 97 (1952).

(8) H. Levi and H. H. Ussing, *Nature*, **164**, 928 (1949).

(9) G. Galeotti, *Z. physik. Chem.*, **49**, 542 (1904).

(10) H. Davson and J. F. Danielli, "The Permeability of Natural Membranes," The Macmillan Co., New York, N. Y., 1943.

Here, P is the pump substance, and the subscripts denote the inside and outside of the cell.

In discussing transcellular sodium transport in a multicellular system like the frog skin, we need to consider it as a specialization of the single cell case. If the pump substance is produced inside the skin cells in much the same way as in other cells and is eliminated or destroyed, not on the outside of the cell but on the inside of the frog skin, the observed potential drop is to be expected. This is because the potential gradient is determined by the concentration gradient of the sodium–pump substance complex, (NaP^+). The concentration of NaP^+ inside the cell is the normal value for a cell interior while the concentration inside of the skin where P is being eliminated will have the value in ordinary ground substance.[11] Thus, a potential around 100 mv., depending on the sodium concentration, is to be expected.

Absolute rate theory and relaxation theory have been applied with success in determining the dependence of the ionic flux on the potential gradient.[5] For the case of diffusion of charged particles through a membrane of n potential energy barriers, Parlin and Eyring have derived an equation for the flux, Q

$$Q = \lambda_0 K_0^0 \frac{x^{-1/2} - x^{1/2}}{x^{-n/2} - x^{n/2}} \left(x^{-n/2} C_0 - \frac{\lambda_n}{\lambda_0} x^{n/2} Cn \right)$$

where

λ_i's are the lattice distances over the ith barrier
k_0^0 is the specific rate constant over the first barrier in the absence of a potential
$x = e^{\mathbf{Z}\mathfrak{F}\epsilon/nRT}$
n is the number of barriers in the membrane
c's are the concn. of a given ion species at the zeroth and nth barriers
$\mathbf{Z}$ is the charge of the ion with sign
F is the Faraday
ϵ is the potential difference between the zeroth and nth minimum

A term g is defined as

$$g = n \frac{x^{-1/2} - x^{1/2}}{x^{-n/2} - x^{n/2}}$$

With these substitutions the permeability constant is defined

$$p(\epsilon) \equiv \frac{\lambda_0 K_0^0 g}{n}$$

By assuming that $\mathbf{Z}\mathfrak{F}\epsilon \ll RT$ and expanding the exponentials, it is found that $g \approx 1$. Extending the approximation to the remaining exponential terms and again retaining only the first terms, the flux equation reduces to

$$Q = p \left[\left(c_0 - \frac{\lambda_n}{\lambda_0} C_n \right) - \frac{1}{2} \left(c_0 + \frac{\lambda_n}{\lambda_0} C_n \right) \frac{\mathbf{Z}\mathfrak{F}\epsilon}{RT} \right]$$

where the permeability constant is now

$$p = \lambda_0 K_0^0 / n$$

The total transport appears in a more familiar form as the sum of a diffusion term and an electrical transport term.

The divergence of g from unity is significant in some cases, depending on the magnitude of n and ϵ. In the discussion to follow it is assumed that $n \geq 20$, *i.e.*, a reasonably thick membrane, which makes g independent of n.

(11) H. Eyring and T. Dougherty, *Am. Scientist*, **43**, 457 (1955).

1. **Sodium Influx.**—The fact that a net inward flux of sodium chloride takes place can be understood in terms of a mechanism involving complex formation as pointed out previously. A typical flux pattern is quite similar to a Langmuir adsorption isotherm curve. The flux equations developed from first principles are available, and hence an explanation of the flux pattern should be possible.

The equation for the net movement of neutral particles is given by the equation[5]

$$Q = P(a_0 - a_n) = Pa_0 - Pa_n$$

The a's are activities at the zeroth and nth barrier. For charged particles a similar relationship can be written[5]

$$Q = P'(\epsilon)(\gamma_0 c_0 e^{-\mathbf{Z}\mathfrak{F}\epsilon/2RT} - \gamma_n c_n e^{\mathbf{Z}\mathfrak{F}\epsilon/2RT})$$

where γ_i is the activity coefficient at concentration c_i. The permeability constant is dependent on the transmembrane potential, and λ_n/λ_0 has been taken to be unity. Extracting the potential-dependent term, defining a new permeability constant, P', and comparing the terms in the equations for charged and uncharged particle flux, we find

$$Q = P'(\gamma_0 c_0 g e^{-\mathbf{Z}\mathfrak{F}\epsilon/2RT} - \gamma_n c_n g e^{\mathbf{Z}\mathfrak{F}\epsilon/2RT})$$

where

$$a_0 \equiv \gamma_0 c_0 g e^{-\mathbf{Z}\mathfrak{F}\epsilon/2RT}, \; a_n \equiv \gamma_n c_n g e^{\mathbf{Z}\mathfrak{F}\epsilon/2RT}$$

and

$$Q = Q_i - Q_0$$

with

$$Q_i = P'\gamma_0 C_0 g e^{-\mathbf{Z}\mathfrak{F}\epsilon/2RT}, \; Q_0 = P'\gamma_n c_n g e^{\mathbf{Z}\mathfrak{F}\epsilon/2RT}$$

Here Q_i is the influx and Q_0 the outflux. A new kind of activity for flux appears.

Let us postulate that influx is proportional to the activity of the sodium complex inside the cells forming the transcellular membrane.

$$Q_i = k' a_{NaP^+}$$

Here P is the pump substance. The sodium complex has been taken to be singly charged in view of Ussing's work on short-circuited frog skin.[12] If the sodium inside the cells is largely in the form of the complex, then the above expression should account for the influx. According to Ussing the active transport of sodium probably takes place in a layer of tissue, one cell thick.[3] An equilibrium will exist between the complex and its components. Since the magnitudes of sodium flux are small, it is quite valid to assume that the equilibrium is disturbed only slightly.

$$Na^+ + P \rightleftarrows NaP^+$$

With the additional assumption that P is constantly being produced within the cell at a given rate regardless of the composition of the bathing solution on the outside of the skin and is also being lost *via* simple diffusion to give a steady-state concentration or activity (P), then the introduction of sodium ions will initiate complexing for which the following formation constant may be written

$$K = \frac{a_{NaP^+}}{a_{Na^+}[(P) - a_{NaP^+}]}$$

(12) H. H. Ussing, *Z. Elektrochem.*, **55**, 470 (1951).

The equation for influx may now be written

$$Q_i = k' a_{Na^+} = k' K a_{Na^+}[(p) = a_{Na^+}]$$

and finally

$$Q_i = \frac{k'K(P)a_{Na^+}}{1 + Ka_{Na^+}}$$

Using the activities defined earlier and assuming the activity coefficients to be unity, the influx can be more explicitly written as

$$Q_i = \frac{k'K(P)g(Na^+)_0 e^{-\mathcal{Z}\mathfrak{F}\epsilon/2RT}}{1 + Kg(Na^+)_0 e^{-\mathcal{Z}\mathfrak{F}\epsilon/2RT}}$$

showing its dependence on the outside sodium concentration $(Na^+)_0$. Neglecting g did not produce large magnitudes of difference in the experimental influx constants. Using the following substitution

$$\xi^- = e^{-\mathcal{Z}\mathfrak{F}\epsilon/2RT}$$

and assuming

$$g \approx 1$$

we have

$$Q_i = \frac{k_1 k_2 (Na^+)_0 \xi^-}{1 + k_2 (Na^+)_0 \xi^-}$$

where $k_1 = k'(P)$ and $k_2 = K$. This form was used in the analysis of the data.

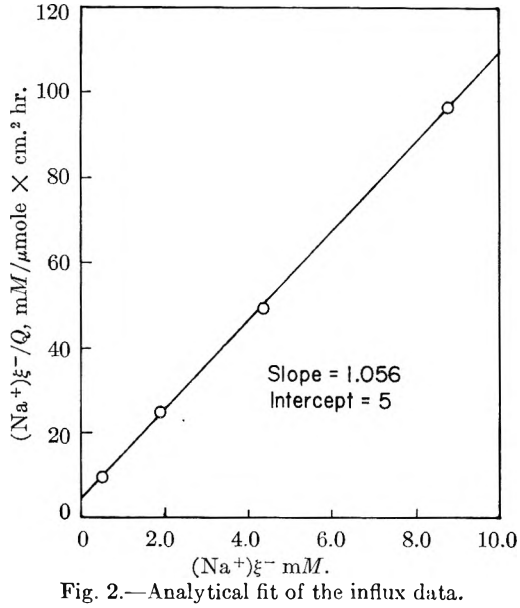

Fig. 2.—Analytical fit of the influx data.

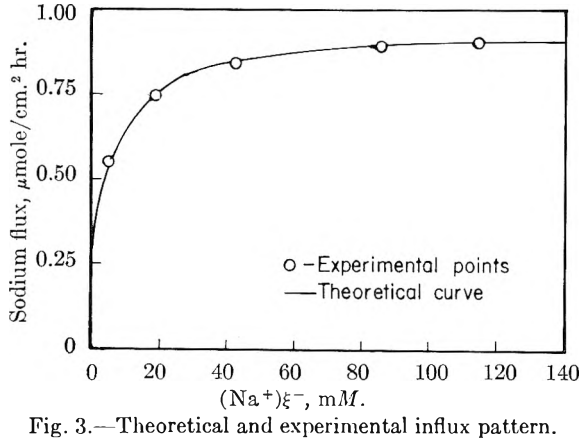

Fig. 3.—Theoretical and experimental influx pattern.

The fitting of the experimental data was accomplished by the point slope form.

$$\frac{Q_i}{(Na^+)_0\xi^-} = \frac{k_1 k_2}{1 + k_2(Na^+)_0\xi^-}$$

$$\frac{(Na^+)_0\xi^-}{Q_i} = \frac{1}{k_1 k_2} + \frac{1}{k_1}(Na^+)_0\xi^-$$

Figure 2 shows a typical plot of the experimental data. The parameters, k_1 and k_2, so evaluated were used to reproduce the data in Fig. 3. In Table II the influx parameters for several frog skins are summarized. The values obtained for the formation constant k_2 indicate that the sodium is largely in complex form.

TABLE II

VALUES OF THE INFLUX PARAMETERS DETERMINED BY EXPERIMENTS

1	0.780	0.146
2	0.947	.211
3	0.806	.413
4	1.32	.076
5	1.09	.092
6	0.804	.124

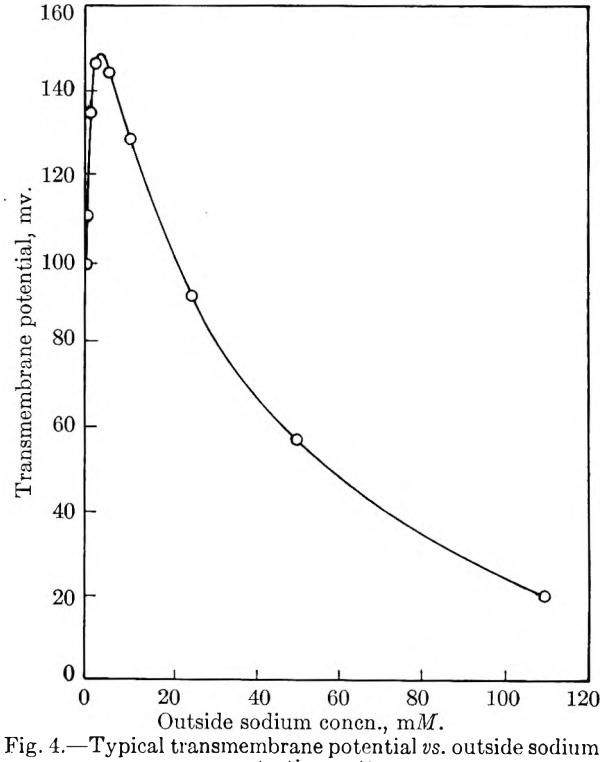

Fig. 4.—Typical transmembrane potential *vs.* outside sodium concentration pattern.

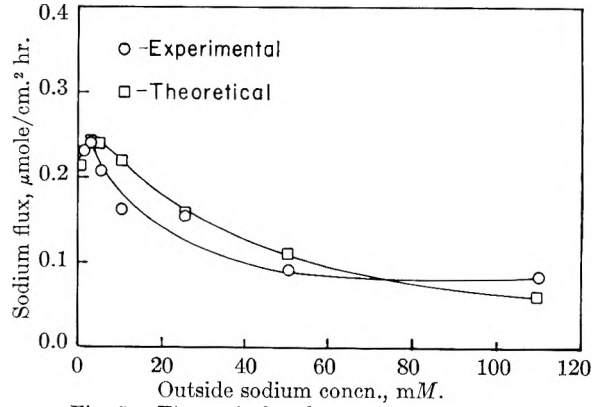

Fig. 5.—Theoretical and experimental outflux.

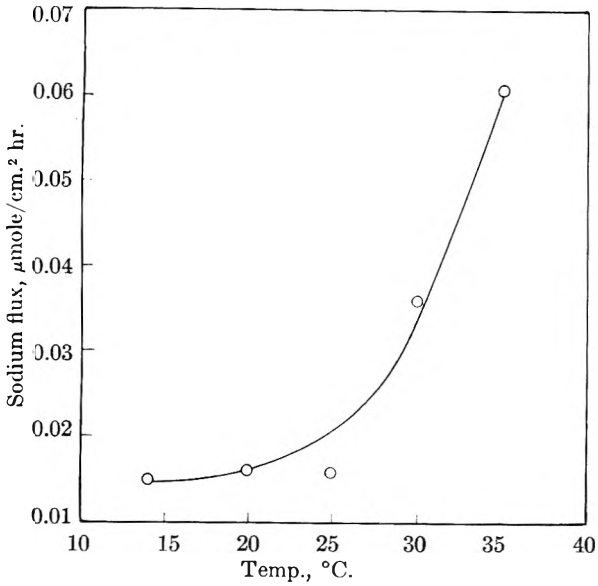

Fig. 6.—Outflux *vs.* temperature.

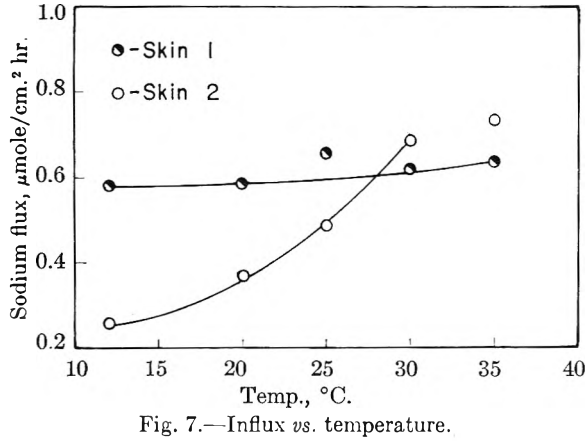

Fig. 7.—Influx *vs.* temperature.

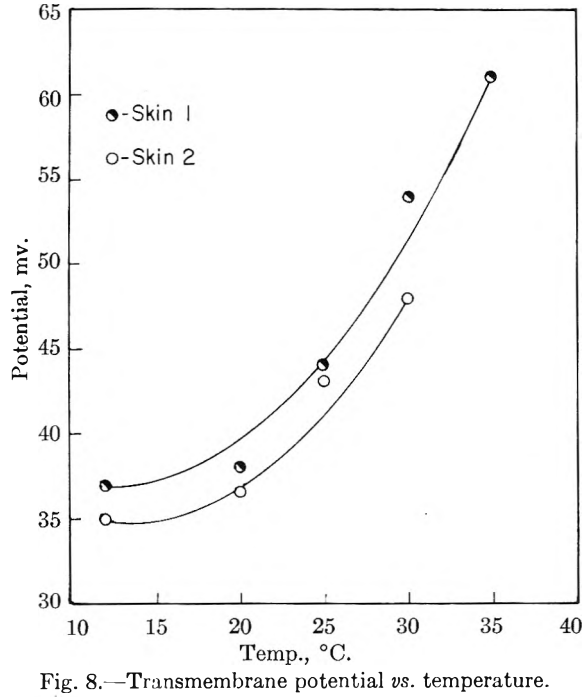

Fig. 8.—Transmembrane potential *vs.* temperature.

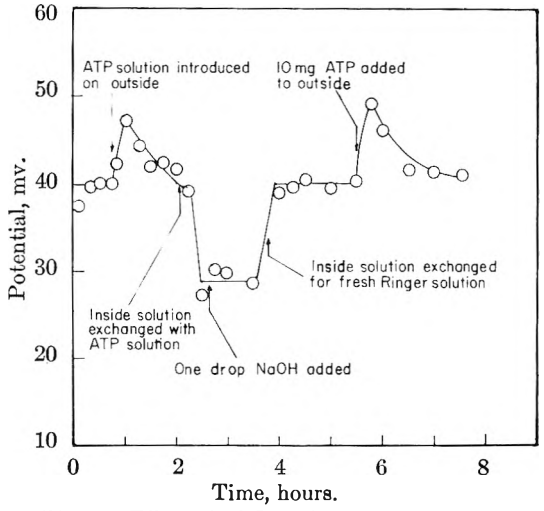

Fig. 9.—Effect of ATP on frog skin potentials.

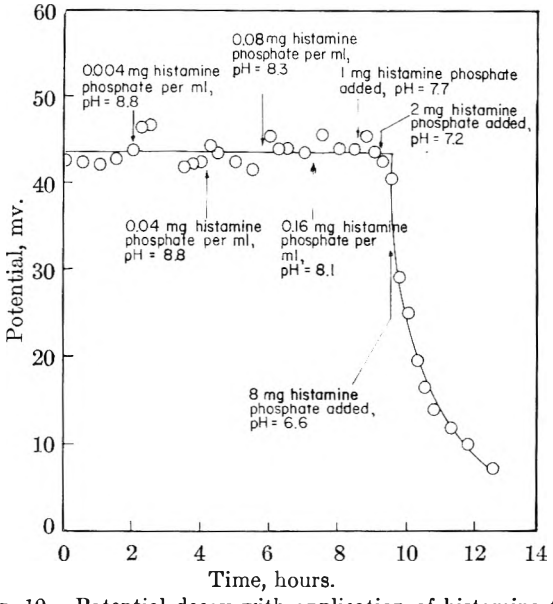

Fig. 10.—Potential decay with application of histamine to the morphological inside of frog skin.

Although the experimental results show considerable variations in the value of the constants, one might speculate as to how the variations among the different skins occur. In view of our theory k_2 ought to be rather constant. The variations from skin to skin are then to be explained as variations in k_1. The factors which enter k_1 include the transmembrane potential, the metabolic rate and the number of energy barriers. The first two are somewhat dependent upon each other according to our theory. Experiments also appear to verify such a relationship. In as much as respiration studies are expressed in terms of dry weight a possible normalizing factor might be the weights of the skins. The other fundamental variable involved, n, the number of barriers, is unfortunately not accessible experimentally.

In view of the basic influx equation

$$Q_i = P' c_0 g e^{-\mathbb{Z}\mathfrak{F}\epsilon/2RT}$$

one is not surprised that the inward movement of sodium ions is found to be retarded or that the

inward movement of anions such as chloride is found to be enhanced by increases in transmembrane potential. The direct response associated with O_2-consumption and transmembrane potential is explained. In terms of the complexing concept, the specificity of active sodium transport is readily justified.

2. Outflux.—The sodium outflux should obey an equation of the form

$$Q_0 = P' c_i^{Na^+} g e^{\mathcal{F}\epsilon/2RT} + P'' c_i^{NaP^+} g e^{\mathcal{F}\epsilon/2RT}$$

Here, two terms are necessary, for the outflux is the result of the diffusion of at least two species of sodium. In these experiments $c_i^{Na^+}$ was held constant while $c_0^{Na^+}$ was varied. The transmembrane potential ϵ depended on $c_0^{Na^+}$. In this case, g deviated from unity markedly at very low outside sodium concentrations when the potentials were high. The second term can be neglected since the concentration of sodium complex inside of the skin is probably very low. Aside from an undeterminable constant, the equation given below should be obeyed

$$Q_0 = P' c_i^{Na^+} e^{\mathcal{F}\epsilon/2RT}\, n \frac{x^{-1/2} - x^{1/2}}{x^{-n/2} - x^{n/2}}$$

where

$$x = e^{\mathcal{F}\epsilon/nRT}$$

A typical potential pattern obtained is shown in Fig. 4. Using these potential values, the flux pattern predicted by the outflux equation is shown in Fig. 5. P' is an experimental parameter chosen to give the best fit. The experimental flux values determined by tracer sodium show good agreement with the calculated flux values. The observation that the outflux of anions exceeds their influx when at the same concentration on both sides of the membrane also appears reasonable.

3. Temperature Effects.—The temperature coefficients of flux and e.m.f. are summarized in Figs. 7, 8 and 9. None of the patterns could be fitted by an Arrhenius plot. In view of the complex temperature dependence of the fluxes, this result was not too surprising.

4. Effects of ATP and Histamine.—Let us speculate a little further as to the details of the active transport process. The formation of the complex is postulated as taking place at one boundary and disappearing at the other. If the correct complexing agent is added at the outside boundary an enhanced influx should result. Alternatively, if the complexing agent is placed on the inside the inward flux should be retarded. The transmembrane potential should be affected in a similar manner. Figures 9 and 10 show the effects of both ATP and histamine, respectively.

The effect of ATP appears to follow just such a requirement. Application of histamine is without effect on the outside but induces a lowering of the transmembrane potential when applied at similar dosages on the inside. However, in the case of histamine the e.m.f. simply decays and never quite levels off. Without a more detailed knowledge of the metabolic processes taking place, their localization, etc., our conclusions on the specific effects of chemical substances must remain somewhat general.

Acknowledgment.—The helpful discussions with Professors Horace Davenport, Department of Physiology; John Spikes, Department of Experimental Biology; and Ransom B. Parlin, Department of Chemistry are gratefully acknowledged. The research was supported in part by the University of Utah Research Committee.

HEAT CAPACITIES AT LOW TEMPERATURES AND ENTROPIES OF FIVE SPINEL MINERALS

BY E. G. KING

Contribution from the Minerals Thermodynamics Experiment Station, Region II, Bureau of Mines, United States Department of the Interior, Berkeley, Cal.

Received September 6, 1955

The heat capacities of five spinel minerals were measured throughout the temperature range 51 to 298°K. All gave a regular type of heat capacity curve. Entropies at 298.16°K. were evaluated, as follows: 25.4 ± 0.2 for $FeAl_2O_4$, 30.0 ± 0.2 for $FeCo_2O_4$, and 32.2 ± 0.2 for $ZnFe_2O_4$ (cal./deg. mole). For $CoFe_2O_4$ and $NiFe_2O_4$, the entropy increments for the temperature range 0 to 298.16°K. are 32.2 ± 0.2 and 30.1 ± 0.2 cal./deg. mole, respectively. The last two substances have zero-point entropies of unknown amounts, attributable to randomness in their structures.

Minerals having the spinel structure are quite common and many of them have technological importance. For example, magnetite and ferrous chromite are important ores, chromite and magnesium aluminate are used as refractories, and several spinels serve as coloring agents for ceramic products. The literature contains low temperature heat capacity and entropy data for eight spinel minerals—magnetite,[1] ferrous and magnesium chromites,[2] titanium–magnesium spinel,[3] titanomagnetite,[4] magnesium ferrite,[5] magnesium aluminate[6] and titanium–zinc spinel.[7] The present paper adds five spinels to this list—cobalt–iron ($CoFe_2O_4$), iron–aluminum ($FeAl_2O_4$), iron–cobalt ($FeCo_2O_4$), nickel–iron ($NiFe_2O_4$) and zinc–iron ($ZnFe_2O_4$).

(1) R. W. Miller, *J. Am. Chem. Soc.*, **51**, 215 (1929). See also G. S. Parks and K. K. Kelley, THIS JOURNAL, **30**, 47 (1926).

(2) C. H. Shomate, *Ind. Eng. Chem.*, **36**, 910 (1944).
(3) S. S. Todd, *J. Am. Chem. Soc.*, **74**, 4669 (1952).
(4) S. S. Todd and E. G. King, *ibid.*, **75**, 4547 (1953).
(5) E. G. King, *ibid.*, **76**, 5849 (1954).
(6) E. G. King, THIS JOURNAL, **59**, 218 (1955).
(7) E. G. King, *J. Am. Chem. Soc.*, **77**, 2150 (1955).

Low temperature heat capacity data are presented for these five substances in the temperature range 51 to 298°K., and entropy increments between 0 and 298.16°K. are evaluated.

Materials.—Cobalt–iron spinel[8] ($CoFe_2O_4$) was prepared from cobaltous oxide (obtained from decomposition of reagent grade cobaltous nitrate hexahydrate) and reagent grade ferric oxide. The ingredients were mixed in stoichiometric proportion and heated five times, for a total of nine days, in the temperature range 950–1350°. During intervals between heats, the material was ground, mixed, analyzed and adjusted in composition as necessary. The final product contained 68.08% ferric oxide, as compared with the theoretical 68.06%. The total iron plus cobalt was determined by hydrogen reduction as 72.76%. After subtracting the iron, 25.14% cobalt was indicated, corresponding to 31.96% cobaltous oxide (theoretical, 31.94%). Silica, in amount of 0.07%, was present as an impurity. The X-ray diffraction pattern agreed with the A. S. T. M. catalog and showed no evidence of any uncombined oxides.

Iron–aluminum spinel[9] was prepared from reagent grade powdered iron, ferric oxide and hydrated alumina. A stoichiometric mixture was pelletized and heated in an evacuated tube, surrounded by another tube through which a slow flow of pure helium was maintained. Seven heats were made (including a total of 40 hours at 1250–1350°) with intervening grindings, mixings, analyses and adjustments of composition. The product contained 41.24% ferrous oxide, 58.62% aluminum oxide and 0.12% silica, as compared with the theoretical 41.34% ferrous oxide and 58.66% aluminum oxide. The X-ray diffraction pattern agreed with the A. S. T. M. catalog and gave no evidence of any uncombined oxides or metallic iron. No magnetic particles were found on testing with a hand magnet.

Iron–cobalt spinel[9] ($FeCO_2O_4$) was prepared from cobaltous oxide (from decomposition of reagent grade cobaltous nitrate hexahydrate) and reagent grade ferric oxide. A stoichiometric mixture was heated in air four times, totaling 130 hours at 1050–1100°, to permit occurrence of the reaction

$$1/2Fe_2O_3 + 2CoO + 1/4O_2 = FeCo_2O_4$$

The usual grinding, mixing, analysis and adjustment of composition were conducted between heats. The final product analyzed 23.47% iron and 26.88% oxygen (determined by complete hydrogen reduction), as compared with the theoretical 23.49 and 26.92%. A small amount of silica, 0.05%, was present. X-Ray diffraction gave a typical spinel pattern as regards spacing, and no evidence of uncombined oxides was found.

Nickel–iron spinel[8] ($NiFe_2O_4$) was prepared by heating a pelletized, stoichiometric mixture of reagent grade nickel oxide and ferric oxide for prolonged periods in the temperature range 990–1270°. Grinding, mixing, analysis and adjustment of composition were conducted at intervals during the preparation process. The product contained 31.86% nickelous oxide and 68.11% ferric oxide, as compared with the theoretical 31.87 and 68.13%. The oxygen content, determined by complete hydrogen reduction, was 27.22%, as compared with the theoretical 27.33%. Silica, in amount of 0.03%, was present. The X-ray diffraction pattern agreed with the A. S. T. M. catalog and no impurity lines were detected.

Zinc–iron spinel[8] ($ZnFe_2O_4$) was prepared by heating a pelletized, stoichiometric mixture of reagent grade zinc oxide and ferric oxide for several periods (totaling 18 days) at temperatures in the range 940–1280°, with the usual grinding, mixing, analysis and adjustment of composition between heats. The product analyzed 33.89% zinc oxide and 66.36% ferric oxide, as compared with the theoretical 33.76 and 66.24%. The isopropyl ether separation of iron from zinc was employed in the analysis. Iron was titrated against standard ceric sulfate solution and zinc against standard potassium ferrocyanide solution. The X-ray diffraction pattern agreed with the A. S. T. M. catalog and no impurity lines were detected.

(8) This substances was prepared by C. J. O'Brien, Chemist, Minerals Thermodynamics Experiment Station, Region II, Bureau of Mines.

(9) This substance was prepared by K. C. Conway, Chemist, Minerals Thermodynamics Experiment Station, Region II, Bureau of Mines.

TABLE I

HEAT CAPACITIES (CAL./DEG. MOLE)

T, °K.	C_p	T, °K.	C_p	T, °K.	C_p
		$CoFe_2O_4$ (mol. wt., 234.64)			
53.29	3.647	114.70	14.52	216.02	29.25
57.66	4.356	124.59	16.25	225.80	30.31
61.98	5.066	135.90	18.16	236.05	31.35
66.32	5.823	145.49	19.76	245.70	32.29
70.66	6.594	155.70	21.39	256.42	33.27
75.17	7.399	165.81	22.86	266.60	34.11
80.58	8.374	175.87	24.26	276.00	34.80
85.01	9.158	185.78	25.57	286.35	35.66
95.04	10.96	195.98	26.90	296.02	36.37
105.02	12.77	206.03	28.13	298.16	(36.53)
		$FeAl_2O_4$ (mol. wt., 173.81)			
53.04	3.420	114.50	10.43	216.14	22.89
57.12	3.741	124.51	11.78	225.66	23.84
61.94	4.184	135.70	13.28	236.04	24.80
66.72	4.674	145.20	14.57	245.55	25.63
71.29	5.168	155.71	15.98	256.48	26.55
76.14	5.700	165.89	17.24	266.61	27.33
80.68	6.222	182.92	19.38	276.02	27.96
85.24	6.739	187.43	19.81	286.31	28.74
94.77	7.876	195.89	20.77	296.03	29.29
105.02	9.185	206.08	21.89	298.16	(29.53)
		$FeCo_2O_4$ (mol. wt., 237.73)			
53.84	3.536	114.73	13.21	216.00	27.42
58.22	4.119	125.12	14.92	226.03	28.41
62.68	4.775	136.12	16.69	236.06	29.41
67.21	5.475	145.43	18.18	245.82	30.30
71.81	6.213	155.56	19.74	256.26	31.18
76.38	6.938	165.69	21.18	266.52	32.00
81.33	7.742	175.84	22.57	275.89	32.67
85.84	8.449	185.63	23.83	286.46	33.45
94.55	9.870	195.84	25.11	295.89	34.15
105.04	11.61	206.15	26.34	298.16	(34.27)
		$NiFe_2O_4$ (mol. wt., 234.39)			
53.58	3.289	114.74	13.40	215.96	27.63
57.89	3.887	124.57	15.05	225.85	28.64
62.32	4.552	135.63	16.85	236.38	29.72
66.85	5.289	145.44	18.43	245.78	30.60
71.25	6.019	155.78	20.01	256.20	31.52
75.53	6.733	165.70	21.42	266.39	32.38
80.85	7.632	175.81	22.81	276.26	33.14
85.44	8.385	185.61	24.06	286.48	33.97
94.75	9.976	195.67	25.32	295.93	34.66
104.95	11.74	206.03	26.54	298.16	(34.81)
		$ZnFe_2O_4$ (mol. wt., 241.08)			
53.26	4.661	114.74	14.41	216.14	27.22
57.63	5.270	124.74	15.98	225.56	28.02
61.92	5.910	136.03	17.67	236.04	28.91
66.19	6.594	145.55	19.09	245.76	29.63
70.51	7.312	155.99	20.55	256.44	30.45
74.85	8.002	166.01	21.82	266.82	31.10
80.73	8.946	175.93	23.03	276.21	31.65
85.36	9.675	185.96	24.16	286.51	32.30
94.92	11.18	195.93	25.23	295.96	32.90
104.74	12.81	206.18	26.29	298.16	(32.99)

Heat Capacity Measurements and Results.—The heat capacity calorimeter and method of operation have been described.[10] Results are reported

(10) K. K. Kelley, B. F. Naylor and C. H. Shomate, U. S. Bur. Mines Tech. Paper 686, 1946.

in defined calories (1 cal. = 4.1840 abs. joules) per deg. mole. All weighings were corrected to vacuum and molecular weights accord with the 1953 International Atomic Weights.[11] The following masses of the compounds were employed in the measurements: $CoFe_2O_4$, 293.66 g.; $FeAl_2O_4$, 217.41 g.; $FeCo_2O_4$, 325.60 g.; $NiFe_2O_4$, 295.50 g.; and $ZnFe_2O_4$, 292.52 g.

The measured heat capacity values are listed in Table I. No anomalous thermal behavior was observed for any of the substances and the results plot as a group of regular curves—Fig. 1. This was not expected beforehand as some analogous substances (magnetite,[1] ferrous chromite,[2] and titanomagnetite[4]) have heat capacity maxima in the investigated temperature range.

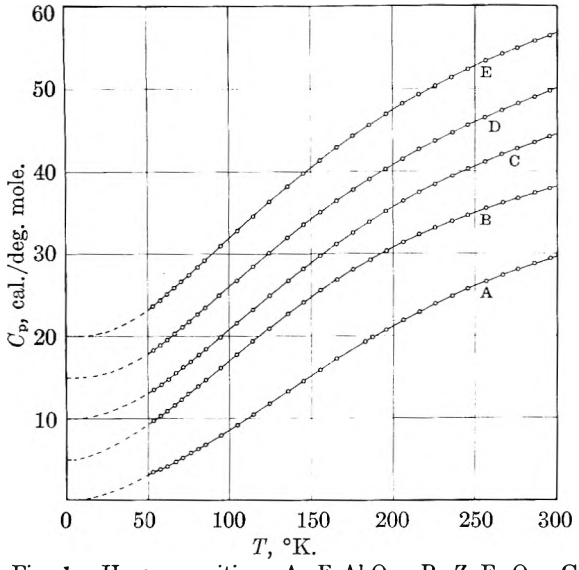

Fig. 1.—Heat capacities: A, $FeAl_2O_4$; B, $ZnFe_2O_4$; C, $FeCo_2O_4$; D, $NiFe_2O_4$; E, $CoFe_2O_4$. (Note: All curves, except A, are displaced by multiples of 5 cal./deg. mole along vertical axis.)

The heat capacity of iron–aluminum spinel runs lower than the other substances at all temperatures between 51 and 298°K., which is to be expected in view of its lower average atomic mass. The results for the cobalt–iron, iron–cobalt and nickel–iron compounds are quite similar, although cobalt–iron spinel has a notably higher heat capacity at 298°K. Zinc–iron spinel has the highest heat capacity at the lowest temperatures and the second lowest heat capacity at 298°K. Thus, the average slope for this substance is lower and a minor difference in trend of its heat capacity curve is evident in Fig. 1.

Entropies.—The measured portions of the entropies, between 51 and 298.16°K., were obtained by Simpson-rule integrations of plots of C_p against log T. The extrapolated portions, between 0 and 51°K., were obtained from Debye and Einstein function sums, which were derived empirically to fit the measured heat capacity data. These sums, together with the represented temperature range and maximum deviation from the measured heat capacity data, are

$CoFe_2O_4$: $D(231/T) + 3E(364/T) + 3E(696/T)$ (51–150° K.; 1.1%)

$FeAl_2O_4$: $D(198/T) + 3E(482/T) + 3E(874/T)$ (51–298° K.; 0.9%)

$FeCo_2O_4$: $D(223/T) + 3E(391/T) + 3E(782/T)$ (51–125° K.; 0.7%)

$NiFe_2O_4$: $D(234/T) + 3E(392/T) + 3E(730/T)$ (51–150° K.; 1.3%)

$ZnFe_2O_4$: $D(166/T) + 3E(371/T) + 3E(741/T)$ (51–298° K.; 1.4%)

The results of the entropy calculations are in Table II.

TABLE II

ENTROPIES (CAL./DEG. MOLE)

Substance	$S_{51} - S_0$ (extrap.)	$S_{298.16} - S_{51}$ (meas.)	$S_{298.16} - S_0$
$CoFe_2O_4$	1.32	30.88	32.2 ± 0.2
$FeAl_2O_4$	1.66	23.75	25.4 ± .2
$FeCo_2O_4$	1.36	28.64	30.0 ± .2
$NiFe_2O_4$	1.24	28.86	30.1 ± .2
$ZnFe_2O_4$	2.34	29.84	32.2 ± .2

Two-component spinel minerals occur mainly in two classes, normal and variate, although some representatives of a mixed class are known.[12–17] The normal class has a regular arrangement of metal ions among the available lattice sites, thus precluding zero-point entropy. Members of the variate class may have zero point entropies up to a maximum of 2 R ln 2 cal./deg. mole.

Of the substances in Table II, $FeAl_2O_4$ and $ZnFe_2O_4$ are known to be regular, $NiFe_2O_4$ is variate, $CoFe_2O_4$ probably is variate, and $FeCo_2O_4$ probably is normal. Consequently, S_0 is zero for $FeAl_2O_4$ and $ZnFe_2O_4$, and the values in the last column of Table II may be taken as their standard entropies. The same probably is true for $FeCo_2O_4$. The other two substances should have standard entropies higher than the values in the last column of Table II by at present unknown amounts, because of randomness in their structures.

(11) E. Wichers, *J. Am. Chem. Soc.*, **76**, 2033 (1954).

(12) T. F. W. Barth and E. Posnjak, *Z. Krist.*, **82**, 325 (1932).

(13) H. M. Richardson, *Iron Steel Inst. Spec. Rept.*, **32**, 170 (1946).

(14) E. J. W. Verwey and E. L. Heilmann, *J. Chem. Phys.*, **15**, 174 (1947).

(15) E. J. W. Verwey, P. W. Haayman and F. C. Romeijn, *ibid.*, **15**, 181 (1947).

(16) F. C. Romeijn, *Philips Research Repts.*, **8**, 304 (1953).

(17) S. Greenwald, S. J. Pickart and F. H. Grannis, *J. Chem. Phys.*, **22**, 1597 (1954).

PHYSICAL PROPERTIES OF AQUEOUS URANYL SULFATE SOLUTIONS FROM 20 TO 90°

BY EDWARD ORBAN, MARTIN K. BARNETT, JANE S. BOYLE, JOHN R. HEIKS AND LERROY V. JONES

Mound Laboratory, Monsanto Chemical Company, Miamisburg, Ohio[1]

Received September 8, 1955

Measurements of the density, surface tension, viscosity and *p*H of aqueous solutions of uranyl sulfate up to as high as 4 molal in concentration and in a temperature range between 20 and 90° are reported.

Introduction

In recent years, interest in the common physical properties of uranium salts has risen sharply, revealing the lack of adequate data. The measurement of the density, viscosity, surface tension and *p*H of a series of aqueous solutions of uranyl sulfate between the temperatures of 20 and 90° is described in the present paper.

Some early work on the densities of solutions between 0.03 and 0.3 molar at temperatures between 10 and 16° was reported by de Coninck.[2] His results do not agree well with the more precise work done by Helmholtz and Friedlander[3] on three concentrations between 0 and 90° and on eight other concentrations at 30°.

The surface tension of aqueous salt solutions has generally been found to increase with increasing concentration. Of approximately 50 salt solutions covered in the International Critical Tables[4] only two salts, ammonium chloride and magnesium acetate, violate this rule. However, Young and Coons[5] found pronounced maxima and minima in the surface tension *versus* concentration curves. Grant,[6] *et al.*, reported that uranyl acetate lowers the surface tension of water although a positive coefficient was found for uranyl nitrate. Values for uranyl sulfate have not been reported. Jones and Ray[7] have noted minima for very low concentrations of KCl, K_2SO_4 and $Ce(NO_3)_3$, but Langmuir[8] has attributed this to an effective decrease in the radius of the capillary tube by an adhering film of solvent.

Two groups of investigators[2,9] made measurements on the *p*H of uranyl sulfate solutions at room temperature, but studies were not made with an excess of uranium trioxide.

There have been no measurements of the viscosity of uranyl sulfate solutions reported in the literature.

Equipment and Material

The uranyl sulfate was prepared from uranium trioxide purchased from the Mallinckrodt Chemical Works. The oxide was first screened through a U. S. Standard Sieve #40 and then a #60. It was washed with distilled water by stirring vigorously at 80 to 90° for six hours and then allowing to stand overnight at room temperature. Following decantation and filtration, the washing process was repeated until no nitrate could be detected in the wash water. The dried oxide was stirred with a stoichiometric amount of 2.6 *M* sulfuric acid. The mixture was heated with stirring to 80° until all of the oxide was dissolved. The solution was filtered and analyzed for uranium and sulfate giving results which permitted the adjustment of the solution by the addition of either oxide or sulfate to a molar ratio of 1.000 ± 0.002. Some of this stock solution was diluted to prepare samples while another portion was recrystallized six times to give pure $UO_2SO_4 \cdot 3H_2O$ crystals. No difference between the solutions prepared from this recrystallized material and the original stock solution could be detected in any of the measurements.

The densities of the solutions were obtained by the hydrostatic weight method. A hollow bob, the weight of which had been adjusted by sealing a number of small steel balls inside, was suspended from the beam of an Ainsworth type DLB Chain-o-matic balance with a length of 36-gage platinum wire. Constant temperature was maintained around the test solution vessel by immersing it in an oil-bath which could be set within ±0.05° of the test temperature.

The viscosities were measured with Ostwald capillary viscometers of 5-ml. volume. A constant temperature water-bath maintained the desired temperature to within ±0.05°.

The surface tension measurements were made with the Pyrex capillarimeter similar in design to that employed by Young, Gross and Harkins.[10] The large tube was about five centimeters in diameter. The capillary tubing was "Precision Grade" and had a nominal bore of 0.5 mm. The capillarimeter was immersed in water in a windowed thermostat that could also be controlled to ±0.05°. The heights of the menisci were observed with a Gaertner Micrometer-slide cathetometer.

A Leeds and Northrup Universal *p*H potentiometer assembly No. 7663-A-1 was used to make *p*H measurements. Out of seven "L and N" glass electrodes available, two were selected which, when set with a buffer of *p*H equal to 4.01, agreed with the value of other buffers at *p*H's of 1.08, 2.08 and 6.86 at 25°. The electrodes, buffers and test solutions were maintained at equilibrium temperatures in a water-bath controlled to ±0.05°.

Procedure and Results

Density.—The volume of the bob used in the density measurements was determined at each temperature by making weighings in doubly-distilled water. From the weight of the bob in air and the literature values[11] of the densities of water at each temperature, the volume of the bob was calculated.

The densities of 12 solutions were measured at 20, 30, 44.8, 59.8, 75 and 90°.

The samples were stirred thoroughly before each determination. Since evaporation occurred at the higher temperatures, a small sample was taken for analysis, immediately after each measurement. Table I presents the density data obtained.

Solutions were originally prepared at 20° on a molar basis, and later converted to a molal basis by means of the meas-

(1) Mound Laboratory is operated by the Monsanto Chemical Company for the United States Atomic Energy Commission under Contract No. AT-33-1-GEN-53.

(2) F. W. O. de Coninck, *Ann. chim. phys.*, [7] **28**, 5 (1903).

(3) L. Helmholtz and G. Friedlander, Atomic Energy Commission Report MDDC-808, December 15, 1943.

(4) "International Critical Tables," Vol. IV, McGraw-Hill Book Co., New York, N. Y., 1923, p. 463.

(5) C. B. F. Young and K. N. Coons, "Surface Active Agents," Chemical Publishing Company, New York, N. Y., 1945.

(6) W. E. Grant, W. J. Darch, S. T. Bowden and W. J. Jones, THIS JOURNAL, **52**, 1227 (1948).

(7) G. Jones and W. A. Ray, *J. Am. Chem. Soc.*, **57**, 957 (1935); **59**, 187 (1937).

(8) I. Langmuir, *Science*, **88**, 430 (1938).

(9) D. A. MacInnes and L. G. Longsworth, U. S. Atomic Energy Commission Report, MDDC-911, November 24, 1942.

(10) A. Weissberger, "Physical Methods of Organic Chemistry," Vol. I, part 1, Interscience Publishers, Inc., New York, N. Y., 1949, p. 367.

(11) C. D. Hodgman, "Handbook of Chemistry and Physics," 30th Ed., Chemical Rubber Publishing Co., Cleveland, Ohio, 1947, p. 1695.

TABLE I

DENSITY OF URANYL SULFATE SOLUTIONS (G./CM.^{3})

Molality	Temperature, °C. 20.0	30.0	44.8	59.8	75.0	90.0
0.176	1.0539	1.0510	1.0445			
.177				1.0343		
.178					1.0293	
.180						1.0193
.452	1.1384	1.1349	1.1282			
.450				1.1208		
.454					1.1113	
.458						1.1008
671	1.2050	1.2012	1.1939	1.1862		
.669					1.1761	
.681						1.1654
.864	1.2630	1.2588	1.2513			
.870				1.2432		
.868					1.2334	
.877						1.2219
1.049	1.3141	1.3098	1.3023	1.2948		
1.053					1.2845	
1.055						1.2720
1.321	1.3911	1.3865	1.3779			
1.323				1.3692		1.3458
1.329					1.3579	
1.753	1.5089	1.5032	1.4956			
1.756				1.4867		
1.761					1.4735	
1.770						1.4620
1.983	1.5672	1.5613	1.5516			
1.986				1.5430		
2.002					1.5328	
2.009						1.5236
2.865	1.7797					
2.862		1.7736				
2.858			1.7633			
2.870				1.7533		
3.872	2.0059	1.9983	1.9856			
3.880				1.9752		
3.959					1.9708	
3.999						1.9646

ured densities. The statistical relation of the original molar concentration (M) to the density (d) in grams per cubic centimeter at 20° was found to be

$$M = 3.1840d - 3.1887$$

Upon extrapolating to $M = 0$, the density does not approach the density of water; to do so the line must assume a more gentle slope at lower concentrations. This is in agreement with the work of Lee,[12] *et al.*, who reported a smaller slope at low than at high concentrations.

Viscosity.—The relative viscosities of the uranyl sulfate solutions were measured with an Ostwald viscometer according to standard procedures.[13] The calculations were made using the literature values for the densities of water,[11] and the densities of the solutions as reported in this publication. The absolute viscosities listed in Table II were calculated from the absolute viscosities of water.[14]

Surface Tension.—For the measurement of surface tension, the solution was introduced into the capillarimeter and the latter was sealed off. The space above the solution contained air at room temperature. The entire apparatus was immersed in a thermostat. Before each measurement the capillarimeter was tipped until the solution flowed up the capillary tube into the overflow trap, thus giving a fresh surface. After leveling precisely and allowing the capillary to come to equilibrium, the difference in the elevation of the large and small menisci were observed with the cathetometer. The bore of the capillary tube was determined by noting the capillary rise exhibited by pure benzene at 20°. From known coefficients of expansion it was determined that the change in size of the capillary because of the temperature change was beyond the limit of accuracy of the experiment. Enlarged photographs of the menisci showed that the contact angle was essentially zero. Also the precision of the measurements did not justify taking account of the density of the gas phase. Therefore, the equation used for the calculations reduces to the familiar form $\gamma = {}^1/_2((h + r/3)dgr)$, where γ is the surface tension, h is the capillary rise, r is the radius of the capillary, g is the acceleration due to gravity and d is the density of the liquid.

(12) J. E. Lee, Jr., R. Rowan, Jr., C. D. Susana and O. Menis, United States Atomic Energy Commission Document ORNL 1332, July 29, 1952.

(13) Joseph Reilly and William Rae, "Physico-Chemical Methods," Vol. 1, D. Van Nostrand Co., Inc., New York, N. Y., 1943, p. 548.

(14) E. C. Bingham and R. F. Jackson, *Bull. Bur. Standards*, **14**, 75 (1918).

TABLE II

ABSOLUTE VISCOSITY OF URANYL SULFATE SOLUTIONS (CENTIPOISE)

Molality	Temperature, °C. 20.0	30.0	45.0	60.0	75.0	90.0
0.176	1.12	0.881	0.659	0.516	0.422	0.349
.452	1.37	1.06	0.779	.610	.494	.403
.671	1.58	1.23	0.893	.685	.547	.460
.864	1.80	1.42	1.01	.779	.608	.501
1.049	2.04	1.58	1.14	.872	.673	.561
1.321	2.50	1.93	1.37	1.04	.836	.656
1.531	2.91	2.22	1.57	1.18	.931	.735
1.753	3.51	2.64	1.89	1.40	1.11	.865
1.978	4.18	3.15	2.21	1.67	1.26	1.01
2.865	8.53	6.21	4.22	3.07	2.30	1.82

Table III summarizes the surface tensions of the uranyl sulfate solutions.

TABLE III

SURFACE TENSION OF AQUEOUS URANYL SULFATE SOLUTIONS (DYNES/CM.)

Molality	Temperature, °C. 20.0	30.0	45.0	60.0	75.0
0.175	73.47	71.95	69.59	67.04	64.55
0.446	74.00	72.56	69.98	67.43	64.83
0.606	74.43	72.75	69.91	67.29	64.60
0.728	74.18	72.58	70.23	67.75	65.06
0.856	74.74	73.10	70.20	67.67	65.13
0.881	74.12	73.22	70.68	68.50	65.87
0.965	75.14	73.38	70.90	68.30	65.64
1.016	74.60	73.12	70.76	68.32	65.56
1.184	75.83	74.13	71.44	68.96	66.26
1.445	76.08	74.29	71.76	69.18	66.55
1.672	76.09	74.26	72.18	69.61	66.68
1.837	76.70	75.03	72.81	70.33	67.70
2.340	77.43	75.90	73.41	70.96	68.24

The data show that the average rate of increase in surface tension with increasing concentration over the concentration range embraced by the study and for five different temperatures is 2.02 dynes per centimeter for each unit increase in molality. Hence, $d\gamma/dm = 2.02$ dynes per cm. per mole. Also, $d\gamma/dt = -0.168$ dyne per cm. per °C. Neglecting the departure from linearity, the equation which described the influence of concentration and temperature on the surface tension becomes

$$\gamma = 2.02m - 0.168(t - 20) + 72.75$$

where m is molality and t is degrees centigrade.

***p*H Measurements.**—Two glass electrodes, used for each *p*H measurement, were standardized before each determination with a reference buffer solution of *p*H 4. The readings from the electrodes did not differ from each other by more than 0.03 *p*H unit in any of the measurements. The electrodes were cleaned with dilute hydrochloric acid after each series of four measurements except at the higher concentrations of uranyl ion where it was found necessary to clean the electrode after each measurement. At high concentrations a slow drift of *p*H was noticed indicating a reaction of the uranyl ion with the glass.

The *p*H of each uranyl sulfate solution was measured at 24.7, 35.0, 44.8 and 59.8°, in the order named. After each measurement had been completed at a particular temperature, the solution was immediately removed from the bath to avoid any change in concentration due to evaporation. A final measurement at the initial temperature agreed with the original measurement in each case.

The measurements at the four temperatures over a concentration range from 0.0006 to 3.85 m are given in Table IV.

TABLE IV

THE *p*H OF URANYL SULFATE SOLUTIONS

Soln. no.	Molality	Temperature, °C. 24.7	35.0	44.8	59.8
1	0.00066	4.09	4.02	3.97	3.89
2	.0013	3.90	3.81	3.76	3.69
3	.0066	3.47	3.39	3.33	3.27
4	.0132	3.27	3.18	3.12	3.04
5	.0758	2.73	2.65	2.58	2.47
6	.157	2.48	2.38	2.29	2.18
7	.321	2.18	2.06	1.98	1.84
8	.824	1.72	1.61	1.52	1.38
9	1.731	1.25	1.13	1.01	0.89
10	3.117	0.68	0.52	0.41	0.30
11	3.850	0.33	0.18	0.04	−0.12[a]

[a] Obtained by extrapolating deflections to a zero reading.

Similar measurements were made with solutions that had excess UO_3 dissolved in them. The data are shown in Table V. The *p*H values of these solutions are considerably higher than the pure uranyl sulfate solutions as would be expected from the basic nature of the oxide.

TABLE V

THE *p*H OF URANYL SULFATE SOLUTIONS CONTAINING EXCESS UO_3

Uranium, *m*	Sulfate, *m*	Ratio, U:SO_4	Temperature, °C. 24.7	35.0	44.8	59.8
1.700	1.700	1.00	1.24	1.18	0.98	0.93
1.904	1.738	1.10	2.10	1.96	1.72	1.36
0.460	0.420	1.10	2.89	2.76	2.42	2.13
.046	.042	1.10	3.54	3.38	3.17	2.83
.0045	.0041	1.10	3.95	3.83	3.68	3.53
2.069	1.730	1.19	2.54	2.38	2.09	1.78
0.497	0.416	1.19	3.19	3.08	2.71	2.41
.049	.041	1.19	3.78	3.59	3.46	3.08
.0049	.0041	1.19	4.09	3.96	3.88	3.75
2.234	1.738	1.29	2.82	2.68	2.35	1.94
0.536	0.417	1.29	3.35	3.18	2.91	2.59
.051	.039	1.29	3.90	3.72	3.60	3.18
.0051	.0039	1.29	4.21	4.08	3.89	3.74
1.344	0.954	1.41	3.29	3.12	2.89	2.40
0.333	0.236	1.41	3.68	3.54	3.42	2.69
.033	.024	1.41	4.08	3.93	3.82	3.69
.003	.0023	1.41	4.32	4.18	4.12	3.99

Discussion

A plot at any one temperature of either surface tension (γ) or the logarithm of the viscosity (η) against molality is approximately a straight line. These linear relations for the two properties may be combined to give a general equation, $\log \eta = a\gamma + b$, where a and b are constants. Both a and b have been found to be linear functions of temperature so that the equation may be written as

$$\log \eta = (0.15 - 0.00046t)\gamma + (-11.32 + 0.046t)$$

where t is the temperature in degrees centigrade.

The hydrolysis of uranyl sulfate to form hydrogen ions may be expressed by a number of equations, some of which include the formation of complexes with the anion. The effect of the sulfate ion on the equilibrium was studied by adding sodium sulfate to a uranyl sulfate solution. If the sulfate ion took part in the reaction, the equilibrium would have shifted, changing the *p*H of the solution. However, the increase in *p*H was almost exactly that calculated from the sulfuric acid equilibrium expression assuming only the addition of the sulfate ion with no other reaction occurring. Thus, the sulfate ion apparently did not enter into the equilibrium involving the hydrolysis of the uranyl ion.

A number of equations may be written to explain the hydrolysis of the uranyl ion to produce hydrogen ions. Nine of these, in which the uranyl ion to water ratio was varied from 1 to 1 up to 6 to 1, were studied. The equilibrium constant for each of these equations was calculated at each concentration by neglecting the small but unknown liquid junction potential present in the glass electrode measurements and calculating the activity of the hydrogen ion directly from the *p*H measurement. The activity coefficients used for the uranyl ion and the complexes were the mean activity coefficients measured by C. H. Secoy[15] for uranyl sulfate. Up to 0.025 *m* solutions of uranyl sulfate, constant values (8.8×10^{-6}) for the equilibrium constant for the equation

$$2UO_2^{++} + H_2O = UO_3 \cdot UO_2^{++} + 2H^+ \qquad (1)$$

were obtained. From about 0.01 *m* up to the highest concentration the equation

$$4UO_2^{++} + H_2O = UO_3 \cdot (UO_2)_3^{6+} + 2H^+ \qquad (2)$$

gave nearly constant equilibrium constants of about 5.5×10^{-2}. A higher form of a uranyl complex would be expected in more concentrated solutions. Equation 1 is similar to the one found by MacInnes and Longsworth[9] to hold for dilute solutions of uranyl nitrate.

It was assumed that by the addition of UO_3 to the solutions a reaction occurred with the simple uranyl ion to form the UO_3 complexes. When a small amount of UO_3 was dissolved (10 mole % in excess of the uranyl ion present) equation 2 did, in fact, give good constant values for the equilibrium constant, but with larger amounts of UO_3 a marked deepening of color occurred, and no equation could be found that would give constant values. Presumably, an ion, more complex than that shown in equation 2, was being formed.

(15) C. H. Secoy, *J. Am. Chem. Soc.*, **70**, 3450 (1948).

SURFACE ACTIVITY AT THE ORGANIC LIQUID/AIR INTERFACE[1]

BY ALFRED H. ELLISON[2] AND W. A. ZISMAN

Naval Research Laboratory and Georgetown University, Washington, D. C.

Received September 9, 1955

Surface activity at the interface of organic liquids with air has been studied by direct observation of the force–area properties of surface films. The all-Teflon film balance developed for this purpose and the special techniques required are discussed. Liquid substrates studied include *n*-hexadecane, white mineral oil and tricresyl phosphate. On *n*-hexadecane and tricresyl phosphate, a linear polymethylsiloxane of high molecular weight was spread from solution to form monolayers having limiting cross-sectional areas which agree well with each other and with those found by other methods. Spreading coefficients of four liquids on white mineral oil could be measured using the piston film technique. From these the liquid/liquid interfacial tensions were calculated. For two of these spreading liquids the interfacial tensions against white mineral oil were determined by the ring method and agreed to 0.1 dyne/cm. with the calculated values. Films of zein could be spread from solution on the surface of tricresyl phosphate. The results suggest that this protein can be spread on the organic liquid substrate without the denaturation that accompanies its spreading on water. Many other compounds were found to be surface active on organic liquids. Among these were other silicones, organic silicates, polyacrylates, polyalkylene ethers and fluorocarbon derivatives. A plausible explanation of the defoaming power of polymethylsiloxanes for organic liquids is offered.

Introduction

Although an impressive amount of knowledge has been obtained from research on surface activity at the air/aqueous-liquid interface, very little has been learned from analogous studies of the interface between air and non-aqueous liquids.

The technique usually employed in the past for investigating the latter has consisted essentially in measuring the surface tension of the non-aqueous liquid as a function of the solute concentration and then applying the Gibbs relation to calculate the surface excess. McBain and Perry[3] studied dilute solutions of laurylsulfonic acid in a variety of hydrocarbon solvents. Jones and Saunders[4] observed the surface tension lowering of nitromethane by a homologous series of *n*-aliphatic acids. Blake, Ahlbrecht and Bryce[5] have recently reported the effect on the surface tension of a mineral oil and two different melted paraffin waxes of very small concentrations of polyfluoroquaternary ammonium compounds. Banks[6] observed the surface tension lowering of a series of organic liquids by a film of a polydimethylsiloxane. A different approach was that of Kaminski[7] who studied the adsorption of lauric acid and lauryl alcohol from solution in mineral oil by the McBain microtome technique.

A more direct approach, however, would be through the use of an apparatus such as the Langmuir film balance. In this way, the existence of adsorbed films could be observed directly, and the essentially insoluble surface films could be characterized by compressing the film and measuring the area occupied. A "Teflon" film balance and trough designed for use with organic liquid substrates has been briefly described by Fox and Zisman.[8] With a few additional improvements introduced during this investigation, it was found possible to develop a very satisfactory film balance. This report is concerned with the results of the subsequent exploratory study of surface activity at the interface between non-aqueous liquids and air.

In selecting chemicals most likely to be surface active in organic liquids, we have used as a guide a rough approximation derived from the Harkins equation for the spreading coefficient

$$S_{b/a} = \gamma_a - (\gamma_b + \gamma_{ab}) \qquad (i)$$

where $S_{b/a}$ is the spreading coefficient of the spreading material "b" upon liquid "a," γ_b is the surface tension of substance "b," γ_a is the surface tension of the substrate liquid "a" and γ_{ab} is the interfacial tension between "a" and "b." Usually γ_{ab} is small compared with γ_b for the interface between two *organic* liquids. Thus spreading behavior can be roughly predicted from the difference $\gamma_a - \gamma_b$. This is analogous to the approximate treatment of the spreading of organic liquids on solids by Fox, Hare and Zisman.[9]

Description of the Apparatus.—Because of the frequent occurrence of appreciable contact angles in the wetting of the Wilhelmy plate by the liquid systems studied, we have preferred the Langmuir method of measuring film pressures. The following are some of the changes made since the balance was first described.[8] The conventional mica float of the torsion head was replaced with a strip of aluminum (0.020″ thick) upon which had been deposited a Teflon coating 0.0015″ thick. A thin strip of solid Teflon would be preferable but lacks the rigidity required for a float. In order to increase the rigidity of the stirrup float assembly, a finely drawn out glass fiber was used instead of the usual silk or nylon thread to connect the stirrup to the float. The oil repellent character of the Teflon surfaces was greatly enhanced by buffing the surface with a cloth wheel to impart a smooth shiny finish.

The end loops connecting the ends of the float to the sides of the tray to prevent escape of the floating film could not be used because in connecting them capillaries would be created through which the substrate liquid would creep. This is because almost all organic liquids have contact angles with polished Teflon of less than 90°.[10] The surface of the creeping liquid would carry film material beyond the confinement of the barriers. Film leakage was prevented by replacing the end loops with fine jets of gas (nitrogen was used here) which blew the film back as it sought to escape

(1) Presented to the Division of Paints, Plastics and Printing Ink Chemistry at the Fall Meeting of the American Chemical Society, Minneapolis, Minnesota, Sept. 11–16, 1955.

(2) Taken from a thesis submitted by A. H. Ellison to the Graduate School of Georgetown University in partial fulfillment of the requirements for the Ph.D. degree.

(3) M. E. L. McBain and L. H. Perry, *J. Am. Chem. Soc.*, **62**, 989 (1940).

(4) D. C. Jones and L. Saunders, *J. Chem. Soc.*, 2944 (1951).

(5) G. B. Blake, A. H. Ahlbrecht and H. G. Bryce, "Perfluoroalkyl Surface Active Agents for Hydrocarbon Systems," preprint of paper presented to the Petroleum Division of the ACS, New York Meeting, September 11–17, 1954.

(6) W. H. Banks, *Nature*, **174**, 365 (1954).

(7) A. Kaminski, "Properties of Surfaces," N6ori-154-T.O. 11 Stanford Research Institute, Report, January 12, 1948.

(8) H. W. Fox and W. A. Zisman, *Rev. Sci. Inst.*, **19**, 274 (1948).

(9) H. W. Fox, E. F. Hare and W. A. Zisman, THIS JOURNAL, **59**, 1097 (1955).

(10) H. W. Fox and W. A. Zisman, *J. Colloid Sci.*, **5**, 514 (1950).

around the ends of the float. Langmuir, in his original film balance for studying insoluble monolayers on water, used air jets for this purpose.[11] Similarly a pair of gas jets was necessary at each movable barrier because capillaries are also created when a conventional type barrier rests on the edges of the balance trough.

The gas jets made from $^1/_8$" i.d. copper tubing were press fitted into diagonal holes drilled in the ends of the barriers and were connected to a gas manifold by flexible Tygon tubing. The gas manifold, which was a piece of $^3/_{16}$" i.d. copper tubing located along the rear of the tray, was provided with gas outlets for each barrier. The gas jet assembly for the ends of the float was made from $^1/_8$" i.d. copper tubing and was permanently mounted on the manifold. The manifold was connected to a tank of compressed dry nitrogen and the flow rate adjusted by a conventional pressure regulator.

In experimenting with non-aqueous substrates, it was necessary to employ some unconventional procedures for cleaning the film balance. The trough, barriers and float assembly were first cleaned by a 30-minute soaking in an aqueous solution of "Tide." A camels'-hair brush was used to scrub gently the movable barriers and the balance parts which came in contact with the film and substrate. This was followed by rinsing the equipment in running tap water for several minutes. The entire procedure was repeated but with a shorter soaking time and a much longer rinsing time. Small droplets of rinse water which remained when the tray was emptied were drawn off with filter paper. The assembly was then allowed to dry for several hours, usually overnight, in a Lucite box to keep it free from dust.

The substrate liquid was added to the clean, dry trough and its level raised to that of the float. The movable barriers were set in position and connected to the air manifold. The pointer on the torsion wire was set at zero and the air jets turned on. This usually caused a very slight displacement of the zero point and so it was readjusted. If necessary, a movable barrier was used to sweep the surface of the liquid free of contaminating film.

The spreading solution was added to the surface between the float and a movable barrier from a micropipet attached to a hypodermic syringe. A convenient amount of film material was obtained by spreading 100 λ (0.100 ml.) of a solution having a concentration of about 1×10^{-4} g./ml. As the solution was delivered dropwise to the surface, the pipet was moved to a new area of surface after each drop. Sufficient time was allowed for the spreading solvent to evaporate, and then the force–area data were obtained. The movable barrier was always adjusted slowly. Due to the higher viscosity of these substrates than water, the time for a newly compressed film to arrive at a steady-state pressure often was long. Thus several minutes were necessary after a change in pressure of only a few tenths of a dyne.

Similar to the technique used for aqueous systems, a few fine particles of Teflon powder often were sprinkled on the surface of the film near each gas jet. Thus any escape of film could be detected since it would carry the Teflon powder with it. The effectiveness of the gas jets was readily observed, for when the gas jets were turned off, the Teflon powder immediately darted past the ends of the float and the surface pressure fell to zero.

Since no end loops were used, the torsion head could be removed from the trough and replaced readily. This feature was helpful when it was desired to sweep the surface or when the trough was being cleaned.

Materials Studied.—The cetane was Eastman Kodak Company *n*-hexadecane "Practical Grade." Before use it was freed from polar impurities by passing it slowly through an adsorption column containing activated alumina and silica. The resulting material had a surface tension in air at 20° of 27.5 ± 0.1 dyne/cm. The white mineral oil used was Fisher's U.S.P. grade Light Mineral Oil. Polar impurities were removed by percolation through alumina and silica. The resulting liquid had a surface tension at 20° of 30.8 ± 0.1 dyne/cm. Tricresyl phosphate was Fisher's Technical grade containing 80% of the *para* and 20% of the *meta* isomers. It has a surface tension at 20° of 40.9[9] and was used as received.

A polymethylsiloxane having a viscosity at 25° of 50 cs., a polymethylphenylsiloxane (DC 510) and a polymethylchlorophenylsiloxane (XF 4050), products of the Dow Corning Corporation were each purified before use by percolation through "Florisil." The trimethyl end-blocked polymethylsiloxane heptadecamer was a pure preparation obtained from the Dow Corning Corporation for earlier research.[12] The ethoxy end-blocked polymethylsiloxane $C_2H_5O[Si(CH_3)_2O]_{110}C_2H_5$, which has been described by Hunter, *et al.*,[13] had a molecular weight of 8250 and a viscosity at 25° of 156 cs. It was percolated through Florisil before use. Silicone L-41, a polyethylsiloxane, and the water-soluble silicones X-520, X-521, X-522, are recent products of the Linde Air Products Company. They were used as received.

Egg albumin and zein (mol. wt.[14] = 40,000) from Eastman Kodak (Technical grade) were used as received. Chymotrypsin and chymotrypsinogen prepared by Armour and Company were used as received. These were obtained from bovine pancreas and were salt free and crystallized.

Solvents used to spread materials on the liquid substrates were: Fisher "Certified Reagent" grade isopropyl alcohol, U. S. Industrial Chemicals Company ethyl alcohol and Eastman Kodak "White Label" trifluoroacetic acid. These were diluted with freshly distilled water as needed.

Polyorganosiloxanes.—The different types of polyorganosiloxane liquids available were found to spread readily on the several non-aqueous substrates used here. On cetane the spreading of three different open-chain polymethylsiloxanes was observed. A liquid polymethylsiloxane having a viscosity at 25° of 50 cs. spread rapidly when a drop was placed on the clean surface of cetane or when a small amount of a solution in isopropyl alcohol was used. As the area of the residual film was decreased or increased by moving the barrier, the surface pressure increased or decreased to give a reproducible curve of film pressure (F) *vs.* surface area (A). No further work was done on this material, since its exact molecular weight was not known.

A trimethyl end-blocked polymethylsiloxane heptadecamer[12] was found to spread on cetane when a drop of the pure material was placed on the surface, but unfortunately it was too oil-soluble for F *vs.* A measurements by the film balance technique. An ethoxy end-blocked polymethylsiloxane having a molecular weight of 8250 spread on cetane when in the pure state or when used in a solution in isopropyl alcohol. With the object of comparing the dimensions of the molecule determined with the film balance with those of a molecular model, the F *vs.* A curve shown in Fig. 1 was obtained. Excellent agreement was found between the runs made with two different spreading solutions having concentrations of 9.2×10^{-5} g./ml. and 3.88×10^{-4} g./ml.

The results in Fig. 1 reveal three regions of interest. The first is at pressures below 0.32 dyne/cm. and at areas greater than 22×10^2 Å.^{2}/molecule (20 Å.^{2}/monomer); the film is gaseous and exhibits a pressure even at the largest areas. The second is between 0.32 and 0.57 dyne/cm. or from 20 to 13 Å.^{2}/monomer in which the film is much less compressible. Extrapolation of the curve in this region to zero pressure results in a limiting area per molecule of 2980 Å.^{2} (or 27 Å.^{2}/monomer). From a pressure of 0.57 dyne/cm. or area of 13 Å.^{2}/monomer up to the collapse pressure of 2.16 dynes/cm. there is the third region in which the film is

(11) I. Langmuir, *J. Am. Chem. Soc.*, **39**, 1848 (1917).

(12) H. W. Fox, P. W. Taylor and W. A. Zisman, *Ind. Eng. Chem.*, **39**, 1401 (1947).

(13) J. M. Hunter, M. S. Gordon, A. J. Barry, J. F. Hyde and R. D. Heidenreich, *ibid.*, **39**, 1848 (1947).

(14) J. Alexander, "Colloid Chemistry," Vol. VI, Reinhold Publ. Corp., New York, N. Y., 1946, p. 1140.

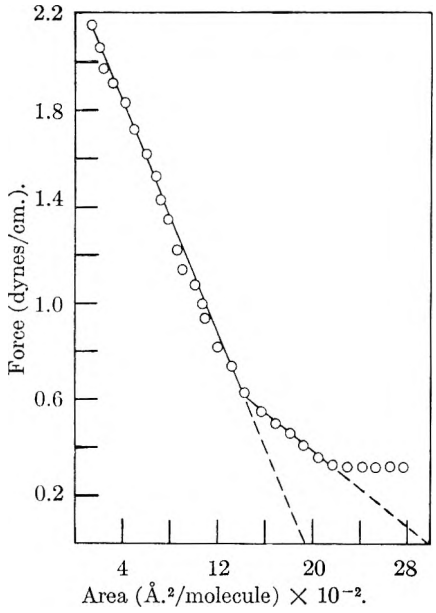

Fig. 1.—*F–A* curve for $C_2H_5O[Si(CH_3)_2O]_{110}C_2H_5$ on cetane.

even less compressible. Extrapolation of this region of the curve to zero pressure yields an area per monomer of 17 Å.².

An explanation of the polymethylsiloxane film properties on cetane can be obtained by comparing the *F–A* curve for cetane with that for water.[12,13] Since higher film pressures are obtainable on water, the three regions found for the curve on water correspond to the three regions on cetane with respect to the area axis only. In the first region on both substrates the polysiloxane chains are fully extended. This allows the maximum number of adsorbing groups to reach the liquid surface. These would be, of course, the Si–O groups on water and the CH_3 groups on cetane.

At an area per monomer in the vicinity of the boundary between the first and second regions (20 Å.²) the fully extended molecules become close-packed. Further compression through the second region on water causes the molecular chains to buckle and form helices.[12] It is believed that the same process occurs in the second region on cetane since this region begins and ends at very nearly the same areas per monomer and the film pressure necessary to force the adsorbing groups out of the surface as the film molecules buckle is, quite logically, less on the cetane surface.

In the vicinity of the boundary of the second and third regions on water (17 Å.²) the molecules have reached the helical configuration with six monomer units per turn.[12] Since the *F–A* curve on cetane showed approximately the same area/monomer at this point (13 Å.²) it was likely that the helical configuration on cetane was also six monomers per turn. A molecular model of this helix shows that the methyl groups must all be on the outside if a complete turn is to be accomplished with as few as six monomer units.

As the film is compressed through the third region on water the film pressure remains essentially constant. This must be due to the fact that in the helical configuration the hydrophilic Si–O groups are shielded within the helix by the hydrophobic methyl groups. In this configuration there is no preference for an orientation where the long axis of the helical molecule is parallel to the water surface. Thus the film collapses and exerts no significant surface pressure until the molecules approach close-packing with the long axis vertically oriented. In the third region on cetane the helical molecules should prefer a horizontal orientation since the coiling of the siloxane chain has not removed all of its adsorbing groups from the liquid surface. Thus the surface pressure rose as the film was compressed through this region and was indicative of the surface pressure required to pack together these horizontally oriented spring-like molecules.

Since this polymethylsiloxane film is reproducible and has properties at low film pressures which are essentially the same as a monolayer of this material on water it can be concluded that it spreads to form a monolayer on cetane.

When the same polymer is spread from isopropyl alcohol solution upon tricresyl phosphate, the resulting film exhibits the *F–A* relationship shown in Fig. 2. The shape of the curve is like that observed by Banks[6] for a polymethylsiloxane on the moderately polar substrates oleic acid and olive oil. Extrapolation of the curve in the region from 2.0 to 4.5 dynes/cm. yields an area per monomer of 24 Å.² which is close to the area on water (23 Å.²) of the extended polysiloxane chain.[12] At 14 Å.²/monomer the film collapses and thus closely parallels the behavior on water. It can be concluded, therefore, that the film is monomolecular in this region with the Si–O groups adsorbed. When the film area has been reduced well below the collapse area, higher film pressures can be obtained which decay with time. This suggests that the molecules of the film are orienting vertically as is found in water but the resulting film is unstable. Thus this polymethylsiloxane film has the same properties on the polar organic liquid substrate, tricresyl phosphate, as on water.

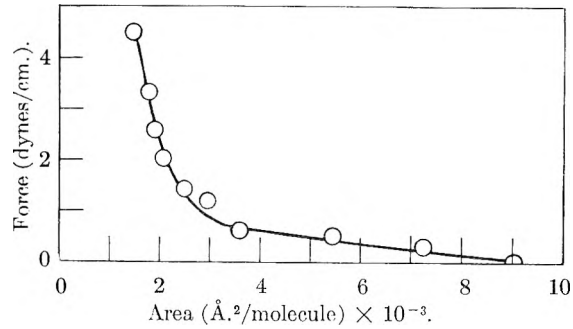

Fig. 2.—*F–A* curve for $C_2H_5O[Si(CH_3)_2O]_{110}C_2H_5$ on tricresyl phosphate.

Since these molecular dimensions compare well with those of a molecular model of a polymethylsiloxane chain and with those obtained by other investigators in studies of such films on water, it can be concluded that the all-Teflon film balance can be used on non-aqueous systems with as much confidence as on aqueous systems.

Other types of polyorganosiloxanes which were found to spread on non-aqueous substrates were:

diethyl, methylphenyl, methylchlorophenyl and the Linde water-soluble silicones.

Proteins.—An attempt was made to see if a monomolecular layer of a protein could be formed on an organic liquid surface, and also to ascertain whether or not the protein had been denatured in the spreading process. If a monomolecular layer of undenatured protein could be formed, this procedure would offer a new method for determining the shape of a protein molecule.

Spreading tests made by placing solid particles of each of a few proteins on the surface of cetane, white mineral oil or tricresyl phosphate gave no evidence of spreading. No spreading occurred when dilute aqueous solutions of the water-soluble proteins, egg albumin, chymotrypsin and chymotrypsinogen were each placed on the clean surface of any of these organic liquid substrates. Since better spreading solutions can usually be made with organic solvents, it was decided to work with the alcohol-soluble protein zein.

Zein is quite soluble in aqueous 90% isopropyl alcohol and aqueous 90% ethanol, and satisfactory spreading solutions could be prepared with these solvents. When a dilute aqueous alcohol solution of zein was spread on either cetane or white mineral oil, the solution spread; but after the solvent had evaporated, the protein was left as tiny particles on the surface. On the higher surface tension substrate tricresyl phosphate, however, the same procedure led to the formation of a film which could be compressed to give a typical force–area curve. It has been reported[15] recently that anhydrous trifluoroacetic acid is a good solvent for proteins. Since this acid also has most of the features desired of a spreading solvent for work on non-aqueous substrates, solutions were made with it. These solutions spread readily on the surface of tricresyl phosphate and large surface pressures were observed immediately. As the solvent evaporated, the surface pressure fell to zero. After this happened the compression of the film was begun.

Figure 3 shows the type of F–A curves obtained on tricresyl phosphate. The position of the curve with respect to the area axis was dependent on the concentration of the spreading solvent, and for a given concentration varied with the solvent. The films spread from aqueous alcohols could be compressed and expanded and recompressed to give the same force–area relationship provided that the film was not collapsed either by exceeding the collapse pressure or by compressing it too rapidly. Films spread from anhydrous trifluoroacetic acid showed hysteresis effects. The curve shows no gaseous region, and thus the molecules in the film must be held together in some fashion so that they cannot spread out indefinitely at zero pressure.

In Table I the results are summarized of the work with zein films spread upon tricresyl phosphate. Since the shapes of all the curves were similar, the results are tabulated and discussed in terms of the thickness of the films. This figure was arrived at by converting the surface concentration of the close-packed film to thickness by using as the film density of zein the value of 1.33 g./cm.^{3} found by

(15) J. J. Katz, *Nature*, **174**, 509 (1954).

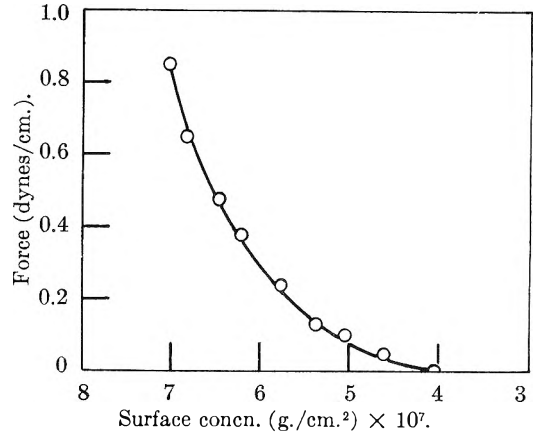

Fig. 3.—F *vs.* surface concentration for zein on tricresyl phosphate. Spread from aqueous 90% EtOH (1.095×10^{-4} g./ml.).

Mitchell[16] for films of zein on water. The surface concentration at close-packing was obtained by extrapolating the high pressure region of the curve to zero pressure. In most cases the extrapolation was less arbitrary than that shown in Fig. 3. However, it is believed that as the work at the organic liquid/air interface is further refined, a better method of characterizing protein films will be required such as the determination of the film dimensions at the point of minimum compressibility suggested by Bull.[17] In making the thickness calculation it was necessary to assume that these zein molecules could arrange themselves so as to be close-packed. The film thickness is of interest here because it should represent one of the dimensions of the molecule if the film is a close-packed monolayer.

TABLE I

THICKNESS OF ZEIN FILMS ON TRICRESYL PHOSPHATE

Spreading solvent	Concn. (g./ml.)	Film thickness (Å.)
90% isopropyl alc. (aq.)	2.49×10^{-3}	80
90% ethanol (aq.)	4.38×10^{-4}	74
	1.09×10^{-4}	44
	5.48×10^{-5}	41
CF_3COOH	1.90×10^{-4}	7
CF_3COOH (91%)-9% H_2O	1.73×10^{-4}	13

Each result given in Table I is the average of several independent runs which agreed to within 5%. The high film thickness of 80 and 74 Å. listed in the table indicates incomplete spreading caused by the high concentration of spreading solution used. Mitchell[16] found that the concentration of the spreading solution should not exceed 1×10^{-4} g./ml. if complete spreading of zein on water were to be obtained. As shown in the table, the same was observed in this study with aqueous ethanol spreading solutions. When the spreading solution was added too rapidly to the surface, cracks could be observed in the film. Such films were swept away and no data taken on them. Satisfactory films were obtained by adding the spreading solution to the surface dropwise from a micropipet, mov-

(16) J. S. Mitchell, *Trans. Faraday Soc.*, **33**, 1129 (1937).

(17) H. B. Bull, "Advances in Protein Chemistry," Vol. III, Academic Press Inc., New York, N. Y., 1947, p. 95.

ing the pipet around so that each drop was delivered to a different area of the surface.

The results in Table I indicate that the zein films are sensitive to the spreading solvent and also to the water content of the spreading solvent. Both actions may be caused by the ability of the solvent to dehydrate the protein. It will be necessary to operate the film balance in controlled atmospheres in order to study the effect of the water in the spreading solvent. However, the following experiments were carried out to show that it is unlikely that the difference observed was caused by retention of the solvent molecules in the film.

To a suitable spreading solution of zein in aqueous ethanol 2.4×10^3 moles of trifluoroacetic acid per mole of zein were added. This represents a large excess of the amount of trifluoroacetic acid necessary to adsorb on or react with the protein molecules. The thickness of the film obtained from spreading this solution on tricresyl phosphate was the same as that found when no trifluoroacetic acid was added. The same result was obtained when heptafluorobutyric acid was used in place of trifluoroacetic acid.

On water, the thickness of a close-packed zein monolayer is about 7 Å. and can be defined by twice the weighted average length of the alkyl branchings on the polypeptide chain.[16] This is so because the polypeptide chain is fully extended and orients itself with the main chain in the surface of the water and all the alkyl branches perpendicular to the water surface: the polar side chains orient below the main chain and the non-polar ones above. Table I shows that zein films spread on tricresyl phosphate from anhydrous trifluoroacetic acid have the same thickness as zein films on water which are denatured, but Katz has reported[16] that proteins recovered from solution in anhydrous trifluoroacetic acid have properties which are not different from the untreated material. Since zein films spread from aqueous alcohols do not have the thickness of denatured films, it is unlikely that spreading alone caused the zein molecules in the film spread from anhydrous trifluoroacetic acid to become fully extended. It is possible that anhydrous trifluoroacetic acid has an effect on the cross-linkages within the zein molecules that is readily reversed after the trifluoroacetic acid is removed, for example, dehydration. Further, in the state produced by the presence of the trifluoroacetic acid the zein molecules could be susceptible to complete unfolding in the spreading process. This explanation is consistent with the earlier observation concerning the water content of the spreading solvent and with present day notions of the cross-linkages within a protein molecule and their role in denaturation.[18]

Reproducibility of the results reported indicates that under each set of spreading conditions the film of zein molecules has a very definite structure. Direct evidence that denaturation did not occur in the spreading of zein on tricresyl phosphate is lacking. However, the films spread from aqueous alcohol were much thicker than denatured zein films on water which suggests a lack of denaturation or the less likely possibility that the films were multilayers composed of denatured zein monolayers.

Spreading Coefficients.—In keeping with the exploratory nature of this investigation, it was desirable to be able to rapidly "screen" from the many promising soluble materials those having surface activity at the organic liquid/air interface. A valuable method is the measurement of the spreading coefficient[19] by the piston film technique.[20] Briefly, the procedure is to allow a drop or small particle of material to spread on a liquid substrate against a piston film which transmits the spreading pressure of the material under test to the float. The pressure on the piston film can be varied by changing its area with the movable barrier. The spreading coefficient ($S_{b/a}$) is the constant pressure created by the spreading liquid on the piston film as the position of the movable barrier is changed. At higher pressures the piston film forces the spreading material into a liquid lens or solid crystallite, and at lower pressures the spreading material is a monolayer which is spread beyond its closest possible packing.

According to Harkins[19] there are three stages of spreading and each has a spreading coefficient. The initial spreading coefficient is that of pure "b" on pure "a," the semi-initial is that of "b" saturated with "a" on pure "a" and the final is "b" saturated with "a" on "a" saturated with "b." In the time necessary to make the measurements reported here, it was unlikely that spreading progressed much beyond the first stage and in no case as far as the third stage since this would have been readily observable. There is little difference in the magnitudes of the initial and semi-initial spreading coefficients and therefore we have made no attempt to distinguish between them in our measurements.

From those materials found to spread as insoluble films on the organic substrates studied, compound F-2 which is $F(CF_2)_7CONH(CH_2)_3N(CH_3)_3$-I[5,21] was chosen as the piston film. A non-polar substrate was considered most desirable for early work, and white mineral oil was chosen over cetane since higher film pressures can be obtained the higher the surface tension of the substrate.

It has been mentioned that the time required for the film to attain equilibrium after a change in film pressure was long because of the rather high viscosity of the oil substrates. For this reason it was not practical to follow the same technique in measuring $S_{b/a}$ that is used on aqueous substrates. The procedure followed here consisted of (A) compressing the spreading drop until it just formed a lens, (B) recording the pressure after time was allowed for the float to become stationary, (C) reducing the pressure until the drop has spread to a thin film about 10 times the diameter of the lens, (D) recording this pressure after equilibrium has been attained, and (E) taking the average value of steps (B) and (D) as $S_{b/a}$. In no case was the difference between these two pressures greater than 0.5 dynes/cm. Repeated measurements of $S_{b/a}$ on the same drop or on different drops of the same material

(18) F. W. Putnam, "The Proteins," Vol. I, Part B, Academic Press, Inc., New York, N. Y., 1953, p. 807.

(19) W. D. Harkins, "The Physical Chemistry of Surface Films," Reinhold Publ. Corp., New York, N. Y., 1952, p. 98.

(20) E. R. Washburn and C. P. Keim, *J. Am. Chem. Soc.*, **62**, 1747 (1940).

agreed to 0.1 dyne/cm. in practically all cases, and the greatest deviation observed was 0.3 dyne/cm. The results are given in Table II.

TABLE II

SPREADING COEFFICIENTS AT 20° OF SOME LIQUIDS ON WHITE MINERAL OIL

(γ_a = 30.8 dynes/cm.)

Spreading liquid "b"	γ_b (dynes/cm.)	$S_{b/a}$ (dynes/cm.)	γ_{ab} (dynes/cm.) Calcd. from $S_{b/a}$	γ_{ab} (dynes/cm.) Ring method
Bis-(*t*-butyl)-bis-(ψ'-heptyl) silicate[b]	21.0	5.9	3.9	4.0
Bis-(*t*-butyl)-bis-(ϕ'-octyl) silicate[c]	18.4	8.0	4.4	4.5
Isopropyl alcohol	21.7[a]	5.4	3.7	..
$C_2H_5O[Si(CH_3)_2O]_{110}$-$C_2H_5$	20.8	6.0	4.0	..

[a] Lange "Handbook of Chemistry," 7th Edition, Handbook Publishers, Inc., Sandusky, Ohio, 1949. [b] ψ' = H-$(CF_2)_nCH_2$-. [c] ϕ' = F$(CF_2)_nCH_2$-.

Using equation (i) the liquid/liquid interfacial tensions were calculated from the measured values of $S_{b/a}$, γ_a and γ_b given in Table II. As a check on the method, the liquid/liquid interfacial tensions were measured for two of these combinations. The other two were not done due to scarcity of material. As the results show, the agreement between the measured and calculated values of γ_{ab} is very good.

The two silicates have the same hydrocarbon radicals. Since it is likely that the molecules will orient with this portion in the oil phase, it is reasonable that their interfacial tensions with oil differ by only 0.5 dyne/cm. The fluorocarbon radicals will orient away from the oil phase, and it is not surprising that the one which had the lower surface tension (the ϕ' compound) had the greater spreading pressure.

General Discussion

Qualitative spreading tests using Teflon indicator powder instead of talc on these organic substrates showed that many other types of materials are surface active on such liquids. Among these are organic silicates, polyacrylates and polyalkylene oxides. Many fluorocarbons and their derivatives are especially surface active. This is not surprising since such compounds have surface tensions which are considerably lower than those of analogous hydrocarbon compounds and their surface activity is predicted by the approximation ($\gamma_a - \gamma_b$) deduced from equation (i). The surface active properties of a variety of fluorocarbon derivatives including materials exhibiting a wide range of oil solubility and molecular structure will be reported shortly.[21]

The results given here on their surface activity lead readily to an explanation of the well known defoaming power of polymethylsiloxanes when added to oils and many other organic liquids.[22,23] It has been shown by McBain, *et al.*,[24] that pure liquids or highly refined oils do not form stable foams. Foaming results when an addition agent or impurity is present which adsorbs at the oil/air interface to produce an elastic film which stabilizes the foam. Many defoamers adsorb at the oil/air interface to produce an unstable film either by interacting with the stabilizing film or by displacing it. Since we have shown here that the polymethylsiloxanes are remarkably surface active in organic liquids it is evident that they can function as defoamers by displacement of the foam stabilizer. This conclusion is borne out by the recent findings of Criddle and Meader[25] who found that the large increase in the surface viscosity of mineral oil caused by the addition of 0.094% sulfurized calcium alkyl phenate was eliminated by the further addition of 0.010% of a polymethylsiloxane. The surface activity of the polymethylsiloxane could not be detected by their approach, however, since the change in surface viscosity of mineral oil caused by addition of 0.010% polymethylsiloxane was nil. Therefore, it is proposed that the defoaming power of polymethylsiloxanes for liquids is due to (a) the displacement of the organic foam stabilizing film by a monolayer of polymethylsiloxane molecules, and (b) to the extraordinary low surface viscosity of such a film. The well known observation that the defoaming effect of silicones is greater the higher the molecular weight is readily explained by the resulting increased adsorptivity at the oil/air interface.

Summary

1. The modified all-Teflon film balance developed has been proved suitable for the study of surface activity at the organic liquid/gas interface.

2. Among the materials found surface active at the organic liquid/gas interface were fluorocarbon derivatives, silicones, a protein (zein), organic silicates, polyacrylates and polyethers.

3. The limiting areas obtained from the force-area curves of a known polymethylsiloxane on cetane and also on tricresyl phosphate were consistent with the results at the water/air interface obtained in other investigations. This served to establish the quantitative reliability of the new methods used.

4. Reproducible films of zein could be formed on tricresyl phosphate. The thickness of these films was found to be dependent on the water content of the spreading solvent. Films spread from aqueous alcohol were much thicker than those spread from anhydrous trifluoroacetic acid which suggested a lack of surface denaturation in the case of the former.

5. The piston film technique for measuring the equilibrium spreading pressure was applied successfully for an organic liquid spreading on another organic liquid. This has been found valuable for a rapid screening of soluble materials. Liquid/liquid interfacial tension calculated from the equilibrium spreading pressure agreed to 0.1 dyne/cm. with direct measurement of the interfacial tension.

6. A general explanation of the defoaming power of polymethylsiloxanes for organic liquids is presented.

(21) A. H. Ellison and W. A. Zisman, "Surface Activity of Fluorinated Compounds on Non-aqueous Substrates," to be published.

(22) R. G. Larsen and H. Diamond, U. S. Patent 2,375,007 (May 1, 1945).

(23) C. E. Trautman and H. A. Ambrose, U. S. Patent 2,416,504 (Feb. 24, 1947).

(24) J. W. McBain, S. Ross, A. P. Brady, J. B. Robinson, I. M. Abrams, R. C. Thorburn and C. G. Lindquist, NACA ARR No. 4105, Sept. 1944.

(25) D. W. Criddle and A. L. Meader, Jr., *J. Applied Phys.*, **26**, 838 (1955).

THE EFFECT OF ALKALI METAL IONS ON THE ACTIVITY OF CRACKING CATALYSTS

BY JOSEPH D. DANFORTH AND DEAN F. MARTIN

Department of Chemistry, Grinnell College, Grinnell, Iowa

Received September 12, 1955

The conversion of cetane in a standard activity test has been reported as a function of the concentration of four alkali metal ions for a silica–magnesia catalyst, an alumina–boria catalyst, and for several silica–alumina catalysts before and after the partial destruction of active sites by calcination. The loss in conversion per milliequivalent of each alkali was considered to be a fundamental characteristic of each catalyst. The constancy of this value before and after site destructive calcination was consistent with a mechanism of site destruction in which large sections of active sites become buried by condensation with an adjacent surface, while the spacing between those sites available for reaction remained relatively unchanged.

Because of the amorphous nature of cracking catalysts, the application of physical methods to the determination of structure has been relatively unsuccessful. An indirect approach to the structure of catalysts has been attempted by studying the reaction of the catalyst with various substances, usually poisons, in an effort to relate cracking activity to chemical changes brought about at the active sites.[1,2]

It was previously shown that the conversion of cetane was inversely proportional to the milliequivalents of an alkali ion over a major portion of the range in which cetane conversion changed appreciably with added alkali.[3] The larger alkali ions were more effective poisons than the smaller ones, and the loss in conversion per milliequivalent of alkali ion appeared to be a function of the radius of the covering ion.

On the assumption that the loss in conversion per milliequivalent of alkali ion was an indirect measure of the distance between the active sites, the losses in conversion per milliequivalent of lithium, sodium, potassium and cesium hydroxide have been determined for cracking catalysts of different chemical constitution.

A comparison of the losses in conversion per milliequivalent of alkali for two silica–alumina catalysts before and after the partial destruction of active sites by calcination indicated no definite change in catalyst spacings, and a mechanism of site disappearance on calcination is implied.

Materials.—A Shell Development Company experimental catalyst was received as 8 to 14 mesh granules containing approximately 25% alumina on silica. Site destructive calcination was accomplished by heating for 8 hr. at 550°. The catalyst gave 54% conversion of cetane, initially, and 47% conversion after site destructive calcination.

A 25% alumina on silica catalyst was prepared by the hydrolysis of alcoholic solutions of ethyl orthosilicate and aluminum isopropoxide as described by Thomas.[2] The catalyst was dried, calcined several hours at 500° and pressed to 6–16 mesh granules. The granules were calcined 15 hr. at 500°, and site destructive calcination was accomplished by an additional 6 hr. at 550° (cetane conversion, 33%).

A silica–magnesia catalyst from the American Cyanamid Company represented a composite of laboratory samples containing approximately 31% MgO. The catalyst as received was calcined for 15 hr. at 500° (cetane conversion, 32%).

The alumina–boria catalyst was obtained from the Shell Development Company as calcined granules containing 11.8% boria on grade A Alorco alumina.

Du Pont Cetane was used in all tests.

Apparatus and Procedure.—The calcined catalyst samples were impregnated as previously described,[3] dried at 110° and calcined 2 hr. at 500° before charging to the reactor. Appreciable quantities of boria were found to dissolve in the aqueous impregnation layer above the alumina–boria catalyst, and this introduced an uncertainty in the alumina–boria data.

The method for determining conversions previously described[3] was modified to charge 25 ml. of cetane at 485° and liquid hourly space velocity, 4, to 12.5 ml. of catalyst. The weight of non-volatile product remaining after stabilization of the liquid to 180° was determined to the nearest mg. and expressed as per cent. of cetane recovered. The conversion of cetane was the difference between this value and 100.

The tables summarizing the conversion data are not given because they do not add appreciably to the information which is presented in the figures.

Precision and Accuracy of Data.—An inspection of the points of Figs. 1–6 shows a definite spread in the data, and lines of somewhat different slopes could be used to represent the data in several cases. The possible error increases as the size of the ion increases because of the very steep slopes obtained on the addition of cesium ion. As is sometimes encountered in catalytic work, an occasional point will fall completely off of a line by an amount far greater than the precision of the standard test would permit. On the other hand, there is a repeating pattern of points which enables lines of approximately reproducible slopes to be drawn to show the change in conversion as a function of the milliequivalents of alkali ion. Because of the possible variation in slopes, ranges of values obtained by the manner in which the line was drawn have been given in Table I. In some cases this range is quite small, while in others the range is large.

Results

The conversion of cetane in a standard activity test has been plotted as a function of the milliequivalents of lithium, sodium, potassium and cesium hydroxides in Figs. 1–6 for two high activity silica–alumina composites, before and after site destructive calcination, and for a silica–magnesia catalyst and an alumina–boria catalyst.

Over that portion of each curve in which added alkali caused a significant change, the conversion appears to be inversely proportional to the milliequivalents of alkali ion per gram of catalyst. At higher concentrations of alkali (not shown) the conversion remains relatively constant. For very small amounts of alkali there is, in some cases, a

(1) G. A. Mills, E. R. Boedeker and A. G. Oblad, *J. Am. Chem. Soc.*, **72**, 1554 (1950).

(2) Charles L. Thomas, *Ind. Eng. Chem.*, **41**, 2564 (1949).

(3) Joseph D. Danforth, THIS JOURNAL, **58**, 1030 (1954).

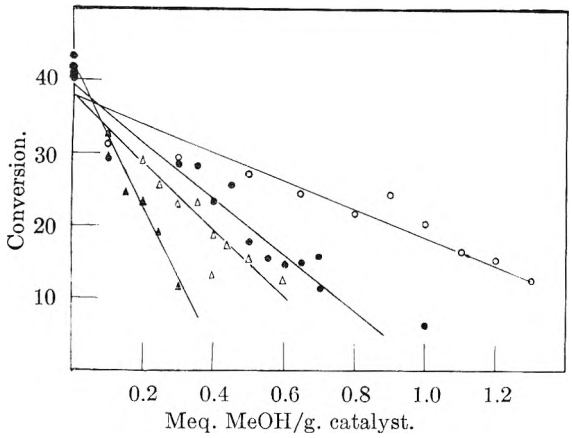

Fig. 1.—25% Al_2O_3 on SiO_2 before site destructive calcination: ○, LiOH; ●, NaOH; △, KOH; ▲, CsOH.

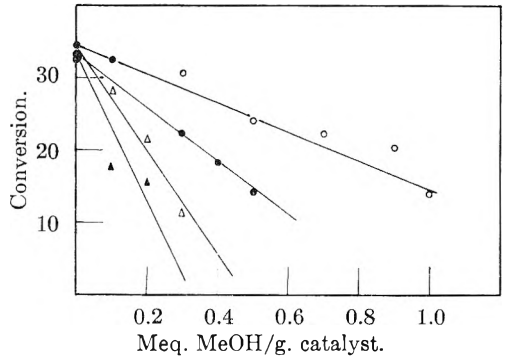

Fig. 2.—25% Al_2O_3 on SiO_2 after site destructive calcination: ○, LiOH; ●, NaOH; △, KOH; ▲, CsOH.

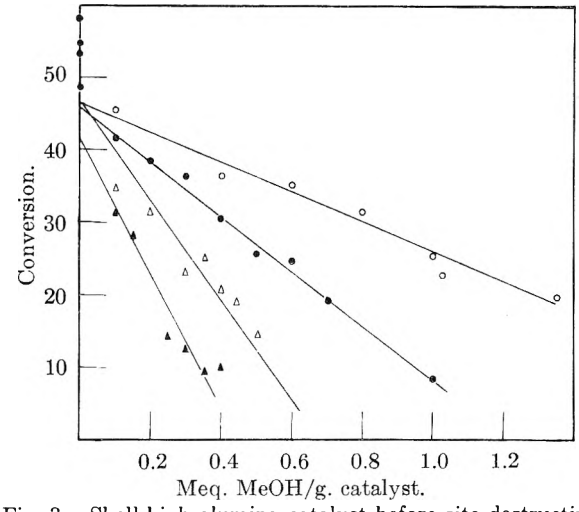

Fig. 3.—Shell high alumina catalyst before site destructive calcination: ○, LiOH; ●, NaOH; △, KOH; ▲, CsOH.

rather sharp decrease in conversion, which is emphasized in the figures by the observation that the straight line portion of every curve does not necessarily extrapolate to the determined conversion for zero alkali content. The curves of Figs. 1–6 have been drawn to emphasize the straight line portions, rather than to depict accurately the conversion of cetane as a function of added alkali over the entire range of alkali content. The slopes of the straight line portion of each curve have been divided by the weight of the catalyst sample to give a value having the units—loss in conversion per milliequivalent of alkali. This value appears to be characteristic for each catalyst as long as comparisons are made with a constant volume of catalyst at the same conditions of operation. These values have been recorded for each alkali ion and each catalyst in Table I.

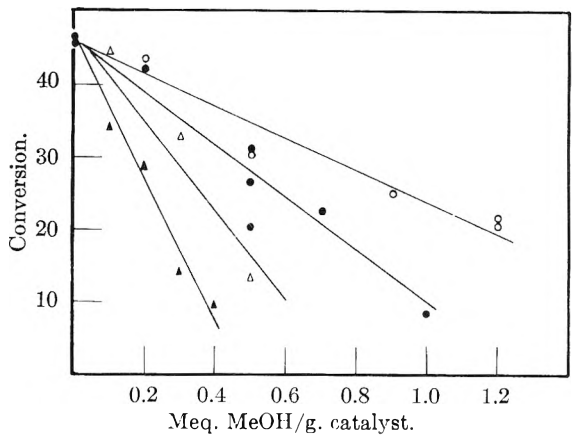

Fig. 4.—Shell high alumina catalyst after site destructive calcination: ○, LiOH; ●, NaOH; △, KOH; ▲, CsOH.

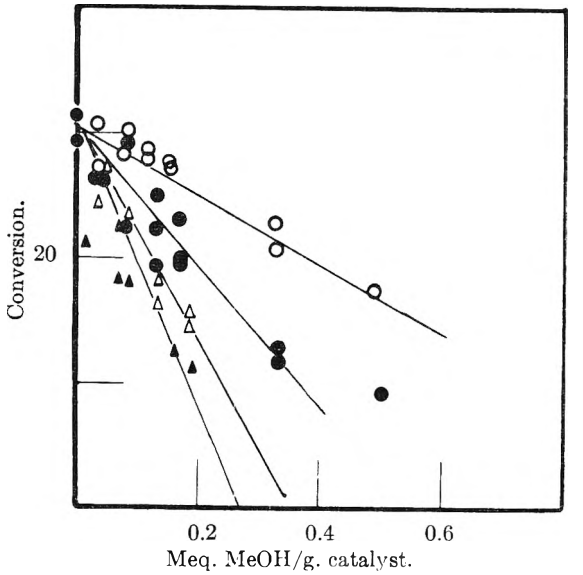

Fig. 5.—Silica–magnesia catalyst: ○, LiOH; ●, NaOH; △, KOH; ▲, CsOH.

A study of Table I indicates that only insignificant variation in the loss in conversion per milliequivalent of alkali is observed on two silica–alumina catalysts of different origin before and after site destructive calcination. The Shell catalyst decreased in conversion from 54 to 47% and the prepared silica–alumina catalyst decreased from 41 to 33% conversion. The fact that the loss in conversion per milliequivalent of any one of the four alkali ions did not change on either catalyst as a result of calcination, has been interpreted to mean that the distance between the active sites does not change, as sites disappear on calcination. This assumes, of course, that the increase of poisoning effect with increase of ion size is a function of the size of the ion, and not an implicit function of some other variable directly related to the size of the ion.

A mechanism for the disappearance of active sites, which is consistent with the observation that

TABLE I

LOSS IN CONVERSION PER MEQ. ALKALI ION

485°; L.H.S.V., 4; duration, hr., 0.5; 12.5 ml. cata.; 25 ml. cetane.

Metal ion	Li	Na	K	Cs
Radius of ion, Å.	0.60	0.95	1.33	1.69
Catalyst				
Shell high alumina catalyst				
Before site dest. calc.	3.2–3.6	6.0–6.2	8.5–11.2	14.0–15.5
After site dest. calc.	3.5–3.6	5.7–6.0	9.2–9.6	15.0–15.2
Prepared 25% Al_2O_3 on SiO_2				
Before site dest. calc.	2.8–3.3	6.1–6.8	8.1–10.3	15.1–17.0
After site dest. calc.	2.8–3.3	6.0–6.3	9.7–11.7	16.4–17.6
Silica–magnesia	5.3–5.7	9.5–11.0	16.0–16.5	20–22
Alumina–boria	6.2–7.0	9.4–9.8	12.5–13.8	16.4–20.4

the spacings between the active sites remain constant during moderate site destructive calcination, can be represented by the disappearance of large sections of active sites by condensation with an adjacent catalyst micelle. Thus, the chains of active sites which have been represented as $\rangle$Al–OH[4] enter into condensation with hydroxyls on an adjacent surface and thereby become buried and unavailable to hydrocarbon molecules. By this mechanism the active sites which do not enter into condensation remain relatively unchanged. This mechanism of active site disappearance is consistent with the observation that only a portion of the acid hydrogens present in precipitated gels of alumina and silica and presumed to be the source of active sites, remains to be titrated after the composite has been calcined in the range of 500°. Presumably a high proportion of the active sites is buried in the catalyst by these condensation processes. When the losses in conversion per milliequivalent of each alkali ion from Table I are plotted as a function of the radius, or as a function of the radius squared for the silica–alumina catalysts, the alumina–boria catalyst and the silica–magnesia catalyst, a dependence of the loss in conversion per milliequivalent of alkali ion on the size of the ion is observed. The precision of the data does not permit a definite choice to be made between the radius and the square of the radius as the correlating variable for these catalysts.

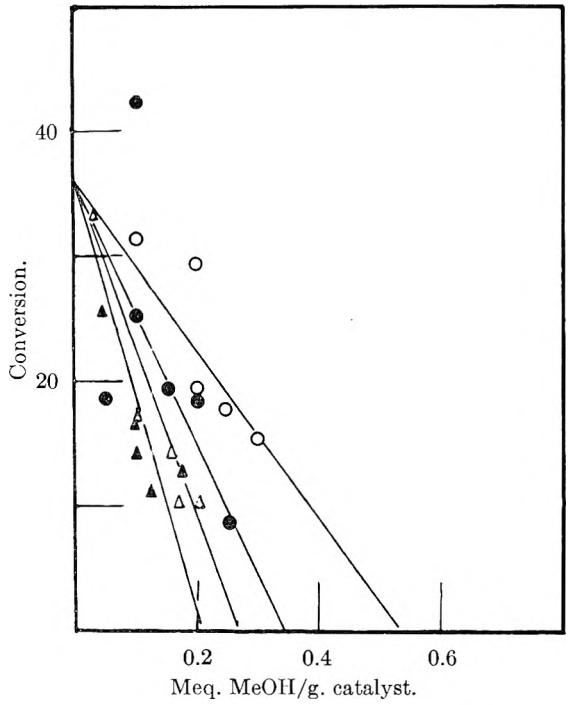

Fig. 6.—Alumina–boria catalyst: ○, LiOH; ●, NaOH; △, KOH; ▲, CsOH.

It is definitely shown that the silica–magnesia and alumina–boria catalysts are more sensitive to alkali ions than those silica–alumina catalysts. This comparison is particularly emphasized for the two smaller ions, lithium and sodium, where the precision of the values is greater. Thus the loss in conversion per milliequivalent of lithium ion is 2.8 to 3.6 on the silica–alumina composites, about 5.5 for the silica–magnesia, and 6.2 to 7.0 for the alumina–boria catalyst.

It would be convenient for purposes of correlation to assign specific drops in conversion per milliequivalent to each different chemical composite. However, data from other sources show that certain high density, low activity silica–alumina catalysts have losses in conversion per milliequivalent that correspond to those observed for the silica–magnesia and alumina–boria catalysts.

The variation for the losses in conversion per milliequivalent was from 3 to 8 with the lithium hydroxide, and from 14 to 22 for cesium hydroxide with the ranges for sodium and potassium falling at intermediate values. The reasons why different catalysts may have different sensitivities to poisoning by alkali ions cannot be given with certainty.

Summary.—The conversion of cetane as a function of the amounts of certain alkali ions has been determined for several silica-alumina catalysts, an alumina–boria catalyst and a silica–magnesia catalyst. A mechanism for the disappearance of active sites on calcination which is consistent with the data has been suggested.

Acknowledgment.—The assistance of Mr. Wayne Ohline and the financial assistance of the Office of Naval Research and the Research Corporation are greatly appreciated.

(4) Joseph D. Danforth, THIS JOURNAL, **59**, 564 (1955).

SORPTION OF VAPORS BY HIGH POLYMERS

BY BRUNO H. ZIMM AND JOHN L. LUNDBERG

General Electric Research Laboratory, The Knolls, Schenectady, N. Y.
Bell Telephone Laboratories, Inc., Murray Hill, N. J.

Received September 13, 1955

Some alternatives to the Flory–Huggins–Guggenheim treatment of sorption of liquids by polymers are examined, using data on three systems, water–collagen, benzene–rubber and toluene–polystyrene. It is found that a simple rigid site type of sorption theory is illuminating for the hydrocarbon systems but breaks down badly when applied to water–collagen mixtures. However, an exact "clustering" theory may be applied to all three of these systems. This theory, which is based on the statistical mechanics of fluctuations, does not compete with the Flory–Huggins–Guggenheim treatment in that it does not predict isotherms, but it does serve to interpret them in molecular terms.

We present in this paper some theoretical considerations that we have found useful for treating data on the vapor pressures of liquids sorbed by polymers. Although extensive advances have been made with the theory of high polymer solutions, it can hardly be said that all the details are yet clear. For solutions dilute in polymer there is the well grounded but imperfectly worked out theory based on virial coefficients.[1-3] In general, there are the theory of Flory[4] and Huggins[5] and the improved quasi-chemical version of the same theory worked out by Guggenheim.[6] Valuable though the latter are, it is still necessary to use a parameter, generally called μ, whose molecular interpretation is obscure and which as yet must be considered to be empirical.[6] Our considerations are not intended as a replacement for the previous theories, but as an adjunct thereto, interpreting experimental data in molecular terms.

Concentrated Solutions.—Let us consider first the initial sorption of liquid by a dry polymer. The Flory–Huggins–Guggenheim theory gives an equation that fits the experimental solvent activities of approximately athermal systems within a factor of about two in this region without using the parameter μ, but the existing derivations of the theory are not notably perspicuous and it is difficult to see clearly the source of the remaining differences with the experimental data. It is not surprising, therefore, that there have been attempts to use theories originally designed for rigid adsorbates. Dole,[7] for example, has discussed several of these possibilities.

We define in the usual way the activity a_1 and volume fraction φ_1 of a volatile material (component 1) dissolved in a high polymer (component 2) by the equations

$$a_1 = f_1/f_1^\circ$$
$$\varphi_1 = N_1 v_1/V \qquad (1)$$

with f_1 and f_1° the fugacities of component 1 in the solution and in the pure state, respectively, and N_1 the number of molecules of component 1 of partial molecular volume v_1 in the mixture of total volume V. The activity a_1 and the volume fraction φ_1 are related by

$$a_1 = \gamma_1 \varphi_1 \qquad (2)$$

where γ_1 is the volume fraction activity coefficient; γ_1 becomes the familiar Henry's law constant if γ_1 is invariant with φ_1 at small values of φ_1.

A discussion of γ_1 at low solvent concentrations may be based on the familiar derivation of the Langmuir adsorption isotherm as given, for example, by Fowler and Guggenheim.[8] We suppose that both the polymer and the pure liquid are divided into cells, each able to receive one molecule of component 1. Then from Fowler and Guggenheim's result we get, at small values of N_1

$$a_1 = \frac{J_1 N_1}{J_s N_s} \exp(q/kT) \qquad (3)$$

where J_1 and J_s are the partition functions for internal degrees of freedom (including vibrations) of the molecules of component 1 in the pure liquid and in the polymer cells, respectively, N_s is the number of cells in the polymer, and q is the energy of transferring a molecule of component 1 from the pure phase to the solution at absolute zero. If this equation is substituted into eq. 2, the activity coefficient is found to be

$$\gamma_1 = (V/N_s v_1)(J_1/J_s) \exp(q/kT) \qquad (4)$$

This expression for γ_1 contains three factors, the last of which is readily understood as a Boltzmann weighting factor accounting for the difference in the zeros of energy of the cells in the pure component 1 and in the solution. The first of the other factors is the ratio of the volume of the solution, which is approximately that of the polymer, to the volume of a "monolayer" of sorbed liquid. The second factor, the ratio of the partition functions, measures the ratio of the free volumes associated with the cells of pure component 1 and of the solution. Since there seems to be no way of observing separately the effects of the first and second factors, we make the convenient simplification of calling the ratio of the partition functions unity.

The experimental results for non-polar polymers are understandable in terms of this model. A marked difference is found between the values of γ_1 for ordinary solutions and for small molecules sorbed by a high polymer. For an ideal solution, γ_1 is unity, but it is typically about four or five for athermal polymer–solvent mixtures at low solvent concentrations. The following tentative interpretation seems reasonable. In ordinary liquids another molecule can be added easily, the molecules already present adjusting to make room for it. In a polymer, however, a space for a new molecule can

(1) B. H. Zimm, *J. Chem. Phys.*, **14**, 164 (1946).
(2) M. L. Huggins, THIS JOURNAL, **52**, 248 (1948).
(3) P. J. Flory and W. J. Krigbaum, *J. Chem. Phys.*, **18**, 1086 (1950).
(4) P. J. Flory, *ibid.*, **10**, 51 (1942).
(5) M. L. Huggins, *Ann. N. Y. Acad. Sci.*, **43**, 9 (1942).
(6) E. A. Guggenheim, "Mixtures," Oxford University Press, London, England, 1952, Chap. XII.
(7) M. Dole, *Ann. N. Y. Acad. Sci.*, **51**, 705 (1949).
(8) R. Fowler and E. A. Guggenheim, "Statistical Thermodynamics," Cambridge University Press, London, England, 1939, p. 427.

be made only by prying several polymer chains apart. Usually this will make a wedge-shaped cavity of the wrong shape for the entering molecule. The factor $(1/\gamma_1)\exp(q/kT)$ then can be thought of as the fraction of the polymer that can form cavities of the proper shape and size.

While this point of view may seem strange to a person used to the current theories of polymer solutions, we feel that it is not really fundamentally different. In our case we recognize the existence of geometrical restrictions to the configurations of the chains by postulating that only a fraction of the polymer can form suitable cavities for the entering solvent molecules. In the Flory–Huggins–Guggenheim theory, for example, geometrical restrictions are implicit in the requirement that the segments of each polymer chain lie on a sequence of adjacent sites of the lattice. Our purpose in returning to a very simple, in fact, naive, point of view is to focus attention on the underlying geometrical problem, a problem that is frequently forgotten in the complexities of the calculations.

The Flory–Huggins–Guggenheim theory of athermal polymer solutions gives

$$a_1/\varphi_1 = \gamma_1 = [1 - 2\mu(1 - \varphi_1)]^{-1/2\mu} \qquad (5)$$

for the activity coefficient of solvent in the presence of polymer of infinite molecular weight. According to Flory's formulation of the theory,[4] μ is zero. Thus, eq. 5 simplifies to

$$a_1/\varphi_1 = \gamma_1 = \exp \varphi_2 \qquad (6)$$

and γ_1 takes on the value 2.718 . . . . in the limit of zero solvent concentration ($\varphi_2 = 1$). In Huggins'[5] and Guggenheim's[6] developments of the theory, the μ of eq. 5 has the value $1/z$ where z is the coördination number of the assumed lattice. Thus, if $z = 6$, the limiting value of γ, is 3.375. These are remarkably close to the experimental values quoted below considering the simplifications in the theories. Of course, the experimental values always can be reproduced exactly by adjusting μ.

The Clustering Function.—The simple theory described above is useful for understanding the gross changes in the limiting value of the activity coefficient γ_1 from system to system, but it is too crude to be of much value for describing the change of activity with concentration in one system. As we remarked before, the Flory–Huggins–Guggenheim theory also is not quite exact enough. Fortunately there is an exact method which at least allows us to recast the problem.

We define the *molecular pair distribution function*, $F_2(i,j)$, by the statement that

$$(1/V^2)\, F_2(\mathrm{i,\ j})\ \mathrm{d(i)}\ \mathrm{d(j)}$$

is the probability that the molecules i and j are each at the positions specified by the coördinates (i,j) in the range of these coördinates d(i) and d(j). The cluster integral G_{11} is defined by

$$G_{11} = (1/V)\int\int [F_2(i,j) - 1]\mathrm{d(i)}\ \mathrm{d(j)} \qquad (7)$$

where i and j are now molecules of components 1. The quantity $\varphi_1 G_{11}/v_1$ is the mean number of type 1 molecules in excess of the mean concentration of type 1 molecules in the neighborhood of a given type 1 molecule; thus, it measures the clustering tendency of the type 1 molecules. A relation[9] has been derived between the activity coefficient, $\gamma_1 = a_1/\varphi_1$, and G_{11}

$$G_{11}/v_1 = -\varphi_2[\partial(a_1/\varphi_1)/\partial a_1]_{P,T} - 1 \qquad (8)$$

where $\varphi_2 = 1 - \varphi_1$ is the volume fraction of component 2. This relation is generally valid for systems of negligible compressibility.

When the activity coefficient does not vary with concentration, as for example in the case of an ideal solution, G_{11} is minus one molecular volume. This means that a particular type 1 molecule in such a system excludes its own volume to the other molecules but otherwise does not affect their distribution. This is what would be expected for an ideal solution, of course.

For athermal polymer solutions, however, we shall see that $\gamma_1 = a_1/\varphi_1$ decreases with increasing φ_1 so that G_{11}/v_1 is greater than -1 and may actually become positive. This can only mean that the concentration of type 1 molecules is higher than average in the neighborhood of a given type 1 molecule, or, in other words, that the type 1 molecules cluster together. We believe that this means that the first solvent molecules to enter the polymer structure loosen the structure and make it easier for subsequent molecules to enter in the neighborhood of the first than to go elsewhere. A string of molecules might occupy one wedge-shaped cavity, for example.

Clustering also occurs, even in solutions of molecules of ordinary size, when there are unequal intermolecular forces such as when heat is absorbed or evolved on mixing.

Huggins' and Guggenheim's derivation of the theory predicts solvent clustering of

$$G_{11}/v_1 = 2/(z - 2) \qquad (9)$$

found by inserting eq. 5 in eq. 8. Similarly, by combining eq. 6 and eq. 8, Flory's treatment gives

$$G_{11}/v_1 = 0 \qquad (10)$$

Thus, Flory's derivation without heat of mixing ($\mu = 0$) corresponds to just enough clustering to overcome the effect of the excluded volume of the central molecule, while the more complicated treatments of Huggins and Guggenheim ($\mu = 1/z$) correspond to increased clustering.

As a further example, eq. 8 may be applied to the Langmuir isotherm

$$a_1 = cN_1/(N_s - N_1) = cv_s\varphi_1/(v_1\varphi_2 - v_s\varphi_1) \qquad (11)$$

where c is a constant, v_s is the volume of adsorbing material per site, and φ_2 the volume fraction of adsorbing material in the mixture. If the differentiations are performed, we obtain the result

$$G_{11}/v_1 = -2 - v_s/v_1 + (1 + v_s/v_1)\varphi_1 \qquad (12)$$

Thus at high coverages (φ_1 approaching $v_1/(v_1 + v_s)$) the excluded volume is the volume of the adsorbed molecule plus the site on which it is adsorbed, while at low coverages it is somewhat greater.

Application to Experimental Data.—The activity coefficients (equation 2) at zero concentration ($\varphi_1 = 0$) and the clustering functions, eq. 7 and 8, have been calculated for the polar system, water-

(9) B. H. Zimm, *J. Chem. Phys.*, **21**, 934 (1953).

collagen,[10] and the non-polar system toluene–polystyrene[11] and benzene–rubber.[12] Activities were calculated from vapor pressure ratios using the Berthelot equation for gas imperfections of toluene and benzene and Keyes' data for water.[13] Additivity of volumes was assumed in calculating volume fractions; this probably leads to some error, but not enough to be important in the present discussion. The data and the calculated results are shown in Figs. 1 and 2 and Table I.

TABLE I

VALUES OF THE VOLUME FRACTION ACTIVITY COEFFICIENT γ_1 EXTRAPOLATED TO ZERO SOLVENT ACTIVITY AND CONCENTRATION

System	$\lim_{\varphi_1 \to 0} (a_1/\varphi_1) = \lim_{\varphi_1 \to 0} \gamma_1$ 25°	40°	50°	75°
Water–collagen	0.30	0.56		
Toluene–polystyrene	4.1		~5.7	~6.7
Benzene–rubber	4.3			

We consider first the non-polar systems. The activity curves for both of them are very similar (Fig. 1). Both values of the activity coefficients, as the solvent concentration approaches zero, are very near four; the possible significance of this in terms of the polymer structure is discussed above. The clustering functions, Fig. 2, show some oscillation, which may not be real, around an average value of about plus one. This is somewhat higher than the theoretical values given above. In part the difference may be caused by clustering resulting from intermolecular attraction; however, since the heat of dilution is positive in the benzene–rubber system[12] and negative in the toluene–polystyrene system,[11] it seems futile to try to estimate a correction. The authors offer the hypothesis that the dilution heats in these systems arise in large part from the internal energy changes associated with changes of shape of the chain molecules on dilution, and that the differences in the intermolecular attractions are probably of small significance in these two systems.

Comparison of these experimental results with theory indicates that the simple Flory theory and, to a lesser extent, the more complicated theories of Huggins and Guggenheim underestimate the inhomogeneity of the solution, with the result that both the Henry's law constant and the clustering function from these theories are too small.

The system water–collagen represents a common type that appears to be quite different from the non-polar mixtures. The initial water is tightly bound, as seen by the large negative heat of sorption (−6600 cal./mole, according to Dole and McLaren[14]) and the small value of the limiting activity coefficient. The heat of sorption is so large that eq. 4 leads to absurdly small results for the volume of a monolayer. The difficulty probably lies in the neglect of the effect of the water molecules on the structure of the protein, which could give rise to an additional entropy term of considerable magnitude.

The clustering function contains no such inaccuracies, so its results should be more significant. We can estimate from Fig. 2 that G_{11} is initially less than minus ten molecular volumes, which can be interpreted to mean that there is less than one mole of initial sorption sites in 180 ml. of collagen, or less than 0.79 mole of sorption sites per 100 g. This may be considered to agree with Dole's figure of 0.56 mole per 100 g.[7] estimated from the Langmuir isotherm, in view of the difficulty in accurately estimating initial slopes from the data. As more

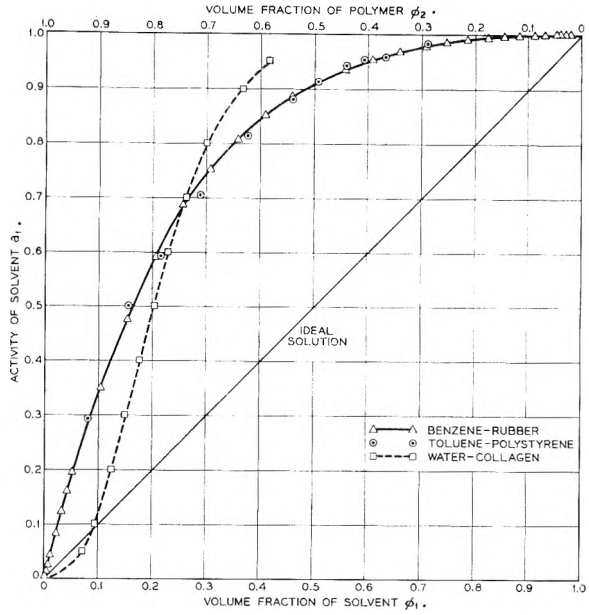

Fig. 1.—Activities of solvents *versus* volume fractions of solvents and polymers for benzene–rubber, toluene–polystyrene and water–collagen at 25°.

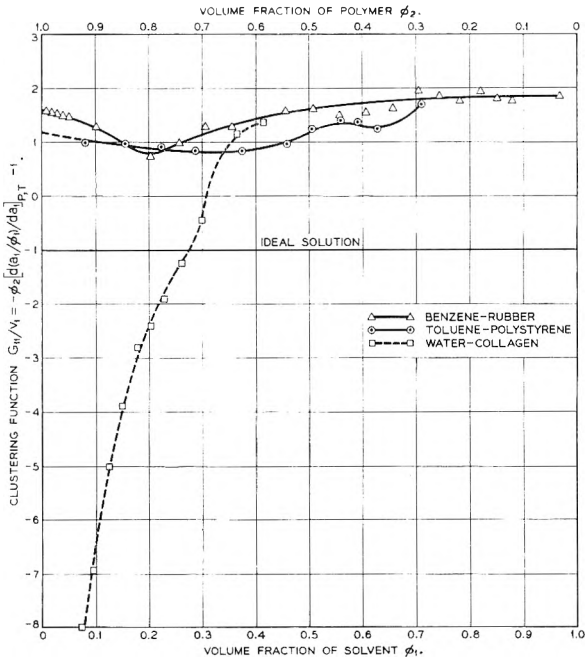

Fig. 2.—Clustering functions of solvents *versus* volume fractions of solvents and polymers for benzene–rubber, toluene–polystyrene and water–collagen at 25°.

(10) H. B. Bull. *J. Am. Chem. Soc.*, **66**, 1499 (1944).

(11) Data of J. L. Lundberg, to be published.

(12) G. Gee and L. R. G. Treloar, *Trans. Faraday Soc.*, **38**, 147 (1942).

(13) F. G. Keyes, *J. Chem. Phys.*, **15**, 602 (1947).

(14) M. Dole and A. D. McLaren, *J. Am. Chem. Soc.*, **69**, 651 (1947).

water is sorbed, the clustering function rises, finally reaching the value of plus one, which is normal for a polymer, just before the collagen is saturated. The clustering function thus shows, without the necessity of a model, how the sorption process changes with increasing water content from one of sorption on a few highly specific sites to a diffuse swelling phenomenon.

THE POLAR PROPERTIES OF SOLVENT AND THE CONDUCTANCE OF ELECTROLYTES AT INFINITE DILUTION[1]

BY EDWARD S. AMIS

Contribution from the Chemistry Department of The University of Arkansas, Fayetteville, Arkansas

Received September 19, 1955

The deviation from Walden's rule calculated as ionic radii show solvation to be selective with the ions clinging preferentially to the more polar constituent of the solvent even at relatively low concentrations (20% or less) of this component. An effective distance of electrostatic attraction of ions and molecules is found to be fairly constant for different solutes in different mixed solvents due to the cancellation of the effect of the moment in the numerator and the dielectric constant in the denominator of the mathematical expression for this distance of electrostatic attraction.

At infinite dilution the electrophoretic and time of relaxation effects vanish. Then the resistance of the medium to the motion of an ion toward an electrode must balance the electrostatic attraction of the electrode for the ion since an ion acquires a velocity proportional to the applied potential and Ohm's law holds for electrolytic solutions.

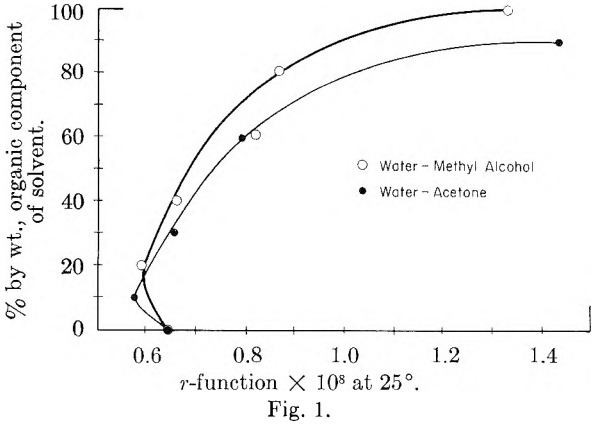

Fig. 1.

Thus by balancing electrostatic and resistance forces, Walden's rule is obtained and is expressed mathematically by the equation

$$\Lambda_0 = \frac{\epsilon\mathfrak{F}}{1800\pi\eta}\left(\frac{Z^+}{r^0_+} + \frac{Z^-}{r^0_-}\right) \qquad (1)$$

where Λ_0 is the equivalent conductance at infinite dilution of an electrolyte possessing positive ions of valence Z^+ and radius r^0_+ and negative ions of valence Z^- and radius r^0_- ϵ is the electronic charge, $\mathfrak{F}$ is the faraday and η is the viscosity of the medium.

For a uni-univalent electrolyte $Z^+ = Z^- = 1$ and

$$\Lambda_0 = \frac{\epsilon\mathfrak{F}}{1800\pi\eta}\left(\frac{1}{r_0^+} + \frac{1}{r_0^-}\right) \qquad (2)$$

If $r_0^+ = r_0^- = r_0$

$$\Lambda_0 = \frac{\epsilon\mathfrak{F}}{900\pi\eta r_0} \qquad (3)$$

Thus if r_0 is constant

$$\Lambda_0\eta = \text{constant} \qquad (4)$$

Actually when $\Lambda_0\eta$ is calculated for the same solute in different solvents, the value is found to vary widely and especially in going from aqueous to organic solvent solutions. These variations which may be over 100% are generally attributed to variations of the r-function with change of solvent.

If from equation 2 the value of $(1/r_0^+ + 1/r_0^-)$ is found and the reciprocal $r_0^+r_0^-/(r_0^+ + r_0^-)$ (hereafter designated as the r-function) of this quantity is obtained, this reciprocal quantity is of the order of r_i an ionic radius. Some interesting conclusions can be drawn from such calculations which are presented in Table I.[2] One would conclude from the values of the r-function that for KCl in water and in water–methyl alcohol at the three temperatures specified and in H_2O–$(CH_3)_2CO$ at one temperature that solvation is to some extent preferential, the K^+ and Cl^- ions clinging rather exclusively to more polar water up to 30 or 40 weight % of the organic component and holding relatively tightly to water even until it is entirely replaced. The latter conclusion is practically inescapably demonstrated by the sudden large increase of the r-function with the replacement of the last few percentage of water by the larger molar volume organic component. A plot of the r-function *versus* percentage organic component for KCl in H_2O–MeOH and H_2O–$(CH_3)_2CO$ solvents is given in Fig. 1. The minima at low percentages of organic component of the solvent may be significant. Landskroener[3] discusses anomalies which occur in the region of ten weight % of the organic component of mixed solvents.

It is apparent therefore that the fact that $\Lambda_0\eta$ changes rapidly in going from water containing solvent to organic solvent can be due to this rapid change of the r-function when the last water is removed from the solvent.

If, instead of an actual radius, one calculates the distance at which the ion can exert a solvation force on dipolar molecules, this will result in a more

(1) The author wishes to thank the National Science Foundation for a grant that made this research possible.

(2) Calculated from the data of: (a) N. G. Foster and E. S. Amis, *J. physik. Chem.*, Neue Folge, **3**, 5/6 (1955); and (b) Argawala and Manderville, *J. Indian Chem. Soc.*, **12**, 699 (1935).

(3) P. A. Landskroener, Dissertation, submitted to the Graduate School of the Catholic University of America in partial fulfillment of the requirement for the degree of Doctor of Philosophy, 1954.

TABLE I

CALCULATED VALUES OF THE r-FUNCTION FROM THE EQUIVALENT CONDUCTANCE AT INFINITE DILUTION

Organic solvent	% by wt.	Λ_0	η	D	$\frac{(r_+^0 + r_-^0)}{(r_+^0 r_-^0)} \times 10^{-7}$	$\frac{(r_+^0 r_-^0)}{(r_+^0 + r_-^0)} \times 10^8$
			Potassium Chloride			
			25.00 ± 0.01°			
MeOH	0.0	150.3	0.008494	78.54	15.58	0.642
	20.2	99.2	.01395	69.2	16.77	.596
	40.2	78.2	.0159	59.6	15.18	.659
	60.7	74.2	.0135	49.8	12.22	.818
	80.7	91.5	.0103	39.1	11.50	.870
	100.0	104.8	.00545	31.5	6.97	1.435
			35.00 ± 0.01°			
MeOH	0.0	180.0	0.00720	74.9	15.82	0.632
	20.2	123.9	.0107	65.8	16.18	.618
	40.2	97.4	.0122	56.3	14.50	.690
	60.7	92.1	.0108	46.9	12.14	.824
	80.7	109.4	.00834	37.5	11.14	.898
	100.0	119.9	.00477	29.9	6.98	1.433
			45.00 ± 0.01°			
MeOH	0.0	211.0	0.00597	71.5	15.37	0.651
	20.2	149.9	.00832	62.6	15.22	.657
	40.2	117.4	.00952	53.5	13.64	.733
	60.7	112.9	.00868	44.2	11.96	.836
	80.7	129.7	.00690	35.3	10.92	.916
	100.0	136.7	.00420	28.3	7.01	1.427
$(CH_3)CO$	0.0 (pure H_2O)	150.3	0.008494	78.54	15.58	0.642
	10.0	129.3	.01054	73.0	16.63	.601
	30.0	97.4	.01286	61.0	15.29	.654
	60.0	82.0	.01264	41.8	12.65	.791
	90.0	105.9	.00504	24.0	6.51	1.536
			Tetramethylammonium chloride			
CH_3OH	100.0	121.7	0.00545	31.5	8.09	1.236
C_2H_5OH	100.0	51.9	0.0109	24.3	6.90	1.449
			Tetraethylammonium picrate			
CH_3OH	100.0	116.7	0.00545	31.5	7.76	1.289
C_2H_5OH	100.0	54.95	0.0109	24.3	7.31	1.368
			Sodium chloride			
	0.0 (pure H_2O)	126.45	0.008494	78.54	13.11	0.763
CH_3OH	100.0	69.90	.00545	31.5	4.65	2.151
C_2H_5OH	100.0	42.5	.0109	24.3	5.65	1.770

constant value since as the dielectric constant goes up and thus tends to reduce the force, the effective moment goes up and tends to increase the force. The reverse holds for the case when the dielectric constant is lowered.

The actual radius r_i of a solvated ion will be considered to be the radius r_i° of the non-solvated ion plus a term proportional to the electrostatic attractive force between the ion and the dipolar molecules of solvent. This can be represented by the equation

$$r_i = r_i^\circ + KF \qquad (5)$$

where r_i° is the radius of the unsolvated ion, F is the coulombic electrostatic force of attraction between the ion and the solvent dipoles and K is a constant. Let us assume that r_i is small compared to the distance at which electrostatic forces can be exerted, *i.e.*, assume $r_i^\circ \angle KF$, then

$$r_i \cong KF \qquad (6)$$

Neglecting higher order effects the coulombic electrostatic force between an ion and a dipole can be represented by the equation

$$F = \frac{2z_i\epsilon\mu\cos\theta}{Dr_s^3} \qquad (7)$$

and for head-on alignment of the ion and the dipole

$$F = \frac{2z_i\epsilon\mu}{Dr_s^3} \qquad (8)$$

In equations 7 and 8 z_i is the valence of the ion, ϵ is the charge on the electron, μ is the dipole moment of the molecule, r_s is the distance between the ion and the dipole at which the force is F, and θ is the angle which a line drawn from the ion to one of the centers of charge of the dipole makes with the line determined by the centers of charge of the dipole, then

$$r_i \cong KF = \frac{2Kz_i\epsilon\mu}{Dr_s^3} = \frac{2K\epsilon\mu}{Dr_s^3} \qquad (9)$$

TABLE II

THE VALUES OF r_s FOR ION–DIPOLE SOLVATION DISTANCES

Wt. % organic component of solvent	Λ_0	D	η	μ of solvent molecule in D	Temp., °C.	$r_s \times 10^8$ ion–dipole solvation distance	Dev. from av.
			KCl				
0.00	150.3	78.54	0.008494	1.84	25	12.06	0.55
0.00	180.0	74.9	.00720	1.84	35	12.31	.30
0.00	211.0	71.5	.00597	1.84	45	12.38	.23
20.2% MeOH	99.2	69.2	.01395	1.82	25	12.87	.26
40.2% MeOH	78.2	59.6	.0159	1.80	25	13.01	.40
60.7% MeOH	74.2	49.8	.0135	1.77	25	12.78	.17
80.7% MeOH	91.5	39.1	.0103	1.73	25	13.47	1.14
100.0% MeOH	104.8	31.5	.00545	1.68	25	12.13	0.48
100.0% MeOH	119.9	29.9	.00477	1.68	35	12.35	.26
100.0% MeOH	136.7	28.3	.00420	1.68	45	12.69	.08
						Av.	± .35
			NaCl				
0.00	126.45	78.54	0.008494	1.84	25	11.38	
100.0% MeOH	69.90	31.5	.00545	1.68	25	10.60	
100.0% EtOH	42.5	24.3	.0109	1.70	25	12.38	
			$(CH_3)_4Cl$				
100.0% MeOH	121.7	31.5	0.00545	1.68	25	12.75	
100.0% EtOH	51.5	24.3	.0109	1.70	25	13.24	
			$(C_2H_5)_4N$ Picrate				
100.0% MeOH	116.7	31.5	0.00545	1.68	25	12.57	
100.0% EtOH	54.9	24.3	0.0109	1.70	25	13.49	

for univalent ions.

Substituting this r_i for r_0 in equation 3 yields

$$\Lambda_0 = \frac{\epsilon\mathfrak{F}}{900\pi\eta r_0} = \frac{\epsilon\mathfrak{F}}{900\pi\eta} \times \frac{Dr_s^3}{2K\epsilon\mu} = \frac{Dr_s^3\mathfrak{F}}{1800\pi\eta K\mu} \quad (10)$$

$$r_s = \sqrt[3]{\frac{1800\pi\eta K\mu\Lambda_0}{D\mathfrak{F}}} \quad (11)$$

As indicated before this r_s has a much greater possibility of being constant than has the radius of the ion. Equation 11 confirms this since when the dielectric constant D, which occurs in the denominator, decreases the dipole moment μ which occurs in the numerator likewise decreases and *vice versa*.

In Table II values of r_s as calculated by equation 11 are tabulated. It can be seen that the constancy is much greater for these than for the Walden's rule r-functions. In fact the average deviation from the average is less than 3% for the entire range of solvent composition for KCl in water and water–methanol solvents and at the three temperatures. When the data for tetramethylammonium chloride and tetraethylammonium picrate are included the average value for r_s is 12.72 and the average deviation from the average is ±0.32 or considerably less than 3%. Sodium chloride in water and in methyl alcohol does give abnormal values of r_s. However, the value for r_s for this salt in ethyl alcohol has a normal value (12.38). No viscosity data were available for water–acetone solvent.

All these calculations were made assuming K to be unity. Since the values do approach molecular dimensions K cannot differ markedly from one. The moment, μ, used in these calculations was taken as $\mu = N_1\mu_1 + N_2\mu_2$, where N_1 and N_2 are the mole fraction and μ_1 and μ_2 the dipole moments of the respective two components. It would probably have been better to have calculated the moments from the additivity of the polarizations of the components, but it is doubtful that the results would have differed enough from those given here to have merited the trouble of making the more nearly correct calculation. The dielectric constant, D, was taken from the data of Åkerlöf.[4]

A mathematical expression corresponding to Walden's rule would be from equation 11

$$\sqrt[3]{\frac{\Lambda_0\eta\mu}{D}} = \text{constant} \quad (12)$$

The third power of this expression will not be so constant, however, since any variations from constancy will be magnified in the cube of the expression. Nevertheless, even the cube will show much greater constancy than does the Walden expression $\Lambda_0\eta$ or than does the r-value calculated from the Walden rule.

(4) G. Åkerlöf, *J. Am. Chem. Soc.*, **54**, 4125 (1932).

VISCOSITY OF ALFIN POLYISOPRENE AT VERY SMALL AND QUITE HIGH RATES OF SHEAR[1]

BY MORTON A. GOLUB

Contribution from the B. F. Goodrich Company Research Center, Brecksville, Ohio

Received September 20, 1955

The shear dependence of viscosity of dilute benzene solutions of Alfin polyisoprene fractions varying in molecular weight from about 700,000 to 5,000,000 was studied at rates of shear from about 100 to 20,000 sec.$^{-1}$. Shear data over the range 0–600 sec.$^{-1}$ are very well represented by the linear expression, $\eta_D = \eta_0(1 - aD)$, while the series expression, $\eta_D = \eta_0(1 - aD + bD^2)$ is adequate for shear rates up to about 3–4000 sec.$^{-1}$. Thereafter the shear dependence takes the form $\eta_D = \eta_\infty + (\eta_0 - \eta_\infty)e^{-kD}$. These relations hold both for the reduced and the intrinsic viscosities. The maximum change in the intrinsic viscosity under shear, *i.e.*, $[\eta]_0 - [\eta]_\infty$, is proportional to the square of the zero shear intrinsic viscosity, and essentially independent of the molecular weight distribution. Likewise, the slope of the limiting tangent to the $[\eta]$ *vs.* D curve is proportional to $[\eta]_0^2$. Since the η *vs.* D plot is virtually linear over the restricted range 100–500 sec.$^{-1}$, extrapolation of such data to the ordinate provides a simple and accurate method for determining the zero shear viscosity. The theoretical equation proposed recently by F. Bueche fits the present data tolerably well up to about 12,000 sec.$^{-1}$, beyond which point the Bueche curve falls steadily below the experimental points. Some modification of the Bueche equation is required in order to take into account the levelling-off of the viscosity–shear curve at high rates of shear.

Introduction

In previous publications[2,3] both the inherent and the intrinsic viscosities of Alfin polyisoprene were shown to be strongly shear dependent, the effect increasing with increasing molecular weight. The viscosity decreases with increasing rate of shear in an approximately linear fashion in the neighborhood of small gradients, while it tends to level off to some limiting value at fairly high shear rates. The data apparently contradict the theoretical prediction, due to Kuhn and Kuhn,[4] of a horizontal tangent to the viscosity–shear curve at zero rate of shear. Instead of being represented by an even-powered series expression

$$\eta_D = \eta_0(1 - aD^2 + bD^4 - \ldots) \qquad (1)$$

where η_D and η_0 are the viscosities at shear rates D and zero, respectively, and a, b, etc., are constants, the data are fitted by

$$\eta_D = \eta_0(1 - aD + bD^2) \qquad (2)$$

quite well, at least over the range of shear rates up to about 3–4000 sec.$^{-1}$. At gradients below about 1000 sec.$^{-1}$, it was assumed that eq. 2 reduces to the linear form

$$\eta_D = \eta_0(1 - aD) \qquad (3)$$

Now, previous viscosity measurements were carried out over the shear range of about 1000 to 10,000 sec.$^{-1}$, and there is consequently the need for accurate data at very small gradients in order to decide the fundamental question whether the viscosity–shear plot has a finite or zero slope at the origin. Moreover, with indications that this plot approaches a limiting viscosity value at high shear rates, there is considerable interest in examining this point more fully, as well as the shear dependence of viscosity over the entire range of gradients possible. Since the preceding papers dealt with unfractionated polyisoprene, there is likewise interest at present in working with fractionated polymer. This paper reports the results of viscosity measurements on fractions of Alfin polyisoprene covering a wide range of molecular weights at shear rates extending from about 100 to 20,000 sec.$^{-1}$, with emphasis being placed on measurements at very small and quite high rates of shear.

Experimental

Viscosity measurements over the range of shear rates of about 1000 to 20,000 sec.$^{-1}$ were made in a special Ostwald-type viscometer, using a sensitive manostat for applying various external pressures to the liquid in the viscometer. The procedure followed was the same as that described previously.[2]

The viscometer employed for measurements at low shear (approximately 100 to 600 sec.$^{-1}$) was an adaptation of a design recently described by Krigbaum and Flory.[5] It consists of a horizontal capillary, and five efflux bulbs arranged vertically in series, enabling measurements to be made at five different hydrostatic heads in a single flow experiment. A reservoir of suitable dimensions permits several dilutions directly in the viscometer, for convenience in the determination of the intrinsic viscosity. Kinetic energy corrections were calculated for each of the bulbs and applied to all viscosity measurements. The constants of the low shear viscometer are given in Table I. This viscometer was firmly supported in a constant temperature bath set at 25 ± 0.01°, as was also the Ostwald-type viscometer.

TABLE I

CONSTANTS OF THE LOW SHEAR VISCOMETER

Capillary length, 50 cm., radius 0.325 mm.

Efflux bulb	Vol. of bulb, cm.^{3}	Mean head,[a] cm.	Efflux time for C_6H_6 at 25°, sec.	Kinetic energy correction,[b] B/A	% Error in time due to kinetic energy correction
E	3.5	17.8	164.2	77	0.29
D	3.0	14.8	169.1	68	.24
C	2.5	11.8	157.7	59	.24
B	2.0	8.5	187.6	53	.15
A	1.5	5.7	177.8	44	.14

[a] Based on normal loading. The hydrostatic heads are smaller, the benzene flow times larger, and the kinetic energy corrections the same, when dilutions are run in the viscometer. [b] Based on extended Poiseuille equation, $\eta/d = At - B/t$, where t is the efflux time and A and B are instrument constants.

The maximum rate of shear, D, at the wall was calculated by means of the relation

$$D = \frac{rghd}{2\eta l} \qquad (4)$$

where r is the radius of the capillary and l its length, g is the gravitational constant, h is the effective hydrostatic head,

(1) Presented at the 128th meeting of the American Chemical Society, Minneapolis, Minn., September 1955.

(2) M. A. Golub, *J. Polymer Sci.*, **18**, 27 (1955).

(3) M. A. Golub, *ibid.*, **18**, 156 (1955).

(4) H. Kuhn and W. Kuhn, *Helv. Chim. Acta*, **28**, 1533 (1945).

(5) W. R. Krigbaum and P. J. Flory, *J. Polymer Sci.*, **11**, 37 (1953).

d is the liquid density and η is the apparent viscosity of the solution.

Several viscosity measurements carried out on the two viscometers on the same polymer solution at the same gradient (about 750 sec.$^{-1}$) agreed within 1%, indicating that the data obtained from the two instruments could be combined to give a single viscosity–shear plot over the entire shear range of 100 to 20,000 sec.$^{-1}$.

Polyisoprene was prepared by means of a conventional Alfin catalyst[6] to a molecular weight of about 1,500,000. Two samples were fractionated by the usual precipitation of polymer from benzene solution with methanol, providing a number of fractions varying in molecular weight from about 700,000 to 5,000,000 (Table II). The polyisoprene solutions contained tetramethylthiuram disulfide to the extent of 1% on polymer for stabilization. Viscosity measurements were made on benzene solutions of the polymer fractions at concentrations extending from about 0.05 g./dl. down to about 0.01 g./dl.

TABLE II

MOLECULAR WEIGHTS OF POLYISOPRENE FRACTIONS

Fraction	$[\eta]_0$	Mol. wt. $\times 10^{-6}$
1a	16.2	4.80
1c	12.8	3.40
3a	10.3	2.55
3b	7.8	1.73
8	6.1	1.15
9	4.1	0.68

Molecular weights were *estimated* from viscosities by means of the relation

$$[\eta] = 5 \times 10^{-4} M^{0.67} \qquad (5)$$

given for *Hevea*.[7] This expression will have to suffice until a viscosity–molecular weight equation is derived for the Alfin polyisoprenes.

Results

Experimental curves of η_{sp}/c *vs.* D for various concentrations of fraction 1a over the entire shear range of about 100 to 20,000 sec.$^{-1}$ are given in Fig. 1. Reduced viscosity values over the restricted

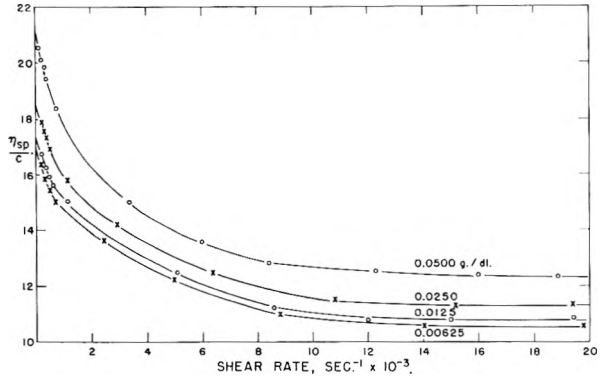

Fig. 1.—Reduced viscosity *vs.* rate of shear for Alfin polyisoprene fraction 1a at various concentrations in benzene at 25°.

range 100 to 600 sec.$^{-1}$ for this fraction, as well as for the other fractions considered in the present work, are given in Fig. 2. It is to be noted that the first four points in each of the curves of Fig. 1 (*i.e.*, at low shear) are the same as those of fraction 1a in Fig. 2, and this indicates that the data obtained from the two viscometers may be properly combined to give the shear dependence over the whole range of gradients under investigation. At quite high rates of shear, the η_{sp}/c *vs.* D curves all level off to limiting viscosity values, beyond which points the polymer solutions behave like Newtonian liquids.

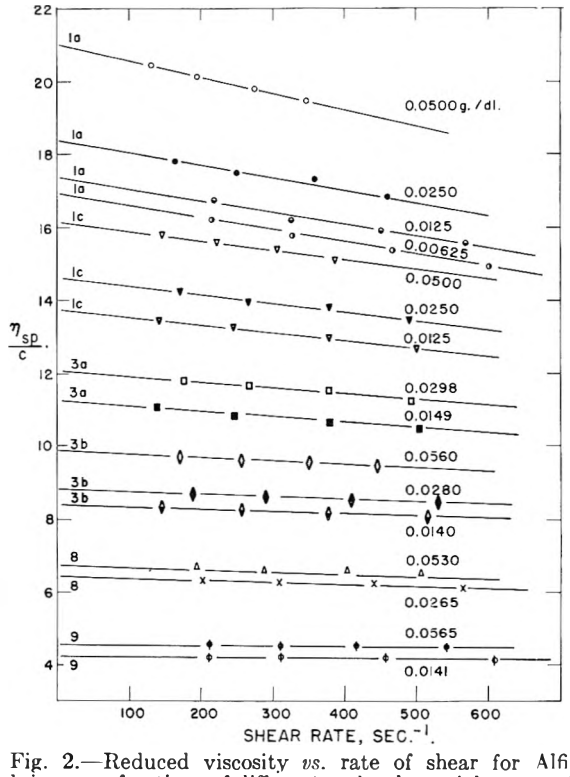

Fig. 2.—Reduced viscosity *vs.* rate of shear for Alfin polyisoprene fractions of different molecular weight at small gradients.

Curves similar to Fig. 1 were obtained for the other polyisoprene fractions but are not presented here. Instead, these η_{sp}/c *vs.* D curves were used to obtain isoshear graphs of η_{sp}/c *vs.* c at various gradients over the whole range. A typical isoshear plot is shown in Fig. 3 for fraction 1a, where η_{sp}/c is seen to vary linearly with c in accordance with the Huggins viscosity–concentration equation. Ex-

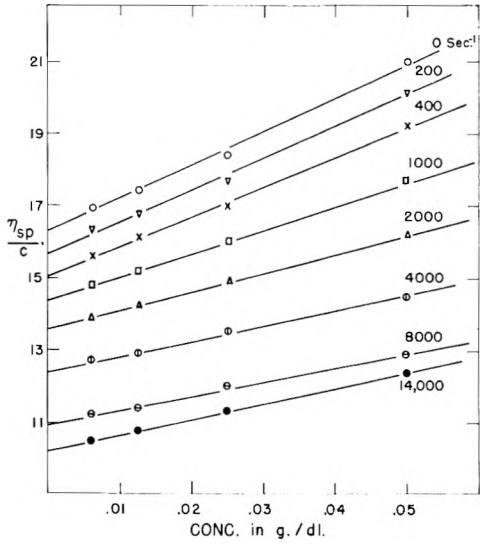

Fig. 3.—Isoshear graph of η_{sp}/c *vs.* concentration for fraction 1a at various gradients.

(6) A. A. Morton, *Ind. Eng. Chem.*, **42**, 1488 (1950).

(7) W. C. Carter, R. L. Scott and M. Magat, *J. Am. Chem. Soc.*, **68**, 1480 (1946).

trapolation of these isoshear lines to zero concentration gives $[\eta]$ at different gradients, and these are plotted in Fig. 4 to give the shear dependence of

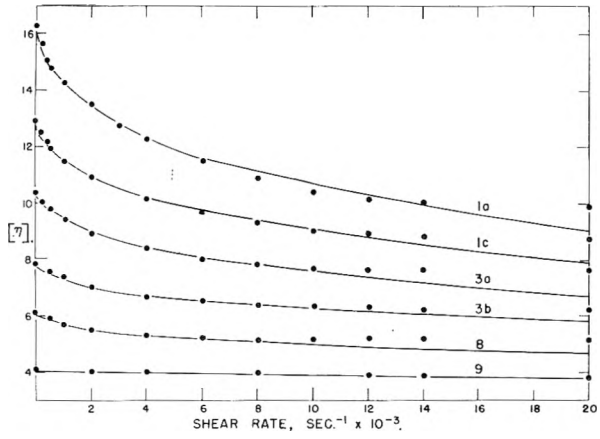

Fig. 4.—Shear dependence of intrinsic viscosity for various fractions of Alfin polyisoprene in benzene at 25°. The points are based on experimental data, while the lines are derived from the Bueche equation.

intrinsic viscosity for the various polymer fractions. Like the reduced viscosity–shear plot, the $[\eta]$ *vs.* D plot levels off at quite high rates of shear. The points of Fig. 4 are based on experimental data, while the lines correspond to attempts to express the data by a theoretical equation proposed recently by Bueche[8] for high molecular weights where segment interactions are important.

Isoshear graphs derived from Fig. 2 were used to obtain the $[\eta]$ *vs.* D curves shown in Fig. 5 for very

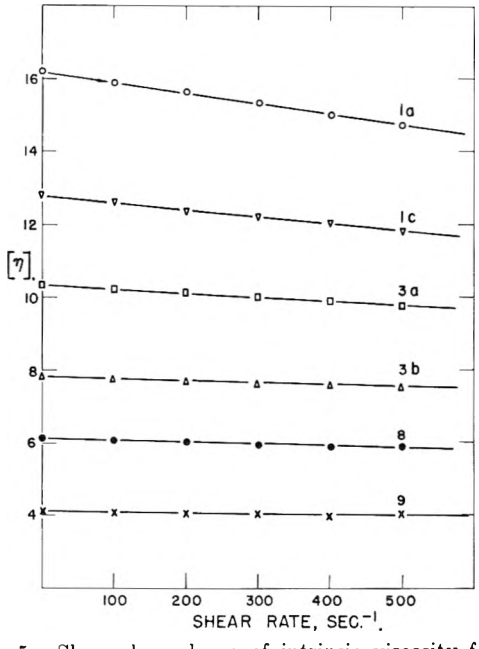

Fig. 5.—Shear dependence of intrinsic viscosity for the various fractions of Alfin polyisoprene in benzene at small gradients.

small gradients. Again, these experimental points may be superimposed on the extended plots of Fig. 4 at the low shear end. They clearly indicate that the limiting effect of shear rate on the intrinsic viscosity is linear in D. The slopes of the $[\eta]$ *vs.* D plots at low rates of shear are proportional to $[\eta]_0^2$, as seen in Fig. 6.

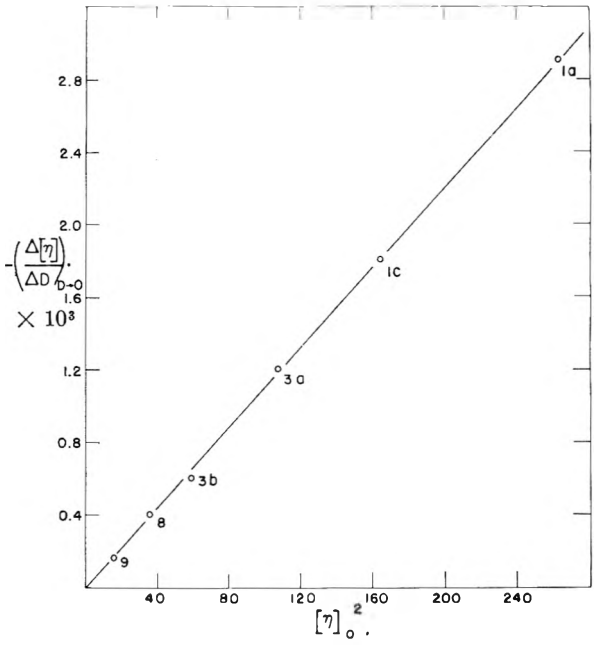

Fig. 6.—The limiting slope of the intrinsic viscosity *vs.* rate of shear curve plotted against the square of the zero shear intrinsic viscosity for various polyisoprene fractions.

The maximum intrinsic viscosity change under shear, *i.e.*, $[\eta]_0 - [\eta]_\infty$, for the various polyisoprene fractions (read off from the curves of Fig. 4) gives a straight line plot against the square of the zero shear intrinsic viscosity, as shown in Fig. 7.

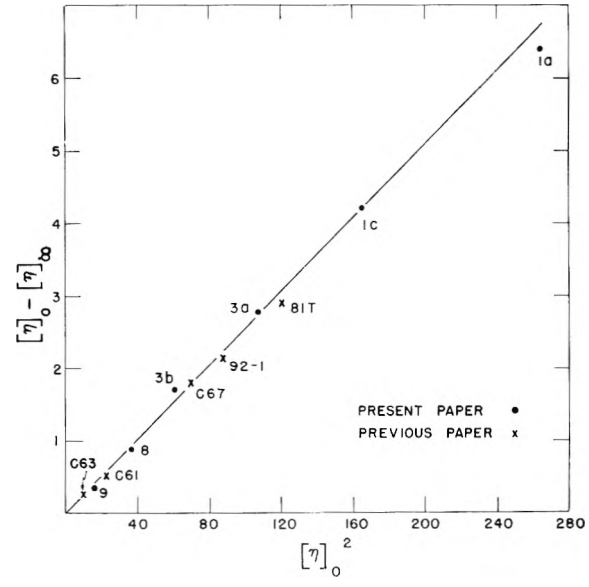

Fig. 7.—The maximum intrinsic viscosity change under shear plotted against the square of the zero shear intrinsic viscosity. The points represent data of fractionated Alfin polyisoprene, and the crosses represent data on unfractionated polyisoprene.

Included in this figure are the results obtained previously[3] for various unfractionated samples of Alfin polyisoprene.

(8) F. Bueche, *J. Chem. Phys.*, **22**, 1570 (1954).

Discussion

The data presented in this paper lead to the following unified picture of the shear dependence of the viscosity for a typical uncharged neutral polymer, such as Alfin polyisoprene. The viscosity decreases rapidly with increase of shear at small gradients, less rapidly at higher gradients and then levels off gradually until at about 10–15,000 sec.$^{-1}$, the polymer solution becomes essentially Newtonian in character (Figs. 1 and 4). Both the reduced viscosity, η_{sp}/c, and the intrinsic viscosity, $[\eta]$, are very well represented by the linear eq. 3 over the range of gradients 0 to 600 sec.$^{-1}$, while the series eq. 2 is adequate for shear rates up to about 3–4000 sec.$^{-1}$. Thereafter, the shear dependence is of the form

$$\eta_D = \eta_\infty + (\eta_0 - \eta_\infty)e^{-kD} \qquad (6)$$

where η_∞ is the limiting viscosity value at very high rates of shear. The suitability of these equations is shown in Table III where representative data for a typical Alfin polyisoprene fraction (1a) are presented. The applicability of each of these forms is confined to the particular range of shear rates just mentioned. Equation 6 is similar to one ob-

TABLE III

SUITABILITY OF VARIOUS EQUATIONS FOR EXPRESSING EFFECT OF SHEAR ON VISCOSITY

Data of Fraction 1a

D, sec.$^{-1}$	η_D, exptl.	η_D from $\eta_D = \eta_0(1 - aD)$	η_D from $\eta_D = \eta_0(1 - aD + bD^2)$	η_D from $\eta_D = \eta_\infty + (\eta_0 - \eta_\infty)e^{-kD}$
0	16.3	16.3	16.3	16.3
500	15.0	15.3	15.4	15.6
1000	14.4	14.4	14.7	15.0
2000	13.5	12.5	13.5	14.0
3000	12.7	...	12.7	13.1
4000	12.3	...	12.3	12.5
6000	11.5	...	12.7	11.5
8000	10.9	...	...	10.9
10000	10.4	...	...	10.4
12000	10.1	...	...	10.2
14000	10.0	...	...	10.1
16000	9.9	...	...	10.0
18000	9.8	...	...	9.9
20000	9.8	...	...	9.8

tained by Philipoff[9] about twenty years ago, *viz.*

$$\eta_D = \eta_\infty + \frac{\eta_0 - \eta_\infty}{1 + \tau^2/b^2} \qquad (7)$$

where τ is the shearing force and b is a constant. It is interesting to note that in several recent studies of the non-Newtonian behavior of high polymer solutions,[10] no formal recognition was made of the levelling-off of the viscosity at high shear rates, even though many of the published curves suggest such an effect. Presumably, had measurements been carried out to high enough rates of shear in those studies, the levelling-off found in the present work would have been observed. Hence, it is safe to assume that the viscosity–shear plot for any other polymer will show the viscosity approach asymptotically a non-zero limit at high rate of shear, although the actual velocity gradient for this to occur will vary from one polymer to the next.

Peterlin[11] and others have shown that for molecules which are not completely soft, the intrinsic viscosity should decrease with increasing velocity gradient as a result of increasing orientation of the polymer molecules in the flow. This serves to explain the observed effect of rate of shear on the viscosity of Alfin polyisoprene. The macromolecules in solution evidently undergo increasing orientation and deformation with increase in shear until at some very high gradient the molecules are as fully oriented or deformed as they possibly can be. Beyond this point, the viscosity remains constant with subsequent increase in shear rate. The quantity $\eta_0 - \eta_\infty$ appears to be of fundamental significance, and may be characteristic for any given polymer–solvent system (at specified molecular weight). Moreover, the ratio of the final and initial values of the viscosity, η_∞/η_0, is related to the rigidity of the molecules. In general, the greater the stiffness of the polymer chains, the greater is the magnitude of the shear effect, and therefore the smaller the actual value of this ratio, other things being the same.

The maximum viscosity change under shear, *i.e.*, $[\eta]_0 - [\eta]_\infty$, was found to be proportional to $[\eta]_0^2$. The results obtained from the present study on fractionated polyisoprene are compared in Fig. 7 with corresponding results obtained previously,[3] on unfractionated polymer, from which it is seen that both sets of data are collinear. These data evidently satisfy an equation of the form

$$[\eta]_0 - [\eta]_\infty = K[\eta]_0^2 \qquad (8)$$

with K being constant for a given polymer–solvent system and essentially independent of molecular weight distribution. This latter fact shows that it is not necessary to have well-fractionated polymer samples in order to determine the dependence of the viscosity on the rate of shear. In practice, however, fractionation is often the only convenient means of obtaining a spectrum of molecular weights for the given polymer species.

A very important consequence of the shear data presented here is that the limiting $[\eta]$ *vs.* D relation at very low rates of shear is a linear one (Fig. 5). This refutes again the theoretical prediction of Kuhn and Kuhn[4] that the limiting slope of the viscosity–shear curve at the origin is zero. Instead, the $[\eta]$ *vs.* D curve has a very steep limiting tangent at low shear rates which is proportional to the square of the zero shear intrinsic viscosity (Fig. 6). In view of the fact that other workers have also failed to detect a bending down of the $[\eta]$ *vs.* D curve at very small gradients, it appears unlikely that extending measurements down to still lower rates of shear will reveal any significant departure from the trends already established. Nevertheless, measurements at shear rates below 100 sec.$^{-1}$ would be of considerable interest in this connection.

The linear nature of the η_{sp}/c *vs.* D plot at low rates of shear (Fig. 2) has an important practical

(9) W. Philipoff, *Kolloid Z.*, **71**, 1 (1935).

(10) L. J. Sharman, R. H. Sones and L. H. Cragg, *J. Appl. Phys.*, **24**, 703 (1953); T. G. Fox, Jr., J. C. Fox, and P. J. Flory, *J. Am. Chem. Soc.*, **73**, 1901 (1951); F. Akkerman, D. T. F. Pals and J. J. Hermans, *Rec. trav. chim.*, **71**, 56 (1952).

(11) A. Peterlin, *J. Polymer Sci.*, **8**, 621 (1952).

consequence in that it provides a simple method for obtaining accurately the zero shear viscosity. Straight line extrapolation of the raw viscosity data, obtained from a low shear viscometer of the type described above, provides $(\eta_{sp}/c)_0$ directly. Finally, plotting the zero shear reduced viscosity against the concentration results in the zero shear intrinsic viscosity, $[\eta]_0$. On the other hand, making measurements over a fairly wide range of shear rates leads to a curved viscosity–shear plot which involves considerable uncertainty in extrapolation. In a previous paper,[2] it was shown that a modified Katchalsky equation could be used to give the zero shear value accurately, but it is now possible to dispense with this somewhat indirect approach and merely extrapolate the data obtained over a restricted range of low shear rates.

An attempt to fit the shear data to an equation proposed recently by Bueche[8] is shown in Fig. 4. The agreement is quite good for shear rates up to about 12,000 sec.$^{-1}$ beyond which point the Bueche curve falls steadily below the experimental points. Inasmuch as his theoretical equation (number 8, ref. 7) was derived by dropping terms which become important only at large shear rates, it appears that the Bueche equation, when modified to incorporate some of these terms, may fit the data quite well even up to about 20,000 sec.$^{-1}$. The equation needs to take into account the ultimate asymptotic levelling-off of the viscosity at very high gradients. Furthermore, because the gradient enters to the one-half power in the equation at low shear rates, it implies a virtually infinite slope of the viscosity–shear curve at the ordinate, which, of course, is not realized experimentally. Nevertheless, the Bueche equation is perhaps the most successful theoretical relation proposed to date connecting the viscosity and the rate of shear.

Any new theoretical equation designed to express the shear dependence of viscosity should be able to account for the following experimental facts. The viscosity reaches an asymptotic limit at some finite value of the gradient. The difference between the initial and final values of the intrinsic viscosity is proportional to the square of the zero shear intrinsic viscosity, for various molecular weight fractions of a given polymer. The limiting slope of the viscosity–shear plot close to the origin is finite and proportional to the square of the zero shear viscosity.

Acknowledgments.—This work was carried out under the sponsorship of the Federal Facilities Corporation, Office of Synthetic Rubber, in connection with the Government Synthetic Rubber Program. The author is much indebted to Hugh E. Diem of these laboratories who kindly supplied the Alfin polyisoprene, and to Mrs. Marilyn E. Gordon for her assistance with the experimental work. It is a pleasure to acknowledge also helpful discussions with R. A. Harrington of the Physical Research Department.

PREPARATION AND CHARACTERIZATION OF BIPOLAR ION-EXCHANGE MEMBRANES

BY VINCENT J. FRILETTE

The Permutit Company, Birmingham, New Jersey

Received September 21, 1955

Synthetic bipolar ion-exchange membranes, one face of which is cation-selective, the other face anion-selective, have been prepared. It is shown that, unlike simple membranes, bipolar membranes must be characterized under dynamic conditions, for the membranes polarize at very low current densities. Polarization is particularly evident with the membrane oriented so that the cation-selective surface is nearest the cathode; with this orientation a high dynamic resistance is obtained and the membrane becomes highly proton-selective. A qualitative explanation for proton-selectivity is suggested in terms of the competitive formation of polarization films and their simultaneous depolarization by electrical and diffusional transport.

Introduction

Synthetic ion-exchange membranes have been described in the recent literature. Such membranes are of biochemical as well as industrial interest; they exhibit a high order of selectivity for either anions or cations. Biochemists use synthetic membranes as simple models or prototypes for more complicated, naturally-occurring structures. In this connection, Sollner has described and constructed model systems of "mosaic membranes," *i.e.*, membranes in which portions of the area are cation-selective while other portions show anion-selectivity.[1] Mention is also made of "layered" membranes, with no further comment on the subject. In this paper we shall describe the behavior of a simple type of layered membrane constructed so that one surface is cation-selective, while the opposite surface is anion-selective. The two surfaces derive their activity from strongly basic and strongly acidic ion-exchange groups, so that the membrane behavior should be relatively independent of the hydrogen ion activity of the environment. To distinguish this particular type of membrane from other conceivable layered membranes, we shall refer to them as "bipolar" membranes, one layer being polar in the electronegative sense, the other in the electropositive sense.

Several approaches could be used to prepare bipolar membranes. As described by Wyllie and Patnode,[2,3] a finely ground ion exchanger may be incorporated in a non-conductive plastic binder to form a heterogeneous membrane. The art of pre-

(1) K. Sollner, S. Dray, E. Grim and R. Neihoff, "Ion Transport Across Membranes," Academic Press, Inc., New York, N. Y., 1954, pp. 144–188.

(2) M. R. J. Wyllie and H. W. Patnode, THIS JOURNAL, **54**, 204 (1950).

(3) H. W. Patnode and M. R. J. Wyllie, U. S. Patent 2,614,976.

paring such membranes is further disclosed by Bodamer,[4] who uses a rubber mill to prepare the dispersions.

Quasi-reversible Characteristics.—Characterization of membranes is usually done by measurements made under conditions approaching reversibility. Thus, the potential difference between the two halves in a concentration cell is usually determined with a potentiometer, and serves to evaluate the selectivity of the membrane. The conductance of the membrane is often measured in an a.c. bridge arrangement. Such characterizations are ineffective for a bipolar membrane, for, as will be seen, its particular characteristics are associated with its polarizability with current flow. Attempts to obtain a potential for the bipolar membrane in a concentration cell utilizing calomel electrodes and solution strengths varying from 0.01 to 0.3 *N* NaCl gave very erratic, irreproducible results, with large drifts of the readings. No particular advantage was found by placing the cation-selective face in contact with either the dilute or concentrated solution. Such fluctuation is in marked contrast to the potentials noted for similarly formed, simple cation or anion-selective membranes, which gave a steady, reproducible value in a matter of minutes, with no marked asymmetric behavior.

The characteristics of simple cation and anion-selective membranes representing the two lamina of the bipolar membrane are given in Table I, along with the thickness and 60 cycle conductance of the bipolar membrane. A Leeds and Northrup type K-2 potentiometer with a thermionic amplifier was used to determine transport values. A Leeds and Northrup 4760 Wheatstone bridge was used for the conductivity measurements, with a 60-cycle bridge current and an a.c. galvanometer. A conductivity cell consisting of a Lucite block bored to form a $^1/_4$-inch cylindrical chamber, $^1/_2$-inch long, fitted with platinized platinum electrodes and bisected by a 1 mm. slot, was used. The difference in resistance of this conductivity cell filled with 0.1 *N* NaCl was measured with and without the membrane in the slot, the difference being the effective areal resistance of the membrane.

TABLE I

MEMBRANE CHARACTERISTICS

Thickness mm.	Permutit[a] Cation 1373 0.15–0.18	Permutit[a] Anion 1374 0.15–0.18	Bipolar 0.25
Effective areal resistance, 0.1 *N* NaCl, ohms-cm.[2]	8.5	9.5	18
Na transport no.			
0.01 *N* NaCl	0.99	0.04	..
0.30 *N* NaCl	.96	.10	..
0.60 *N* NaCl	.93	.15	..
1.50 *N* NaCl	.85	.25	..

[a] Permutit is the registered trademark of Permutit Co., New York.

Preliminary Experiments

Preliminary Hittorf-type experiments to determine transport characteristics of bipolar membranes under dynamic conditions showed that their behavior was dependent on the direction in which the membrane was oriented. With the anion-selective surface nearest the cathode, the membrane exhibited low resistance, while with the reverse orientation the resistance was quite high. The latter orientation proved most interesting, for it was found that a large portion of the current was carried not by the cations or anions of the electrolyte, but apparently by hydrogen ion which originated from the ionization of water.

The behavior of bipolar membranes may be qualitatively understood if we consider the lamina as separated by a thin chamber of dilute electrolyte. If, in this model, the anion membrane is nearest the cathode, then anions and cations will concentrate in the dilute electrolyte until the rate of outward diffusion through the lamina is equivalent to the rate of electrical concentration. The resistance of such a cell, assuming we have large quantities of electrode-chamber solution, will become somewhat lower, the exact values depending on the specific dimensions of the model. With the reverse orientation, however, the depleted solution which separates the lamina becomes less conductive, and if one continues to raise the potential to maintain a constant current, the competitive ionization of water begins to occur. In this case acid appears at the surface of the cation membrane, and alkali at the anion membrane. When the potential drop across the membrane becomes large, and acid and alkali are produced, the model will be referred to as "polarized." Although bipolar membranes do not have a measurable thickness of electrolyte that separates the lamina, the model described was found a useful aid in predicting their behavior.

In a real membrane, no measurable separation of the cation- and anion-selective lamina exists; the formation of acid and alkali may be regarded as the result of the abstraction of a proton from the water at the anion membrane surface and its transport through both lamina toward the cathode. One might ask whether the actual locus of the abstraction is at the surface or somewhere within the membrane structure. While the question is not trivial from the quantitative point of view, qualitatively the result still is the formation of acid and alkali. If one chooses the surface of the membrane as the locus, then the hydrogen-ion mobility (or proton-transfer) in the anion membrane should be reasonably large, in order to support any measurable conduction by this mechanism. Actual measurements show that this indeed is the case, as can be seen in Table II; the anion lamina is not a good barrier for hydrogen ion, and exhibits a high dialysis rate even at low acid concentrations. The lack of selectivity with hydrochloric acid is in marked contrast to the behavior of this membrane with sodium chloride.

TABLE II

BEHAVIOR OF PERMUTIT ANION MEMBRANE 1374 IN HYDROCHLORIC ACID

Mean concn. HCl, *N*	Transport no., H^+	Dialysis rate, $\times 10^4$ Meq./cm.^{2}/min.
0.01	0.11	0.02
.15	.32	2.28
.60	.60	16.0
1.50	.69	48.0

Since preliminary experiments with dilute solutions indicated that even at low current densities a major portion of the current was carried by hydrogen ion, it seemed appropriate to designate bipolar membranes as "proton-selective" by analogy with the terms "anion-selective" and "cation-selective" now in use.

Experimental Characterization

To evaluate quantitatively the dynamic behavior of the described bipolar membrane, a series of molded polyethylene rings was used to assemble the eight-chambered cell shown diagrammatically in Fig. 1. Each chamber had an area of 25 cm.^{2} and a thickness of about 1.3 cm. Very thin rubber gaskets were used on either side of the membrane to prevent leakage. The average volume of each chamber was found to be 33.4 ml., with a variation from chamber-to-chamber of *ca.* 0.6 ml. due to deflection of membranes. Acheson graphite electrodes were used both for the cathode and anode. As shown in Fig. 1, the bipolar membranes are alternated with cation-selective membranes. The need for a membrane separator is evident since in its absence the

(4) G. W. Bodamer, U. S. Patents 2,681,319 and 2,681,320.

TABLE III

PROTON-TRANSPORT EFFICIENCY, 0.2 *N* NaCl

Expt. no.	*E*,[a] v.	Current density, amp./cm.² × 10³	Time of operation, min.	Approx. concn. H^+, OH^-, *N*[b]	% Coulomb efficiency for proton transfer From OH^-, Chambers 2, 4, 6	From H^+, Chambers 3, 5, 7	From H^+, Chamber 1
1	9.8	3.8	10	0.006	34	31	50
2	21.6	7.5	5	.008	48	46	73
3	33.3	15.2	5	.02	55	52	87
4	55.3	30.2	2.5	.02	63	60	80
5	51.6	30.2	12.5	.06	34	30	80
6[c]	18.7	30.2	12.5	.003	<2	<2	<5

[a] Applied e.m.f. in steady state, less 2.7 volts for terminal electrodes. [b] Determined from titration of solutions collected from chambers, 2, 4, 6 and 3, 5, 7. [c] Electrodes reversed.

alkali produced in chamber 2, *e.g.*, would be neutralized by the acid formed in chamber 3. Actually, cellophane or an anion selective membrane could replace the cation membranes with similar effects so far as acid and alkali separation is concerned; the final location of the transported sodium chloride would be different, however.

In order to evaluate the proton-selectivity, the cell shown in Fig. 1 was rinsed several times and filled with NaCl solution of a known concentration; the current was then applied and maintained constant with suitable rheostats. After a selected interval of time the current was discontinued and the individual chambers were drained immediately to prevent changes of acid or alkali concentration by diffusion. A series of such experiments with 0.2 *N* NaCl at various current densities is summarized in Table III. At low current densities, the initial, low voltage rose rapidly and attained the voltage shown within less than half a minute, which is presumably the time required for the membrane to polarize. At higher current densities polarization appeared proportionately faster. The electrodialysis time was chosen to be sufficiently long to avoid introduction of gross error due to the interval required for polarization; also, it was chosen short enough to avoid excessive loss of hydrogen ion by competitive migration with sodium across the cation-membranes. Expt. no. 5 in Table III illustrates the apparent loss in coulomb efficiency when the conversion of salt to acid is increased threefold. Since the loss of hydrogen ion by competitive electromigration would be expected to be proportional to salt conversion, it is estimated that the calculated coulomb efficiencies are low by not more than several per cent. due to this source of error. This error together with that arising from the time required for initial polarization, lead to the estimation of the resultant values as within 5% of the true values.

Results for concentrations other than 0.2 *N* are shown in Table IV. It is evident that with higher concentrations of solution higher current densities are required to obtain efficient proton selectivity.

TABLE IV

EFFECT OF ELECTROLYTE CONCENTRATION AND CURRENT DENSITY ON PROTON-TRANSPORT EFFICIENCY

Expt. no.	Concn. NaCl, *N*	Current density, amp./cm.² × 10³	% Coulomb efficiency for proton transport From OH^- and H^+, av. for Chambers 2-7 incl.	From H^+, Chamber 1
7	0.1	3.8	53	91
1	0.2	3.8	32.5	50
8	1.0	3.8	26.5	45
2	0.2	7.5	47	73
9	.5	7.5	15.8	47
4	.2	30.2	61.5	80
10	.5	30.2	48	42

The effect of reversal of membrane orientation with respect to anode and cathode is shown in expt. 6, Table III. Note that in this experiment the voltage required to sustain the current is small, and no significant amounts of acid or alkali are formed.

Theoretical Basis for Behavior.—The present state of our knowledge of membranes together with the apparent complexity of the problem involved makes it impractical to attempt an exact quantitative treatment of bipolar membrane behavior. However, an attempt to estimate the extent of polarization and the components of the steady-state potential drop across a polarized membrane does lead to some interesting rational concepts.

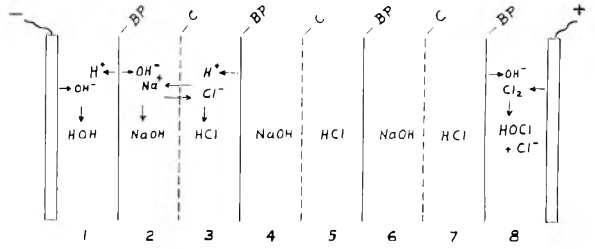

Fig. 1.—Multichamber salt-hydrolyzing cell; BP = bipolar membrane; C = cation membrane.

In the initial unpolarized state, a bipolar membrane immersed in dilute electrolyte will contain some migrant electrolyte, the exact internal concentration being determined by the Donnan equilibrium. The initial effect of the passage of current probably is the removal of migrant Na^+ and Cl^- ions through the cation and anion lamina, respectively. This process would rapidly terminate due to the high electrostatic potential developed by the separation of ions, except for the fact that residual sorbed electrolyte migrates into the depleted interface to provide counterions to maintain electroneutrality. The net effect of this mechanism is that the migrant electrolyte within the membrane is no longer in Donnan equilibrium with the external concentration throughout, but rather a gradient is established which has a minimum concentration value at the interface between the lamina, and a maximum concentration value at the interfaces in contact with free solution. The development of the gradient results in a polarization, which is characterized by a reverse potential computable from the Nernst equation. If, for example, it is assumed that the interface between the lamina has a Donnan salt level equivalent to what it would have if the individual surfaces were in contact with electrolyte of concentration C_i and the external faces in contact with electrolyte of concentration C_0, then the total reverse potential, assuming perfect membrane behavior and substituting concentrations for activities, would be

$$-E_{rev} = \frac{-2RT}{F} \ln \left(\frac{C_0}{C_i}\right) = -0.12 \log \left(\frac{C_0}{C_i}\right) \quad (1)$$

We now may consider the competitive process, the transport of a proton from the surface of the anion lamina to the surface of the cation lamina. This reaction is characterized by a minimum reverse potential computable from simple considerations.

$$-E_{rev_2} = \frac{-RT}{F} \ln \frac{a_{H_3O^+}\text{ (acid side)}}{a_{H_3O^+}\text{ (base side)}} = \frac{-RT}{F} \ln \frac{(a_{H_3O^+})(a_{OH^-})}{K} \quad (2)$$

Taking $K = 10^{-14}$, assuming concentrations equal to activities, and assuming the activity of water as 1, we have

$$-E_{rev_2} = -0.83 - 0.059 \log C_{H^+}C_{OH^-} \quad (3)$$

For the case where no preferential removal of either ion occurs, *i.e.*, for the non-terminal bipolar membranes, C_{H^+} and C_{OH^-} will be essentially equal. Accordingly, for either C_{H^+} or C_{OH^-}

$$-E_{rev_2} = -0.83 - 0.12 \log C_{H^+} \quad (4)$$

E_{rev1} and E_{rev2}, because they are restoring potentials which exist simultaneously between the same two planes, must be equal. We may now write

$$-0.83 = 0.12 \log C_{H^+}\left(\frac{C_i}{C_0}\right) \quad (5)$$

or

$$C_{H^+} = 10^{-6.9}(C_0/C_i) \quad (6)$$

Equation 6, which relates the hydrogen (or hydroxyl) ion concentration at the surface of the membranes in the steady state to the removal of Donnan electrolytes at the interface, indicates a very drastic reduction of migrant electrolyte for even low surface concentrations of acid and alkali. We may, in fact, estimate the concentration of migrant electrolyte indirectly, provided we have some way to estimate C_{H^+} and C_{OH^-}. The latter evaluation has been treated recently by King for a simple electrode[5] and a similar estimate may be derived for a bipolar membrane. For this estimation, it is necessary to assume a value for δ, the effective diffusion layer thickness. As a first approximation, let $\delta = 0.01$ cm., a reasonable value for free convection.[6] Since this value probably is an underestimation, it serves to set the lower limit for the concentration of hydrogen and hydroxyl ions in immediate contact with the surface of the membrane. If the bulk of the solution has a negligible hydrogen ion concentration, it can be shown that the concentration at the surface of the membrane is given by

$$C_{H^+} = 10^3 \frac{\delta I_p}{DF} \quad (7)$$

where C_{H^+} is the normality of acid, δ is the effective diffusion layer thickness in cm., D is the diffusion coefficient for HCl in cm.^{2}-sec.$^{-1}$, F is the Faraday, and I_p is the proton current density in amps. per cm.^{2}. From the literature, D may be taken as 3×10^{-5}.[6] Substitution in equation 7 gives

$$C_{H^+} = 3.34I_p \quad (8)$$

Because the diffusion coefficients for NaOH and HCl are similar, equation 8 also approximates the surface concentration of hydroxyl ion. In Table V are shown the surface concentrations for expts. 1–4 calculated from this equation. The values obtained are distinctly low, in view of the average normality of the liquid drained from chambers (Table III); the reason for the discrepancy probably is that δ in our small, convection-damping system is considerably larger than the chosen value, and perhaps close to 0.05 cm. Even from the calculated values, however, the use of equation 6 indicates that the migrant electrolyte in the membrane interface is in equilibrium with 10^{-3} to 10^{-4} N NaCl. Qualitatively, then, we may picture the operating bipolar membrane as almost completely stripped of migrant electrolyte at the interface.

TABLE V

CALCULATED POLARIZATION AND EFFECTIVE AREAL RESISTANCE OF BIPOLAR MEMBRANES IN 0.2 N NaCl

Expt. no.	$I_p + I_i$, amp./cm.^{2} $\times 10^3$	I_p, amp./cm.^{2} $\times 10^3$	C_{H^+}, C_{OH^-}, N[a]	E_{rev}, v./b.p. membrane	R_m[b] ohms/cm.^{2}
1	3.8	1.3	0.004	0.49	360
2	7.5	3.5	.012	.56	490
3	15.2	8.1	.028	.61	350
4	30.2	18.7	.06	.65	280
5	30.2	18.7	.06	.65	250
6[c]	30.2	*ca.* 0	...	.0	−0.8[d]

[a] From equation 8 for non-terminal bipolar membranes. [b] Specific conductance at 23° for 0.2 N NaCl taken as 0.018 mhos. Effective areal resistance of cation-membrane separators taken from Table I. Resistance contribution of solution plus cation-selective separators estimated at 625 ohms per cm.^{2} of cell area. R_m calculated from $E - 4E_{rev} = (I_p + I_i)(4R_m + R_{soln})$. [c] Electrodes reversed. [d] Negative effective areal resistance indicates membrane more conductive than 0.2 N solution. Actually, low figures such as this are not reliable, since small errors in assumption easily can change the value by several ohms.

The dynamic potential across the bipolar membrane, E_m, may now be described in terms of the reverse potential, E_{rev}, and an ohmic loss

$$E_m = E_{rev} + (I_p + I_i)R_m \quad (9)$$

where I_p and I_i are the proton and ion currents, respectively, and R_m is the dynamic membrane resistance. I_p is sustained by convective-diffusive depolarization of the polarized layer adjacent to the membrane, and is reinforced by electromigration when either the current density becomes relatively high or the level of supporting electrolyte becomes low. The other portion of the current, I_i, can be sustained only by the reverse leakage of Na^+ and Cl^- through the membrane, *i.e.*, by diffusion or electromigration of anions through the cation lamina, or cations through the anion lamina.

Reverse ion leakage and proton conduction in a polarized membrane, if the conceptions developed are correct, should be high resistance processes. In the immediate vicinity of the membrane interface, gaps between contiguous ion-exchanger particles presumably are filled with very pure water, which should offer considerable resistance to conduction. As for reverse ion leakage, it has been found that the diffusion coefficient for chloride ion in a synthetic cation-exchange membrane is of the order of 10^{-8} cm.^{2}/sec. in 0.04 N solution.[7] If the

(5) C. V. King, *J. Electrochem. Soc.*, **102**, 193 (1955).

(6) C. W. Tobias, M. Eisenberg and C. R. Wilke, *ibid.*, **99**, 359C (1952).

(7) R. J. Stewart, Thesis, University of Toronto, 1953.

corresponding coefficient for sodium ion in an anion membrane is of the same order of magnitude, the dynamic resistance, R_m, of the bipolar membrane should be quite high as contrasted with a 60 cycle resistance of 18 ohms. Values computed from Table III for R_m are shown in Table V, and are about twenty times the unpolarized resistance.

Proton transport efficiency, *i.e.*, the relative values of I_p and I_i, will evidently be favored by factors which minimize the reverse ion leakage and maximize the depolarization of the caustic and acid diffusion films. High current densities, for example, would be expected to favor proton transport efficiency by reason of increased polarization, especially if the caustic and acid film concentration is high relative to the supporting electrolyte; in this case electrical migration would assist diffusion as a depolarizing mechanism, while the high level of polarization of the membrane would increase the reverse leakage resistance. High external electrolyte concentrations would have just the opposite effect, as shown in Table IV. These relationships are confirmed by Fig. 2, in which is plotted an empirical relation between current density and proton transport number described by the function

$$t_p = b \log I_p \qquad (10)$$

in which t_p = the proton transport number, I_p the current carried by protons and b is an empirical factor. As seen from the graph, b initially increases with current density, but apparently becomes constant above a threshold density. The total current density required for b to level off increases with supporting electrolyte concentration, while the maximum value for b is highest for the most dilute salt solution used. In all cases studied an increase of current density increases the proton transport number, while increased electrolyte concentrations favor the ionic transport number.

Generalized Bipolar Membrane.—The synthetic bipolar membrane studied was formed of two efficient lamina. Similar effects may be expected, however, for any two lamina with different cation transport values. For example, in a simple membrane the adjacent solution film may be considered as a component lamina; the magnitude of the effects probably will be much smaller than with both lamina in the solid state, and correspondingly higher current densities and more dilute solutions will be required for any sizable proportion of proton-transfer. With proper conditions, differences of *p*H on two sides of a cation membrane have been found,[8] while a recent patent describes practical difficulties encountered due to *p*H changes in a unit designed to demineralize water.[9]

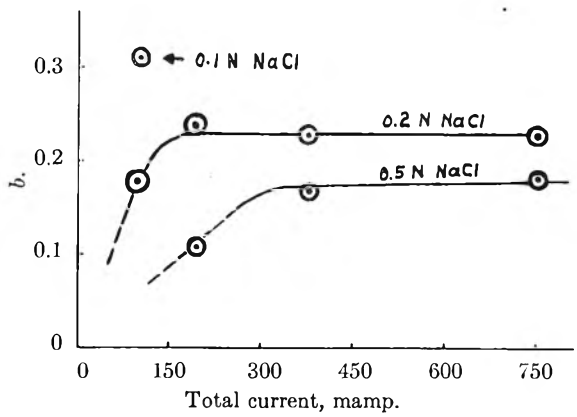

Fig. 2.—Proton selectivity *vs.* current density: $t_p = b \log I_p$; t_p = proton transport no.; I_p = proton current, ma.

It is also interesting to speculate on the role of bipolar membrane phenomena in biochemical systems. Such phenomena could arise, for example, from the reversible sorption of a soluble polyanion on a cation-selective membrane. Or, with a membrane containing both weakly basic and acidic fixed groups, the bipolar membrane effects could appear and disappear with metabolically produced *p*H changes on either side. Complex valving effects might arise in this way to control the rate of elimination or sorption of salts in living organisms.

Acknowledgment.—The writer wishes to thank Mr. M. E. Gilwood, Director of Research of The Permutit Company, for permission to publish these results.

(8) Report T. A. 270, "Survey of Water Desalting Investigations, in Particular the Electrodialytic Method," General Technical Dept., T. N. O., The Hague, Netherlands, 1954, p. 90.

(9) N. W. Rosenberg, U. S. Patent 2,708,658.

COLLOIDAL STRUCTURE IN LITHIUM STEARATE GREASES[1]

BY MARJORIE J. VOLD

Contribution from the Chemistry Department, University of Southern California, Los Angeles, Calif.

Received September 22, 1955

In a series of greases prepared by aging dispersions of 25% lithium stearate in *n*-hexadecane at various temperatures, the practical macroscopic properties of consistency and liquid loss rate divide the greases into groups according to the phase state of the system during aging. Hard, stable greases are produced from the liquid state. The processing conditions affect both the size of ultimate crystallites and the manner of their aggregation. As a colloidal system, greases should be classed as flocculated dispersions, in which a dominant factor in interparticle interaction is the London–van der Waals force.

This investigation had a twofold purpose. One purpose was to investigate the effect on the gross macroscopic properties of a grease of the phase state of the system from which its constituent crystallites are formed. A second purpose was to investigate the structure of the systems at the colloidal level with the hope of accounting at least qualitatively for the magnitudes of the observed bulk properties.

The role of shape of the soap crystallites in determining grease consistency has been studied by

(1) This work was supported by the Office of Ordnance Research, Contract No. DA 04-495-Ord-557.

several investigators.[2,3] In a number of cases the consistency of the grease was found to increase linearly with the length/width ratio of the elongated primary particles. However, the large differences in the slopes of these lines, particularly in the extensive results reported by Leet[3] led the writer to suggest[4] that particle geometry might be playing only a secondary role. It could govern the number of interparticle contacts whose rupture consumes some of the energy dissipated in flow of the material. The role of particle aggregation has not been studied so extensively although Vold, Coffer and Baker[5] found evidence that extensive interparticle aggregation is associated with low liquid loss rates in the system calcium stearate–*n*-hexadecane–water. Particle size as such also has not been extensively studied. However, the wide variety of sizes of primary particles of different materials functioning as effective thickening agents casts doubt on its importance, at least as a primary variable.

That particle size and shape should be influenced by the phase state of the system from which the crystallites grow is surely to be expected. For growth from a normal more or less molecularly homogeneous solution supersaturated with respect to a single crystal form, a background of theoretical work on rates of nucleation and of crystal growth[6] could provide a basis for predictions. But in the case of soap–oil systems, the micellar nature of the isotropic solution[7] and the existence of a sequence of mesomorphic forms in the equilibrium phase states as the systems are cooled[8] introduces additional variables.

Experimental Part

The subject greases were prepared by melting 5 g. of pure dry lithium stearate with 15 g. of *n*-hexadecane in a sealed Pyrex glass tube, maintaining the molten solution at 220° for 24 hours, quick chilling by immersing the hot tube in a freezing mixture of solid carbon dioxide and acetone, replacing it in a second air oven for a 24 hour aging period at the desired temperature, again quick chilling and finally (after rewarming to room temperature) working the resultant gel 60 double strokes in a perforated piston type manually operated grease worker. A second series of greases was prepared in the same way except for omission of the first chilling operation. The difference between the two sets is that in the first case preformed crystallites of colloidal dimensions are heated to an aging temperature, while in the second the phase state at the aging temperature is realized by cooling directly from isotropic solution.

The lithium stearate used was prepared by neutralization of Merck and Co. lithium hydroxide with a stearic acid of m.p. 68.7–69.0° (cor.), iodine value 0.33 and equivalent weight 285.8 purified from Armour "Neo-fat 65" by recrystallization from acetonitrile. Its transition temperatures, phase behavior and X-ray diffraction pattern were identical with those found previously.[8] Du Pont *n*-hexadecane (cetane) was used without further treatment.

The greases were characterized as to consistency by worked penetration, following A.S.T.M. procedure using a miniature cone penetrometer as described by Hotten and Kibler.[9] The values were reproducible within 10–20 units on independently prepared samples, and within 10 units on the same sample, independent of the age of the grease from 30 minutes after working to about three months.

They were characterized as to stability by measuring the rate of loss of oil to filter paper from a 1 cc. block of grease pressed into good contact with a single sheet of Whatman No. 4 paper held in a frame. The area of the oily spot followed a rate law of the form $\log A = \alpha \log t + K$. The exponent α was virtually $^2/_3$ in all cases while values of k varied with the grease and were reproducible within 5%.

Dispersions of the greases (0.167% by wt.) were prepared in *n*-heptane. A few cc. of the solvent were placed in an inclined cylindrical tube and the weighed grease dispersed by rolling it between a large diameter (12 mm.) glass rod and the side of the tube. The fluid dispersion thus obtained was then diluted with additional solvent.

Electron micrographs were obtained of the particles present in each of these dispersions by placing minute droplets on collodion coated screens and allowing the solvent to evaporate. The mean particle size was the same in a fresh suspension and one which had stood at room temperature for six weeks, showing that recrystallization in *n*-heptane is slow at room temperature.

The dispersions so prepared are initially fairly homogeneous, showing a blue Tyndall light, but flocculate in a few moments standing to coarse, loose aggregates which settle rapidly leaving a clear supernatant solvent layer. The settled material gradually compacts, reaching a steady-state volume in a few days which is unchanged for weeks. On shaking mildly the cycle of flocculation and settling repeats exactly; on subjecting the dispersions to very violent agitation (5 min. in a Waring blendor at 12,000 r.p.m.), some still repeat very nearly the same cycle while others give a much larger final settled volume. The actual soap concentration in the settled volumes is from 0.25 to 2%. The flocculated particles form a gel which does not flow under its own weight when the 2 cm. i.d. settling tubes are laid in a horizontal position. These final gel volumes (measured after at least 3 weeks) were recorded both for agitated and unagitated dispersions.

Results and Discussion

Table I gives for each grease, the worked penetration at 25°, liquid loss rate at 25°, and the gel volume of both agitated and unagitated dispersions in *n*-heptane. At 220° the system is a single homogeneous liquid phase; at 200, 186 and 175° a liquid crystalline solution phase coexists with isotropic solution at equilibrium. At 163, 149 and 125° crystal form II coexists with more dilute solution and at 105° crystal form I coexists with very dilute solution. In the H-series of greases (heated to the aging temperature), classification according to grease properties subdivides the greases in complete correspondence with their phase state. In the C-series (cooled to the aging temperature from 220°) the same properties are observed as in the case of the H-series when only liquid and liquid crystalline phases are involved. However, it would appear from the magnitudes of the penetrations and liquid loss rates that undercooling with respect to crystallization occurred down to between 125 and 149°. These observations are consistent with the results of Evans, Hutton and Matthews[10] obtained for a technical lithium stearate grease containing 8% soap in oil.

The results of Table I may be summarized in the observation that the crystallites formed by rapid cooling of either liquid or liquid crystalline solutions of lithium stearate in *n*-hexadecane yield greases

(2) (a) A. Bondi, *et al.*, 3rd World Petr. Congr. Sec. VII, 1951, p. 373; (b) R. J. Moore and A. M. Cravath, *Ind. Eng. Chem.*, **43**, 2892 (1951).

(3) R. H. Leet, *N. L. G. I. Spokesman*, **XIX**, No. 1, 20 (1955).

(4) M. J. Vold, *ibid.*, **XIX**, No. 1, 24 (1955).

(5) R. D. Vold, H. F. Coffer and R. F. Baker, *Inst. Spokesman*, **XV**, No. 10, 8 (1952).

(6) J. A. Christiansen and A. E. Neilsen, *J. Electrochem.*, **56**, 465 (1952).

(7) C. R. Singleterry and L. A. Weinberger, *J. Am. Chem. Soc.*, **73**, 4574 (1951).

(8) M. J. Vold, *J. Colloid Sci.*, **5**, 1 (1950).

(9) B. W. Hotten and G. M. Kibler, *Anal. Chem.*, **22**, 1574 (1950).

(10) D. Evans, J. F. Hutton and J. B. Matthews, *J. Appl. Chem.*, **2**, 252 (1952).

which are quite similar in properties irrespective of the actual temperature, though small variations exist within the group. The greases are relatively hard and stable. The fact that the gel volume of dilute dispersions of the greases depends strongly on whether or not the dispersion has been agitated vigorously, suggests that the grease may contain sub-units or crystallite aggregates such as have been postulated by Bondi and Penther[11] on the basis of dielectric studies and Hutton and Matthews[12] on the basis of rheological studies at low shearing stress.

Electron micrographs typical of the several hundred areas examined have been reproduced elsewhere.[13] The sketches of Fig. 1 are intended only to supplement the following description of the phenomena observed. The reader should examine the genuine photographic reproductions for further details.

Examination of the photographs shows that there are two distinct types of particles involved in building the gels. One type is a heterogeneous rod-shaped particle, usually averaging 0.6–1.5μ in length and 0.1–0.3μ in projected width. These particles have many smaller, generally rod shaped units adhering to them at random angles. The projections give the rods a somewhat irregular contour. They dominate in samples cooled quickly from liquid or liquid crystalline phases. It is possible that structures of this form exist in the liquid crystalline phase itself and persist, despite the crystallization, when the system is cooled rapidly.

The second type is a more homogeneous rod which seems to have uniform density and sharply defined edges. These predominate in systems cooled to aging temperatures in which one or the other of the crystalline forms is stable but which are still high enough to permit relatively slow growth from more concentrated and thus more viscous soap solutions.

TABLE I

PROPERTIES OF GREASES WITH 25% LITHIUM STEARATE IN *n*-HEXADECANE[a]

Aging temp., °C.	Worked Pen.	Liquid loss rate[b]	Gel Vol. (unagitated) cc./g.	Gel Vol. (agitated) cc./g.
H. Greases heated to aging temp.				
220	161	31	72	241
200	189	26	72	..
186	185	28	49	180
175	198	36	62	192
163	264	46	168	132
149	253	49	180	216
125	249	51	156	204
105	230	25	138	..
C. Greases cooled to aging temp. from 220°				
200	201	..	58	198
186	197	25	52	162
175	205	..	54	186
163	208	..	66	71
149	199	32	132	252
125	307	60	138	240
105	203	..	180	..

[a] The horizontal lines drawn in the table separate the greases into groups on the basis of the four properties. In group H the subdivision coincides with subdivision according to equilibrium phase state. [b] Arbitrary units (sq. cm. spot area at 1000 sec.).

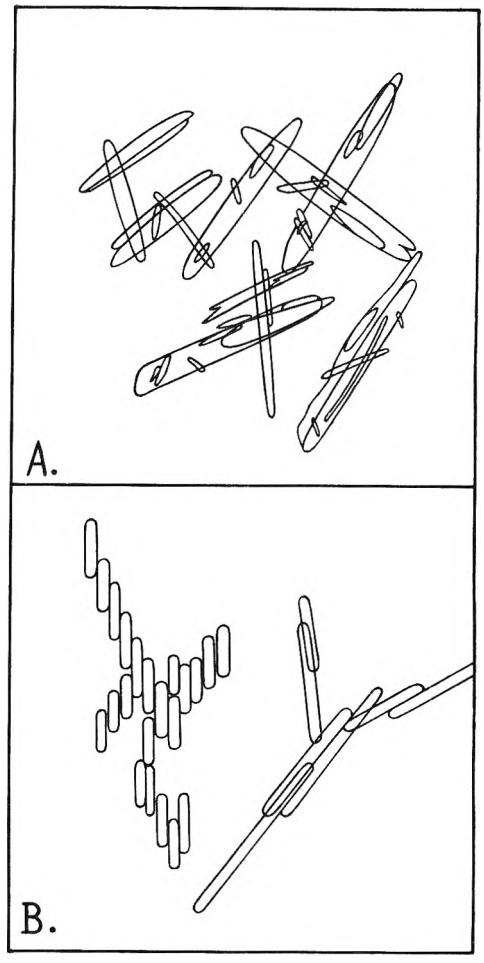

Fig. 1.—Schematic representation of typical electron micrographs of suspensions of lithium stearate greases: A, heterogeneous rods forming randomly piled aggregates. The larger rod-shaped units generally average 1μ in length. These structures predominate in samples cooled rapidly from liquid or mesomorphic states. B, homogeneous rods forming branched aggregates by cohesion with axes parallel. The rods vary in length from <0.1μ to as much as 0.8μ depending on growth temperature.

In greases formed by heating preformed crystallites the average length of the particles increases from too small to measure statistically in samples quenched to freezing temperatures and aged only at room temperature (<0.1μ), to 0.25μ in samples aged at 105° to as much as 0.6–0.8μ in samples aged at 163°. If aging is carried on above 172°, the crystallites are transformed to mesomorphic form and the factors governing the particle sizes in the cooled greases changes abruptly.

Thus the observed sizes of ultimate particles as a function of the conditions under which they were developed are almost entirely as expected. The electron micrographs, however, reveal a second structural characteristic of the greases which seems to be even more significant in determining their properties than the ultimate particle size. This is a great spread in type of particle aggregate.

(11) A. Bondi and C. J. Penther, THIS JOURNAL, **57**, 72 (1953).

(12) J. F. Hutton and J. B. Matthews, "Proc. Second Int. Congr. on Rheology," V. G. W. Harrison, Ed., Academic Press, Inc., New York, N. Y., 1954, p. 408.

(13) M. J. Vold, Final Technical Report, Contract DA-04-495-ORD557, Aug. 31, 1955.

In some cases mutual cohesion occurs along the length of the ultimate particles, with one or more such particles forming parts of more than one aggregate, resulting in branched structures. The extent of the thickening action with this type of structure appears to depend qualitatively on the size of the mesh in this network structure. With short stubby rods the mesh is finer and the grease harder, in contrast with other situations[2b,3] in which decrease in length/width ratio reduces consistency.

A second type of aggregate appears to be formed by quite random piling up of the crystallographically heterogeneous rod-like entities which are themselves aggregates of very tiny crystallites. Greases in which this type occurs are harder and more stable than those in which the aggregates are more stringy.

Finally, there also occur very large ($0.5 \times 5\mu$) agglomerates which seem to result from incomplete dispersion of crystallites formed by cooling the liquid crystalline phases. It seems likely that these, which are relatively uncommon, do not contribute significantly to the rheological properties of the greases except indirectly by reducing the effective soap content.

The gelation of the dilute dispersions of the grease occurs because the dispersion is essentially unstable. Convection due to thermal gradients and to settling phenomena, and to a much lesser degree Brownian motions, brings individual particles in contact and cohesion occurs at once. The result is an expanded gel which gradually compacts under sustained gravitational pressure to a steady-state volume.

By treating the individual particle as "monomer" and the gel as "polymer" Frisch and Vold[14] were able to apply Flory's[15] approach to development of an equation for the critical gel volume as

$$V = \frac{2\beta}{d_s}\left(1 + \frac{\rho s}{v}\right)(f-1)^{1/2}$$

Here V is the gel volume in cc. per gram dispersed phase of density d_s, ρ is the average radius of the elongated particle, s its surface area and v its volume; β is a factor put in empirically to account for the fact that probability of forming a bond between two particles, analogous to the chance of reaction of two functional groups of separate monomers, contains both geometrical and energetic terms of which only the former were explicitly considered; f is the potential number of branches at a branch point in the network and is set equal to the number of sites on one particle at which a second could cohere.

Application to the two types of cases presented by the data of Table I shows that for those in which the gel volume is nearly independent of agitation, critical volumes of the right order of magnitude are obtained using a value for the shape factor $(1 + \rho s/v)$ calculated by Isihara[16] for elongated ovaloids and an effective functionality f, equal to twice the length/width ratio. The factor β was set equal to unity which amounts to assuming that any two contacting fibers will bond but two coming into proximity of each other without touching will not be attracted or repelled, *i.e.*, the interaction forces are short range. The calculation applies also to systems showing an increase in settling volume after agitation. For these the volume before agitation is in accord with assumption of large roughly isometric aggregates for which the shape factor is the same as for spheres[4] and the functionality very high (40–150) since each protruding rod-like component of the aggregate is a potential site for bonding to another aggregate. These aggregates (the gel units of Bondi) are presumed to be dispersed into component smaller elongated ultimate particles when the system is stirred vigorously.

If the dominant factor causing cohesion is van der Waals attraction, it should be calculable as a sum of A/r^6 terms for the component atoms of each particle less the sum of A/r^6 terms for the atoms of solvent displaced by the particles, with the value of A dependent on the chemical nature of each atom pair. In first approximation only the oxygen atoms need be considered since the carbon atoms of the soap particle replace a nearly equal number of carbon atoms of solvent.

Calculation has shown[4] that for infinitely long soap crystallites in contact at large angles, the net attraction is of a reasonable order of magnitude if it is assumed that the hydrocarbon "tails" of the soap molecules are exposed in the contacting surfaces. However, the result is also available[17] that for similar particles in contact with long axes parallel the attraction is so much greater (10–20 times) that rapid destruction of the grease into a stringy soap curd and supernatant solvent would be expected after a short period of stirring.

Two hypotheses, each applicable in its proper sphere, lead out of this seeming dilemma which was also pointed out by Bondi.[18] In the case of the heterogeneous particles the close contact required for the exertion of those large attractions cannot be realized because adherent tiny soap crystallites on the surfaces of the larger rods act as "spacers" and the bond is formed between these with the A/r^6 terms of the balance of the atoms in the particle contributing only a small amount of the total because of the larger separations.

In the case of the more homogeneous particles strong cohesion between parallel aligned particles displaced along their long axes reduces the probability of their ever forming bonds along their whole length (which would result in soap separation from the grease) to much less than that calculated on purely geometrical grounds.

The most significant general conclusion from this work viewed as a whole is the clear demonstration that interparticle forces dependent on factors other than particle shape alone are of controlling importance in determining the rheological properties of soap-containing greases.

Acknowledgment.—The writer wishes to express her appreciation to Miss Valeria Artel and Dr. Richard F. Baker for their valuable assistance in the techniques of electron microscopy.

(14) H. L. Frisch and M. J. Vold, *J. Colloid Sci.*, in press.

(15) P. J. Flory, "Principles of Polymer Chemistry," Cornell University Press, Ithaca, N. Y., 1953, p. 347ff.

(16) A. Ishihara, *J. Chem. Phys.*, **21** 1142 (1951).

(17) M. J. Vold, *J. Colloid Sci.*, **9**, 451 (1954).

(18) A. Bondi, *N. L. G. I. Spokesman*, **XIX**, No. 1, 33 (1955).

THE CRYSTAL STRUCTURE OF Cr_5Si_3

BY CAROL H. DAUBEN, D. H. TEMPLETON AND C. E. MYERS

Contribution from Radiation Laboratory, Department of Chemistry and Division of Mineral Technology, University of California, Berkeley; and Department of Chemistry, Purdue University, Lafayette, Indiana

Received September 22, 1955

The compound Cr_5Si_3 is tetragonal, space group I4/mcm with $a = 9.170 \pm 0.006$ Å., $c = 4.636 \pm 0.003$ Å., 4 Si in (a) 8 Si in (h) with $x = 0.165$, 4 Cr in (b), and 16 Cr in (k) with $x = 0.075$, $y = 0.224$. Other compounds which have this structure are Mo_5Si_3, W_5Si_3, Mo_5Ge_3, Nb_5Si_3, V_5Si_3, Ta_5Si_3 and probably Cr_5Ge_3.

We have prepared single crystals of a chromium silicide by heating the elements in an induction furnace and cooling from a temperature probably about 1500°. Determination of the crystal structure shows the compound to be Cr_5Si_3. It is isostructural with Mo_5Si_3, W_5Si_3,[1] Mo_5Ge_3[2] and probably Cr_5Ge_3[3] which had been reported previously under various designations. Recently we have learned that Aronsson[4] has reported briefly very similar atomic coördinates for W_5Si_3, and that other work has added Nb_5Si_3,[5,6] V_5Si_3[6,7] and Ta_5Si_3[8] to the list of isostructural compounds. There is also another form of Nb_5Si_3 and Ta_5Si_3 which does not have this structure.[1,6] Parthé, Nowotny and Schmid[8] have shown that the diffraction data for Cr_5Si_3, V_5Si_3, Nb_5Si_3 and Ta_5Si_3 agree with Aronsson's structure.

Weissenberg diagrams were obtained about [001] with Fe Kα and Mo Kα radiation and powder patterns with Cu Kα and Cr Kα radiation. The unit cell is tetragonal with dimensions (from the chromium data, $\lambda = 2.2909$ Å.);

$$a = 9.170 \pm 0.006 \text{ Å.}$$
$$c = 4.636 \pm 0.003 \text{ Å.}$$

There are four molecules of Cr_5Si_3 in the unit cell and the absences correspond to symmetry I-c-. The X-ray density is 5.9 g. cm.$^{-3}$ and that obtained by displacement[9] is 5.6 g. cm.$^{-3}$. By considerations of symmetry, and by conventional Fourier methods, the atoms were located in the following positions

Space group I 4/mcm $- D_{4h}^{18}$
(0, 0, 0; $\frac{1}{2}, \frac{1}{2}, \frac{1}{2}$;)+
4 Si in (a) 0, 0, $\frac{1}{4}$; 0, 0, $\frac{3}{4}$:
8 Si in (h) $\pm(x, \frac{1}{2}+x, 0; \frac{1}{2}+x, \bar{x}, 0:)$ with $x = 0.165$
4 Cr in (b) 0, $\frac{1}{2}, \frac{1}{4}$; $\frac{1}{2}$, 0, $\frac{1}{4}$:
16 Cr in (k) $\pm(x, y, 0; \bar{y}, x, 0; x, \bar{y}, \frac{1}{2}; y, x, \frac{1}{2}:)$ with $x = 0.075$, $y = 0.224$

The positions given by Aronsson for W_5Si_3 are the same as these (after shift of origin), with x (Si) = 0.17 and x, y (W) = 0.074, 0.223. His structure description is based on space group I $\bar{4}2$m but with special values of the z parameters which correspond to the higher symmetry. Deviations from these special values would result in violations of the glide plane absences and in differences in intensities for the same hk in various odd layers, neither of which is observed up to the fifth layer.[10]

Observed and calculated structure factors are listed in Table I. The values of R calculated for zero, first and second layers were 16, 14 and 14%, respectively. No absorption or temperature corrections were made. Since all odd layers are alike and the zero and fourth layers are alike, calculations were not made for the other layers.

Figure 1 shows the electron density projection parallel to [001]. Each atom has nearest neighbors as

Cr (b): 2 Cr at 2.32 Å., 8 Cr at 2.87 Å.
4 Si at 2.43 Å.

Cr (k): 1 Cr at 2.61 Å., 2 Cr at 2.70 Å., 2 Cr at 2.87 Å., 2 Cr at 3.06 Å.
1 Si at 2.42 Å., 1 Si at 2.44 Å., 2 Si at 2.46 Å., 2 Si at 2.66 Å.

Si (a): 8 Cr at 2.46 Å.
2 Si at 2.32 Å.

Si (h): 2 Cr at 2.42 Å., 2 Cr at 2.43 Å., 2 Cr at 2.44 Å., 4 Cr at 2.66 Å.

One third of the silicon atoms form straight chains parallel to c, but otherwise there are no silicon–silicon bonds. The atomic arrangement is shown in Fig. 2.

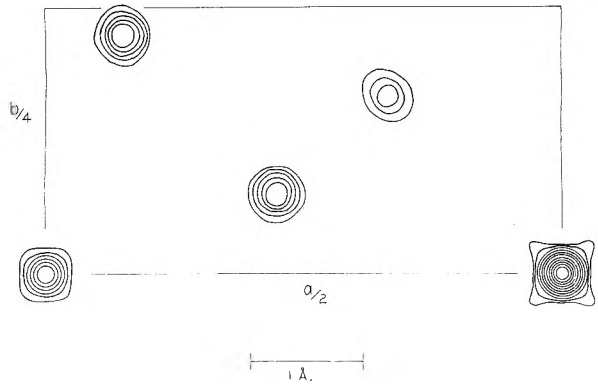

Fig. 1.—Electron density projection on (001).

In Table II are listed lattice dimensions for W_5Si_3 and Mo_5Si_3 derived from diffraction patterns (Cr Kα) of the samples prepared by Searcy.[1] There is disagreement with the values published by Aronsson[4] and by Parthé, Schachner and No-

(1) L. Brewer, A. W. Searcy, D. H. Templeton and C. H. Dauben, *J. Amer. Ceram. Soc.*, **33**, 291 (1950).
(2) A. W. Searcy and R. J. Peavler, *J. Am. Chem. Soc.*, **75**, 5657 (1953).
(3) H. J. Wallbaum, *Naturwissenschaften*, **32**, 76 (1944).
(4) B. Aronsson, *Acta Chem. Scand.*, **9**, 137 (1955).
(5) E. Parthé, H. Schachner and H. Nowotny, *Monatsh. Chem.*, **86**, 182 (1955).
(6) A. G. Knapton, *Nature*, **175**, 730 (1955).
(7) P. Pietrowsky, private communication (June, 1955).
(8) E. Parthé, H. Nowotny and H. Schmid, *Monatsh. Chem.*, **86**, 385 (1955).
(9) The discrepancy is not considered significant because of difficulty in measuring the density.
(10) NOTE ADDED IN PROOF.—In a recent publication Aronsson (*Acta. Chem. Scand.*, **9**, 1107 (1955)) has adopted the space group I 4/mcm in agreement with our choice.

TABLE I

OBSERVED AND CALCULATED STRUCTURE FACTORS FOR Cr_5Si_3

hkl	F_o	F_c	*hkl*	F_o	F_c	*hkl*	F_o	F_c	*hkl*	F_o	F_c	*hkl*	F_o	F_c
0,2,0	..[a]	6	5,13,0	<5	−4	14,14,0	24	21	6,11,1	10	−13	0,18,2	<7	1
0,4,0	30	32	5,15,0	17	11	14,16,0	<5	2	6,13,1	<5	1	0,20,2	30	−29
0,6,0	9	−4	5,17,0	13	−8	14,18,0	8	10	6,15,1	<6	4	0,22,2	<6	−6
0,8,0	<3	1	5,19,0	9	−12	15,15,0	18	−15	6,17,1	9	13	0,24,2	<4	−6
0,10,0	10	9	5,21,0	6	−5	15,17,0	<5	1	6,19,1	<6	5	1,1,2	..[a]	8
0,12,0	31	29	5,23,0	<5	−9	16,16,0	<5	4	6,21,1	<6	−1	1,3,2	5	3
0,14,0	31	33	6,6,0	46	52	16,18,0	10	10	6,23,1	10	−9	1,5,2	16	−16
0,16,0	<6	2	6,8,0	13	16	17,17,0	6	−3	7,8,1	4	−6	1,7,2	20	−21
0,18,0	19	18	6,10,0	9	6	121	10	10	7,10,1	19	15	1,9,2	24	26
0,20,0	20	−13	6,12,0	18	18	1,4,1	47	50	7,12,1	<5	2	1,11,2	14	−12
0,22,0	12	6	6,14,0	11	−7	1,6,1	<3	−1	7,14,1	<6	−5	1,13,2	16	15
0,24,0	<4	6	6,16,0	15	12	1,8,1	14	−13	7,16,1	<6	−2	1,15,2	<7	1
110	..[a]	−9	6,18,0	10	6	1,10,1	18	−20	7,18,1	<6	−2	1,17,2	<7	6
130	12	−13	6,20,0	23	22	1,12,1	3	−1	7,20,1	<6	−2	1,19,2	<7	0
150	7	6	6,22,0	<5	−2	1,14,1	<5	−6	7,22,1	<4	5	1,21,2	<6	1
170	37	−34	6,24,0	11	13	1,16,1	26	23	8,9,1	19	14	1,23,2	<5	6
190	20	19	7,7,0	29	27	1,18,1	<6	9	8,11,1	<5	8	2,2,2	41	−53
1,11,0	21	−20	7,9,0	9	−8	1,20,1	<6	−4	8,13,1	<5	2	2,4,2	12	4
1,13,0	10	8	7,11,0	<5	4	1,22,1	<4	−3	8,15,1	<6	−2	2,6,2	14	−12
1,15,0	<6	−7	7,13,0	35	−31	1,24,1	7	−4	8,17,1	18	−21	2,8,2	10	−3
1,17,0	<6	−1	7,15,0	<6	0	2,3,1	33	34	8,19,1	<5	4	2,10,2	13	−11
1,19,0	8	−6	7,17,0	11	−6	2,5,1	20	−22	8,21,1	<4	0	2,12,2	32	−32
1,21,0	<5	−4	7,19,0	10	3	2,7,1	18	17	8,23,1	8	10	2,14,2	18	−17
1,23,0	<4	1	7,21,0	4	10	2,9,1	10	−7	9,10,1	14	13	2,16,2	21	−17
1,25,0	6	−9	8,8,0	7	8	2,11,1	13	−16	9,12,1	13	−12	2,18,2	7	2
2,2,0	10	−9	8,10,0	17	14	2,13,1	11	11	9,14,1	10	8	2,20,2	<7	−2
2,4,0	42	53	8,12,0	16	16	2,15,1	<5	−4	9,16,1	<6	−4	2,22,2	<6	5
2,6,0	32	30	8,14,0	11	6	2,17,1	<6	8	9,18,1	<6	1	2,24,2	10	−13
2,8,0	42	38	8,16,0	21	19	2,19,1	<6	−4	9,20,1	<4	1	3,3,2	17	−14
2,10,0	16	19	8,18,0	<6	−4	2,21,1	<5	7	10,11,1	<5	−5	3,5,2	22	22
2,12,0	8	−8	8,20,0	14	12	2,23,1	10	−12	10,13,1	10	−12	3,7,2	18	19
2,14,0	<5	4	8,22,0	<4	0	3,4,1	11	−5	10,15,1	18	16	3,9,2	<5	0
2,16,0	<6	1	9,9,0	31	−27	3,6,1	26	−27	10,17,1	<6	4	3,11,2	<6	1
2,18,0	20	19	9,11,0	17	11	3,8,1	30	32	10,19,1	14	11	3,13,2	<6	3
2,20,0	13	12	9,13,0	9	9	3,10,1	<4	−2	10,21,1	12	−11	3,15,2	<6	−8
2,22,0	22	19	9,15,0	<6	4	3,12,1	28	22	11,12,1	13	−13	3,17,2	<7	6
2,24,0	<4	−1	9,17,0	<6	−6	3,14,1	21	−15	11,14,4	14	13	3,19,2	<6	10
3,3,0	27	−30	9,19,0	10	−8	3,16,1	<6	−4	11,16,1	<6	−6	3,21,2	<6	2
3,5,0	15	13	9,21,0	9	−12	3,18,1	13	−10	11,18,1	<5	2	3,23,2	<5	5
3,7,0	13	12	10,10,0	14	14	3,20,1	<6	−2	11,20,1	<4	3	4,4,2	30	−29
3,9,0	10	−8	10,12,0	4	6	3,22,1	<4	10	12,13,1	<6	−2	4,6,2	35	−38
3,11,0	<4	−8	10,14,0	8	10	3,24,1	<3	1	12,15,1	<6	−2	4,8,2	24	−25
3,13,0	<5	−3	10,16,0	8	11	4,5,1	19	−16	12,17,1	15	−13	4,10,2	9	−14
3,15,0	17	−16	10,18,0	<6	4	4,7,1	<3	2	12,19,1	<4	2	4,12,2	<6	−8
3,17,0	<6	−1	10,20,0	<5	4	4,9,1	6	8	12,21,1	<3	−1	4,14,2	<6	−5
3,19,0	<5	4	10,22,0	7	8	4,11,1	16	13	13,14,1	<6	−4	4,16,2	<7	−4
3,21,0	<5	−3	11,11,0	21	−16	4,13,1	<5	4	13,16,1	<5	−3	4,18,2	23	−19
3,23,0	<4	−1	11,13,0	13	−11	4,15,1	16	−16	13,18,1	<4	−4	4,20,2	<6	−11
4,4,0	13	14	11,15,0	13	−13	4,17,1	<6	8	13,20,1	<3	−1	4,22,2	12	−11
4,6,0	3	−3	11,17,0	<6	0	4,19,1	15	−16	14,15,1	<5	4	5,5,2	26	−21
4,8,0	<4	8	11,19,0	<5	4	4,21,1	12	10	14,17,1	6	7	5,7,2	<5	0
4,10,0	19	19	11,21,0	7	5	4,23,1	<4	2	14,19,1	<4	3	5,9,2	9	−10
4,12,0	21	16	12,12,0	12	5	5,6,1	9	−9	15,16,1	9	9	5,11,2	17	18
4,14,0	21	19	12,14,0	10	9	5,8,1	13	15	15,18,1	<4	4	5,13,2	<6	3
4,16,0	17	18	12,16,0	<6	−4	5,10,1	32	−32	16,17,1	<4	6	5,15,2	19	18
4,18,0	<6	−3	12,18,0	23	20	5,12,1	6	3	0,2,2	..[a]	−55	5,17,2	<7	−2
4,20,0	<6	2	12,20,0	4	2	5,14,1	<5	1	0,4,2	18	−18	5,19,2	<6	−4
4,22,0	<5	2	12,22,0	9	11	5,16,1	9	9	0,6,2	39	−43	5,21,2	<5	0
4,24,0	10	10	13,13,0	20	13	5,18,1	<6	4	0,8,2	32	−34	6,6,2	23	18
5,5,0	36	−33	13,15,0	<6	0	5,20,1	<5	3	0,10,2	21	−20	6,8,2	16	−15
5,7,0	8	−10	13,17,0	<5	−1	5,22,1	<5	−5	0,12,2	6	3	6,10,2	17	−19
5,9,0	19	−18	13,19,0	14	−12	6,7,1	<4	−1	0,14,2	<6	10	6,12,2	<6	−5
5,11,0	14	12	13,21,0	10	−8	6,9,1	13	−15	0,16,2	18	−20	6,14,2	31	−25

TABLE I (*Continued*)

hkl	F_o	F_c	*hkl*	F_o	F_c	*hkl*	F_o	F_c	*hkl*	F_o	F_c	*hkl*	F_o	F_c
6,16,2	<7	−4	8,8,2	22	−19	9,17,2	<7	1	11,17,2	<6	5	14,14,2	<6	6
6,18,2	<7	−10	8,10,2	<6	−10	9,19,2	<6	−3	11,19,2	<6	9	14,16,2	10	−12
6,20,2	<6	6	8,12,2	<6	−6	9,21,2	<5	−8	11,21,2	8	10	14,18,2	<5	−3
6,22,2	12	−14	8,14,2	<7	−12	10,10,2	8	−8	12,12,2	6	−12	14,20,2	12	−18
7,7,2	32	34	8,16,2	<7	2	10,12,2	18	−12	12,14,2	<7	−1	15,15,2	10	−10
7,9,2	<5	−1	8,18,2	19	−16	10,14,2	<7	−7	12,16,2	16	−18	15.17.2	6	7
7,11,2	<7	11	8,20,2	<6	−1	10,16,2	<7	−6	12,18,2	<6	7	16,16,2	8	−9
7,13,2	27	−22	8,22,2	10	−12	10,18,2	<6	−10	12,20,2	12	−11	16,18,2	<4	−2
7,15,2	<7	6	9,9,2	22	−18	10,20,2	<5	−6	13,13,2	24	22			
7,17,2	<7	2	9,11,2	21	19	11,11,2	10	−9	13,15,2	<7	5			
7,19,2	13	12	9,13,2	14	14	11,13,2	<7	−5	13,17,2	<6	4			
7,21,2	<6	14	9,15,2	<7	9	11,15,2	<7	−6	13,19,2	<5	−8			

[a] Not on film.

TABLE II

LATTICE DIMENSIONS OF TETRAGONAL Cr_5Si_3-TYPE CRYSTALS

Crystal	*a*, Å.	*c*, Å.
W_5Si_3		
This work	9.605 ± 0.005	4.964 ± 0.005
Aronsson[a]	9.645	4.969
Parthé, *et al.*[b]	9.56	4.94
Mo_5Si_3		
This work	9.642 ± 0.005	4.905 ± 0.005
Aronsson[a]	9.617	4.899
Parthé, *et al.*[b]	9.66	4.99
Mo_5Ge_3[c]	9.82 ± 0.03	4.97 ± 0.02

[a] Reference 4. [b] Reference 5, converted from kx. units. [c] Derived from the pattern of Searcy and Peavler, ref. 2.

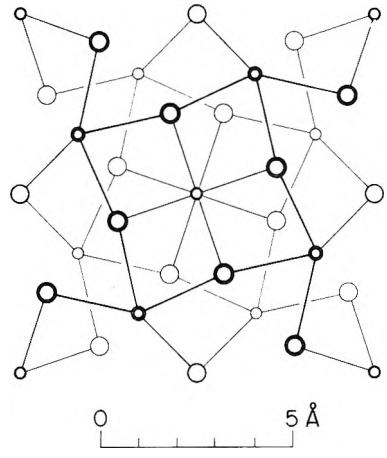

Fig. 2.—Atomic arrangement in Cr_5Si_3, projected on (001). The larger circles represent Cr atoms, the smaller ones Si atoms. The lines represent distances less than 3.50 Å. The vertical chains at 0,0; $0,{}^1/_2$; ${}^1/_2,0$; ${}^1/_2,{}^1/_2$ are not visible in this projection.

wotny,[5] which are listed for comparison. The cause of this disagreement is unknown. Solid solubility is not sufficient under the conditions of Searcy's experiments[1] to explain the differences, but we cannot rule out solid solubility under other conditions of heat treatment. Also listed in Table II are lattice dimensions for Mo_5Ge_3, derived from the pattern of Searcy and Peavler.[2]

We are indebted to Professor A. W. Searcy, under whose direction the crystals were prepared, for valuable discussions and for giving us the photograph of the Mo_5Ge_3 diffraction pattern, and to Mrs. Helena W. Ruben for taking some of the powder patterns and making some of the film measurements. We thank Professor H. Nowotny for calling to our attention some of the recent work of his group and others and for a copy of one of his papers in advance of publication. This research was supported in part by the United States Atomic Energy Commission and in part by the Office of Naval Research.

THE THERMODYNAMIC PROPERTIES OF THE MODERATELY DILUTE LIQUID SOLUTIONS OF COPPER, SILVER AND GOLD IN THALLIUM, LEAD AND BISMUTH

BY O. J. KLEPPA

Institute for the Study of Metals, University of Chicago, Chicago, Illinois

Received September 23, 1955

Some new measurements are reported on the heats of solution of silver and gold in liquid thallium, lead and bismuth. Most of the experiments were performed at 450°, although a few runs also were carried out at 350°. The heats of formation of the intermetallic phases "Au_2Pb" and "Au_2Bi" were determined at 350° by dissolving the alloys in pure liquid lead and bismuth, respectively. Some new observations are reported on the solubility of solid silver in liquid thallium, lead and bismuth at temperatures up to 4–500°. The new heat data are compared with earlier data from calorimetry and from e.m.f. investigations, and with thermodynamic data derived from the equilibrium phase diagrams. In order to facilitate this correlation an analytical method is proposed which in certain cases will permit a derivation of important free energy, heat and entropy data from phase diagram information alone. A summary is presented of all available thermodynamic data for the moderately dilute solutions of copper, silver and gold in thallium, lead and bismuth. The significance of the data is discussed briefly.

Introduction

In past communications the author has reported on the thermodynamic properties of the liquid systems gold–thallium, gold–lead and gold–bismuth as determined by e.m.f. cell measurements at 6–700°.[1] More recently he has discussed the corresponding copper systems, based on measurements of the solubility of solid copper in the low-melting liquids metals.[2] In the present work calorimetric data are reported on the solutions of silver and gold in liquid thallium, lead and bismuth. The calorimetric experiments were carried out in a high temperature reaction calorimeter described previously.[3] Most of the calorimetric work was performed at 450°, while a few runs were carried out at 350°. At this temperature the heats of formation of "Au_2Pb" and "Au_2Bi" were also determined. It was originally planned to include in the present study a calorimetric determination of the heats of solution of copper in thallium, lead and bismuth. However, it was found that copper dissolved too slowly in these metals at 450°, and the heats of solution could not be obtained.

The earlier work on the gold and copper systems showed that these mixtures have large positive excess entropies of mixing. In order to obtain additional entropy data, notably on the silver solutions, the calorimetric heat data have been combined with free energy information from the phase diagrams. In the course of this work it became evident that the location of the liquidus curves for the silver systems was too uncertain to permit reasonably reliable thermodynamic calculations. Therefore the solubility of solid silver in liquid thallium, lead and bismuth was determined between the eutectic temperatures and 400–500°.

Experimental

Calorimetry.—The metals used in the present work were all of 99.9+% purity. Readers are referred to earlier communications for details of experimental technique.[3,11]

At 450° the solution of silver in bismuth proceeded moderately fast, going to completion in 20–30 minutes. At 350° the corresponding reactions were more sluggish and took about 45 minutes. Approximately the same time was required to dissolve silver in lead at 450°, while the solution of silver in thallium required as much as 60 minutes. Generally the highest silver concentrations required the longest reaction periods.

The solution of gold was very rapid in all three liquid metals, with reaction periods lasting 15–20 minutes, even at 350°. As the error in the calorimetric heat leak correction is roughly proportional to the length of the reaction period, it is not surprising to find that the silver experiments are less precise than the gold experiments. During the work on silver–bismuth some additional loss in precision resulted from unsatisfactory operation of the controller which keeps the calorimeter at temperature. This condition was corrected when the other systems were studied.

Solubility Measurements.—The solubility of silver in liquid thallium, lead and bismuth was determined by a method previously described by the author[4]: Solid silver was equilibrated with the appropriate liquid alloys in evacuated Pyrex ampoules. After 24 hours in a thermostated (±1°), tilting furnace, the equilibrium liquid was separated from the solid phase. The silver content of the liquid phase was then determined by conventional chemical analysis. The furnace temperatures were measured by means of a ehromel–alumel thermocouple calibrated at the melting points of tin, bismuth and zinc.

Results. Comparison with Earlier Data

Calorimetry. Silver Alloys.—In three experiments at 450° solid silver was dissolved in liquid thallium, yielding alloys containing from 2 to 5 atomic % silver. Similarly silver was dissolved in liquid lead in 7 experiments (1 to 9% silver), and in bismuth in 10 experiments (2 to 33% silver). The variations in maximum silver content reflect the extent of liquid range in the systems at 450° (see Fig. 4). Three solution experiments also were performed with silver in bismuth at 350°. In the latter experiments the alloys formed all contained about 4 atomic % silver.

The molar heats of formation (ΔH^M) determined in these experiments are recorded in Table I, along with values of the quantity $\Delta H^M/x_{Ag}$. The data on silver–lead and silver–bismuth obtained at 450° were subjected to a least squares treatment, and may be represented by the equations

$$\Delta H^M(\text{Ag(s)} + \text{Pb(l)}, 450°) = 24.03x_{Ag} - 26.3x^2_{Ag} \text{ kjoule/g. atom} \quad (1)$$

$$\Delta H^M(\text{Ag(s)} + \text{Bi(l)}, 450°) = 24.01x_{Ag} - 24.7x^2_{Ag} \text{ kjoule/g. atom} \quad (2)$$

Values of $\Delta H^M/x_{Ag}$ calculated according to these equations have been included in Table I for comparison with the experimental results.

(1) O. J. Kleppa, *J. Am. Chem. Soc.*, **71**, 3275 (1949); **73**, 385 (1951).
(2) O. J. Kleppa, *ibid.*, **74**, 6047 (1952).
(3) O. J. Kleppa, THIS JOURNAL, **59**, 175 (1955).
(4) O. J. Kleppa and J. A. Weil, *J. Am. Chem. Soc.*, **73**, 4848 (1951).

TABLE I

MOLAR HEATS OF FORMATION OF LIQUID ALLOYS FROM SOLID SILVER AND LIQUID SOLVENT METALS

	Alloy composition x_{Ag}	Total g. atoms	ΔH^M, joule/g. atom	$\Delta H^M/x_{Ag}$, kjoule exp.	Calcd. eq. 1
(a) Ag–Tl, 450°	0.02060	0.5858	522	25.34	...
	.0338	.4256	838	24.79	...
	.05353	.3482	1297	24.23	...
(b) Ag–Pb, 450°	0.00732	1.1144	170.7	23.31	23.84
	.01907	0.9483	452	23.71	23.53
	.02115	.9872	503	23.78	23.48
	.04533	.5643	1048	23.12	22.84
	.06679	.3725	1479	22.14	22.27
	.08682	.2623	1875	21.60	21.75
	.09399	.2220	2029	21.59	21.55
				Mean dev. from eq. 1: 0.23 kj.	
					Calcd. eq. 2
(c) Ag–Bi, 450°	0.01953	0.8179	461	23.60	23.53
	.02956	.4963	688	23.56	23.28
	.04177	.4247	936	22.41	22.98
	.06197	.5134	1393	22.48	22.48
	.08791	.2391	1883	21.42	21.84
	.09738	.2695	2195	22.54	21.60
	.1297	.1936	2628	20.26	20.80
	.1800	.1626	3592	19.96	19.56
	.2032	.1759	3853	18.78	18.94
	.3338	.2001	5342	16.00	15.76
				Mean dev. from eq. 2: 0.36 kj.	
(d) Ag–Bi, 350°	0.03741	0.5145	847	22.64	Av.
	.04039	.4203	890	22.04	22.28 ± 0.24
	.04259	.4168	944	22.16	

The experimental data for 450° have been plotted in Fig. 1, ($\Delta H^M/x_{Ag}$ for all systems, ΔH^M for silver–bismuth). The appropriate curves have been drawn for the silver–bismuth system only. We note that the limiting heat of solution of silver in thallium is about 26 kjoule/g. atom, while the corresponding figures for silver in lead and in bismuth are both 24.0 kjoule. It is also worth noting that the limiting "curvatures" for these two systems are very nearly the same, −26.3 and −24.7 kjoule, respectively. The difference between these figures is not significant when the experimental precision is taken into account. Presumably the curvature for silver–thallium will be of the same order of magnitude, although the three observations on this system do not permit a reliable determination of the curvature.

The three experiments on silver–bismuth carried out at 350° show that when the temperature is reduced from 450 to 350°, the limiting heat of solution falls from 24.0 to about 23.3 kjoule/g. atom. Thus in this temperature range the average relative partial molal heat capacity of silver in pure liquid bismuth is of the order of +7 joule/degree.

The heats of mixing of liquid silver–lead and silver–bismuth alloys containing about 20 to 80 atomic % silver were determined calorimetrically at 1050° by Kawakami.[5] The experimental precision in this work was at best of the order of ±5–10%. By a tenuous extrapolation of Kawakami's data for higher silver contents, we find that the partial molal heats of solution of liquid silver in liquid lead and bismuth should be +12–14 kjoule and +8–10

(5) M. Kawakami, *Sci. Rep. Tohoku Imp. Univ.*, **19**, 521 (1930).

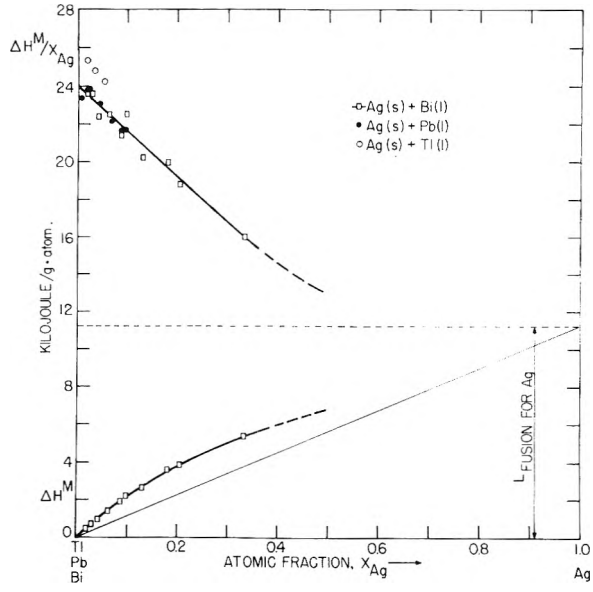

Fig. 1.—Heat of solution of silver in thallium, lead and bismuth at 450°.

kjoule/g. atom, respectively. If we set the heat of fusion of silver equal to 11.2 kjoule,[6] and take the difference in temperature into consideration, these values are in reasonable agreement with the present results.

Calorimetry. Gold Alloys.—Pure, solid gold was dissolved in liquid thallium in 8 experiments at 450° and 2 experiments at 350°; in liquid lead in 7 experiments at 450° and 2 at 350°; and in liquid bismuth in 8 experiments at 450° and 3 at 350°. The experiments at 450° gave alloys ranging from 1–2 to about 30 atomic % gold, while the runs at 350° generally were duplicate experiments at low gold concentrations.

The molar heats of formation are recorded in Table II, along with values of the quantity $\Delta H^M/x_{Au}$. The data for 450° were subjected to a least squares treatment, which gave the following equations for the molar heats of formation

$$\Delta H^M[\text{Au(s)} + \text{Tl(l)}, 450°] = 11.06x_{Au} - 0.7x^2_{Au} \text{ kjoule/g. atom} \quad (3)$$

$$\Delta H^M[\text{Au(s)} + \text{Pb(l)}, 450°] = 5.09x_{Au} + 8.6x^2_{Au} \text{ kjoule/g. atom} \quad (4)$$

$$\Delta H^M[\text{Au(s)} + \text{Bi(l)}, 450°] = 14.80x_{Au} - 5.3x^2_{Au} \text{ kjoule/g. atom} \quad (5)$$

Values of $\Delta H^M/x_{Au}$ calculated according to these equations have been included in Table II for comparison with the experimental results.

The experimental data on gold alloys obtained at 450° are plotted in Fig. 2. The experiments at 350° were carried out chiefly in order to throw some light on the temperature dependence of the heat of solution. We note that in all cases the heat (ΔH) of solution increases with increasing temperature. The effect appears to be strongest for gold in lead where the limiting heat of solution increases by about 1.6 kjoule when the temperature is raised from 350 to 450°. The corresponding figures for

(6) O. Kubaschewski and E. L. Evans, "Metallurgical Thermochemistry," London, 1951.

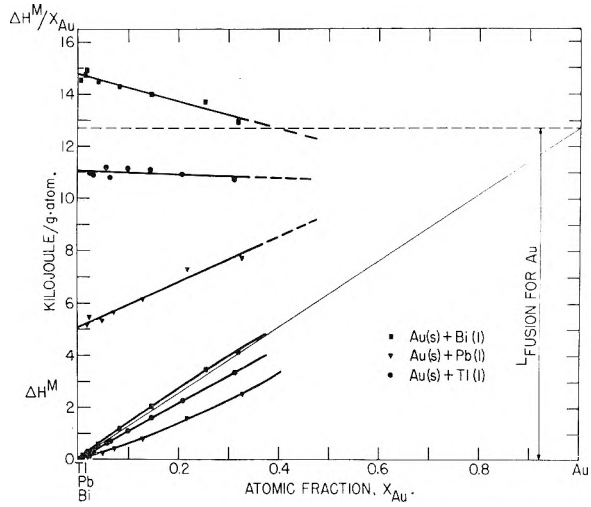

Fig. 2.—Heat of solution of gold in thallium, lead and bismuth at 450°.

gold in bismuth and thallium are 0.9 and 0.3 kjoule, respectively.

TABLE II

MOLAR HEATS OF FORMATION OF LIQUID ALLOYS FROM SOLID GOLD AND LIQUID SOLVENT METALS

	Alloy composition x_{Au}	Total g. atoms	ΔH^M, joule/g. atom	$\Delta H^M/x_{Au}$, kjoule Exp	Calcd. eq. 3
(a) Au–Tl, 450°	0.02431	0.6335	267.0	10.98	11.04
	.03143	.4361	342.6	10.90	11.04
	.05775	.2517	646	11.19	11.02
	.06480	.4516	701	10.81	11.01
	.09954	.1427	1111	11.16	10.99
	.1457	.1029	1620	11.12	10.96
	.2084	.1255	2280	10.94	10.91
	.3128	.07178	3354	10.72	10.84
				Mean dev. from eq. 3: 0.13 kj.	
					Calcd. eq. 4
(b) Au–Pb, 450°	0.01908	0.8787	98.8	5.18	5.25
	.02363	.5724	129.7	5.49	5.29
	.04820	.3418	256.3	5.32	5.50
	.07198	.2374	408.5	5.67	5.71
	.1298	.1405	798	6.15	6.21
	.2173	.08246	1592	7.33	6.96
	.3271	.07016	2525	7.72	7.91
				Mean dev. from eq. 4: 0.16 kj.	
					Calcd. eq. 5
(c) Au–Bi, 450°	0.01151	1.1651	167.1	14.52	14.74
	.01774	0.7655	262.2	14.78	14.71
	.01953	.6223	291.1	14.91	14.70
	.04118	.3256	596	14.48	14.58
	.08294	.1766	1186	14.30	14.36
	.1466	.1038	2054	14.01	14.03
	.2542	.07540	3487	13.72	13.46
	.3198	.07023	4137	12.94	13.12
				Mean dev. from eq. 5: 0.14 kj.	
(d) Au–Tl, 350°	0.04287	0.3558	462	10.78	10.75 ± 0.03
	.04306	.3579	462	10.73	
(e) Au–Pb, 350°	0.02569	0.6123	98.0	3.81	3.69 ± 0.13
	.02033	.9508	72.4	3.56	
(f) Au–Bi, 350°	0.01718	0.6266	241.1	14.04	13.84 ± 0.21
	.01760	.6434	239.8	13.63	
	.2068	.06755	2697	13.04	

We may compare the present results with corresponding heat data obtained indirectly from e.m.f. cell work at 600–700°. In order to facilitate this comparison we have in Fig. 3 plotted values of $\Delta H^M/x_{Au}$ and $\Delta F^E/x_{Au}$ (calculated from the e.m.f. data) *versus* x_{Au}. From this figure we obtain values of the relative partial molal heat content for liquid gold in thallium, lead and bismuth, as well as the

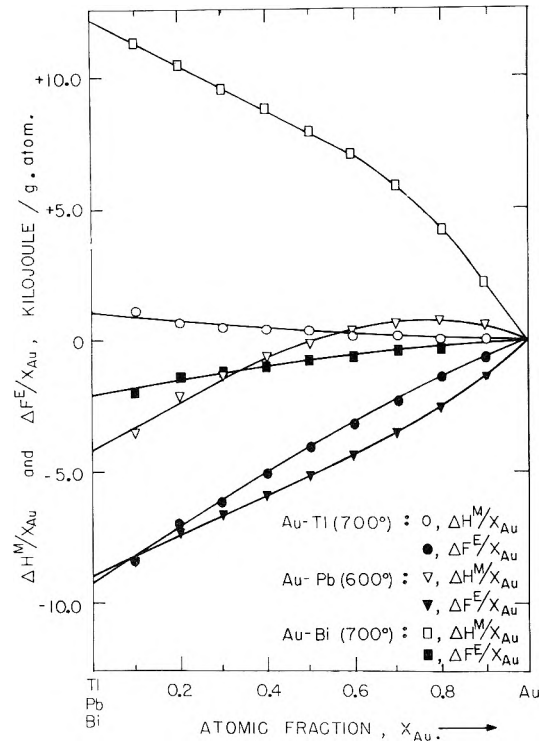

Fig. 3.—Heat of mixing and excess free energy in the liquid systems gold–thallium, gold–lead and gold–bismuth from e.m.f. measurements.

limiting "curvatures" for the heat of mixing at low gold concentrations. If we adopt 12.8 kjoule/g. atom for the heat of fusion of gold,[6] and assume this value to be essentially independent of temperature, we may calculate values of the limiting heats of solution of solid gold at the temperature of the e.m.f. measurements. We compare these e.m.f. data with the new calorimetric values in Table III.

TABLE III

CHARACTERISTIC HEAT DATA (IN KILOJOULES) FROM E.M.F. WORK[1] AND FROM CALORIMETRY

System	Limiting heat of soln. E.m.f. (temp., °C.)		Calorimetry 450°	Calorimetry 350°	Limiting "curvature" E.m.f. 6–700°	Limiting "curvature" Calorimetry 450°
Au(s) in Tl(l)	14	(700)	11.1	~10.8	−1.5	−0.7
Au(s) in Pb(l)	8.5	(600)	5.1	~ 3.5	9	8.6
Au(s) in Bi(l)	25	(700)	14.8	~13.9	−8	−5.3

This comparison indicates that the heat data calculated from the e.m.f. work are somewhat high, even if we allow for the temperature dependence of the heat of mixing. Still, the agreement must be considered as reasonably satisfactory for gold in thallium and lead. For gold in bismuth, however, the discrepancy is more serious. An examination of the original e.m.f. measurements shows that the temperature coefficients of the e.m.f.s determined for this system were associated with considerable uncertainty, particularly in the high temperature

(high gold) region. It also should be pointed out that the work on the gold–bismuth system is the only high temperature e.m.f. study where bismuth was used as the more electropositive component. While the data for moderate temperatures do not appear to show any anomalies, it may be worth exploring whether Bi/Bi^{+++} electrodes in salt melt systems are unreliable at very elevated temperatures.

The molar heats of formation of "Au_2Pb" and "Au_2Bi" (from solid gold and liquid lead resp. bismuth) were determined at 350° by dissolving the alloys in the liquid low-melting metals. In evaluating the molar heats of formation use was made of the heats of solution of gold quoted in Table II. The results are given in Table IV.

TABLE IV

MOLAR HEATS OF FORMATION OF "Au_2Pb" AND "Au_2Bi" FROM SOLID GOLD AND LIQUID LEAD AND BISMUTH AT 350°

Alloy	g. atoms	Solvent + alloy, g. atoms	Observed, joule	$-\Delta H^M$, kjoule/g. atom Result	Av.
"Au_2Pb"	0.009750	0.5580	44.2	2.15	
	.01929	.5676	85.2	1.95	2.05 ± 0.10
"Au_2Bi"	.00982	.4361	106.6	1.62	
	.01991	.4462	218.6	1.79	1.70 ± 0.09

The heat of formation of "Au_2Bi" was not previously known. For "Au_2Pb," however, a value of the heat of formation was calculated by the author from phase diagram information combined with activity data for the liquid gold–lead alloys at 600° extrapolated to lower temperatures.[1] This calculation gave the value −8.4 kjoule/g. atom for formation of the alloy from liquid, undercooled gold and liquid lead at about 350°. With a heat of fusion for gold of 12.8, this would indicate little or no heat effect associated with the formation from solid gold and liquid lead. The present work shows that this heat effect is actually −2.0 kjoule/g. atom.

Solubility Measurements.—The solubility data for solid silver in liquid thallium, lead and bismuth are given in Table V, and plotted in Fig. 4. In this figure we have included what appears to be the most reliable earlier liquidus data for these three systems,[7,8] as well as the solubility information for thallium, lead and bismuth in solid silver reported by Raub and Engel.[9]

For solutions of gold in bismuth the freezing point depression curve given by Hansen[10] appeared to be uncertain. Therefore some exploratory solubility and thermal analysis runs were carried out with alloys containing about 10 atomic % gold. As a result it was found that at this composition the freezing point depression is 22 ± 1° (liquidus at 249°).

Thermodynamic Calculations

It is a problem of considerable interest to derive reliable excess free energy, heat and entropy data for a binary system from the equilibrium phase diagram.[2] In general, this problem is quite laborious and involves tedious and time-consuming calculations.

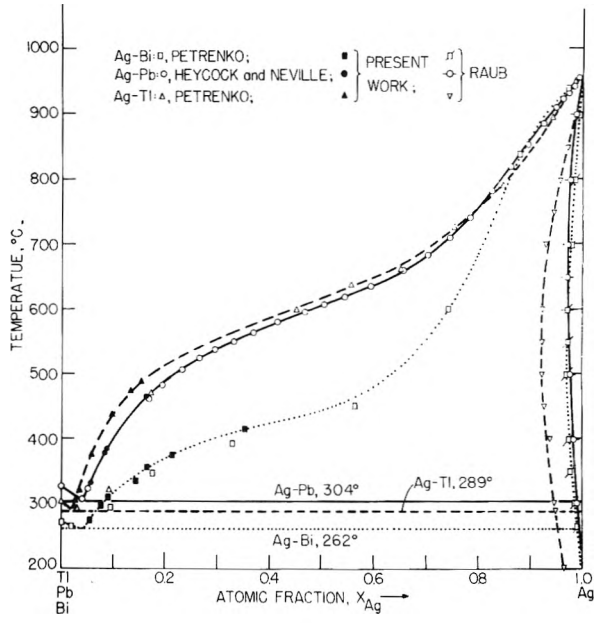

Fig. 4.—Phase diagrams of the systems silver–thallium, silver–lead and silver–bismuth.

TABLE V

SOLUBILITY OF SILVER IN LIQUID THALLIUM, LEAD AND BISMUTH

	T, °K.	x_{Ag}
(a) Ag–Tl	569	0.0266
	578	.0286
	593	.0345
	647	.0577
	710	.0971
	746	.1332
	761	.1531
(b) Ag–Pb	595	0.0517
	605	.0566
	650	.0828
	656	.0881
	737	.1631
(c) Ag–Bi	547	0.0552
	569	.0763
	583	.0904
	607	.1420
	628	.1634
	647	.2147
	688	.354

In the present work, however, we are concerned chiefly with moderately dilute liquid solutions, in which case these calculations sometimes can be simplified to a considerable extent.

In moderately dilute solutions it is convenient to expand the excess thermodynamic functions (*i.e.*, ΔF^E, ΔH^M and ΔS^E) in powers of the mole fraction of the minor component.[11] In the case of ΔF^E we get

$$\Delta F^E = Ax_1 + Bx_1^2 + \text{h.o.t.} \qquad (6)$$

For a given temperature A and B are characteristic excess free energy constants of the solution. As long as x_1 is not too large we may retain the two

(7) C. T. Heycock and F. H. Neville, *Phil. Trans. Roy. Soc. (London)*, **A189**, 37 (1897).

(8) G. J. Petrenko, *Z. anorg. allgem. Chem.*, **50**, 133, 136 (1906).

(9) E. Raub and A. Engel, *Metallforschung*, **1**, 76 (1946).

(10) M. Hansen, "Aufbau der Zweistofflegierungen," Berlin, 1936.

(11) O. J. Kleppa, THIS JOURNAL, **59**, 354 (1955).

first terms only. In this case we obtain for the two relative partial molal excess free energies

$$\bar{F}_1^E \text{ (minor component)} = (A + B) - Bx_2^2 \quad (7a)$$

$$\bar{F}_2^E \text{ (major component)} = -Bx_1^2 \quad (7b)$$

We may, of course, write completely analogous expressions for ΔH^M in terms of characteristic enthalpy constants a and b, and for the excess entropy in terms of constants α and β. Because of the fundamental relation between excess free energy, heat and excess entropy we have

$$A = a - \alpha T \text{ and, } B = b - \beta T$$

Over limited ranges in temperature we may to a first approximation assume a, b, α and β to be independent of temperature, while A and B depend on temperature only through the entropy constants α and β.

We are at present particularly interested in the solutions of copper, silver and gold (below designated component 1) in liquid thallium, lead and bismuth (component 2). If we assume the heats of fusion of 1 and 2 to be independent of temperature, it can be shown that the equilibrium between nearly pure solid 1 or 2 and the moderately dilute liquid solutions of 1 in 2 will yield the following relations.

(a) For the freezing point depression of 2

$$B_S x_1^2 - B_L y_1^2 = \Delta S_2(f)(T - T_2) - RT \ln (y_2/x_2) \quad (8)$$

(b) For the solubility of 1 in 2

$$A_L + B_L - B_L y_2^2 + B_S x_2^2 = \Delta S_1(f)(T - T_1) - RT \ln (y_1/x_1) \quad (9)$$

In these expressions y and x are the equilibrium mole fractions in the liquid and solid phase, respectively, while the subscripts L and S similarly refer to formation of the liquid or solid phase from the elements in the equivalent state. $\Delta S(f)$ is the entropy of fusion, while T_1 and T_2 are the melting points of 1 and 2. If the appropriate solid solubilities (x) are very small, we may in (8) and (9) neglect the terms $B_S x^2$. Under these conditions one set of equilibrium observations (x,y,T) in (8) should be sufficient for evaluation of B_L, while two sets of observations (at reasonably well-separated compositions and temperatures) should, at least in principle, permit a separation of B_L into b_L and β_L.

We may use equation 8 to calculate B_L from the freezing point depression curves for silver and gold dissolved in the low melting liquid metals. However, for the silver alloys the eutectic temperatures are quite close to the melting points of the pure metals. This tends to make the calculated values of B_L very inaccurate. For the gold systems, on the other hand, the freezing point curves extend to higher gold concentrations and lower temperatures. From liquidus data quoted by Hansen[10] and heats of fusion given by Kubaschewski and Evans[6] we calculate B_L at about 300° for gold in thallium to be $\sim +5.5$ kjoule, and for gold in lead $\sim +8$ kjoule. From the information on gold in bismuth quoted above we similarly get $B_L \sim 0$. The limited temperature range and the inaccuracy of the equilibrium data prevent a reliable separation of the excess free energy constants B_L into b_L and β_L. We may, on the other hand, compare the values of B_L calculated from the phase diagram with corresponding data obtained from the author's e.m.f. work at 6–700°. From Fig. 3 we find the following values of B_L: Au in Tl (700°): +10.5; Au in Pb (600°): +8; Au in Bi (700°): +3 kjoule. When the temperature dependence of these quantities is taken into account (primarily through the terms $\beta_L \Delta T$, see values of β_L given in Table VI), the agreement must be considered as very satisfactory.

If we now consider equation 9, which refers to the solubility of 1 in 2, we note that each set of equilibrium data (x,y,T) here will give us one relation between A_L and B_L. However as A_L and B_L are temperature dependent quantities (containing to a first approximation a, b, α, β, T), we require equilibrium data for at least four reasonably well-separated temperatures (and compositions) in order to obtain all four solution constants. In certain cases y_2 remains close to 1 over a wide range in temperature. Then one may neglect the terms containing B_L compared to A_L in eq. 9 and determine a_L and α_L without evaluating b_L and β_L. For the solutions of copper in thallium, lead and bismuth this method of evaluation yields essentially the same results as the previously described graphical method.[2] In other cases it will not be possible to evaluate all four constants, although fairly good values of A_L and B_L for a given temperature may be secured.

From the data in Table V the following values of A_L and B_L were calculated for the solutions of silver in thallium, lead and bismuth: Ag–Tl (450°): 11.4 and −15.3 kjoule; Ag–Pb (450°): 9.8 and −11.3 kjoule; Ag–Bi (350°): 7.6 and −12.5 kjoule. However, only for the system silver–lead was it possible to achieve a reliable separation of heat and entropy terms from phase diagram information alone. The calculation gave the following results: $a_L \sim 12$ kjoule, $b_L \sim -23.6$ kjoule; $\alpha_L \sim 3$ joule/degree and $\beta_L \sim -17$ joule/degree. The calculated values may be compared with the calorimetric values of a_L and b_L for 450°: $a_L = 24.0 - 11.2 = 12.8$ kjoule, and $b_L = -26.2$ kjoule. Thus the agreement is quite good. For this system and also for silver in thallium and bismuth the most reliable complete set of solution constants are obtained by combination of A_L and B_L from the phase diagram with a_L and b_L obtained calorimetrically. In this way we calculate the characteristic constants given in Table VI for the systems involving silver. In this table we give also as far as possible equivalent data for the gold solutions (calculated from e.m.f., freezing point depressions and calorimetry), as well as values of A_L, a_L and α_L for the corresponding copper systems (obtained from solubility data alone and arbitrarily referred to 450°).

Discussion

The thermodynamic data given in the present work and summarized in Table VI show certain interesting features which call for some discussion. It is first important to recall that the reported heat and entropy constants (a, b, α and β) in general may vary with temperature, and that a comparison of data for different temperatures may be questionable. Unfortunately we know little about the temperature dependence of these constants. Our

TABLE VI

SUMMARY OF CHARACTERISTIC SOLUTION CONSTANTS FOR THE MODERATELY DILUTE LIQUID SOLUTIONS OF COPPER, SILVER AND GOLD IN THALLIUM, LEAD AND BISMUTH

System	A_L	a_L	α_L, joule/deg.	B_L	b_L, kjoule	β_L, joule/deg.	Method
Cu–Tl, ~450°	28	34	8.5	....	.....	.....	Solubility data alone
Cu–Pb, ~450°	24	28	6	....	.....	.....	
Cu–Bi, ~450°	15	19	6	....	.....	.....	
Ag–Tl, 450°	11.4	15	5	−15.3	−30?	−20?	Solubility and calorimetry
Ag–Pb, 450°	9.8	12.8	4	−11.3	−26.2	−21	
Ag–Bi, 350°	7.6	12.1	7	−12.5	~−25	~−20	
Au–Tl, 700°	−9	1	10	10.5	−1.5	−12	E.m.f. alone
Au–Pb, 600°	−9	−4	5.5	8	9	1	
Au–Bi, 700°	−2	~4	~6	3	.....	.....	E.m.f. and calorimetry
Au–Tl, ~300°	...	−2	...	~ 5.5	~− 0.7	~−10	Freezing point depression and calorimetry
Au–Pb, ~300°	...	−10	...	~ 8	~ 8.6	~ 1	
Au–Bi, ~300°	...	1	...	~ 0	~− 5.3	~− 9	

information is largely restricted to what we observed about a_L for the three gold systems and for silver–bismuth (see above). In these four cases we found that a_L (and accordingly also α_L) increases algebraically with increasing temperature. Between 350 and 450° the effect is roughly of the same order for silver–bismuth and for gold–bismuth (~7 and ~9 joule/degree, respectively). It is about twice as large for gold in lead and about one half for gold in thallium. We should here perhaps also mention that a_L for gold in tin varies with temperature roughly as for gold in lead.[12] However, the actual values of a_L for gold–tin are more negative than for any of the present systems (~ −33 kjoule at 450°).

Possibly the most interesting common feature of the data presented in Table VI is that all the systems show considerable excess entropies of solution, with values of α_L ranging from 4 to 10 joule/degree. The corresponding heat terms cover a range from −10 kjoule (gold–lead at ~300°) to +34 kjoule (copper–thallium). It is noted that the highest values of α_L are found for gold–thallium and copper–thallium, while the lowest values are exhibited by silver–lead at 450° and by gold–lead at lower temperatures.[13] The mentioned information on the temperature dependence of a_L and α_L suggests that it may be worthwhile to consider further the origin of the excess entropy terms observed in the present systems. In earlier communications the author suggested that the excess entropies found in the gold and copper systems might be due to vibrational heat capacity effects and/or to a volume expansion associated with the packing of atoms of different size.[1,2] Vibrational heat capacity effects may in principle be of two types: (a) associated with a change in the characteristic temperature on alloying or (b) due to anharmonicity of the thermal vibrations. It is possible that the heat capacity deviations observed in the present work could be related to the latter of these effects. It appears improbable, on the other hand, that they can be explained by a volume expansion: It seems likely that the packing difficulties which in turn lead to volume expansions become less serious as the temperature is increased.[11] Finally it is of course quite possible that the increase in heat and entropy with temperature may result from a weakening of the chemical bond proper,[12] or from the combined work of several factors. The latter explanation is particularly attractive because the observed heat terms a_L have both *positive* and negative values.

Another interesting feature of the data given in Table VI is the remarkable constancy of β_L for the three silver systems. Thus for moderately dilute liquid solutions of silver in thallium, lead and bismuth, the excess partial molal entropies of the solvent metals are all positive and have essentially the same value for the same silver content. Among the gold systems gold–thallium and gold–bismuth show somewhat analogous behavior, while gold–lead is entirely out of line. We have previously mentioned the great similarity of the heat data for the silver alloys. In fact among the three silver systems the most significant difference in thermodynamic properties is the difference in the entropy constant, α_L, which is much higher for silver–bismuth than for silver–lead and silver–thallium. It is in large measure due to this high value of α_L that the silver–bismuth phase diagram differs significantly from those of the two other systems (see Fig. 4).

In recent communications[12] the author has shown how for certain alloy systems the experimental data on the limiting "curvatures" of the heat of mixing (*i.e.*, the constants b_L in Table VI) agree with a rule derived theoretically by Friedel.[14] The derivation of Friedel's rule is based on the displacement of the Fermi level of the solvent metals by solute atoms of different valence. The rule predicts that, in the absence of the complicating effects of large size differences and of strong chemical interaction between the components, the limiting curvature should be negative for a solute of lower valence than the solvent and positive for solutes of higher valence. Furthermore, for the same solvent, the magnitude of the curvature for different solutes should be roughly proportional to the valence difference.

It will be noted that, with the exception of gold–lead, all the considered systems show negative values

(12) O. J. Kleppa, submitted for publication.

(13) This is not evident from Table VI, but is a consequence of the strong temperature dependence of a_L for this system.

(14) J. Friedel, *Adv. in Physics*, **3**, 446 (1954).

of b_L. However, for solutions of silver and gold in the same solvent, where we according to Friedel might expect somewhat similar values of b_L such a similarity is not actually observed. Now it may be recalled that the atoms of silver and gold have very nearly the same atomic size. Therefore, we are not able to explain this discrepancy as a size effect. On the other hand we note that the chemical interaction (as measured, *e.g.*, by the magnitude and sign of the constants a_L in Table VI) is considerably stronger for the gold systems than for the silver systems. This may, at least in part, explain why Friedel's rule is not obeyed in a more quantitative manner.

Acknowledgments.—The author wishes to acknowledge the assistance of Miss M. C. Bachelder in performing the chemical analyses. This work has been supported in part by the Office of Naval Research through Contract No. 6-ori-02004 with the University of Chicago.

PROTON RELAXATION ON CATALYTIC SOLIDS

BY T. W. HICKMOTT AND P. W. SELWOOD

Contribution from the Department of Chemistry of Northwestern University, Evanston, Illinois, and the Department of Physics of Harvard University, Cambridge, Mass.

Received September 26, 1955

Proton relaxation time measurements by means of the spin–echo method have been made for liquids absorbed on high area, diamagnetic catalyst supports. It was found that the diamagnetic substances markedly reduce proton relaxation times. Associated liquids such as methanol, ethanol and water, and the non-associated hydrocarbon *n*-hexane were absorbed on γ-Al_2O_3 and the relaxation time plotted as a function of the weight of liquid. For all the liquids studied a linear relation between relaxation time and weight of liquid was found over a fourfold increase of variables, with γ-Al_2O_3 being markedly more effective in lowering the relaxation time of protons in associated liquids compared to the effect on protons in *n*-hexane. A qualitative theory in terms of the porous structure of the diamagnetic solid and hydrogen exchange with the defect structure of the catalyst has been developed. Limited measurements for water absorbed on high area silica–alumina catalysts lend support to the theory, as do observations of the change in proton relaxation time for liquids absorbed on paramagnetic oxides that are supported on γ-Al_2O_3.

Introduction

Among the most used catalysts are those based on high area, diamagnetic oxides such as γ-Al_2O_3 or silica gel. The oxides themselves are catalysts for reactions such as dehydrogenation, dehydration or cracking of hydrocarbons. In addition they are used to support and disperse paramagnetic substances such as oxides of copper, manganese or chromium and thus to increase the catalytic activity of these substances for specific reactions. The proton spin-lattice relaxation time, T_1, can be measured directly by the techniques of nuclear resonance absorption.[1,2] This quantity, a measure of the interaction of the nuclear spin system with its surroundings, is characteristic of a pure liquid, and is extremely sensitive to any changes in the electronic and magnetic environment of nuclei and therefore to the motion of nuclei. The present work is concerned with the effect of liquid–solid interactions on the proton relaxation time of liquids absorbed on diamagnetic solids, particularly γ-Al_2O_3. It also extends previous measurements of the relaxation time of protons in water absorbed on supported paramagnetic oxides.[3,4]

Experimental

Proton Relaxation.—Relaxation time measurements were made by means of the spin–echo method for detecting nuclear resonance. The 180°–90°–180° pulse method for measuring T_1 was used; the details of the equipment as well as the theory of the method are available elsewhere.[5,6,7] Since this is a null method, and the time of separation between 180 and 90° pulses can be measured accurately, it is possible to measure T_1 for very small samples and to estimate the error in any measurement. In addition, a range of T_1 from two milliseconds to several seconds can be covered with uniform accuracy throughout the whole range. A permanent magnet with field strength of 3510 oersteds was used, with homogeneity of 0.1 oersted over a sample size of 0.3 cc., just small enough that the decay tail following a pulse was not completely obscured by saturation of the amplifier and receiver. The permanent magnet had an advantage of greater stability over an electromagnet, thus making it possible to take several minutes in the measurement of a relaxation time. With an electromagnet considerable field drifts would be likely to occur over this length of time.

In making a measurement, the frequency of the r.f. pulse generator was first adjusted to the resonant frequency of the nuclei. The pulse amplitude and duration were then varied until the appearance of a three pulse sequence on the oscilloscope showed that both 90 and 180° pulses were independently available from separate gating circuits. During the course of a series of measurements, the pulse widths would be checked frequently since there was some tendency to drift. In practice, the simultaneous adjustment of the resonant frequency of the oscillator, the tuning capacitor of the tank circuit containing the sample, the coupling capacitor between tank circuit and oscillator, and the pulse width were all crucial, and all had to be carefully set.

To measure T_1, a 180° pulse was followed by a 90° pulse coincident with the triggering of the oscilloscope sweep, and then by an indicating 180° pulse. The time separation of the 180–90° pulses was changed until the echo following the second 180° pulse vanished into the noise. The time separation at which the echo reappeared from the noise was also observed and a point midway in time between them was used for a value of τ_{null}, with $\tau_{null} = T_1 \ln 2$. The accuracy in the T_1 measurements was considered to be the value at each of the two points where the signal vanished into the noise. In order to avoid corrections to the observed values

(1) N. Bloembergen, E. M. Purcell and R. V. Pound, *Phys. Rev.*, **73**, 679 (1948).

(2) F. Bloch, *ibid.*, **70**, 460 (1946).

(3) R. B. Spooner and P. W. Selwood, *J. Am. Chem. Soc.*, **71**, 2184 (1949).

(4) P. W. Selwood and P. K. Schroyer, *Disc. Faraday Soc.*, **8**, 337 (1950).

(5) E. L. Hahn, *Phys. Rev.*, **80**, 580 (1950).

(6) H. Y. Carr and E. M. Purcell, *ibid.*, **94**, 630 (1954).

(7) G. B. Benedek, *J. Chem. Phys.*, **22**, 2003 (1954).

of T_1,[8] the time between inverting pulses was made at least eight times as long as the relaxation time measured. This meant that the repetition time for water where $T_1 = 2.5$ seconds was about 20 seconds, and the stability of the permanent magnet over a period of several minutes became important. On some samples, the spin–spin relaxation time, T_2, was measured by the "one-shot" method.[6] Since this depends on a determination of the echo amplitude instead of its vanishing point, fairly large samples were needed, and the accuracy of the measurements was difficult to estimate. Instrumental non-linearities, particularly in the broad-band amplifier used, also caused errors in the measurement of T_2 without affecting observed values of T_1.

Preparation of Samples.—Preparation of the γ-Al_2O_3 has been described.[9] Supported oxides of manganese were prepared[10] by impregnating a fixed weight of γ-Al_2O_3 with manganous nitrate solution, filtering off the excess solution, and igniting the dried filtrate at 200° for 24 hours to produce the so-called "low-ignition" series. Various concentrations of manganese, by weight, were achieved by varying the concentration of manganese in the impregnating solution. Magnetic and analytical studies[11] indicate that at low concentrations the manganese is present as the sesquioxide while a valence of four is found at higher concentrations. The transition between oxidation state of three and four is gradual. Catalytic data on these oxides have also been reported,[12] a peak in the activity for hydrogen peroxide decomposition occurring at about 4% manganese. Supported copper oxides were prepared[13,14] by impregnation of γ-alumina with cupric nitrate solution, the dried solid being calcined at 390° for 24 hours.

In order to provide a basis of comparison between samples with different amounts of paramagnetic ion, all supported oxides were mechanically diluted to a common percentage of paramagnetic ion by the addition of diamagnetic γ-alumina. For manganese, dilutions of 1 and 0.75% were used, while all copper samples were diluted to 0.50% by weight. An additional reason for the dilution is that supported oxides containing several per cent. of paramagnetic ions would reduce proton relaxation times so greatly that they would be difficult to measure. However, the necessity of dilution greatly complicates interpretation of the results since γ-alumina alone markedly reduces proton relaxation times. The notation for a diluted sample is, for example, 3.4/1% MnO_2/Al_2O_3. This indicates that a sample which originally contained 3.4% manganese, by weight, has been diluted to 1% manganese by weight, by the addition of a suitable amount of γ-alumina. In practice, the amount of γ-alumina diluent in a manganese sample varied from 47.3% for a 1.9/1% dilution to 92.2% for a 9.6/0.75% sample. For the copper oxides, it ranged from 0% for a 0.50/0.50% sample to 93.1% for a 7.29/0.50% sample. It is evident that the effect of γ-alumina also must be considered in any interpretation of results. For all samples, 0.0400 ± 0.0005 g. of powder was weighed into a corked 1/8 dram vial of 6 mm. o.d. which fitted snugly into the tank coil of the spin–echo equipment. To this vial a few drops of proton-containing material were added by means of a pipet, and the amount of liquid was weighed. After at least 15 minutes, relaxation time measurements were made. An additional aliquot of liquid would then be added and weighed and another measurement taken. The weight of liquid at any time was considered to be additive, thus neglecting any evaporation from the vial. More liquid was added until the powder became saturated, a condition shown by the formation of a small puddle of liquid on adding more liquid. In practice, four or five measurements could be made on any one sample. The weighing errors were cumulative and about ±0.0002 g. for each weighing.

Proton-containing liquids used were water, methanol, ethanol and *n*-hexane. The water, prepared by passing glass distilled water through an ion-exchange column, had a measured $T_1 = 2.5 \pm 0.15$ second. The methanol was Merck absolute methanol that assayed 99.5% CH_3OH by volume and conformed to A.C.S. specifications. No attempt was made to purify it further, and $T_1 = 2.46 \pm 0.15$ second. The ethanol had a measured $T_1 = 1.80 \pm 0.10$ second and was absolute alcohol from the Commercial Solvents Company, used without further purification. *n*-Hexane was obtained from the Matheson Company and had $T_1 = 2.40 \pm 0.15$ seconds. It contained at least 99% *n*-hexane, the most probable impurity being methylcyclopentane. All measurements were made at room temperature and no temperature dependence was studied. Since values of T_2 for the pure liquids were uncertain due to diffusion[5,6] and modulation[15] effects, and since the accuracy of such measurements in the presence of catalyst is uncertain, measured values of T_2 for absorbed liquids have not been included in this paper; they may be found elsewhere,[16] along with estimates of errors in specific T_1 measurements.

Results

Diamagnetic Supports.—Graphs of the value of proton relaxation times as a function of weight of liquid on 0.0400 g. of γ-Al_2O_3 are shown in Fig. 1 for

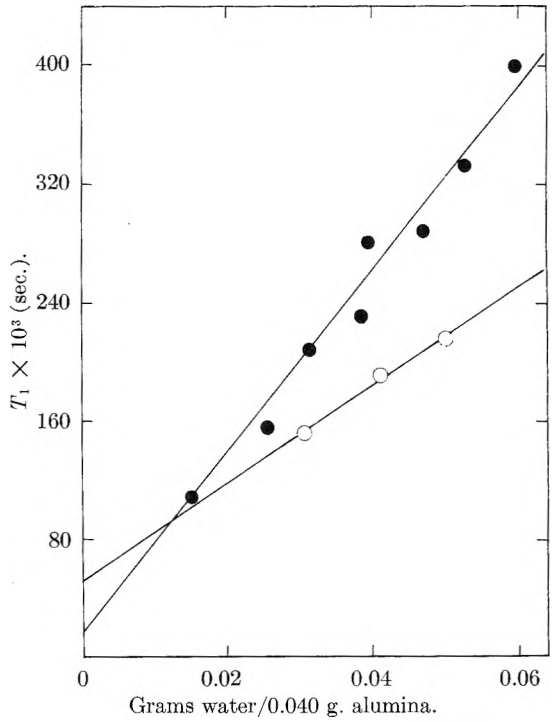

Fig. 1.—Proton relaxation time as a function of water absorbed on γ-alumina: ●, on γ-Al_2O_3; ○, on γ-Al_2O_3-B.

water, Fig. 2 for methanol and ethanol, and Fig. 3 for *n*-hexane. The γ-Al_2O_3 studied principally had an area of about 200 square meters per gram (BET nitrogen), and was free of ferromagnetic impurities. γ-Al_2O_3-B had a specific area of about 280 square meters per gram with a magnetic susceptibility $\chi = -0.382 \times 10^{-6}$. Measurements on two separate samples of γ-Al_2O_3 are included in Fig. 1, while only one sample of γ-Al_2O_3-B was studied. The dehydrated γ-Al_2O_3 in Fig. 3 was obtained by heating the regular γ-Al_2O_3 for 4.5 hours at 470°. This was not a high enough temperature to affect appreciably the surface area or pore structure of the alumina, but it did drive off 6.3% by weight of volatile impurities, most probably water.

To provide a basis of comparison for the behavior

(8) G. B. Benedek, Thesis, Harvard University, 1953.

(9) R. P. Eischens and P. W. Selwood, *J. Am. Chem. Soc.*, **69**, 1590 (1947).

(10) P. W. Selwood, T. E. Moore, M. Ellis and K. Wethington, *ibid.*, **71**, 693 (1949).

(11) P. W. Selwood, *Advances in Catalysis*, III, 27 (1951).

(12) J. Mooi and P. W. Selwood, *J. Am. Chem. Soc.*, **74**, 1750 (1952).

(13) P. W. Selwood and N. S. Dallas, *ibid.*, **70**, 2145 (1948).

(14) P. E. Jacobson and P. W. Selwood, *ibid.*, **76**, 2641 (1954).

(15) E. L. Hahn and D. E. Maxwell, *Phys. Rev.*, **88**, 1070 (1952).

(16) T. W. Hickmott, Thesis, Northwestern University, 1954.

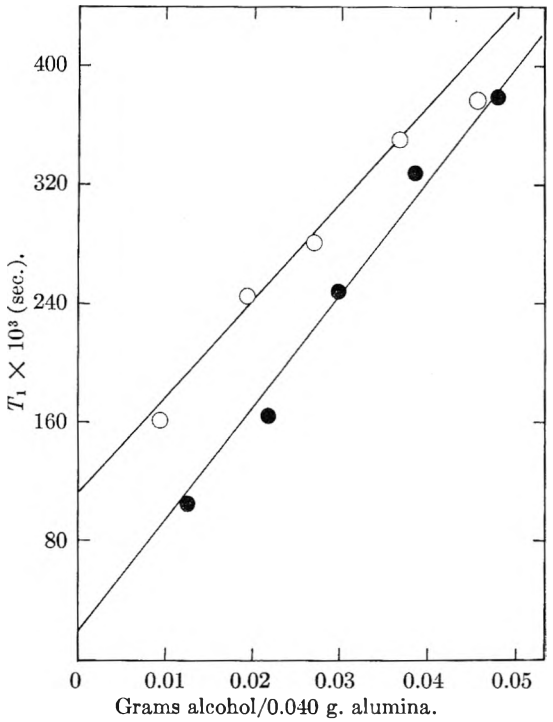

Fig. 2.—Proton relaxation time as a function of methanol (●), and of ethanol (○) absorbed on γ-alumina.

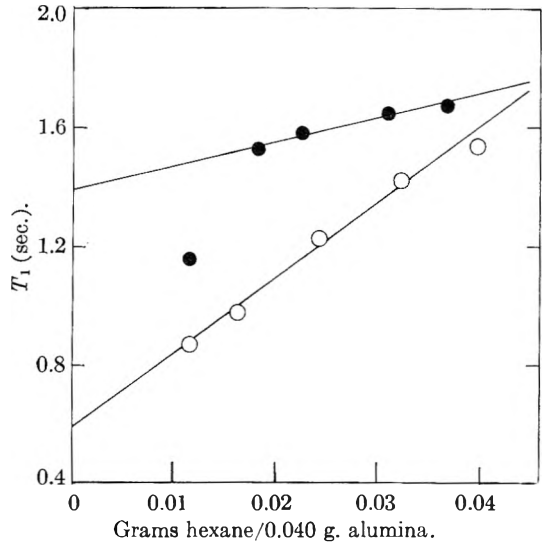

Fig. 3.—Proton relaxation time as a function of hexane absorbed on γ-alumina: ●, γ-Al_2O_3; ○, dehydrated γ-Al_2O_3.

of different substances on the same catalyst, use the slopes of the graphs of relaxation time *versus* weight of liquid to define a quantity, β, by means of the equation, $T_1 = T_{1(0)} + \beta N$ where $T_{1(0)}$ is the intercept of the relaxation time curve on the ordinate and N is the number of moles of proton-containing liquid added to the 0.04-g. sample used in the present work. To provide a further basis of comparison, divide β by the total number of hydrogen atoms per molecule, since every hydrogen atom contributes equally to the resonance. This quantity will be designated by δ in this paper. Table I shows the values of β,δ and $T_{1(0)}$ for liquids on γ-Al_2O_3. These quantities have no theoretical justification but provide a means of comparing results of measurements on different liquids.

TABLE I

β, δ AND $T_{1(0)}$ FOR LIQUIDS ON 0.0400 g. OF γ-ALUMINA

Liquid	β (sec./mole)	δ (sec./mole-H atom)	$T_{1(0)}$ (sec.)
Water	110	55	0.016
Methanol	209	52	.038
Ethanol	353	59	.112
n-Hexane	690	49	1.39
n-Hexane (dehydrated γ-Al_2O_3)	2210	158	0.59

Figure 4 shows relaxation time *versus* grams of water for two cracking catalysts. The UOP cracking catalyst was obtained from Dr. H. Pines. It was UOP type B, a zirconia-silica-alumina catalyst, containing 86.2% silica, 9.4% zirconia and 4.3% alumina by weight. The second commercial cracking catalyst was obtained from the Standard Oil Company (Indiana). It contained about 20% volatile content and, on a dry basis, 13% alumina, the rest being silica. Its surface area was stated to be about 740 square meters per gram. It is not known whether any magnetic impurities were present in either cracking catalyst. No detailed studies have been made on cracking catalysts since it was outside the scope of this work, but the linear relationship between the relaxation time and weight of liquid seems to hold as well for such systems as for alumina.

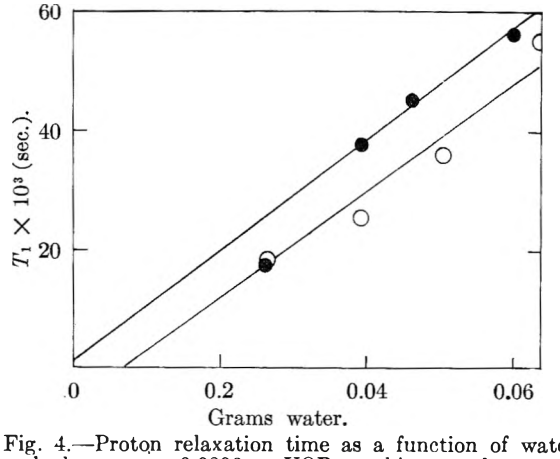

Fig. 4.—Proton relaxation time as a function of water absorbed on: ●, 0.0806 g. UOP cracking catalyst; ○, 0.0516 g. commercial cracking catalyst.

Figures 5 through 8 illustrate three major types of behavior for liquids absorbed on diluted, supported paramagnetic oxides. The first, and most common, is typified by Fig. 5 for ethanol on 1% MnO_2/Al_2O_3. It is observed for associated liquids on supported manganese, and partially for alcohols on supported copper. Characteristic is a regular increase of slope and intercept of the line joining experimental points, with the lowest relaxation times measured being one-hundredth the relaxation time for pure liquid. The second type is that of *n*-hexane on supported copper oxide. Here, a linear relation between relaxation time and weight of liquid is again observed, but the lowest observed relaxation times, even on undiluted oxide as for 0.50/

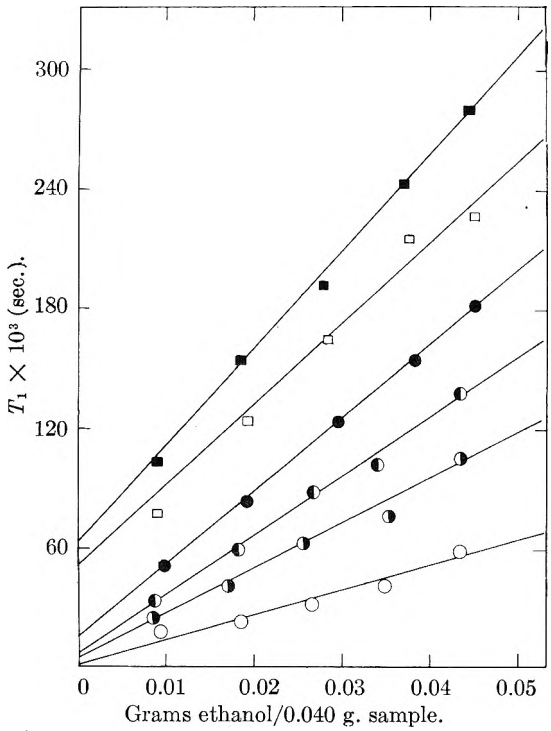

Fig. 5.—Proton relaxation time as a function of ethanol absorbed on supported manganese oxide diluted to 1%: ○, 1.9/1; ◑, 3.4/1; ◐, 4.5/1; ●, 6.1/1; □, 7.0/1; ■, 9.6/1. (See text for explanation of dilution terminology.)

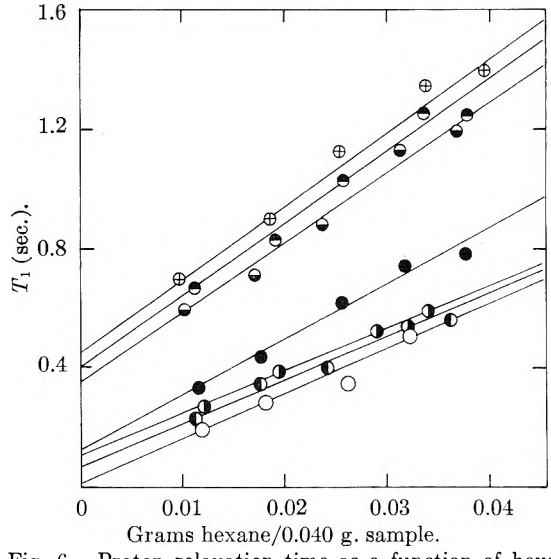

Fig. 6.—Proton relaxation time as a function of hexane absorbed on supported cupric oxide diluted to 0.5%: ○, 0.50/0.50; ◐, 1.36/0.50; ◑, 1.96/0.50; ●, 3.64/0.50; ◒, 4.70/0.50; ◓, 6.12/0.50; ⊕, 7.29/0.50.

0.50% copper oxide, is only about one-tenth that of the pure liquid. It is analogous to the behavior of *n*-hexane on diamagnetic supports and shows the importance of hydrogen bond interactions and proton exchange with the support in reducing relaxation times, even if paramagnetic impurities are present. The third type of curve is shown in Fig. 7, water on supported copper oxide. Here all lines show nearly the same slope, and even the most diluted catalyst samples are extremely effective in reducing the proton relaxation time. A related effect is observed for ethanol and methanol on supported copper oxide, for the data for 1.36/0.50% and 1.96/0.50% dilutions are fitted best by two intersecting lines of different slope. To attempt to verify the reality of the effect, two separate samples were measured and points from both measurements are plotted on the same graph. The break in the line seems well outside experimental error.

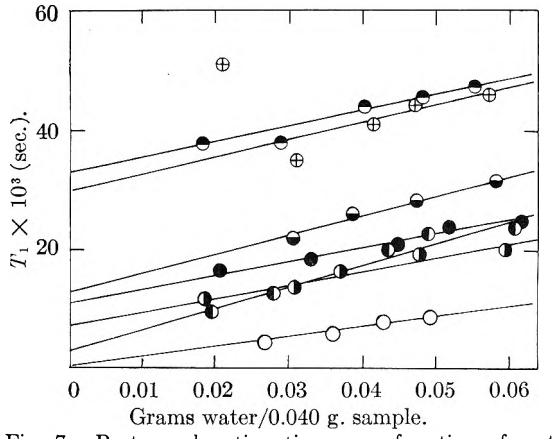

Fig. 7.—Proton relaxation time as a function of water absorbed on supported cupric oxide diluted to 0.5%: ○, 0.50/0.50; ◐, 1.36/0.50; ◑, 1.96/0.50; ●, 3.64/0.50; ◒, 4.70/0.50; ◓, 6.12/0.50; ⊕, 7.29/0.50.

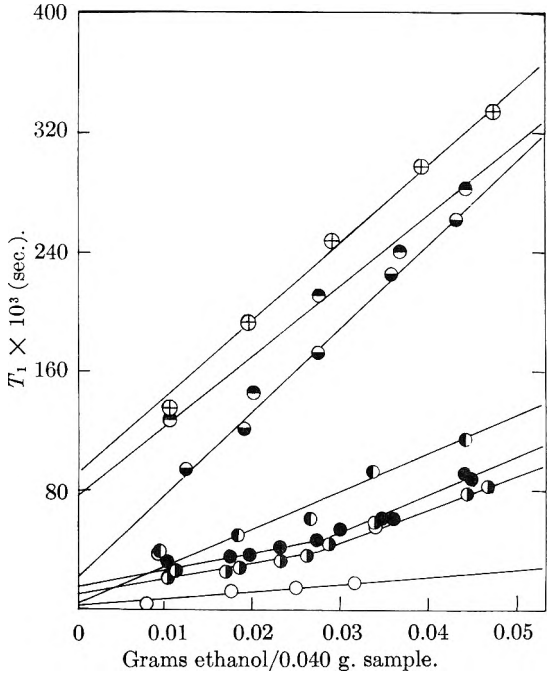

Fig. 8.—Proton relaxation time as a function of ethanol absorbed on supported cupric oxide diluted to 0.5%: ○, 0.50/0.50; ◑, 1.36/0.50; ◐, 1.96/0.50; ●, 3.64/0.50; ◒, 4.70/0.50; ◓, 6.12/0.50; ⊕, 7.29/0.50.

Discussion

The effect of paramagnetic ions in reducing the relaxation time of protons in both liquids[1] and solids[17] is well known. The results on high area catalyst supports show that diamagnetic substances may also have the same effect on protons in liquids absorbed on them.

Examination of Figs. 1 through 4 shows a number of features requiring explanation. (1) The ex-

(17) N. Bloembergen, *Physica*, **15**, 386 (1949).

perimental points for relaxation time *versus* weight of liquid fall on a reasonably good straight line over a fourfold increase of both variables. (2) A difference exists in the behavior of water, ethanol and methanol, associated liquids in which hydrogen bonding is important, compared to the behavior of *n*-hexane which comes much closer to the properties of an ideal liquid. Typical of this difference is the value of the intercept $T_{1(0)}$ which is one-twentieth of T_1 for bulk ethanol, and only half of the value of T_1 for pure hexane. (3) A general similarity of the alumina and silica–alumina systems is found, with the cracking catalysts of higher specific area being appreciably more effective in reducing the relaxation time for water than the aluminas. Likewise, of the two aluminas examined, the one of higher specific areas is more effective in reducing T_1. (4) Dehydrated alumina, having lost about 6.3% of water, has a much larger value of β for *n*-hexane than regular alumina has. The experimental points lie consistently below those for regular alumina, indicating a greater interaction of hexane with dehydrated alumina. (5) Only one relaxation time can be observed in any particular measurement though there must be considerable variation in the environment of individual protons in different portions of the catalyst. (7) The near equivalence of δ for all four liquids on alumina may be coincidence, but it seems rather unusual in view of the complexity of the systems studied.

A relaxation mechanism for nuclei[1] is provided by magnetic interactions between neighboring dipoles, the Brownian motion of molecules in the liquid providing frequency components that induce a transfer of energy from the nuclear spin system to the remaining degrees of freedom in the liquid. The important factor is any relative reorientation between magnetic nuclei. Using a model of a spherical molecule in a viscous medium, an expression for the relaxation time of protons in water was derived, $(1/T_1) = (1/T_1)_p + (1/T_1)_n$. The first term represents the effect of the proton in the same molecule and is inversely proportional to the sixth power of the internuclear distance. The second term, directly proportional to the viscosity of the liquid and to the number of molecules per cc., describes the effect of the bulk of the liquid. Calculations for water show that the proton in the same molecule is more important in determining the observed T_1.

In addition to the interactions affecting the relaxation time of protons in pure liquids, two other factors are important for absorbed liquids. One is the effect of minute traces of paramagnetic ions, undetectable by conventional magnetic susceptibility measurements. If such impurities were incorporated into the surface of the solid during preparation they could markedly reduce proton relaxation times by a "spin-diffusion" mechanism of the type that has been postulated[17] to account for observed relaxation times in solids containing paramagnetic impurities. A second factor is interaction and collisions with the confining walls of the micro- and macropores of the diamagnetic catalyst support. Such interactions could be the formation of chemical compounds with the substrate, or could simply be the adsorption of protons into vacancies of the crystal lattice or a rapid exchange with protons incorporated during the preparation of the porous structure. They would produce a different type of motion of the molecules as compared with motion in the bulk liquid and would also cause deformation of the molecule resulting in changes in the magnetic field of a nucleus. These deformations, or wall effects, would be most important in small pores where the ratio of surface to volume is largest and any molecule is only a few molecular diameters from the wall at any time. Liquids with labile protons and hydrogen bonding would be most strongly affected.

The present results must be considered of a preliminary nature since a detailed explanation would need to be correlated with surface area, pore distribution and magnetic studies of the supports. The existence of both macropores, and micropores of the order of molecular dimensions, is well established for substances of high specific area.[18] The nature and properties of liquids absorbed in pores is not well known, but some experimental evidence[19,20] shows that the density of liquids in micropores decreases, that the freezing point is much lowered for an absorbed liquid and that the latent heat of vaporization of absorbed liquid exceeds that of the bulk liquid. Magnetic susceptibility measurements[21] show that the diamagnetic susceptibility of water and of *n*-propyl alcohol increases for the first layer added to high area, diamagnetic silica gel, but approaches the bulk value for greater coverage. The susceptibility remains constant for *n*-heptane on silica gel. The changed susceptibility is attributed to breaking of hydrogen bonds of water molecules on pore surfaces.

A qualitative explanation of observed results for water and alcohols absorbed on high area porous substances is that the first liquid added is closely bound to the surface, proton exchange occurring with lattice vacancies and protons incorporated in the alumina during preparation. Interaction with the substrate modifies the relative orientation of nuclear dipoles in complex fashion. This results in an increasing number of spin transitions and thus in shorter relaxation times. As more liquid is added, a smaller fraction of the total amount of liquid interacts directly with the surface and therefore the properties of absorbed liquid more closely approach that of bulk liquid with its longer relaxation time. In contrast, *n*-hexane possesses no labile hydrogens and thus interacts only weakly with the catalyst support. Heating γ-alumina drove off about 6% of volatile impurities by weight. The resulting sample was appreciably more effective in reducing proton relaxation in *n*-hexane, indicating that *n*-hexane, immiscible in water, could come in closer contact with the substrate.

Figures 5 through 8, presenting typical results for liquids absorbed on supported manganese and copper oxides, show that the general behavior is very similar to that found for liquids absorbed on dia-

(18) S. Brunauer, "Adsorption of Gases and Vapors," Princeton University Press, Princeton, N. J., 1943.
(19) P. C. Carman, THIS JOURNAL, **57**, 56 (1953).
(20) C. Pierce and R. N. Smith, *ibid.*, **57**, 64 (1953).
(21) W. O. Milligan and H. B. Whitehurst, *ibid.*, **56**, 1073 (1952).

magnetic γ-alumina. Since the samples were diluted with γ-alumina to a common percentage of paramagnetic ion, a linear relation between relaxation time and amount absorbed is to be expected; any attempt to explain the reduction of relaxation times as due solely to paramagnetic ions is unwarranted.

Water absorbed on supported copper oxide behaves anomalously. For samples with widely differing initial concentrations of paramagnetic ion the change in relaxation time with amount absorbed is nearly constant. Further, the absorbed water has a definite bluish tinge. These two facts indicate that there may be an appreciable amount of free cupric ion on the surface of supported copper oxides. Copper in this form is capable of being taken into solution instead of being firmly incorporated into the catalyst structure as supported manganese ions are. The result is equivalent to measuring the relaxation time of solutions of different concentrations of cupric ion absorbed on γ-alumina, rather than the relaxation time for water affected by interaction with a firmly bound supported copper oxide. The break in the graphs for ethanol and methanol absorbed on supported copper oxides is associated with the more limited solubility of cupric ion in these solvents.

Acknowledgment.—The courtesy of the Department of Physics of Harvard University, in particular of Professors E. M. Purcell and N. Bloembergen in providing laboratory space and facilities as well as helpful guidance, is gratefully acknowledged. This work was done under contract with the Office of Naval Research, and one of us (T.W.H.) was supported by fellowships from the Sinclair Refining Company and the National Science Foundation.

THE CATALYTIC REDUCTION OF COBALT FROM AMMONIACAL COBALT SULFATE SOLUTIONS[1,2]

BY THOMAS M. KANEKO AND MILTON E. WADSWORTH

Department of Metallurgy, University of Utah, Salt Lake City, Utah

Received September 26, 1955

Ammoniacal cobalt sulfate solutions were reduced under hydrogen pressure in a specially designed autoclave. The rates of reduction were measured analytically by following the depletion of cobalt from solution. Linear reduction rates were obtained under the conditions of this study covering a temperature range of 150 to 245° and hydrogen partial pressures of 150 to 800 p.s.i. Colloidal graphite was added in all runs and was found to act as a heterogeneous hydrogenation catalyst. Maximum rates of reduction were obtained for an ammonia to cobalt ratio of 2 to 1, indicating that the most easily reduced cobalt complex is the diammine. These results are consistent with the proposed mechanism which involves adsorption of hydrogen and cobalt ammine complex on the catalyst surface. An exponential hydrogen pressure dependency is explained in terms of structural variations associated with the quinonoid character of colloidal graphite.

Introduction

The precipitation of metals by hydrogen reduction of aqueous solutions of their salts was first suggested by Beketov,[3] and subsequently a wide variety of applications have been reported.[4,5] In recent years, high temperature–high pressure techniques of hydrogen reduction have been applied to the commercial production of metals.[6,7]

Although general descriptions of the various processes can be found in the literature, there is an absence of basic information on the operating variables and the reaction kinetics involved. This investigation, therefore, was initiated to make a kinetic study of the reduction of ammoniacal solutions of cobalt sulfate using hydrogen under elevated temperatures and pressures.

Apparatus and Experimental Procedure

A high temperature–high pressure reaction unit has been specially designed and constructed for this investigation and already has been described elsewhere.[8]

The cobalt–ammine complex solutions were prepared just prior to each experimental run by adding concentrated ammonium hydroxide, reagent grade, to cobalt sulfate.[9] Colloidal graphite[10] was used to aid in the precipitation of cobalt metal powder. In the absence of colloidal graphite, the rate of reduction was extremely slow.

After placing the sample solution in the autoclave, the latter was evacuated, flushed with nitrogen, and then re-evacuated to make certain that atmospheric oxygen had been removed from the system. The autoclave was then allowed to come to operating temperature. After thermal equilibrium was reached, the reaction was initiated with the introduction of hydrogen gas to the desired working pressure. The vapor pressure of the solution was accounted for so that the true partial pressure of hydrogen was known for the conditions of each test. Liquid samples were withdrawn from the autoclave at periodic intervals.

The cobalt content of these samples was determined electrolytically.[11] A quick test to determine if the autoclave liquor had been depleted was carried out by adding a drop of

(1) Supported by the Atomic Energy Commission under Contract No. AT(11-1)-82.

(2) This paper comprises part of a thesis to be presented by T. M. Kaneko in partial fulfillment of the requirements for the degree of Doctor of Philosophy, Department of Metallurgy, University of Utah.

(3) N. Beketov, *Compt. rend.*, **48**, 442 (1859).

(4) V. N. Ipatieff, "Catalytic Reactions at High Pressures and Temperatures," The Macmillan Co., New York, N. Y., 1936.

(5) V. G. Tronev, S. M. Bodin, *et al.*, *Izvest. Sektora Platinyi Drugikh Blagorod. Metal., Inst. Obshchei i Neorh. Kim., Akad. Nauk S.S.S.R.*, **22**, 194 (1948).

(6) J. G. Baraguanth and J. B. Chalelain, *Mining and Metallurgy*, **26**, 391 (1945).

(7) F. A. Forward, *Mining Eng.*, **5**, 577 (1953).

(8) W. H. Dresher, T. M. Kaneko, W. M. Fassell, Jr., and M. E. Wadsworth, *Ind. Eng. Chem.*, **47**, 1681 (1955).

(9) All cobalt sulfate solutions used in the experimental work were prepared by dissolving "Analytical Reagent" (Mallinckrodt Chemical Co.) cobalt sulfate crystals, $CoSO_4 \cdot 7H_2O$, in distilled water.

(10) Colloidal graphite was prepared by dissolving concentrated "Aquadag" (Acheson Colloids Co.) in distilled water.

(11) A. H. Low, A. J. Weinig and W. P. Schoder, "Technical Methods of Ore Analysis," John Wiley and Sons, Inc., New York, N. Y., 1947, p. 109.

the sample to a Nitroso R salt solution, which forms a color complex sensitive to extremely small concentrations of cobalt. During the normal run, any cobalt metal which may have discharged into the sample was removed with a Teflon covered Alnico magnet prior to analysis.

The rate of reduction is expressed in milligrams of cobalt precipitated per cc. of solution per hour, the weight being determined from the depletion of cobalt ion from solution.

Results and Discussion

Ammoniacal solutions of cobalt sulfate were found to reduce linearly under all conditions investigated, covering the ranges of 150 to 245° in temperature and 150 to 800 p.s.i. in hydrogen partial pressure. The effect of stirring speed on the rate of reduction indicated that agitation was eliminated as a variable at the stirring speed of 650 r.p.m. All subsequent experiments were performed at this limiting speed or above.

The rate of reduction as a function of the concentration of graphite was found to vary linearly in the concentration range of 40 to 240 mg./l. from a series of runs at 225° and 600 p.s.i. hydrogen partial pressure. Such a dependency is expected for a solid catalyst, the rate being a function of the surface area. The rate diminished to an extremely low value in the absence of the catalyst. The choice of "Aquadag" (colloidal graphite) was somewhat fortuitous since the many forms of carbon vary considerably in their catalytic behavior. It was at first thought that the colloidal graphite added served as a seed or nucleating agent. Such an assumption is not consistent with the linear rates observed.

Experiments at constant temperature (225°), hydrogen partial pressure (600 p.s.i.) and colloidal graphite concentration (120 mg./l.), but at varying ratios of ammonia to a constant amount of cobalt sulfate (0.425 mole/l.), indicated that a maximum rate of reduction was obtained at the ratio of two moles of ammonia to one of cobalt (Fig. 1). This

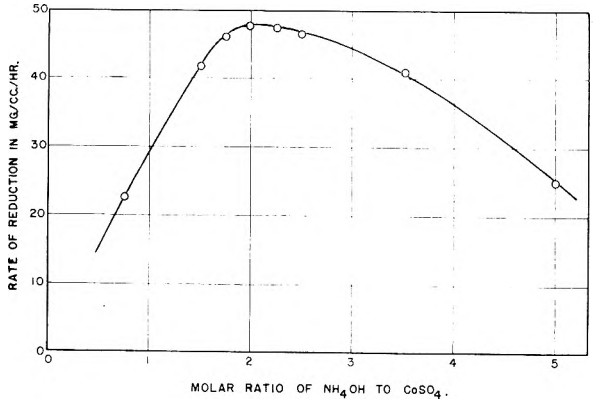

Fig. 1.—Effect of the molar ratio of NH_4OH to $CoSO_4$ on the rate of reduction of cobalt–ammine complex.

ratio suggests that the most active species in such a system is the cobalt(II)–diammine sulfate

$$Co\left|\begin{matrix}2NH_3\\4H_2O\end{matrix}\right|^{++} SO_4^{--}$$

The NH_3 ligand is covalently bonded to the cobalt, forming a very stable complex. This bond is sufficiently strong to make it very difficult to hydrolyze. The *p*H of the cobalt sulfate solution after addition of NH_4OH in the 2 to 1 ratio was practically neutral and indicative of the reaction

$$Co^{++} + NH_4OH \longrightarrow \left|\begin{matrix}-Co-NH_3\\ \diagup\ \diagdown\end{matrix}\right|^{++} + H_2O$$

The diammine complex is also consistent with the reduction of Co^{++}, which requires two electrons and forms two ammonium (NH_4^+) ions, resulting in the product $(NH_4)_2SO_4$.

From the data obtained in studying the effect of the partial pressure of hydrogen on the rate of reduction of cobalt(II)-diammine sulfate at constant concentration of 0.425 mole per liter (25 g. Co/l.), three isotherms for the hydrogen partial pressure range of 150 to 700 p.s.i. were plotted for the temperatures of 175, 225 and 245° (Fig. 2). The curves indicate an exponential dependency of the rate on the hydrogen partial pressure. Such an exponential dependency is not unique, however, since it has been observed in other catalyst systems[12,13] in which it was found that the rate varied exponentially with the fraction of the catalyst surface covered.

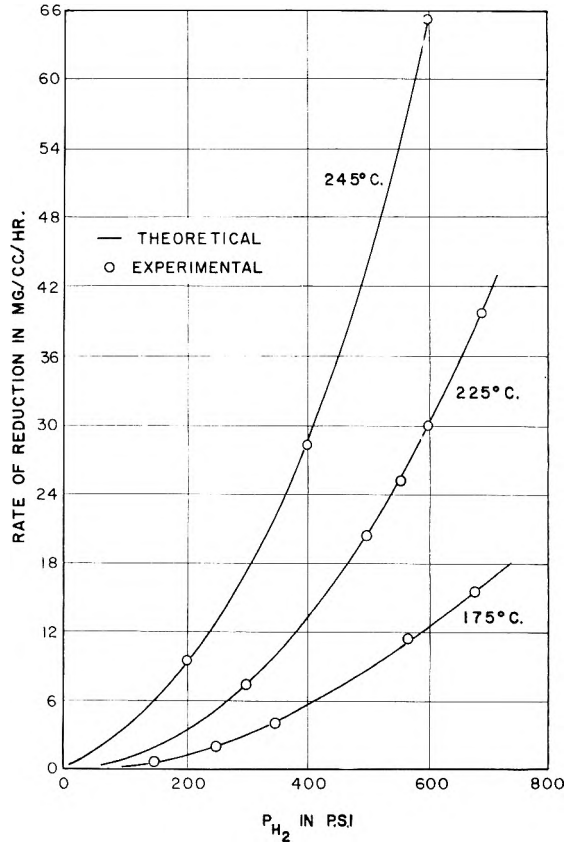

Fig. 2.—Effect of hydrogen partial pressure on the rate of reduction of cobalt–ammine complex.

The adsorption of hydrogen on the surface of the graphite catalyst may be explained by a reversible oxidation–reduction couple and involves the presence of both phenolic and olefinic groups which have been identified[14] by infrared absorption.

(12) H. A. Taylor and N. J. Thon, *J. Am. Chem. Soc.*, **74**, 4169 (1952).

(13) M. A. Cook and A. G. Oblad, *Ind. Enp. Chem.* **45**, 1456 (1953).

(14) E. A. Kmetko, *Phys. Rev.*, **82**, 456 (1951).

The recent work of Garten and Weiss[15] clearly points out the quinone–hydroquinone character of activated carbon and carbon black. They distinguish between the reduced form ("L" carbon) and the oxidized form ("H" carbon) and show that low temperature preparation of carbon results in the formation of "L" (phenolic) form while high temperature preparation results in the formation of "H" (quinonoid) form. The reversible reaction of the adsorption of hydrogen on graphite may be represented by the equation

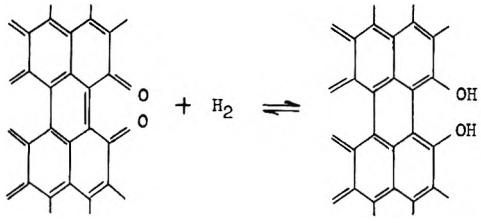

(1a)

"H" form "L" form

The "H" or quinoid form of the graphite structure results in the formation of fixed olefinic bonds and produces surface strain which is relieved by the resonance shift associated with the adsorption of hydrogen. The resulting "L" or phenolic form has an underlying structure which is essentially aromatic. The surface strain is evident from the fact that the C–C distance in graphite is 1.42 Å. whereas the C=C distance is only 1.34 Å.[16] The hydrogen should therefore split on a surface site such as is shown in eq. 1a. For this reason, the adsorption process kinetically appears to involve molecular adsorption. The presence of surface strain affects both the adsorption potential of hydrogen and the ease with which it may be removed in subsequent reactions. Consequently, the activation energy involving hydrogen adsorption should vary with surface coverage. The importance of structural shifts has been proposed for several systems including a number of catalysts.[13,17–19] Structural shifts in catalyst surfaces have been demonstrated in this Laboratory by means of differential infrared spectroscopy.[20]

The experimental results obtained, at first glance, appear to indicate a homogeneous reaction. Linear rates of reduction would not be expected if the rate controlling step takes place at the surface of the growing cobalt particle. These curves suggest an intermediate product whose formation represents the slow or rate-controlling step. This intermediate could then complete the over-all sequence of reactions necessary to produce cobalt metal at the surface of the growing particle. Such a sequence of events is further supported by the fact that the rate of reduction of the cobalt–ammine complex is virtually independent of the nature of the cobalt metal deposit produced. Concentration gradients with the solid catalyst itself are readily produced by the centrifuging action of the impeller, whereas the molecular adsorbates, H_2 and cobalt(II)–diammine sulfate, are not affected. Since the catalyst is the source of the intermediate product from which the metallic cobalt is produced, concentration gradients of this intermediate product will occur. Therefore, metallic cobalt will precipitate in regions of high graphite (or of the intermediate product) concentration. This effect should occur primarily at the walls of the autoclave if proper baffling is not present. Also, the inertia of the solid catalyst will cause "piling up" of these particles near the impeller, particularly in front of it. It has been observed in this study that the metal deposit on the impeller blades is greatest on the forward side.

It was found that the insertion of a cylindrical baffle around the impeller, providing flow parallel to the autoclave walls and more uniform distribution of the catalyst throughout the system, virtually eliminated "plating out," except on the impeller itself. These results suggest the importance of proper agitation through improved impeller and baffle design or the use of simple gas bubbling systems.

Using the 2 to 1 molar ratio of ammonia to cobalt sulfate, a series of runs were made at various concentrations of cobalt–ammine complex at constant temperature (175°) and hydrogen partial pressure (670 p.s.i.). The results are shown in Fig. 3. The shape of this isotherm suggests an adsorption process involving the cobalt(II)–diammine complex associated with the active or phenolic surface sites on the graphite. The concentration of the phenolic sites depends in turn upon the concentration of H_2 in solution according to eq. 1a. Consequently, the measured rate of reduction should be a function of the hydrogen partial pressure and the concentration of the cobalt complex.

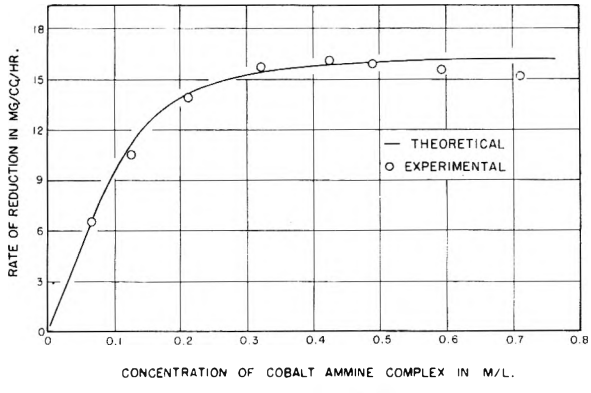

Fig. 3.—Effect of the concentration of cobalt–ammine complex on the rate of reduction at constant temperature (175°) and hydrogen partial pressure (670 p.s.i.).

The following mechanism is consistent with the experimental results

$$H_2(\text{gas}) \underset{}{\overset{k}{\rightleftharpoons}} H_2(\text{solution}) \qquad (1)$$

(15) V. A. Garten and D. E. Weiss, *Austr. J. Chem.*, **8**, No. 1, 68 (1955).

(16) A. F. Wells, "Structural Inorganic Chemistry," Oxford University Press, London, 1945, p. 82.

(17) T. H. Milliken, Jr., G. A. Mills and A. G. Oblad, *Disc. Faraday Soc.*, No. 8, 279 (1950); *Advances in Catalysis*, **III**, 199 (1950).

(18) M. A. Cook, D. H. Pack and A. G. Oblad, *J. Chem. Phys.*, **19**, 367 (1951).

(19) E. B. Cornelius, T. H. Milliken and A. G. Oblad, THIS JOURNAL, **59**, 810 (1955).

(20) R. O. French and M. E. Wadsworth, "Differential Infrared Spectra of Surfaces: Ammonia on Cracking Catalysts," presented before the Gordon Research Conference, Catalysis Section, June, 1955.

$$\text{¦S}_{(q)} + H_2 \overset{K_1}{\rightleftharpoons} \text{¦S}_{(p)} \quad (2)$$

$$\text{¦S}_{(p)} + Co\{\} \overset{K_2}{\rightleftharpoons} \text{¦S}_{(p)} - Co\{\} \quad (3)$$

$$\text{S}_{(p)} - Co\{\} \longrightarrow |\ |^{\ddagger} \longrightarrow \text{¦S}_{(q)} + Co\{\}\cdot 2H \text{ (slow)} \quad (4)$$

$$Co\{\}\cdot 2H \longrightarrow Co^{\circ} + 2NH_4^{+} + SO_4^{--} \text{ (fast)} \quad (5)$$

The symbols ¦S$_{(q)}$ and ¦S$_{(p)}$ represent the quinonoid and phenolic sites, respectively, on the graphite surface; Co{} represents the surface active cobalt(II)–diammine complex, and Co{}·2H represents the intermediate product which is formed during the rate-determining step represented by eq. 4. None of these symbols are intended to represent the actual structures involved.

Equations 1, 2 and 3 are here considered to be equilibrium reactions. These steps may actually represent steady-state conditions. The distinction, which lies in the determination of the temperature coefficients for the K values of each reaction, is not within the scope of the data presented in this paper. According to eq. 1, the concentration of hydrogen in solution equals kP_{H_2}, where k is the Henry constant. Letting the fraction of the surface sites covered with hydrogen, ¦S$_{(p)}$, be θ_1, the fraction of the ¦S$_{(p)}$ sites covered with the adsorbed cobalt–ammine complex, ¦S$_{(p)}$-Co{}, be θ_2, the fraction of the uncovered sites, ¦S$_{(q)}$, be $1 - \theta_1$, and the bulk concentration of Co{} be represented by ψ, one obtains from eq. 2 and 3

$$K_1 = \frac{\theta_1}{(1 - \theta_1)kP_{H_2}} = e^{-\Delta F_1/RT} \quad (6)$$

and

$$K_2 = \frac{\theta_2}{(\theta_1 - \theta_2)\psi} = e^{-\Delta F_2/RT} \quad (7)$$

where K_1, K_2 and k are the equilibrium constants.

According to the absolute reaction rate theory[21,22]

$$\text{Rate} = \kappa \frac{kT}{h} \pi_i C_i e^{-\Delta F^{\ddagger}/RT} \quad (8)$$

where κ is the transmission coefficient (conventionally considered to be equal to 1), k and h are the Boltzmann and Planck constants, respectively, $\pi_i C_i$ represents the product of the concentrations of the reactants, and $\Delta F^{\ddagger}$ is the activation energy. Since eq. 4 represents the rate-determining step, the rate of reaction according to eq. 8 becomes

$$R = \kappa \frac{kT}{h} k_0 \theta_2 e^{-\Delta F^{\ddagger}/RT} \quad (9)$$

where k_0 is a factor containing surface roughness and the conversion units to keep the left- and right-hand portions of eq. 9 consistent with each other. Combining eq. 6, 7 and 9 gives the over-all rate

$$R = \kappa \frac{kT}{h} k_0 \left(\frac{K_1' P_{H_2}}{1 + K_1' P_{H_2}}\right)\left(\frac{K_2\psi}{1 + K_2\psi}\right) e^{-\Delta F^{\ddagger}/RT} \quad (10)$$

where K_1' equals $K_1 k$.

According to the structural model for hydrogen adsorption, the variation of the activation energy with surface coverage may be considered to be a linear function of the surface coverage. This assumption implies a long-range relief of strain following adsorption. Figure 4 represents diagrammatically the energy barriers associated with the structural model. The adsorption potential of hydrogen on the graphite increases as the amount of hydrogen adsorbed decreases. The adsorption potential, ΔF_1, may therefore be represented by the equation

$$\Delta F_1 = \Delta F_1^{\circ} + \alpha\theta_1 \quad (11)$$

where ΔF_1° is the adsorption potential at zero coverage and α is a constant. The plus sign must be used since ΔF_1° is negative and α is a positive number. Similarly, the activation energy, $\Delta F^{\ddagger}$, may be represented by the equation

$$\Delta F^{\ddagger} = \Delta F_0^{\ddagger} - \alpha\theta_1 - \beta\theta_1 \quad (12)$$

where $\Delta F_0^{\ddagger}$ is the activation energy a zero hydrogen surface coverage, and α and β are constants.

The results of this study, as will be shown, indicate that the quantity, $K_1' P_{H_2}$, is small compared to 1. Therefore, the combination of eq. 10, 11 and 12 results in the equation

$$R = \kappa \frac{kT}{h}\left(\frac{K_2\psi}{1 + K_2\psi}\right) \times k_0 P_{H_2} e^{-(\Delta F_1^{\circ} + \alpha\theta_1)/RT} e^{-(\Delta F_0^{\ddagger} - \alpha\theta_1 - \beta\theta_1)/RT} \quad (13)$$

The $\alpha\theta_1$ terms cancel, and at constant temperature and cobalt–ammine concentration, eq. 13 becomes

$$R = K_0' P_{H_2} e^{\beta' P_{H_2}/RT} \quad (14)$$

where

$$\beta' = \beta K_1' \quad (15)$$

and

$$K_0' = \kappa \frac{kT}{h}\left(\frac{k_0 K_2\psi}{1 + K_2\psi}\right) e^{-\Delta F_1^{\circ}/RT} e^{-\Delta F_0^{\ddagger}/RT} \quad (16)$$

In logarithmic form, eq. 14 may be written

$$\log R/P_{H_2} = \beta' P_{H_2}/2.3RT + \log K_0' \quad (17)$$

whereupon, a plot of $\log R/P_{H_2}$ *versus* P_{H_2} should result in a straight line whose slope is $\beta'/2.3RT$. Figure 5 is such a plot for the three isotherms of pressure *versus* rate of Fig. 2. The agreement is very good for all three curves at 175, 225 and 245°. The corresponding β' values were found to be 2.28, 2.07 and 1.98, respectively. This correlation shows that the assumption $K_1' P_{H_2} \ll 1$ is valid and also that the results are in excellent agreement with the structural model proposed for the adsorption of hydrogen on the graphite catalyst surface. The constancy of the K_1' value indicates that the $\beta\theta_1$ correction to ΔF_1 is very small, that is, the absorption band of Fig. 4 is very narrow. The small variation in β' with temperature indicates temperature compensation of k and K_1. At constant temperature, eq. 13 becomes

$$R = K_0''\left(\frac{K_2\psi P_{H_2}}{1 + K_2\psi}\right) e^{\beta' P_{H_2}/RT} \quad (18)$$

where

$$K_0'' = \kappa \frac{kT}{h} k_0 e^{-\Delta F_1^{\circ}/RT} e^{-\Delta F_0^{\ddagger}/RT} = \text{constant}$$

The experimental rates plotted in Fig. 3 are not single valued functions of the cobalt(II)–diammine sulfate solution concentration. The concentration term, ψ, must be set equal to the product, $(Co\{\}^{++})(SO_4^{--})$, that is, the sulfate ion concentration as well as that of the $Co\{\}^{++}$ contributes to the rate of reduction. Therefore, an increase in sulfate ion concentration beyond that added as $CoSO_4$

(21) S. Glasstone, K. J. Laidler and H. Eyring, "The Theory of Rate Processes," McGraw–Hill Book Co., New York, N. Y., 1941, p. 197.

(22) K. Laidler, "Chemical Kinetics," The McGraw–Hill Book Co., New York, N. Y., 1950, p. 152.

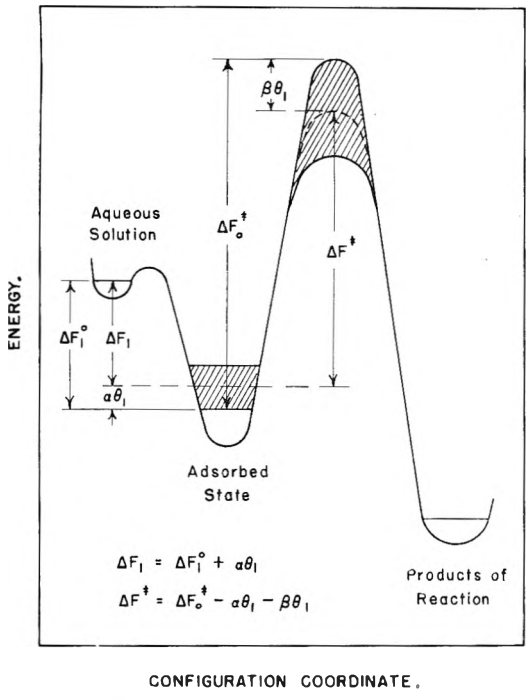

Fig. 4.—Energy barrier diagram illustrating the variation of ΔF_1 and $\Delta F^{\ddagger}$ with surface coverage, θ_1.

should provide a corresponding increase in the rate. To study this effect, a solution was prepared containing 0.425 mole of K_2SO_4 plus 0.425 mole of $CoSO_4$ per liter, and the rate of reduction was measured at 225 and 670 p.s.i. P_{H_2}. The rate was 31.8 mg. cc.$^{-1}$ hr.$^{-1}$ which is double that obtained in the absence of K_2SO_4 and measured under identical conditions. The adsorption of the ion

$$Co\begin{vmatrix}2NH_3\\4H_2O\end{vmatrix}^{++}$$

alone is unlikely, since electrical neutrality must be maintained. For this reason, the adsorption of the cobalt–ammine complex must involve ion pair or neutral molecule adsorption. Such a neutral complex could form according to the reaction

$$Co\begin{vmatrix}2NH_3\\4H_2O\end{vmatrix}^{++} + SO_4^{--} \rightleftharpoons Co\begin{vmatrix}2NH_3\\2H_2O\\SO_4\end{vmatrix}^{\circ} + 2H_2O \quad (19)$$

The above neutral complex, perhaps written in an overly simplified form, would be termed sulfato-diaquo-diammine–cobalt(II). The neutral complex should be much more surface active than the ion. Such compounds have been prepared,[23] in which the bidentate character of the SO_4^{--} ion results in the displacement of two of the H_2O molecules. If the neutral complex is the true adsorbate, its concentration may be represented by the equation

$$\psi = [Co\{\}^{\circ}] = K_3[Co\{\}^{++}][SO_4^{--}] \quad (20)$$

where K_3 is the equilibrium constant, and ψ is the adsorbate solution concentration. Accordingly, the rate of the reaction should increase with an increase in sulfate ion concentration, and eq. 18 may be written to include eq. 20 as

$$R = \frac{K_0''K_2K_3(Co\{\}^{++})(SO_4^{--})}{1 + K_2K_3(Co\{\}^{++})(SO_4^{--})} P_{H_2}e^{\beta' P_{H_2}/RT} \quad (21)$$

The solid curve of Fig. 3 represents the theoretical curve according to eq. 21, using values of 142 for the product, K_2K_3, and 4.48×10^{-3} for K_0 obtained from the experimental data. Close agreement of the theoretical curve with the measured rates was obtained for cobalt–ammine solution concentration up to 0.5 molar. Above this concentration, the measured rates dropped slightly below the theoretical plateau value. This decrease in the rate was at first interpreted in terms of competitive adsorption,[24] which did not adequately account for the sulfate ion dependency. A more probable explanation for the decrease in the rate at high concentrations involves the expected decrease in the solubility of H_2 and variations in activity of solution components as the ionic strength increases. Table I lists a series of measured rates and the corresponding rates calculated according to eq. 21 for various values of ψ and P_{H_2} at 175°.

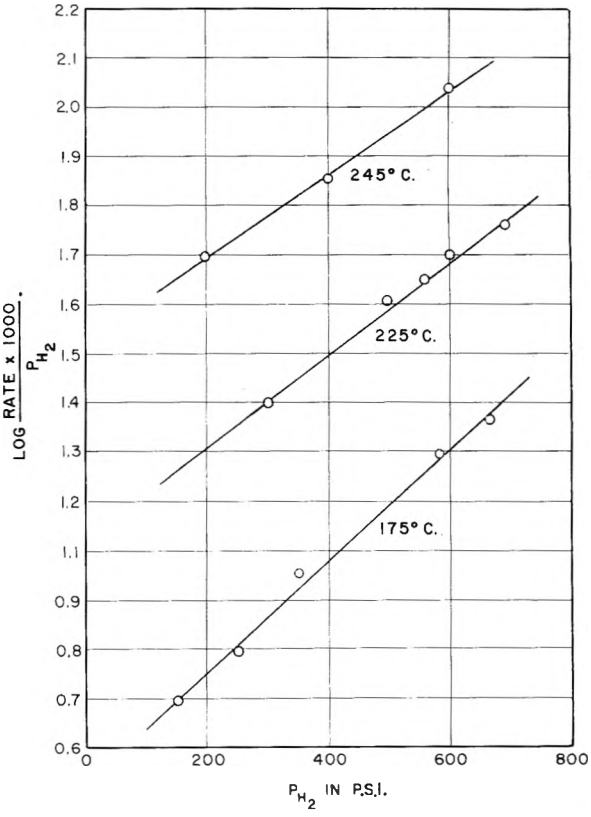

Fig. 5.—Plot of log rate/P_{H_2} *versus* P_{H_2} showing linear dependency in agreement with the structural adsorption model.

Just how the neutral cobalt complex adsorbs on the phenolic sites cannot be determined since the K_2 and K_3 values are not known separately. If one assumes, however, that the adsorption takes place by hydrogen bonding on two phenolic sites, it is possible to calculate the solution concentration, ψ. A reasonable value for hydrogen bonding on two such sites would be of the order of 10 kcal./mole

(23) P. C. L. Thorne and E. R. Roberts, "Inorganic Chemistry," Interscience Publishers, New York, N. Y., 1948, p. 299.

(24) Thomas M. Kaneko and Milton E. Wadsworth, Technical Report No. XXII (September 1, 1955), Atomic Energy Commission Contract, AT (11-1)-82, Project No. 1.

TABLE I

MEASURED AND CALCULATED RATES AT 175° FOR VARIOUS COBALT–AMMINE CONCENTRATIONS AND HYDROGEN PARTIAL PRESSURES

Concn. (moles/l.)	P_{H_2} (p.s.i.)	ψ/K_3	Rate (mg. cc.$^{-1}$ hr.$^{-1}$) Found	Calcd.
0.065	670	0.004	6.6	6.2
.125	670	.016	10.6	11.3
.210	670	.044	13.9	14.2
.320	670	.102	15.8	15.4
.425	670	.180	16.2	15.9
.490	670	.240	15.9	16.0
.595	670	.354	15.7	16.2
.710	670	.503	15.1	16.3
.425	565	.180	11.2	10.3
.425	345	.180	4.0	3.5
.425	245	.180	2.0	2.0
.425	150	.180	1.0	0.9

or greater.[16] Using this value as the adsorption potential, K_2 would be 7×10^4. Since K_2K_3 was determined experimentally to be 142, the value of K_3 under this assumption would be approximately 2×10^{-3}. For a solution whose total cobalt(II)–diammine sulfate concentration is 0.425 molar, ψ would be approximately 4×10^{-4} molar, according to eq. 20. Although this concentration is very small, it is sufficient to saturate all available sites if a potential approximating that of hydrogen bonding is operative. If, on the other hand, ion pair adsorption of $Co\{\}^{++}$ plus SO_4^{--} is assumed, the adsorption potential would be 4.45 kcal. based on calculations from experimental data. This value implies physical adsorption which seems somewhat low to explain a specific catalytic process. Additional studies involving cryoscopic or conductivity measurements are necessary to determine the value of K_3.

An Arrhenius plot of log of reduction rate *versus* reciprocal temperature for a series of runs at 0.425 molar cobalt(II)–diammine sulfate concentration and 670 p.s.i. hydrogen partial pressure resulted in an over-all apparent activation energy of 15.7 kcal./mole. The slope of such a plot, however, depends upon the sum of $\Delta H_1' + \Delta H_2 + \Delta H^{\pm}$. A more detailed temperature study is required to determine ΔH_2. The value of $\Delta H_1'$, determined from the variation of β' with temperature, results in a value of -920 cal./mole. The value of ΔH_2 should also be negative. Therefore, $\Delta H^{\pm}$ should be appreciably greater than 15.7 kcal./mole.

The presence of the intermediate product, $Co\{\}\cdot 2H$, shown in eq. 4 and 5 is not a new concept. Similar intermediates have been proposed for other systems.[25-28]

(25) Sol Weller and G. A. Mills, *J. Am. Chem. Soc.*, **75**, 769 (1953).
(26) E. Peters and J. Halpern, *Can. J. Chem.*, **33**, 356 (1955).
(27) J. Halpern and E. Peters, *J. Chem. Phys.*, **23**, 605 (1955).
(28) E. Peters and J. Halpern, THIS JOURNAL, **59**, 793 (1955).

Hydroquinone as a Homogeneous Hydrogenation Catalyst.—The rate of reduction of cobalt(II)–diammine sulfate using hydroquinone instead of graphite was greatly increased over the rates observed for the latter at the same molar concentrations of each catalyst. The catalytic properties of this system are not surprising in view of the hydroquinone–quinone character of activated carbon.[15] Experiments at constant concentration of hydroquinone showed that the rate of reduction as a function of the partial pressure of hydrogen was linear. Such a rate dependency is in contrast to the exponential increase obtained with graphite and demonstrates the absence of structural effects associated with the adsorption of hydrogen on the latter. The resonance structure of such compounds as hydroquinone resulting in a reversible, oxidation–reduction couple is instrumental to their catalytic activity. It appears, therefore, that a structure having a high oxidation potential should be selected in oxidizing systems, whereas a low oxidation potential is indicative of strong reducing properties. Such a correspondence occurs when rates are compared for the *o*-, *m*- and *p*-dihydroxybenzene. As suspected, the *meta* form (resorcinol) does not behave as a catalyst, since the corresponding *m*-benzoquinone is not formed. On the other hand, both catechol (*o*-dihydroxybenzene) and hydroquinone (*p*-dihydroxybenzene) behave as catalysts for the reduction of cobalt(II)–diammine sulfate. The rate observed for catechol was not as great as that obtained for hydroquinone. This difference in rate is to be expected, since the oxidation potential is greater for the *o*-benzoquinone (0.792 v.) than for the quinone (0.699 v.).[29]

The over-all effects observed indicate very advantageous use of such reagents in both oxidation and reduction hydrometallurgical systems. Also, the application of other heterogeneous hydrogenation and oxidation catalysts is suggested.

Acknowledgments.—The authors wish to express appreciation to the Atomic Energy Commission for its support of this work. Equipment for this study was purchased through the University of Utah Research Fund. Thanks are extended to Dr. John R. Lewis, Head of the Department of Metallurgy, University of Utah, for his support and interest in this work. Particular thanks are due Dr. W. Martin Fassell, Jr., for his help during the initial development of this work and for his suggestions regarding the use of "Aquadag" as a seeding agent and the subsequent use of hydroquinone. Thanks are also extended to Mr. William H. Dresher for his helpful suggestions regarding impeller and baffle design.

(29) L. F. Fieser and M. Fieser, "Organic Chemistry," D. C. Heath and Co., Boston, Mass., 1944, p. 728.

TURBULENT COAGULATION OF COLLOIDS

BY H. L. FRISCH

Department of Chemistry, University of Southern California, Los Angeles 7, Calif.

Received September 29, 1955

The theory of both rapid and slow turbulent coagulation of a colloidal suspension in a homogeneously and isotropically turbulent medium is developed in terms of the principal physical parameters characterizing the turbulence. The coagulation time, ϑ, as expected, for large ϑ satisfies a relation similar to one derived by Smoluchowski for coagulation as a result of molecular Brownian motion, except that the molecular diffusion coefficient is replaced by an appropriate eddy diffusivity constant. For more rapid coagulations this similarity breaks down and the exact form of ϑ is shown to depend strongly on the form of the Lagrangian correlation coefficient. The effect of boundary effects and repulsive forces due to electrostatic charges on the particles is considered.

I. Introduction—Turbulent Diffusion

Consider a swarm of particles whose velocities form a field of homogeneous and isotropic turbulence in a fluid macroscopically at rest.[1] We shall assume that there is no correlation between the molecular agitation and turbulent fluctuations in the positions of the suspended particles. Thus we can write for the variances in the position of the particles $\overline{y^2}_{\text{tot}}$.[1]

$$\overline{y^2}_{\text{tot}} = \overline{y^2}_{\text{turb}} + \overline{y^2}_{\text{mol}} \tag{1}$$

It has been shown[1] that if $c(x, y, z; t)$ is the mean concentration of particles located in a volume element dv centered about x, y, z at time t, then

$$\frac{\partial c}{\partial t} = n^*(t)\nabla^2 c \tag{2}$$

where n^* is defined to be the factor of turbulent diffusion[2]

$$n^*(t) = \frac{1}{2}\frac{\overline{dy^2}}{dt} \tag{3}$$

Introducing the Lagrangian correlation coefficient $R_h(h)$ of the field of turbulence we can write instead of eq. 3

$$n^*(t) = \overline{v^2}\int_0^t R_h(\alpha)d\alpha \tag{4a}$$

where $\overline{v^2}$ is the variance of turbulent velocities. If we wish to take into account also molecular agitation for which

$$\overline{y^2}_{\text{mol}} = 2Dt$$

D the diffusion (molecular) coefficient, eq. 4a becomes[1]

$$n^*(t) = \overline{v^2}\int_0^t R_h(\alpha)d\alpha + D \tag{4b}$$

The purpose of this paper will be to describe the kinetics of the mutual coagulation of the suspended particles in terms of the parameters characterizing the turbulent motion of the particles themselves. The physical systems to which these results are to apply can be either hydrosols or aerosols being subjected to extremely turbulent stirring without net macroscopic convection of the suspending medium. The viscosity of the suspending medium is taken to be sufficiently large so that in good approximation the motion of the suspended particles characterizes the motion of the medium itself.

(1) F. N. Frankiel, *Advances in Appl. Mech.*, **III**, 61 (1953).

(2) F. N. Frankiel, *Compt. rend.*, **224**, 98 (1947).

II. Rapid Turbulent Coagulation

As a preliminary step to further consideration, we verify that, in view of the usual assumption[1,3] of a Gaussian distribution for the probability density $\Psi(\vec{r}, t)$ for the particles at a time t, the probability of a relative displacement of two particles, initially, together at $t = 0$ which lies between $\vec{r}$ and $\vec{r} + d\vec{r}$ is

$$\Psi_{1,2}(\vec{r}, t)\,d\vec{r} = d\vec{r}\int_{(r_1)}\Psi_1(\vec{r}_1, t)\Psi_2(\vec{r}_1 + \vec{r}, t)d\vec{r}_1 = \frac{d\vec{r}}{(2\pi\overline{y_1^2})^{3/2}(2\pi\overline{y_2^2})^{3/2}}\int_{-\infty}^{+\infty}\exp(-|\vec{r}_1|^2/2\overline{y_1^2})\times$$

$$\exp[(-|\vec{r}_1 + \vec{r}|^2)/2\overline{y_2^2}]\,d|\vec{r}_1| = \frac{d\vec{r}}{[2\pi(\overline{y_1^2} + \overline{y_2^2})]^{3/2}}\exp\{-|\vec{r}|^2/2(\overline{y_1^2} + \overline{y_2^2})\} \tag{5}$$

Equation 5 follows directly from the random nature of the turbulence and is a direct analogy to a result in Brownian motion due to Smoluchowski,[4] whence

$$\overline{y^2}_{1,2} = \overline{y_1^2} + \overline{y_2^2} \tag{6}$$

Combining eqs. 3 and 6, we find

$$n^*_{1,2}(t) = \frac{1}{2}\frac{d\overline{y^2}_{1,2}}{dt} = n_1^*(t) + n_2^*(t) \tag{7}$$

which is the basic result we require in the theory of coagulation.

Following Smoluchowski[4] we suppose that (fast) coagulation results from the coalescence of particles colliding with one another. By virtue of eq. 7 we can calculate the flux of particles colliding with a given one of the swarm by holding that one fixed at the origin of our coördinate system, where it is surrounded by an effective "sphere of influence" for coagulation of radius $R_{1,2}$. Assuming further that our particles are distributed uniformly at time $t = 0$ in a medium of infinite extent, we find the concentration of particles about our central one by solving, *cf.* eq. 2

$$\frac{\partial c}{\partial t} = n^*_{1,2}(t)\nabla^2 c = n^*_{1,2}(t)\left\{\frac{\partial^2 c}{\partial r^2} + \frac{2}{r}\frac{\partial c}{\partial r}\right\}$$

$c = c_0$ a constant at $t = 0$ for $r > R$

$c = 0$ at $r = R_{1,2}$ for $t > 0$.

(3) G. K. Batchelor, "Theory of Homogeneous Turbulence," Cambridge University Press, Cambridge, 1953.

(4) M. v. Smoluchowski, *Z. physik. Chem.*, **93**, 129 (1917); see also S. Chandrasekhar, *Rev. Mod. Phys.*, **15**, 1 (1943).

We find

$$c(r,t) = c_0\left[1 - \frac{R_{1,2}}{r} + \frac{2R_{1,2}}{r\sqrt{\pi}}\int_0^{(r\,-\,R_{1,2})^2/\overline{y^2_{1,2}}} \exp(-x^2)\,dx\right] \quad (8)$$

since

$$\frac{\partial c}{\partial \overline{y^2_{1,2}}} = \frac{\partial^2 c}{\partial r^2} + \frac{2}{r}\frac{\partial c}{\partial r}$$

by virtue of eq. 7. From eq. 8 the rate at which particles arrive at the surface $r = R_{1,2}$ is given by

$$J_{1,2}\,dt = 4\pi n^*_{1,2}(t)\left(r^2\frac{\partial c}{\partial r}\right)_{r\,=\,R_{1,2}} dt \quad (9)$$

$$= 4\pi n^*_{1,2}R_{1,2}c_0\left\{1 + \frac{R_{1,2}}{\left(\frac{\pi}{2}\overline{y^2_{1,2}}\right)^{1/2}}\right\}\dot{c}t$$

More generally, as a result of the coalescence of single, double, etc., particles, we can write for the specific rate of formation of a particle of size $i + k$

$$J_{i+k}dt = 4\pi n^*_{i,k}R_{i,k}c_ic_k\left\{1 + \frac{R_{i,k}}{\left(\frac{\pi}{2}\overline{y^2_{i,k}}\right)^{1/2}}\right\}dt \quad (10a)$$

$$= V_{i,k}c_ic_k\,dt$$

where c_i, c_k are the concentrations of particles of size i and k, respectively, and

$$n^*_{i,k}(t) = n^*_i(t) + n^*_k(t)$$

$$\frac{1}{2}\frac{d}{dt}\overline{y^2_{i,k}} = n^*_{i,k} \quad (10b)$$

Following Smoluchowski[4] we can write for the variation of k-fold particles with time

$$\frac{dc_k}{dt} = \frac{1}{2}\sum_{i+j=k} c_ic_jV_{i+j} - c_k\sum_{j=1}^{\infty} c_jV_{k+j} \quad (11)$$

In order to integrate eq. 11 we shall make the rather questionable assumption[4] that there exists an average in some sense over i and j of V_{i+j} such that

$$\frac{dc_k}{dt} \approx 2V(t)\left\{\frac{1}{2}\sum_{i+j=k} c_ic_j - c_k\sum_{j=1}^{\infty} c_k\right\} \quad (12)$$

$$V_{i+j}(t) \approx 2V(t) \quad (i, j = 1, 2, \ldots).$$

Solving we find[4]

$$c_k(t) = c_0[(c_0\tau)^{k-1}/(1 + c_0\tau)^{k+1}] \quad (13)$$

$k = 1, 2, \ldots$

and

$$c(t) = \sum_{k=1}^{\infty} c_k(t) = c_0/(1 + c_0\tau) \quad (14)$$

with c_0 the number concentration of single particles present at $t = 0$

$$\tau = \int_0^t V(\alpha)\,d\alpha$$

$$= 4\pi\int_0^t n^*(\alpha)R\left\{1 + \frac{R}{\left[\frac{\pi}{2}\overline{y^2}(\alpha)\right]^{1/2}}\right\}d\alpha \quad (15)$$

where R is a representative average radius of a particle whose Lagrangian correlation coefficient is $R_h(\alpha)$ and $n^*(\alpha)$ is given by eq. 4b. Neglecting in first approximation $R/\left[\frac{\pi}{2}\overline{y^2}(\alpha)\right]^{1/2}$ in comparison to unity we find

$$\tau \approx 4\pi R\int_0^t n^*(\alpha)\,d\alpha$$

$$\tau \approx 2\pi R\overline{y^2}(t)$$

while more generally

$$\tau = 2\pi R\left\{\overline{y^2}(t) + \left[\frac{8R^2\overline{y^2}(t)}{\pi}\right]^{1/2}\right\} \quad (16)$$

An important physical parameter first introduced by Smoluchowski to describe a coagulation process is the coagulation time ϑ, where, *cf.* eq. 14

$$c(\vartheta) = {}^1/_2c_0$$

The corresponding quantity in turbulent coagulation depends markedly on the form of the Lagrangian correlation coefficient and satisfies by virtue of eq. 16 and 14

$$\overline{y^2}(\vartheta) + \left[\frac{8R^2\overline{y^2}(\vartheta)}{\pi}\right]^{1/2} = (2\pi Rc_0)^{-1} \quad (17a)$$

Two limiting relations can be derived, the first for very short times and the second for long times, respectively, without detailed knowledge of the turbulence field. For times long in comparison with the Lagrangian scale of turbulence L_h, where

$$L_h = \int_0^{\infty} R_h(\alpha)\,d\alpha$$

we can write

$$\overline{y^2}_{turb.} \approx 2\overline{v^2}L_ht \quad \text{or}$$

$$\overline{y^2} \approx [2\overline{v^2}L_h + 2D]t = 2Kt$$

where K is the constant eddy diffusivity. Neglecting the term $0(\vartheta^{1/2})$ we have from eq. 17a

$$\vartheta = (4\pi KRc_0)^{-1}, \vartheta \gg L_h \quad (17b)$$

This result goes over smoothly into the value in the absence of turbulence $\vartheta = [4\pi DRc_0)^{-1}$.

For times which are small in comparison to L_h as well as the Lagrangian microscale of turbulence[1] $\lambda_h = [-{}^1/_2d^2R_h(0)/dh^2]^{-1/2}$ one finds

$$\overline{y^2}_{turb.} \approx \overline{v^2}\,t^2 \quad \text{or}$$

$$\overline{y^2} \approx \overline{v^2}\,t^2 + 2Dt$$

This result implies that for very short times $t < D/\overline{v^2}$ molecular agitation produced by Brownian motion is more important than the effects of turbulence. We find on substituting the above in eq. 17a that

$$\vartheta = \frac{D}{\overline{v^2}} + \frac{1}{\overline{v^2}}\left\{D^2 + \overline{v^2}\left[\beta - 2\left(\frac{4R^4}{\pi^2} + \frac{2R^2\beta}{\pi}\right)^{1/2}\right]\right\}^{1/2} \quad (17c)$$

$\beta = (2\pi Rc_0)^{-1}, \vartheta \ll L_h, \lambda_h$

This equation simplifies considerably if we consider two cases

(1) $D^2 > \overline{v^2}\beta$ for which

$$\vartheta \approx (4\pi RDc_0)^{-1} = \frac{1}{D}\left(\frac{4R^4}{\pi} + \frac{R}{\pi^2c_0}\right)^{1/2} \quad (18a)$$

$$= (4\pi RDc_0)^{-1} - O\left(\frac{R^{1/2}}{Dc_0{}^{1/2}}\right)$$

and

(2) $D^2 < \overline{v^2}\beta$ for which

$$\vartheta \approx = (2\pi R\overline{v^2}c_0)^{-1/2} \quad (18b)$$

Thus in a very rapid coagulation the coagulation time can be almost uninfluenced by turbulent

mixing (*cf.*, eq. 18a) while in a somewhat less rapid coagulation the larger coagulation time is already very markedly influenced. Particularly significant from the point of view of experimental verification of this theory is the transition in ϑ^{-1} from a concentration dependence varying as the first power to a half power and back again to a first power in the concentration, depending on the scale of turbulence.

In general, ϑ can be found by introducing a suitable correlation function $R_h(\alpha)$, often a representative one such as a Gaussian type suffices,[1] in the relation

$$\overline{y^2}(\vartheta) = 2D + 2\overline{v^2}\int_0^{\vartheta}(\vartheta - \alpha)R_h(\alpha)\,d\alpha \qquad (19)$$

which together with eq. 17a determines ϑ as a function of all the physical parameters. For a Gaussian $R_h(\alpha)$, $\overline{y^2}/2t \approx K$ for $t \geqslant (10 - 12)L_h$, hence for $\vartheta \geqslant (10 - 12)L_h$ eq. 17b already applies.

III. Boundary Effects in Turbulent Diffusion

In the preceding discussion of turbulent coagulation it was assumed that every particle adheres on collision with the stationary, central particle and following Smoluchowski the boundary condition, $c = 0$ at the boundary, was employed. This assumption is at best an approximation and if the average particle size is small compared to an average mixing length of the fluid then a more appropriate boundary condition is[5]

$$\gamma\left(\frac{\partial c}{\partial r}\right)_{r=R} = c(R,t)$$

where γ is a length of the order of a mixing length which, for a small condensation coefficient α between particles, varies inversely with α. In the case of turbulence, γ is itself a function of the time which we will for the sake of mathematical simplicity treat as roughly constant. Letting $\xi = \gamma R/(R + \gamma)$ we find that the appropriate solution of the diffusion equation is no longer eq. 8 but

$$\frac{c(r,t)}{c_0} = 1 - \left(\frac{R-\xi}{r}\right)\left\{\operatorname{erfc}\left[\frac{r-R}{(\overline{y^2})^{1/2}}\right] - \exp\left(\frac{\overline{y^2}}{\xi^2} + \frac{r-R}{\xi}\right)\operatorname{erfc}\left[\frac{r-R}{(\overline{y^2})^{1/2}} + \frac{(\overline{y^2})^{1/2}}{\xi}\right]\right\} \qquad (20)$$

Using this solution we find that the concentration of k-fold particles as well as the total number of particles is still given by eq. 13 and 14, respectively, since their derivation is unchanged except for the definition of $\tau(t)$. Assuming as before that a suitable average radius R for the coagulating colloid can be defined, then we have instead of eq. 15

$$\tau(t) = \frac{4\pi R^2}{R+\gamma}\int_0^t n^*(\alpha)\left\{1 + \frac{R}{\gamma}\exp\left[\frac{\overline{y^2}(\alpha)}{\xi^2}\right]\operatorname{erfc}\left[\frac{(\overline{y^2}(\alpha))^{1/2}}{\xi}\right]\right\}d\alpha = \frac{2\pi R^2}{R+\gamma}\int_0^{\overline{y^2}(t)}\left\{1 + \frac{R}{\gamma}\exp\left[\frac{\overline{y^2}(\alpha)}{\xi^2}\right]\operatorname{erfc}\left[\frac{(\overline{y^2}(\alpha))^{1/2}}{\xi}\right]\right\}d\overline{y^2}(\alpha), \text{ or } \tau(t) = \frac{2\pi R^2}{R+\gamma}\left\{\overline{y^2}(t) + \frac{R\xi^2}{\gamma}\int_0^{[\overline{y^2}(t)]/\xi^2}\exp(Z)\operatorname{erfc}(Z^{1/2})\,dZ\right\} \qquad (21a)$$

In particular when $[\overline{y^2}(t)]/\xi^2 > 1$ we find that $\tau(t)$ is given asymptotically as

$$\tau(t) \doteq \frac{2\pi R^2}{R+\gamma}\left\{\overline{y^2}(t) + \frac{2}{\pi^{1/2}} \times \frac{R^3}{(R+\gamma)}[\overline{y^2}(t)]^{1/2}\right\} \qquad (21b)$$

Thus for large times and $R \ll \gamma$ eq. 21b further reduces to

$$\tau(t) \approx \frac{2\pi R^2}{R+\gamma} \times \overline{y^2}(t)$$

whence it follows that the coagulation time ϑ is given by (*cf.* eq. 14)

$$\vartheta \approx \frac{R+\gamma}{4\pi R^2 K c_0} \qquad (22a)$$

More generally ϑ must be found as a solution of

$$\tau(\vartheta) = c_0^{-1} \qquad (22b)$$

where τ as a function of $\overline{y^2}(\vartheta)$ is given by eq. 21a and $\overline{y^2}(\vartheta)$ as a function of ϑ by eq. 19.

IV. Slow Turbulent Coagulation

We have restricted our discussion so far to "rapid" coagulation in the sense that any electrostatic repulsive forces between the "spheres of interaction" of two particles are sufficiently weak to be neglected. When this is not the case Fuchs[6] has shown how to modify the Smoluchowski coagulation theory for the presence of these forces as long as these are derivable from a potential $\psi(r)$, *i.e.*, the forces are conservative. For lyophobic colloids the form of $\psi(r)$ is known and the effect of this correction is tabulated.[7] When these forces are appreciable then the rate of coagulation is materially slowed down so that one refers to the process as one of "slow" coagulation.

Extending these ideas to the case of turbulent coagulation there should be an analog of a slow coagulation process resulting from the mutual repulsion of the particles. In the case that $\vartheta_s \gg L_h$ and if an analog to a friction coefficient f exists for the particle in turbulent flow and inertial effects can be neglected, then

$$\vartheta_s = \frac{\vartheta}{x} \qquad (23)$$

Here ϑ is the coagulation time in the absence of repulsive forces and x is obtained by solving an appropriate Smoluchowski equation[4] with the ordinary molecular diffusion coefficient replaced by the eddy diffusion coefficient K, since for large t

$$n^* \longrightarrow K$$

The parameter x is given by the analog of a formula due to Fuchs[6]

$$x = \int_0^1 \exp\left[\psi\left(\frac{R}{x'}\right)/fK\right]dx' \qquad (24)$$

(5) F. C. Collins and G. E. Kimball, *Ind. Eng. Chem.*, **41**, 2551 (1949); H. L. Frisch and F. C. Collins, *J. Chem. Phys.*, **20**, 1797 (1952); F. C. Collins, *J. Colloid Sci.*, **5**, 499 (1950).

(6) N. Fuchs, *Z. Physik*, **89**, 736 (1934).

(7) E. Verwey and J. Th. Overbeek, "Theory of the Stability of Lyophobic Colloids," Elsevier Press, Inc., New York, N. Y., 1948.

In the case of molecular diffusion the analog of the product fK is given by the theory of Brownian motion as kT where T is the absolute temperature and k is Boltzmann's constant. This no longer applies but if the colloid particles behave hydrodynamically like macroscopic bodies then a number of semi-empirical expressions for f can be substituted in eq. 24. In general $fK \gg kT$ and hence the contribution of x is much smaller than in the case of molecular diffusion.

V. Discussion

A number of relations characterizing the coagulation of particles in turbulent flow have been obtained on the assumption that the turbulence is homogeneous and isotropic and the fluid remains macroscopically at rest. The possibility of extension of these results to fluids which are displaced with a constant velocity, say along the x-axis, can be relatively easily formulated since the basic turbulent diffusion theory exists.[1,3,8] A more serious difficulty is encountered when an analog of these results is required for turbulence fields which are neither homogeneous nor isotropic. It is hoped that at least a first guide to the type of coagulation behavior to be expected in turbulent media is given by the simpler types of fields.

Finally the possibility suggests itself that a global (as opposed to a local property) characteristic of field of turbulence could be established based on the coagulation time of a sufficiently well-characterized colloidal suspension. Needless to say, extensive further investigation would be required to implement such a suggestion.

(8) E. W. Hewson, "Int. Symp. on Atmospheric Turbulence in the Boundary Layer," Geophys. Res. Paper #19, Cambridge, 1952.

ENERGY LEVELS AND THERMODYNAMIC FUNCTIONS FOR MOLECULES WITH INTERNAL ROTATION. IV. EXTENDED TABLES FOR MOLECULES WITH SMALL MOMENTS OF INERTIA[1]

BY JAMES C. M. LI AND KENNETH S. PITZER

Contribution from the Department of Chemistry and Chemical Engineering, University of California, Berkeley, California

Received October 3, 1955

Additional theoretical developments have made it possible to present general tables for the thermodynamic properties of a restricted rotator which are applicable to molecules with very small moments of inertia. Additional eigenvalues for the Mathieu equation were obtained for these calculations. These eigenvalues will be of use also in the interpretation of spectral data for restricted rotators.

When the general tables for the thermodynamic functions for a restricted internal rotator were presented in Paper I of this series,[2] it did not appear to be practical to extend general tables into the region of low moments of inertia where the partition function depends on the over-all rotation quantum numbers. Recently, however, in treating the case of methyl alcohol in which the partition function for internal rotation does depend significantly upon over-all rotation quantum number, Halford[3] showed that it was still possible to separate the internal and external rotational partition functions in good approximation. We will show that this separability is generally valid for molecules comprising coaxial tops. From the nature of the energy level pattern for less symmetrical molecules it seems virtually certain that the same approximation is still valid and that the extended tables to be presented herewith are applicable to all molecules which consist of a symmetrical top attached to a rigid frame.

We shall find that the partition function for internal rotation is a periodic function of a boundary value parameter ρ which depends on the over-all rotational state. The essential approximation is that the actual molecules at temperatures of interest be widely distributed over external rotational levels and as a result uniformly distributed over the range in ρ. Therefore we take the average over ρ for our final partition function for internal rotation.

$$Q = \frac{1}{2\pi}\int_0^{2\pi} Q(\rho)\mathrm{d}\rho \qquad (1)$$

The reduced moment of inertia and similar quantities were defined in Paper I.

Extended Tables of Thermodynamic Functions for Internal Rotation.—We first give in Tables I–IV supplements to Tables I, III, V and VI in Paper I for smaller moments of inertia and hence larger values of the reciprocal of the partition function for free rotation. In terms of current values of physical constants[4] we have

$$Q_f = 2.7935(10^{38}IT)^{1/2}/n \qquad (2)$$

where I is the reduced moment of inertia for internal rotation. In the present tables R is 1.9872 which does not differ significantly from the value 1.9869 used previously.

It should be noted that equation 2 is the classical approximation to the partition function for free rotation. We use this expression as a definition of Q_f even down to $Q_f = 1$ where the classical approxi-

(1) This work was assisted by the American Petroleum Institute through Research Project 50 and by the Atomic Energy Commission through the Radiation Laboratory.

(2) K. S. Pitzer and W. D. Gwinn, *J. Chem. Phys.*, **10**, 428 (1942); see also K. S. Pitzer, *ibid.*, **5**, 469 (1937); **14**, 239 (1946); J. E. Kilpatrick and K. S. Pitzer, *ibid.*, **17**, 1064 (1949).

(3) J. O. Halford, *ibid.*, **18**, 1051 (1950).

(4) F. D. Rossini, F. T. Gucker, Jr., H. L. Johnston, L. Pauling and G. W. Vinal, *J. Am. Chem. Soc.*, **74**, 2699 (1952).

TABLE I

$(-F/T)$

V/RT \ $1/Q_t$	0.55	0.60	0.65	0.70	0.75	0.80	0.85	0.90	0.95	1.00
0	1.190	1.014	0.856	0.710	0.575	0.443	0.323	0.208	0.102	0.001
0.2	1.182	1.009	.852	.707	.570	.441	.321	.207	.101	.000
.4	1.164	.997	.842	.699	.565	.438	.318	.206	.099	− .002
.6	1.136	.974	.826	.687	.555	.431	.315	.204	.097	− .002
.8	1.099	.947	.804	.670	.543	.424	.310	.200	.096	− .002
1.0	1.056	.912	.777	.647	.526	.411	.302	.195	.094	− .004
1.5	.937	.815	.700	.588	.481	.379	.277	.178	.084	− .009
2.0	.817	.713	.615	.521	.428	.338	.249	.160	.074	− .011
2.5	.705	.616	.534	.454	.375	.298	.219	.141	.063	− .015
3.0	.608	.530	.458	.390	.324	.258	.191	.122	.053	− .018
3.5	.525	.457	.395	.336	.278	.222	.165	.105	.042	− .021
4.0	.455	.393	.339	.288	.239	.190	.140	.088	.034	− .024
4.5	.398	.340	.290	.247	.205	.162	.117	.074	.027	− .026
5.0	.347	.297	.253	.214	.177	.139	.102	.063	.020	− .025
6.0	.273	.230	.193	.161	.131	.103	.074	.045	.012	− .024
7.0	.218	.181	.149	.123	.100	.078	.056	.032	.008	− .022
8.0	.179	.145	.118	.096	.078	.060	.042	.024	.005	− .018
9.0	.149	.120	.095	.078	.062	.047	.032	.019	.004	− .014
10.0	.124	.100	.079	.063	.049	.037	.026	.015	.002	− .012
12.0	.092	.071	.054	.042	.033	.025	.018	.010	.001	− .008
14.0	.069	.052	.038	.030	.023	.016	.012	.007	.000	− .007
16.0	.053	.039	.028	.021	.016	.012	.008	.004	.000	− .004
18.0	.042	.030	.022	.016	.012	.008	.006	.003	.000	− .003
20.0	.033	.023	.017	.012	.009	.006	.004	.002	.000	− .002

TABLE II

S

V/RT \ $1/Q_t$	0.55	0.60	0.65	0.70	0.75	0.80	0.85	0.90	0.95	1.00
0	2.182	2.009	1.850	1.703	1.567	1.438	1.316	1.203	1.097	0.995
0.2	2.180	2.003	1.848	1.701	1.563	1.433	1.312	1.196	1.091	.991
.4	2.170	1.996	1.837	1.691	1.555	1.428	1.307	1.193	1.085	.983
.6	2.151	1.980	1.823	1.677	1.541	1.415	1.295	1.184	1.076	.976
.8	2.125	1.957	1.800	1.654	1.523	1.399	1.284	1.171	1.068	.966
1.0	2.094	1.928	1.774	1.629	1.499	1.377	1.262	1.153	1.052	.952
1.5	1.997	1.833	1.685	1.552	1.428	1.310	1.201	1.094	1.000	.906
2.0	1.874	1.718	1.578	1.450	1.332	1.224	1.122	1.024	0.936	.846
2.5	1.739	1.589	1.456	1.335	1.224	1.126	1.031	0.942	.860	.779
3.0	1.576	1.456	1.330	1.217	1.114	1.021	0.936	.855	.779	.710
3.5	1.458	1.323	1.206	1.100	1.004	0.919	.841	.769	.703	.638
4.0	1.328	1.199	1.087	0.988	0.901	.821	.748	.683	.623	.568
4.5	1.209	1.086	0.978	.884	.804	.730	.662	.607	.551	.501
5.0	1.097	0.982	.881	.794	.716	.648	.588	.535	.486	.442
6.0	0.915	.808	.715	.637	.568	.509	.457	.412	.372	.339
7.0	.774	.672	.588	.516	.453	.401	.357	.319	.285	.257
8.0	.660	.566	.486	.422	.366	.320	.281	.248	.220	.195
9.0	.570	.483	.407	.350	.300	.258	.223	.195	.171	.150
10.0	.496	.414	.348	.293	.248	.211	.180	.154	.134	.116
12.0	.388	.315	.255	.213	.176	.146	.122	.101	.084	.073
14.0	.309	.247	.196	.157	.126	.100	.084	.069	.056	.046
16.0	.251	.196	.155	.119	.092	.075	.059	.048	.038	.029
18.0	.205	.158	.121	.093	.072	.056	.042	.034	.026	.020
20.0	.170	.129	.097	.073	.056	.042	.032	.024	.018	.014

mation is clearly invalid. Also we find that the average of $Q(\rho)$ over ρ can give values less than unity. We will see that $Q(0)$ cannot be less than one, but $Q(\rho)$ can be lower for other values of ρ. This is the explanation of the negative values in the last column of Table I.

For Tables II, III and IV, the related functions Q' and Q'' are needed. These were calculated by standard methods and treated in exactly the method to be described for Q.

The energy levels for the restricted rotator are eigenvalues for the Mathieu equation. These eigenvalues are available[5] for $\rho = 0$ and π. The ei-

(5) "Tables Relating to Mathieu Functions," from the Computation Laboratory of the National Bureau of Standards, Columbia University Press, New York, N. Y., 1951.

TABLE III

H/T

V/RT \ $1/Q_f$	0.55	0.60	0.65	0.70	0.75	0.80	0.85	0.90	0.95	1.00
0	0.994	0.994	0.994	0.994	0.994	0.994	0.994	0.994	0.994	0.994
0.2	0.996	.994	.994	.994	.992	.992	.991	.990	.989	.990
.4	1.006	.999	.994	.992	.990	.988	.988	.986	.985	.985
.6	1.014	1.004	.995	.990	.987	.984	.982	.980	.979	.979
.8	1.026	1.009	.996	.984	.980	.976	.974	.972	.971	.970
1.0	1.038	1.014	.996	.982	.972	.965	.962	.960	.959	.960
1.5	1.059	1.019	.987	.962	.945	.932	.922	.916	.915	.917
2.0	1.057	1.005	.962	.928	.904	.886	.873	.864	.860	.861
2.5	1.032	0.972	.922	.882	.850	.827	.811	.801	.796	.797
3.0	0.988	.924	.870	.828	.791	.763	.744	.732	.728	.729
3.5	.933	.868	.811	.765	.727	.697	.676	.663	.659	.662
4.0	.872	.806	.749	.701	.661	.630	.609	.595	.590	.592
4.5	.810	.744	.687	.638	.599	.567	.545	.531	.526	.528
5.0	.750	.685	.628	.580	.540	.508	.485	.470	.465	.467
6.0	.644	.580	.523	.476	.437	.406	.383	.368	.361	.363
7.0	.554	.491	.437	.392	.354	.324	.302	.286	.279	.279
8.0	.480	.420	.368	.326	.290	.261	.239	.223	.215	.213
9.0	.421	.363	.312	.273	.240	.211	.191	.176	.168	.165
10.0	.370	.314	.269	.231	.200	.174	.154	.140	.132	.129
12.0	.296	.244	.202	.170	.143	.121	.104	.091	.084	.081
14.0	.240	.195	.158	.127	.103	.084	.072	.062	.056	.053
16.0	.198	.157	.127	.098	.076	.061	.051	.044	.038	.034
18.0	.164	.128	.099	.077	.060	.047	.036	.029	.026	.023
20.0	.138	.105	.080	.061	.047	.036	.028	.022	.018	.016

TABLE IV

C

V/RT \ $1/Q_f$	0.50	0.55	0.60	0.65	0.70	0.75	0.80	0.85	0.90	0.95	1.00
0	0.994	0.994	0.994	0.994	0.994	0.994	0.994	0.994	0.994	0.994	0.994
0.2	1.000	1.000	1.000	1.000	1.000	1.000	1.000	0.999	0.999	0.999	0.999
.4	1.018	1.017	1.015	1.013	1.012	1.010	1.008	1.007	1.005	1.004	1.004
.6	1.049	1.046	1.041	1.036	1.031	1.026	1.021	1.017	1.014	1.011	1.010
.8	1.092	1.084	1.075	1.067	1.058	1.049	1.040	1.031	1.025	1.020	1.015
1.0	1.144	1.131	1.118	1.105	1.091	1.078	1.065	1.052	1.040	1.031	1.024
1.5	1.299	1.273	1.247	1.218	1.192	1.165	1.141	1.115	1.090	1.070	1.053
2.0	1.465	1.424	1.382	1.341	1.300	1.258	1.218	1.180	1.146	1.113	1.083
2.5	1.619	1.562	1.504	1.448	1.393	1.341	1.289	1.238	1.190	1.146	1.105
3.0	1.732	1.663	1.597	1.532	1.466	1.401	1.337	1.276	1.217	1.164	1.114
3.5	1.803	1.727	1.654	1.580	1.506	1.432	1.361	1.293	1.226	1.165	1.108
4.0	1.834	1.754	1.674	1.593	1.513	1.435	1.359	1.286	1.215	1.148	1.085
4.5	1.832	1.749	1.664	1.578	1.496	1.413	1.333	1.259	1.185	1.115	1.051
5.0	1.808	1.718	1.631	1.543	1.457	1.373	1.292	1.214	1.140	1.068	1.004
6.0	1.711	1.614	1.520	1.429	1.342	1.255	1.173	1.096	1.022	0.954	0.888
7.0	1.588	1.487	1.390	1.296	1.207	1.120	1.040	0.962	0.890	.826	.767
8.0	1.468	1.366	1.262	1.164	1.074	0.988	0.908	.834	.765	.704	.647
9.0	1.362	1.250	1.144	1.048	0.956	.869	.789	.717	.652	.593	.542
10.0	1.262	1.151	1.045	0.943	.850	.765	.688	.618	.556	.499	.450
12.0	1.107	0.989	0.877	.774	.682	.600	.528	.463	.407	.358	.313
14.0	0.978	.855	.744	.644	.554	.479	.411	.352	.303	.262	.226
16.0	.873	.749	.639	.542	.457	.387	.324	.272	.229	.194	.162
18.0	.780	.657	.549	.456	.378	.312	.259	.215	.175	.144	.119
20.0	.701	.580	.477	.389	.316	.256	.208	.168	.135	.109	.089

genvalues for $\rho = \pi/2$ (*i.e.*, the Mathieu functions periodic in 4π but not in 2π) were kindly computed for us by Robert Pexton of the Theoretical Section, Livermore Laboratory, Radiation Laboratory, University of California. Table V gives these eigenvalues which should be of value in calculating spectral frequencies in internal rotator problems in addition to the present problem and possibly others.

In addition to Tables I–IV, the thermodynamic functions are presented in Tables VI–IX in terms of variables related directly to Mathieu function parameters. These tables, which will be discussed below, will be found more convenient for certain calculations because the temperature appears in only one variable, rather than both of the variables of Tables I–IV.

TABLE V

MATHIEU EQUATION EIGENVALUES

θ	$\theta_{0,0}$	$\theta_{0,1}$	$\theta_{0,2}$	$\theta_{0,3}$	$\theta_{0,4}$	$\theta_{0,5}$	$\theta_{0,6}$	$\theta_{0,7}$	$\theta_{0,8}$	$\theta_{0,9}$
0.25	0.208949	2.274369	6.255967	12.252779	20.251624	30.251068	42.250758	56.250566	72.250439	90.250350
.50	.092337	2.340760	6.274030	12.261122	20.256504	30.254274	42.253030	56.252263	72.251755	90.251401
.75	− .084899	2.433751	6.304650	12.275058	20.264620	30.259618	42.256819	56.255091	72.253950	90.253153
1.00	− .307285	2.537181	6.348449	12.294629	20.276003	30.267102	42.262124	56.259051	72.257024	90.255606
1.25	− .562707	2.638247	6.406033	12.319901	20.290654	30.276728	42.268945	56.264143	72.260977	90.258761
1.50	− .842670	2.727976	6.477777	12.350990	20.308586	30.288500	42.277286	56.270367	72.265811	90.262619
1.75	− 1.141382	2.800509	6.563612	12.387986	20.329813	30.302421	42.287145	56.277724	72.271527	90.267179
2.00	− 1.454857	2.852375	6.662826	12.431050	20.354375	30.318497	42.298526	56.286215	72.278125	90.272443
2.25	− 1.780282	2.881905	6.774095	12.480344	20.382265	30.336733	42.311429	56.295841	72.285606	90.278411
2.50	− 2.115613	2.888745	6.895458	12.536090	20.413524	30.357135	42.325857	56.306601	72.293877	90.285083
2.75	− 2.459323	2.873486	7.024558	12.598502	20.448182	30.379711	42.341813	56.318498	72.303095	90.292460
3.00	− 2.810233	2.837294	7.158754	12.667837	20.486275	30.404466	42.359298	56.331531	72.313193	90.300438
3.25	− 3.167422	2.781657	7.295355	12.744301	20.527825	30.431411	42.378317	56.345703	72.324171	90.309198
3.50	− 3.530152	2.708185	7.431776	12.828091	20.572907	30.460556	42.398871	56.361014	72.336029	90.318660
3.75	− 3.897815	2.618455	7.565455	12.919413	20.621561	30.491911	42.420962	56.377466	72.348768	90.328823
4.00	− 4.269911	2.513956	7.694393	13.018332	20.673846	30.525488	42.444598	56.395061	72.362389	90.339690
4.25	− 4.646019	2.396052	7.816734	13.124883	20.729853	30.561298	42.469779	56.413799	72.376891	90.351259
4.50	− 5.025777	2.265952	7.930712	13.238932	20.789622	30.599360	42.496512	56.433683	72.392276	90.363531
4.75	− 5.408889	2.124731	8.035237	13.360270	20.853250	30.639683	42.524800	56.454710	72.408543	90.376506
5.00	− 5.795073	1.973339	8.129310	13.488511	20.920797	30.682286	42.554647	56.476889	72.425694	90.390184
5.25	− 6.184114	1.812598	8.212282	13.623158	20.992400	30.727185	42.586060	56.500219	72.443730	90.404566
5.50	− 6.575788	1.643238	8.283713	13.763515	21.068172	30.774402	42.619043	56.524701	72.462649	90.419652
5.75	− 6.969928	1.465902	8.343425	13.908874	21.148188	30.823948	42.653608	56.550339	72.482536	90.435443
6.00	− 7.366371	1.281160	8.391462	14.058307	21.232537	30.875858	42.689751	56.577134	72.503247	90.451938
6.25	− 7.764973	1.089517	8.427866	14.210958	21.321411	30.930150	42.727484	56.605088	72.524849	90.469138
6.50	− 8.165598	0.891417	8.452919	14.365680	21.414838	30.986859	42.766812	56.634204	72.547343	90.487043
6.75	− 8.568133	.687267	8.467041	14.521570	21.513003	31.046001	42.807745	56.664485	72.570729	90.505746
7.00	− 8.972473	.477423	8.470638	14.677645	21.615939	31.107612	42.850280	56.695942	72.595011	90.525082
7.25	− 9.378517	.262230	8.464031	14.832845	21.723756	31.171714	42.894439	56.728563	72.620188	90.545128
7.50	− 9.786184	.041912	8.447799	14.986332	21.836492	31.238356	42.940224	56.762359	72.646263	90.565883
7.75	−10.195386	− .183173	8.422363	15.136962	21.954224	31.307586	42.987645	56.797331	72.673238	90.587350
8.00	−10.606050	− .412823	8.388190	15.284212	22.076962	31.379426	43.036710	56.833484	72.701113	90.609528
8.25	−11.018110	− .646818	8.345675	15.427032	22.204611	31.453905	43.087445	56.870821	72.729815	90.632420
8.50	−11.431503	− .884933	8.295253	15.565008	22.337188	31.531119	43.139837	56.909335	72.759478	90.656025
8.75	−11.846159	−1.126996	8.237319	15.697350	22.474465	31.611060	43.193907	56.949047	72.790044	90.680344
9.00	−12.262037	−1.372820	8.172240	15.823622	22.616434	31.693839	43.249649	56.989954	72.821513	90.705380
9.25	−12.679082	−1.622247	8.100359	15.943356	22.762836	31.779462	43.307102	57.032058	72.853889	90.731131
9.50	−13.097248	−1.875117	8.022001	16.056300	22.913155	31.868010	43.366286	57.075365	72.887170	90.757601
9.75	−13.516487	−2.131302	7.937465	16.162150	23.067546	31.959538	43.427191	57.119894	72.921361	90.784687
10.00	−13.936760	−2.390669	7.847028	16.260728	23.225194	32.054086	43.489820	57.165624	72.956533	90.812574

TABLE VI

$-F/RT$

4θ \ τ	4.5	4.0	3.5	3.0	2.5	2.0	1.75	1.5	1.25	1.0
0	0.6313	0.5724	0.5056	0.4285	0.3374	0.2258	0.1590	0.0820	−0.0092	−0.1208
1	.6270	.5679	.5010	.4238	.3326	.2216	.1554	.0794	− .0100	− .1183
2	.6148	.5551	.4877	.4102	.3193	.2097	.1453	.0723	− .0119	− .1117
3	.5960	.5355	.4674	.3896	.2993	.1924	.1308	.0624	− .0142	− .1018
4	.5723	.5110	.4422	.3643	.2752	.1721	.1143	.0517	− .0160	− .0900
5	.5455	.4833	.4141	.3366	.2494	.1511	.0977	.0416	− .0169	− .0776
6	.5170	.4542	.3849	.3083	.2236	.1310	.0823	.0328	− .0172	− .0657
7	.4877	.4248	.3559	.2806	.1990	.1126	.0688	.0256	− .0160	− .0548
8	.4588	.3959	.3277	.2543	.1764	.0965	.0573	.0200	− .0144	− .0454
9	.4307	.3682	.3011	.2300	.1560	.0826	.0477	.0157	− .0128	− .0373
10	.4037	.3419	.2763	.2077	.1380	.0708	.0400	.0124	− .0111	− .0306
12	.3541	.2944	.2325	.1696	.1082	.0525	.0285	.0081	− .0081	− .0206
14	.3107	.2539	.1962	.1392	.0857	.0396	.0208	.0056	− .0058	− .0139
16	.2732	.2197	.1665	.1153	.0687	.0304	.0156	.0041	− .0040	− .0095
18	.2413	.1918	.1423	.0963	.0558	.0238	.0119	.0031	− .0028	− .0065
20	.2140	.1673	.1225	.0813	.0458	.0189	.0093	.0024	− .0020	− .0045
25	.1621	.1231	.0870	.0552	.0294	.0112	.0052	.0014	− .0008	− .0019
30	.1265	.0938	.0644	.0393	.0198	.0070	.0031	.0008	− .0004	− .0009
35	.1012	.0735	.0491	.0288	.0138	.0045	.0019	.0005	− .0002	− .0004
40	.0827	.0589	.0383	.0217	.0099	.0030	.0012	.0003	− .0000	− .0002

Mathematical Treatment.—The essential derivations will be presented briefly for the case of two coaxial symmetrical tops. In addition to the work of Halford[3] and the earlier papers of this series,[2] reference should be made to the important work of Dennison and collaborators[6] on the energy levels of molecules of this type and to a recent revision of

(6) J. S. Koehler and D. M. Dennison, *Phys. Rev.*, **57**, 1006 (1940); D. G. Burkhard and D. M. Dennison, *ibid.*, **84**, 408 (1951); E. V. Ivash and D. M. Dennison, *J. Chem. Phys.*, **21**, 1804 (1953).

TABLE VII

S/R

4θ \ τ	4.5	4.0	3.5	3.0	2.5	2.0	1.75	1.5	1.25	1.0
0	1.1313	1.0724	1.0056	0.9285	0.8374	0.7258	0.6590	0.5819	0.4908	0.3792
1	1.1290	1.0696	1.0022	.9241	.8316	.7180	.6499	.5712	.4783	.3653
2	1.1222	1.0614	0.9920	.9112	.8148	.6956	.6239	.5409	.4436	.3274
3	1.1111	1.0479	.9754	.8904	.7882	.6608	.5841	.4958	.3937	.2759
4	1.0959	1.0297	.9531	.8627	.7534	.6169	.5350	.4420	.3370	.2215
5	1.0770	1.0071	.9258	.8295	.7125	.5672	.4812	.3854	.2807	.1719
6	1.0548	0.9808	.8945	.7920	.6677	.5152	.4268	.3306	.2289	.1305
7	1.0297	.9515	.8601	.7516	.6210	.4636	.3745	.2804	.1851	.0979
8	1.0024	.9199	.8235	.7096	.5740	.4143	.3264	.2362	.1488	.0731
9	0.9731	.8866	.7857	.6672	.5282	.3685	.2833	.1983	.1193	.0547
10	.9425	.8521	.7472	.6253	.4845	.3270	.2454	.1665	.0958	.0412
12	.8789	.7821	.6714	.5456	.4054	.2570	.1846	.1181	.0627	.0238
14	.8147	.7135	.5998	.4739	.3388	.2030	.1402	.0851	.0420	.0143
16	.7523	.6487	.5347	.4117	.2842	.1619	.1079	.0625	.0289	.0089
18	.6931	.5897	.4768	.3589	.2399	.1306	.0843	.0468	.0203	.0057
20	.6383	.5352	.4260	.3138	.2041	.1066	.0668	.0356	.0146	.0037
25	.5215	.4249	.3266	.2300	.1408	.0671	.0393	.0190	.0068	.0014
30	.4316	.3437	.2568	.1743	.1011	.0443	.0243	.0108	.0034	.0006
35	.3628	.2834	.2066	.1355	.0748	.0303	.0157	.0064	.0018	.0003
40	.3094	.2375	.1692	.1075	.0566	.0212	.0104	.0040	.0011	.0001

TABLE VIII

H/RT

4θ \ τ	4.5	4.0	3.5	3.0	2.5	2.0	1.75	1.5	1.25	1.0
0	0.5000	0.5000	0.5000	0.5000	0.5000	0.5000	0.5000	0.5000	0.5000	0.5000
1	.5020	.5017	.5012	.5004	.4990	4965	.4945	.4919	.4883	.4836
2	.5074	.5062	.5043	.5010	.4955	4859	.4786	.4686	.4555	.4391
3	.5150	.5124	.5080	.5008	.4888	4685	.4533	.4334	.4080	.3777
4	.5235	.5187	.5109	.4984	.4781	.4448	.4207	.3903	.3531	.3115
5	.5315	.5238	.5117	.4928	.4631	.4161	.3836	.3439	.2976	.2495
6	.5379	.5266	.5096	.4836	.4441	.3843	.3445	.2978	.2461	.1962
7	.5420	.5268	.5043	.4710	.4220	.3510	.3058	.2548	.2011	.1527
8	.5435	.5240	.4958	.4553	.3976	.3178	.2691	.2162	.1632	.1185
9	.5424	.5184	.4845	.4373	.3722	.2859	.2355	.1826	.1321	.0921
10	.5388	.5102	.4709	.4176	.3465	.2562	.2054	.1541	.1070	.0718
12	.5248	.4876	.4389	.3759	.2971	.2045	.1561	.1100	.0708	.0444
14	.5040	.4596	.4036	.3347	.2531	.1634	.1194	.0795	.0478	.0282
16	.4790	.4289	.3682	.2964	.2155	.1315	.0924	.0585	.0329	.0183
18	.4519	.3979	.3345	.2623	.1841	.1069	.0724	.0437	.0231	.0122
20	.4243	.3679	.3035	.2325	.1582	.0878	.0576	.0332	.0165	.0083
25	.3594	.3018	.2396	.1748	.1114	.0559	.0340	.0177	.0076	.0033
30	.3051	.2499	.1924	.1350	.0813	.0373	.0212	.0100	.0038	.0014
35	.2615	.2099	.1575	.1067	.0610	.0258	.0137	.0059	.0020	.0007
40	.2267	.1786	.1309	.0858	.0467	.0182	.0092	.0036	.0011	.0003

the calculations for methanol.[7] The asymmetry of the OH group is so small that the model of two coaxial tops is still satisfactory for methanol. However, it is important to distinguish between examples such as ethane or methylchloroform where both tops have strict n-fold symmetry and examples like methanol where one top is asymmetric but of a nature to leave two moments of inertia nearly equal. We shall also mention the probable effects in cases of large asymmetry.

For the case of coaxial tops, the external rotation perpendicular to the symmetry axis is readily separated and the partition function integrated. The complete rotational partition function in good approximation is then

$$Q_T = \frac{8\pi^2 AkT}{h^2\sigma} \sum_k \sum_l e^{-\delta K^2} - F_{l,\rho(K)} \qquad (3)$$

$$\delta = h^2/8\pi^2 CkT$$

$$F_{l,\rho(K)} = (E_{l,\rho(K)} - E_{0,0})/kT$$

where A is the total moment of inertia perpendicular to the symmetry axis, C, the total moment about the symmetry axis, σ, the symmetry number for over-all rotation, and $E_{l,\rho(K)}$ the internal rotation energy for the indicated level. It is to be noted that E depends upon the quantum number K, which gives the total angular momentum about the symmetry axis, as well as the quantum number for internal rotation, l. The sum in K runs from $-\infty$ to $+\infty$.

Koehler and Dennison[6] showed that the variation of E with K was periodic. Let us define a

(7) E. V. Ivash, J. C. M. Li and K. S. Pitzer, *J. Chem. Phys.*, **23**, 1814 (1955).

TABLE IX

C/R

4θ \ τ	4.5	4.0	3.5	3.0	2.5	2.0	1.75	1.5	1.25	1.0
0	0.5000	0.5000	0.5000	0.5000	0.5000	0.5000	0.5000	0.5000	0.5000	0.5000
1	.5038	.5046	.5055	.5067	.5082	.5097	.5104	.5105	.5090	.5042
2	.5152	.5180	.5215	.5260	.5313	.5366	.5381	.5372	.5300	.5096
3	.5335	.5394	.5468	.5557	.5658	.5742	.5748	.5689	.5492	.5030
4	.5577	.5675	.5792	.5928	.6066	.6143	.6102	.5938	.5444	.4760
5	.5868	.6005	.6163	.6335	.6483	.6495	.6361	.6038	.5403	.4310
6	.6194	.6366	.6556	.6743	.6862	.6743	.6481	.5965	.5088	.3755
7	.6540	.6740	.6946	.7120	.7168	.6863	.6450	.5738	.4655	.3179
8	.6894	.7108	.7311	.7444	.7380	.6853	.6276	.5392	.4166	.2637
9	.7241	.7457	.7635	.7698	.7492	.6728	.6007	.4990	.3673	.2163
10	.7572	.7773	.7906	.7877	.7508	.6514	.5671	.4556	.3202	.1763
12	.8150	.8277	.8269	.8006	.7301	.5918	.4913	.3713	.2400	.1166
14	.8580	.8587	.8396	.7881	.6880	.5239	.4170	.2986	.1793	.0780
16	.8850	.8710	.8234	.7580	.6356	.4580	.3514	.2400	.1349	.0530
18	.8967	.8682	.8108	.7178	.5807	.3988	.2963	.1939	.1023	.0366
20	.8955	.8517	.7798	.6733	.5278	.3479	.2508	.1578	.0788	.0257
25	.8543	.7831	.6871	.5642	.4155	.2502	.1691	.0971	.0424	.0112
30	.7880	.7027	.5978	.4730	.3314	.1844	.1173	.0619	.0239	.0052
35	.7188	.6282	.5220	.4006	.2682	.1384	.0831	.0404	.0139	.0025
40	.6556	.5640	.4593	.3426	.2195	.1053	.0598	.0270	.0083	.0013

variable ρ in which E will have the period 2π. The μ used in I is related by $\mu = i\rho/\pi$. For examples where both tops have the same n-fold symmetry (as CH_3-CF_3) or where only one top has a strict symmetry (as CH_3-OH), the expression for ρ in terms of K is

$$\rho = (2\pi C_1/nC)K + 2\pi\beta/n \qquad (4)$$

where C_1 is the moment of inertia of one top (one which is strictly symmetrical), n is the symmetry number for internal rotation, and β is an integer such that $0 \leq |\beta| \leq n/2$. The value of β depends upon the nuclear spin orientation of the symmetrically placed nuclei. In a CH_3 group $\beta = 0$ for the spin species of symmetry A, and $\beta = \pm 1$ for species E. If both tops have strict symmetry, either may be taken for C_1, but for optimum accuracy in the calculation to follow the top with smaller moment of inertia should be selected.

Let us now sum the partition function over the internal rotational energy levels for various values of ρ. The results may be expanded in Fourier series.

$$Q(\rho) = \sum_l e^{-F_{l,\rho}} = \sum_m a_m \cos m\rho \qquad (5)$$

$$a_m = \frac{1}{\pi}\int_0^{2\pi} Q(\rho)\cos m\rho \mathrm{d}\rho,\ m \neq 0 \qquad (6a)$$

$$a_0 = \frac{1}{2\pi}\int_0^{2\pi} Q(\rho)\mathrm{d}\rho \qquad (6b)$$

Only the cosine terms are needed since Q is an even function of ρ.

We may now insert this result in the total partition function

$$Q_T = \frac{8\pi^2 AkT}{h^2\sigma}\sum_K\sum_m e^{-\delta K^2} a_m \cos\,[m\rho(K)]\mathrm{d}K \qquad (7)$$

Since δ is small in all cases of interest, we may replace the sum over K by an integral provided the cosine factor also varies slowly with K. The latter condition will hold for $m = 0$ and 1 at least.

$$\cos\,[m\rho(K)] = \cos(2\pi\beta m/n)\cos(2\pi C_1 mK/nC) - \sin(2\pi\beta m/n)\sin(2\pi C_1 mK/nC)$$

$$Q_T = \frac{8\pi^2 AkT}{h^2\sigma}\left(\frac{\pi}{\delta}\right)^{1/2}[a_0 + a_1\cos(2\pi\beta/n)e^{-\pi^2 C_1^2/n^2C^2\delta} + \ldots] \qquad (8)$$

$$Q_E = \frac{8\pi^2 AkT}{h^2\sigma}\left(\frac{\pi}{\delta}\right)^{1/2}$$

$$Q_I = a_0 + a_1\cos(2\pi\beta/n)e^{-\pi^2 C_1^2/n^2C^2\delta} + \ldots \qquad (9)$$

The result in equation 8 is immediately factorable into the standard partition function for external rotation Q_E and the desired result for internal rotation Q_I, equation 9. The subscript I will be omitted hereafter.

In Paper I, Q as defined in equation 5 was assumed to be independent of ρ whereupon $a_0 = Q$ and all other a's are zero. The tables were discontinued whenever $Q(0)$ and $Q(\pi)$ were observed to be significantly different. The next approximation is the first term in the series in equation 9, *i.e.*, $Q = a_0$. This corresponds to the average of $Q(\rho)$ over ρ. Halford's result is essentially this approximation, although he further concluded that $a_0 = {}^1/_2Q(0) + {}^1/_2Q(\pi)$. He verified that the additional terms were negligible for methanol at 200°K.; however, it is instructive to note their magnitude. With the molecular data of Ivash and Dennison, we obtain at 200°K., $a_0 = 1.190$, $a_1 = 0.007$, and the exponent in equation 9 is -23.5 for the a_1 term. For the A nuclear spin species, $\beta = 0$, and the second term contributes a correction of $+10^{-10}\%$. For the E species, $\beta = \pm 1$, and $\cos(2\pi\beta/n) = -{}^1/_2$. Thus the correction is half as large and of the opposite sign.

We have also studied molecules where the two tops have different orders of symmetry. The expression for ρ becomes more complex in these cases but as K increases the values of ρ always oscillate rapidly over their full range in a manner to make $Q_I = a_0$ a good approximation. For example if $n_1 = 3$ and $n_2 = 2$, one may express the energy levels by taking

$$\rho = (2\pi C_1/6C)K \quad \text{for even } K$$
$$\rho = (2\pi C_1/6C)K - \pi \quad \text{for odd } K$$

TABLE X

a_0

4θ \ τ	1.00	1.25	1.50	1.75	2.00	2.5	3.0	3.5	4.0	4.5
0	0.8862	0.9908	1.0854	1.1724	1.2533	1.4012	1.5350	1.6580	1.7725	1.8800
1	.8883	.9901	1.0826	1.1681	1.2480	1.3947	1.5277	1.6503	1.7646	1.8720
2	.8942	.9881	1.0750	1.1564	1.2333	1.3761	1.5071	1.6285	1.7422	1.8494
3	.9032	.9858	1.0644	1.1398	1.2124	1.3489	1.4764	1.5958	1.7083	1.8149
4	.9139	.9841	1.0531	1.1211	1.1878	1.3168	1.4396	1.5560	1.6669	1.7724
5	.9253	.9832	1.0424	1.1026	1.1631	1.2832	1.4002	1.5131	1.6214	1.7254
6	.9364	.9829	1.0333	1.0858	1.1399	1.2505	1.3611	1.4695	1.5749	1.6769
7	.9466	.9841	1.0259	1.0712	1.1192	1.2202	1.3239	1.4274	1.5292	1.6286
8	.9556	.9857	1.0202	1.0590	1.1013	1.1929	1.2896	1.3878	1.4857	1.5822
9	.9633	.9873	1.0158	1.0490	1.0861	1.1689	1.2586	1.3514	1.4451	1.5383
10	.9698	.9889	1.0125	1.0408	1.0733	1.1479	1.2309	1.3183	1.4076	1.4974
12	.9796	.9919	1.0081	1.0289	1.0539	1.1143	1.1849	1.2617	1.3424	1.4249
14	.9862	.9943	1.0056	1.0210	1.0404	1.0895	1.1494	1.2168	1.2890	1.3644
16	.9906	.9957	1.0041	1.0157	1.0309	1.0713	1.1222	1.1811	1.2458	1.3142
18	.9935	.9972	1.0031	1.0120	1.0240	1.0574	1.1011	1.1529	1.2107	1.2728
20	.9955	.9980	1.0024	1.0093	1.0190	1.0469	1.0847	1.1303	1.1821	1.2386
25	.9981	.9992	1.0014	1.0053	1.0112	1.0298	1.0568	1.0910	1.1310	1.1759
30	.9991	.9996	1.0008	1.0031	1.0070	1.0200	1.0400	1.0665	1.0984	1.1348
35	.9996	.9998	1.0005	1.0019	1.0045	1.0139	1.0293	1.0503	1.0763	1.1065
40	.9998	.9999	1.0003	1.0012	1.0030	1.0100	1.0220	1.0390	1.0607	1.0862

TABLE XI

$a_1 \times 10^4$

4θ \ τ	1.0	1.25	1.5	1.75	2.0	2.5	3.0	3.5	4.0	4.5
0	1503	907	536	312	180	59	19	6	2	1
1	1468	888	526	308	178	58	18	6	2	1
2	1369	836	499	293	170	56	18	6	2	1
3	1228	760	459	272	160	53	17	5	2	0
4	1067	672	412	248	146	49	16	5	2	
5	906	582	363	221	132	45	15	5	2	
6	756	500	314	194	118	41	14	4	1	
7	624	417	270	169	104	37	13	4	1	
8	512	348	229	146	91	33	12	4	1	
9	418	290	194	126	79	30	10	4	1	
10	341	240	164	108	69	26	10	3	1	
12	227	164	116	79	52	21	8	3	1	
14	152	113	82	57	38	16	6	2	1	
16	103	78	58	41	28	13	5	2	1	
18	71	54	41	30	21	10	4	2	1	
20	49	38	29	22	16	7	3	1	0	
25	21	16	13	10	8	4	2	1		
30	9	7	6	5	4	2	1	0		
35	4	3	3	2	2	1	1			
40	2	2	1	1	1	1	0			

These expressions are for symmetry A for both of the tops. The calculation leading from equation 7 to equation 8 now yields a zero coefficient for a_1, and the coefficient of a_2 will be extremely small in any practical example.

We are unable to think of any real molecules (at meaningful temperatures) in which the terms beyond a_0 in equation 9 will be significant.[8] Nevertheless, we give in the Appendix values of a_1 and a_2, in addition to a_0, which should certainly suffice to establish the value of Q in all cases.

In addition to the partition function itself, we need the related functions written as Q' and Q'' and defined as the sums of $F_l e^{-F_l}$ and $F_l^2 e^{-F_l}$, respectively, where F_l is the quantity defined in equation 3. These functions are similarly related to the variable ρ and are treated correspondingly.

The following expressions, which should be of fully adequate accuracy, were used in the numerical calculations.

$$\begin{aligned} a_0 &= [Q(0) + 2Q(\pi/2) + Q(\pi)]/4 \\ a_1 &= [Q(0) - Q(\pi)]/2 \\ a_2 &= [Q(0) - 2Q(\pi/2) + Q(\pi)]/4 \end{aligned} \qquad (10)$$

The equations for the a' and a'' are of identical

(8) Halford (ref. 3) indicates concern about molecules such as *t*-butyl alcohol in which C becomes very large and therefore the exponent in equation 9 might become small. However, he presumably thought C_1 could be the OH group moment, which is not correct since the OH group does not have the threefold symmetry. Actually $C_1 \cong C$ in this case so that the argument in the cosine in equation 5 changes by $2\pi/3$ for successive K values with a given nuclear spin species. Halford's detailed arguments lead to this same conclusion.

TABLE XII

$-a_1' \times 10^4$

4θ \ τ	1.0	1.25	1.5	1.75	2.0	2.5	3.0	3.5	4.0	4.5
0	2957	2344	1716	1193	799	333	129	48	17	6
1	2867	2282	1678	1170	786	328	128	47	17	6
2	2621	2114	1571	1105	748	315	124	46	17	6
3	2278	1873	1416	1010	691	296	117	44	16	6
4	1903	1602	1238	898	623	273	110	42	15	5
5	1544	1334	1055	782	551	247	101	39	14	5
6	1230	1088	884	669	480	221	92	36	13	5
7	968	876	730	566	414	196	83	33	12	4
8	757	699	598	474	356	173	75	30	11	4
9	592	555	486	394	300	151	67	27	10	4
10	463	440	394	326	254	132	59	25	10	4
12	287	276	256	222	179	99	47	20	8	3
14	181	175	167	150	126	74	37	16	7	3
16	117	112	109	101	88	55	28	13	6	2
18	78	73	72	69	61	41	22	10	5	2
20	53	49	48	47	43	30	17	8	4	2
25	21	19	18	18	18	14	9	5	2	1
30	9	8	8	8	8	7	5	3	1	1
35	4	4	3	3	3	3	2	2	1	0
40	4	2	2	2	2	2	1	1	0	

TABLE XIII

$a_1'' \times 10^4$

4θ \ τ	1.0	1.25	1.5	1.75	2.0	2.5	3.0	3.5	4.0	4.5
0	−848	916	1793	2013	1856	1191	624	291	126	51
1	−876	842	1719	1952	1812	1170	616	288	124	51
2	−937	652	1516	1783	1686	1112	591	278	121	50
3	−987	402	1237	1544	1504	1025	555	264	116	48
4	−994	157	936	1274	1294	920	510	247	109	46
5	−944	− 41	656	1009	1079	810	462	227	102	43
6	−845	−180	422	768	878	701	413	207	94	40
7	−730	−259	240	561	700	598	365	187	86	37
8	−603	−293	103	405	547	504	320	168	79	34
9	−487	−295	17	277	420	423	279	150	72	32
10	−384	−277	−41	181	318	351	241	134	65	29
12	−227	−216	−91	59	173	238	179	105	53	24
14	−129	−152	−95	0	86	158	131	81	43	20
16	− 72	−102	−81	−24	37	103	95	62	34	17
18	− 40	− 63	−62	−31	11	66	68	48	27	14
20	− 22	− 42	−46	−29	− 6	41	49	36	22	11
25	− 5	− 13	−19	−18	− 9	11	20	18	12	7
30	− 1	− 4	− 7	− 8	− 7	2	8	9	7	4
35	− 0	− 1	− 3	− 4	− 4	0	3	4	4	2
40		− 0	− 1	− 2	− 2	0	1	2	2	1

TABLE XIV

4θ \ τ	$a_2 \times 10^4$		$-a_2' \times 10^4$			$a_2'' \times 10^4$		
	1	1.25	1	1.25	1.5	1	1.25	1.5
0	0.9	0.1	8.6	1.0	0.1	62.9	10.1	1.4
1	.9	.1	8.3	1.0	.1	60.7	9.5	1.4
2	.8	.1	7.6	0.9	.1	54.8	9.1	1.3
3	.7	.1	6.5	.8	.1	47.7	8.0	1.2
4	.6	.1	5.4	.7	.1	37.9	6.9	1.0
5	.5	.1	4.4	.6	.1	29.5	5.5	0.9
6	.4	.1	3.4	.5	.1	22.3	4.7	0.7
7	.3	.0	2.6	.4	.1	16.5	3.5	0.6
8	.2	.0	2.0	.3	.0	11.1	2.7	0.5
9	.2	.0	1.5	.2	.0	8.6	2.0	0.4
10	.1	.0	1.1	.2	.0	6.1	1.6	0.3
12	.1	.0	0.6	.1	.0	3.0	1.1	0.1
14	.1	.0	0.3	.1	.0	1.5	0.5	0.0

form. For these quantities it was more convenient to use variables which relate more closely to the Mathieu equation parameters.

$$4\theta = 5.000 \times 10^{38} IV_0/n^2 = \tau V_0/RT \qquad (11)$$
$$\tau = 4Q_t^2/\pi = 32\pi^2 IkT/n^2h^2$$

Here V_0 is the potential barrier height in cal./mole, and I is in g. cm.^{2}.

In these terms the Mathieu equation is

$$M'' + (\theta_0 + 2\theta \cos 2x)M = 0 \qquad (12)$$
$$M(x + \pi) = e^{i\rho}M(x)$$

and the partition function for a given ρ is

$$Q(\rho) = \sum_{l=0}^{\infty} \exp\left[\theta_{0,0}(0) - \theta_{0,l}(\rho)\right]/\tau \qquad (13)$$

Since we do not believe it will be necessary to use the a_1 and a_2 quantities in practical cases, we shall not present the detailed formulas for thermodynamic properties involving these terms. The derivations follow in a straightforward fashion from equation 9.

The θ and τ variables are more convenient for some thermodynamic calculations than Q_f and (V/RT) since T appears in both the latter but in only τ and not θ. Thus in calculating properties for a given molecule at a series of temperatures one has only to vary τ and may hold θ constant. Both for this reason and because they represent the original calculated values, we present thermodynamic functions in Tables VI to IX as functions of τ and 4 θ. The values in Tables I to IV were interpolated from these directly calculated values.

The derivation in this section was presented for the example of two coaxial tops. While we are not prepared to present a rigorous derivation for the general case of a symmetric top attached to a rigid frame it seems practically certain that the tables will be applicable in the extended region just as they were in the region discussed in Paper I. The only requirement is that the coupling with overall rotation be of such a nature as to weight $Q(\rho)$ equally over the full range of ρ. Since varying rotational states will require different ρ values and there will be a broad distribution over various rotational states, it seems safe to assume that the range of ρ will be covered evenly. Thus we believe it is safe to use the present tables in the same manner as was recommended in Paper I.

Appendix

In Tables X through XIV are given values of the functions a_0, a_1, a', a_1'', a_2, a', a_2'' as defined in equation 6 and 10 and the accompanying text. The corresponding values of a_0' and a_0'' can be obtained from Tables VIII and IX by the equations relating the partition function and the thermodynamic properties.

$$a_0' = a_0(H/RT) \qquad (14)$$

$$a_0'' = a_0\left[\frac{C}{R} + \left(\frac{H}{RT}\right)^2\right] \qquad (15)$$

ELECTRICAL PROPERTIES OF SOLIDS. XIX. CARBON BLACK IN POLAR AND NON-POLAR POLYMERS

BY BERNHARD GROSS[1] AND RAYMOND M. FUOSS

Sterling Chemistry Laboratory, Contribution No. 1319, Yale University, New Haven, Connecticut

Received October ?, 1955

The electrical properties (d.c. conductance κ, dielectric constant ϵ and loss tangent, tan δ) of non-polar (butadiene–styrene) and polar (butadiene–acrylonitrile) polymers containing 0–96 parts by weight of various types of carbon black per 100 parts elastomer have been measured; frequency range, 30 c. $\leq f \leq$ 0.5 Mc. With carbon blacks whose particles average greater than 100 mμ in diameter, the dielectric constant can be computed by Bruggemann's mixture rule up to about 60 parts of carbon by weight; for smaller particles or higher concentrations, the observed dielectric constant is greater than calculated. Chain formation can account for this result. With coarse blacks, κ decreases initially with concentration of carbon, due to adsorption of electrolyte on the surface of the particles, while fine blacks cause a rapid increase in κ. Marked transients were found in κ, which satisfy a power law in time; the transients are ascribed to an ionic atmosphere surrounding the carbon particles and to the semiconducting layer of adsorbed ions. The magnitude of the transient component increases with increasing concentration of coarse blacks. For the polar acrylonitrile polymer, the maximum a.c. loss factor appears at about 200 kc., independent of carbon content. In the non-polar polymer, losses are decreased by initial addition of carbon due to adsorption; the adsorbed layer of ions then gives rise to a pure a.c. loss mechanism.

Introduction

Earlier work on the electrical properties of rubber–carbon mixtures has been reviewed by McPherson;[2] recent investigations[3,4] have shown that with regard to conductance these systems possess two clearly distinct regions, one in which their behavior approaches that of an insulator and another where it approaches that of a conductor. These regions are separated by a rather narrow interval, across which a relatively small increase in concentration of the black causes the conductance to increase by about 4–5 orders of magnitude. The present paper deals only with the first zone.

Conductance, like other electrical properties, depends mainly on particle size and concentration of the (carbon) black. For sufficiently high concentrations and/or sufficiently small particle size, it increases strongly due to chain formation by the particles, but before this happens it may show a

(1) On leave of absence from the Instituto Nacional de Tecnologia, Rio de Janeiro, Brazil. Grateful acknowledgment is made to the California Research Corporation and to the National Research Council of Brazil for research grants for the academic year 1954–55.

(2) A. T. McPherson, "Electrical Properties of Rubber," Chapter in C. C. Davies and J. T. Blake, "Chemistry and Technology of Rubber," Reinhold Publ. Corp., New York, N. Y., 1937.

(3) B. B. S. T. Boonstra and E. M. Dannenberg, *Ind. Eng. Chem.* **46**, 218 (1954).

(4) P. E. Wack, R. L. Anthony and E. Guth, *J. Appl. Phys.*, **18**, 456 (1947).

temporary decrease[5,6] due to absorption of electrolytic contaminants at the surface of the black. The dielectric constant also increases with increasing concentration and decreasing particle size. Values up to 1000 were reported by Kemp and Herrmann,[7] fine blacks again giving the highest values. Dielectric dispersion and dielectric loss over the frequency interval of 50 c. up to 50 Mc. for polar and non-polar rubbers have been investigated by Dalbert.[8]

So far the diversity of results makes it difficult to attain a satisfactory understanding of the relative importance of the various underlying physical factors. Kickstein[6] emphasized the role of the dispersion of the black and the nature of the contact between particles. Uniform dispersion gives relatively low dielectric constants. With the formation of larger aggregates of particles with semi-conducting interfaces, the dielectric constant still remains low, but a considerable dielectric after-effect appears. Finally when chain formation sets in, dielectric constant and conductance increase, and the after-effect practically disappears.

The resistivity of the graphite, which constitutes the particles of the black, is approximately 1000 times greater than that of a metal, but is still very low compared to that of ordinary elastomers. Therefore with the frequency range concerned here, the particles may be considered to act as perfectly conducting spheres (the spherical form has been confirmed by electron microscope studies[9]). As a first approximation, the properties of the systems should then be simply those of a suspension of conducting particles in a dielectric continuum and we may therefore apply the formulas which have been established for such mixtures. For our purposes, two theoretical results are important. Bruggeman[10] has calculated the dielectric constant for systems comprising spheres immersed in a continuous medium, such as suspensions, emulsions and colloidal solutions. His result for the special case of perfectly conducting spheres gives for the relative increase in dielectric constant

$$\epsilon/\epsilon_0 = 1/(1 - p)^3 \qquad (1)$$

where ϵ is the dielectric constant of the mixture, ϵ_0 that of the continuum and p the volume concentration of disperse phase. This formula should therefore represent the observed increase in capacitance so long as the dispersion remains uniform. The d.c. conductance would change in the same way as the capacitance if adsorption at the interfaces did not occur or was negligible. For a non-uniform dispersion, no quantitative results can be expected since the degree of non-uniformity and chain-formation cannot be predicted. Wiener,[11] however, has obtained a general rule for the dielectric constant of mixtures of particles with arbitrary shape which may be stated as follows for the present case: The dielectric constant of a mixture is always greater than the value that would be obtained if the two components of the mixture were arranged into the two layers with a plane interface parallel to the electrodes of the capacitor.[12] Therefore, once Bruggeman's relationship is found to hold over a certain range of concentration of the black, we would attribute any excess elsewhere of the measured dielectric constant over the calculated one to non-uniformity of dispersion. Chain formation is but a special case of non-uniformity, with the conducting particles forming cylinders that may be partially oriented in the direction of the applied field.

An additional (but presumably secondary) effect will be produced by the influence of the semi-conducting surface layers of the black particles, as was emphasized by Kickstein. Evidence for the existence of these layers may be derived from density measurements. While the density of graphite is 2.2, the density of the black in the rubber as determined by a helium displacement method[13] is about 1.8. The difference must be caused by adsorbed gases which are still present when the particles are mixed into the rubber. This layer may have properties of an oxide layer, and while not perfectly insulating it certainly is much less conducting than the black itself. Its relaxation time may fall into the time interval of ordinary measurements.

Experimental

Materials.—The polymers used were commercially available copolymers of butadiene and styrene (75:25, GRS 1504) and of butadiene and acrylonitrile (60:40, Hycar 1041). The gum was milled until soft on a laboratory mill; master batches of the following compositions (by weight) were first made up: Hycar, 100.0; zinc oxide, 5.0; stearic acid, 1.0; Altax (benzothiazyl disulfide), 1.5; sulfur, 1.5; and GR-S, 100.0; zinc oxide, 5.0; stearic acid, 1.0; Captax (mercaptobenzothiazole), 1.0; sulfur, 2.5. Then aliquots were weighed out and carbon blacks of various kinds in varying amounts were milled into the rubber. Milling was sufficient to give a uniform mixture; excessive milling was avoided in order to change the electrical characteristics as little as possible.[3] The carbon blacks are described in Table I. We take this opportunity to thank the Connecticut Hard Rubber Company (New Haven, Connecticut) for supplying the materials, and for the use of their laboratory facilities.

Samples for electrical measurements were cured for 30 min. at 150° in a closed mold. To ensure good electrical contact, the discs (5.0 cm. diam., 3 mm. thick) were coated

(5) P. Dunsheath, *Trans. Inst. Rubber Ind.*, **2**, 460 (1926–27).
(6) G. Kickstein, *Rubber Chem. Technol.*, **27**, 940 (1954).
(7) A. R. Kemp and D. B. Herrmann, *ibid.*, **12**, 317 (1939).
(8) R. Dalbert, *Rev. gén. caoutchouc*, **29**, 515, 588, 649 (1952).
(9) W. D. Schaeffer, W. R. Smith and M. H. Polley, *Ind. Eng. Chem.*, **45**, 1721 (1953).
(10) D. A. G. Bruggeman, *Ann. Phys.*, **24**, 636 (1935).
(11) O. Wiener, *Phys. Z.*, **5**, 332 (1904).

(12) This result can be obtained in an elementary way. Consider a two layer condenser in which the conductance of the upper layer of thickness d is negligible compared to that of the bottom layer. Then the capacitance of the condenser will be proportional to $1/d$. Now rearrange the material in a condenser as follows: interchange a slab of thickness D of the upper dielectric from the left half with a slab of the same thickness of the lower (conducting) layer from the right half. This operation divides the condenser into two parallel sections, each having half the original area; in the left section, the thickness of the non-conducting layer has been decreased to $(d - D)$ while in the right, it has been increased to $(d + D)$. The increase of capacitance due to the section with the smaller thickness will overcompensate the decrease of capacitance due to the section with the larger thickness, and the net result is an increase in capacitance.

$$\frac{1}{2}\left(\frac{1}{d-D} + \frac{1}{d+D}\right) = \frac{1}{2d}\left(1 + \frac{D}{d} + \frac{D^2}{d^2} + \ldots + 1 - \frac{D}{d} + \frac{D^2}{d^2} - \ldots\right) > \frac{1}{d}$$

(13) R. P. Rossman and W. R. Smith, *Ind. Eng. Chem.*, **35**, 972 (1943).

TABLE I

PROPERTIES OF CARBON BLACKS

Name	Type	Av. diam. (mμ)
Thermax	Medium thermal furnace	473
P-33	Fine thermal furnace	172
Philblack A	Medium abrasion furnace	80
Shawinigan	Acetylene	55
Philblack O	High abrasion furnace	45
Vulcan SC	Superconductive furnace	27

before measurements with diluted Aqua-dag on both sides, leaving an uncoated ring between guard and test areas.[14] The cell constant was calculated from the diameter of the test electrode and the average thickness of the sample; the latter was computed from the diameter, weight and density of each sample.

Apparatus and Method.—The cell was constructed of copper with platinum electrode faces.[15] Measurements were made at room temperature (25–28°); at 30–960 c.p.s., a Schering bridge[16] was used, while a General Radio 716C Bridge equipped with Guard Circuit 716-P4 was used for higher frequencies. Values given later in Table II for the Hycar samples were measured with the less sensitive General Radio Bridge and therefore cannot claim the same degree of precision as those for the GRS samples which were measured with the low frequency bridge. It must, however, be taken into consideration that the absolute value of the dielectric constants of the samples depends on milling and pressing conditions and therefore high precision is not justified. Since dispersion of the polar Hycar by far exceeds that of the non-polar GRS, the General Radio bridge was adequate for the more polar systems. Measurements of resistance were made on a d.c. Wheatstone bridge.[17]

Density.—For calculation of the increase of dielectric constant according to eq. 1, the volume concentration p of the black must be known. The samples were made up with a known weight ratio r of black to gum. Therefore the actual density of the black in the rubber must be determined. As mentioned above, in consequence of the adsorbed air, this is not the density of graphite, but it does not seem obvious that it will be equal to the value determined by a method like that used by Rossman and Smith;[13] smaller values might be expected, because the gum cannot penetrate as well as helium into all the pores of the black. We determined the dimensions and weights of the samples and calculated the densities from these data. The results of the measurements are shown in Fig. 1. Assuming simple volume additivity, the densities of the mixtures were calculated from the known densities of the gum and trial values for the density of the black. The latter were then adjusted, until adequate agreement between calculated and measured curves was reached. Figure 1 represents the final results; here the curves are drawn using the following values for the densities of the blacks: 1.80, Thermax in Hycar; 1.74, Thermax in GRS; and 1.68, Vulcan SC in Hycar. The control samples containing no carbon black had densities 1.060 (Hycar) and 0.988 (GRS). If ρ_b is the density of the black and ρ_0 the density of the gum, the relation between volume fraction p and mass ratio r is given by

$$r = (\rho_b/\rho_0)p/(1 - p) \qquad (2)$$

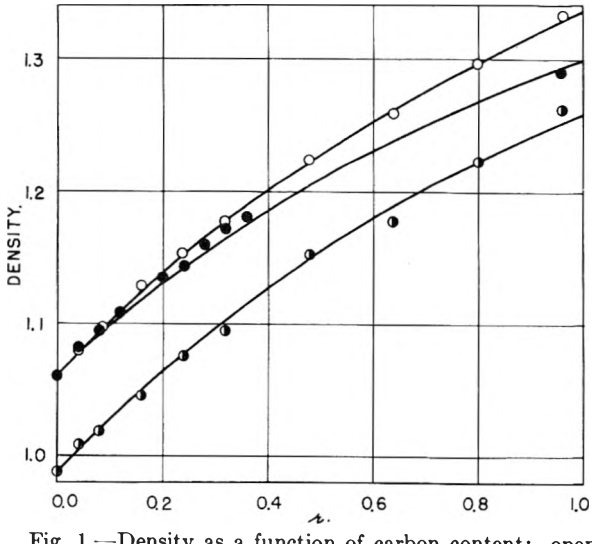

Fig. 1.—Density as a function of carbon content: open circles, Hycar-Thermax; solid circles, Hycar-SC; half-shaded circles, GRS-Thermax.

Results and Discussion

Capacitance at 60 Cycles.—For comparison with theoretical formulas, the relative increase in dielectric constant (or capacitance) is of particular interest. Accordingly, the dotted curves in the upper part of Fig. 2 represent observed capacitance

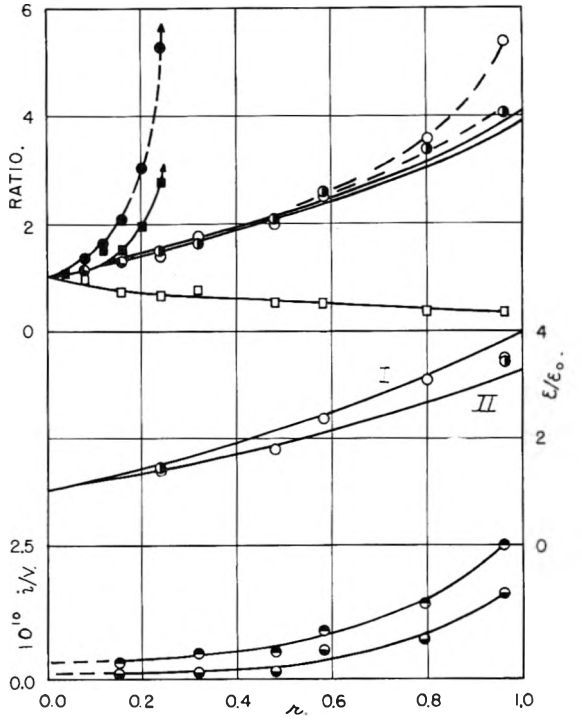

Fig. 2.—Electrical properties as a function of carbon content: upper curves; (circles), ratio of dielectric constant (60 c.) of filled to unfilled stock; same code as Fig. 1; (squares), ratio of d.c. conductances of filled and unfilled stocks; (open squares), Hycar-Thermax; (solid squares), Hycar-SC. Curves in center: dispersion at 0.5 Mc.; same code as Fig. 1. Bottom curves: transient currents in Hycar-Thermax. Top-shaded circles, after 10 sec.; bottom-shaded circles, after 30 sec.

ratios relative to the stocks without carbon black for Thermax and Vulcan SC in Hycar and Thermax in GRS. The solid curves are calculated from eq. 1 and 2 using the numerical values given above for densities. Inspection of the figure shows that for concentrations up to $r \approx 0.6$, the values for the Thermax samples with both Hycar (open circles) and GRS (right-shaded circles) are practically identical and within the experimental limits fall on the theoretical curves, thus confirming the simple mixture law. For the higher concentrations deviations are observed; while the GRS samples still

(14) R. M. Fuoss, *J. Am. Chem. Soc.*, **59**, 1703 (1937).
(15) R. M. Fuoss, *ibid.*, **63**, 369 (1941).
(16) D. Edelson, W. N. Maclay and R. M. Fuoss, *J. Chem. Educ.*, **27**, 644 (1950).
(17) M. Yamin and R. M. Fuoss, THIS JOURNAL, **58**, 477 (1954).

are rather close to the curve, the capacitance increase for the Hycar samples is nearly 50% above theoretical values. With Vulcan SC (solid circles), however, no agreement between experimental and theoretical curves is found. Capacitance ratios are very much higher from the start than calculated; for $r = 0.24$ they have already reached approximately the same value as was found with Thermax for $r = 0.96$. Higher values could not be measured, because at $r = 0.28$ the resistance of the SC samples had fallen to 10 ohms. It seems obvious that two different phenomena are involved here. At low and medium concentrations, the Thermax samples behave like a uniform dispersion of conducting spheres in a dielectric, since they conform to Bruggeman's formula, independent of the dielectric constant of the suspending continuum (Hycar, $\epsilon = 20.16$; GRS, $\epsilon = 2.79$, both at 60 c.). The deviations at high concentrations and with a different black are in the sense of Wiener's rule, with the measured values lying *above* the theoretical ones. This deviation indicates the formation of heterogeneities, which may well be chains.

The appearance of positive deviations with the fine SC much sooner than with the relatively coarse Thermax suggests that chain formation with constant concentration must increase with decreasing particle size. Therefore measurements were made at constant concentration ($r = 0.24$) with the wide range of blacks listed in Table I. For the coarsest black (Thermax), both Hycar and GRS gave about the same capacitance ratio at 24 parts black (*cf.* Fig. 2); the Thermax samples were therefore taken as the reference samples for the next figure. In Fig. 3, the capacitance ratio of various stocks to that of the Thermax samples is plotted against particle diameter. Again we find no very significant difference between the GRS and Hycar samples; the values scatter considerably, but the trend of all the curves is the same. The influence particle size manifests itself only below approximately 100 mμ, while for larger diameters, the capacitance stays constant, indicating a wide range of validity of eq. 1, the law of mixtures. But with small particle size, especially below 100 mμ, the increase in capacitance becomes very strong, and the Hycar values again exceed the GRS values. We therefore conclude that the more finely dispersed the black, the stronger its tendency for chain formation becomes.

D.C. Conductance.—For the kind of systems considered here, d.c. conductance should be proportional to capacitance, on account of their equal dependence on geometrical factors. Therefore it can be expected that at least the strong increase in capacitance observed in some of the curves of Figs. 2 and 3 should be accompanied by a corresponding increase in conductance. Results of d.c. measurements of Hycar samples with the Wheatstone bridge at 600 volts are also represented in Figs. 2 and 3. The squares in the upper part of Fig. 2 show the observed ratios of conductance at various carbon contents to the conductance of the corresponding rubber containing no carbon black. The squares in Fig. 3 show the influence of particle size on relative conductance, with the Thermax-Hycar sample as the reference. The expected correlation between chain formation and increase in conductance is confirmed. For the coarse black, however, a different effect is found. Conduction with Thermax (*cf.* Fig. 2) decreases while the mass ratio increases; the negative slope persists up to $r = 0.96$. Such a decrease has already been reported by others, although apparently not up to such high concentrations. D.C. conductance in rubber is presumably due to the presence of electrolytic impurities. As a consequence of the influence of the electric image force, preferential adsorption of ions occurs at the surfaces of the particles of the black, thereby reducing the number of available charge carriers. The total effect of adsorption is in fact greater than suggested by a first glance at Fig. 2, where the conductance ratio is calculated with respect to the conductance of the control sample. Since the relative capacitance was observed to increase over the same range of the variable, the corresponding geometric effect should increase conductance. Therefore conductance values should be considered for each mass ratio (concentration) with respect to the corresponding value of the capacitance curve.

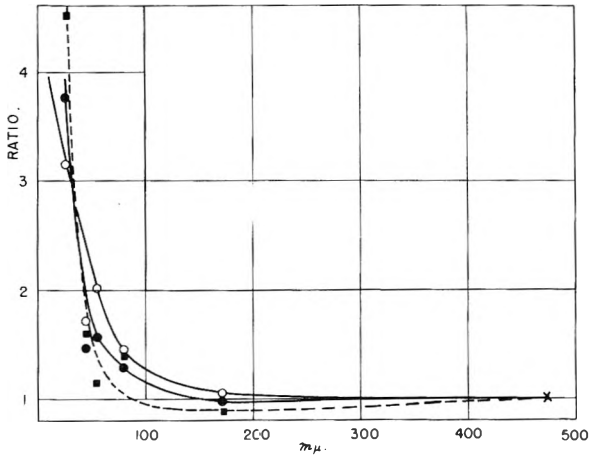

Fig. 3.—Electrical properties as a function of particle size. Values given as ratios to Thermax samples (X). Open circles, dielectric constant (60 c.) of GRS; solid circles, dielectric constant (60 c.) of Hycar; solid squares, conductance of Hycar.

The conductance values of Figs. 2 and 3 refer to the steady-state values which are reached after the voltage has been applied for a sufficient time. Steady state, however, requires time to establish itself. For Thermax samples in particular, a considerable after-effect was noticed, the intensity of which increased strongly with increasing concentration of the black: immediately after application of the voltage, a strong current was observed, the intensity of which decreased rapidly. As an example, Fig. 4 shows current per unit voltage as a function of time for a Hycar-Thermax sample with $r = 0.96$. The inset gives the time-dependent component $\Delta(i/V)$ (obtained as the difference of observed and steady state conductances) on a double logarithmic scale; the familiar power law ct^{-n} is followed. For different Thermax samples, values of n between 0.6 and 1.0 were found. The

TABLE II

DISPERSION OF DIELECTRIC CONSTANT

f, kc.	ϵ_0	ϵ/ϵ_0 r = 0.24	0.48	0.64	0.80	0.96	0.24 SC
			Butadiene–acrylonitrile polymer				
0.1	20.4	1.38	1.91	2.43	3.57	5.19	5.02
0.5	20.0	1.39	1.91	2.39	3.40	4.98	4.85
1.0	19.7	1.38	1.91	2.08	3.38	4.86	4.76
2.5	19.4	1.40	1.89	2.32	3.32	4.54	4.58
5.0	19.0	1.34	1.85	2.32	3.29	4.46	4.38
10	17.9	1.35	1.86	2.33	3.42	4.17	4.35
25	16.2	1.34	1.85	2.30	3.17	4.14	4.21
50	14.1	1.34	1.86	2.39	3.16	4.07	4.18
100	12.20	1.33	1.86	2.24	3.06	3.88	4.09
250	9.76	1.34	1.85	2.24	3.06	3.78	4.00
500	8.04	1.37	1.78	2.36	3.07	3.48	3.92
			Butadiene–styrene polymer				
30 cps	2.7945	1.4775	2.0929	2.5173	3.426	4.083	4.634
60	2.7935	1.4757	2.0900	2.5137	3.407	4.065	4.571
120	2.7921	1.4755	2.0879	2.5090	3.406	4.046	4.510
240	2.7920	1.4746	2.0858	2.5030	3.398	4.023	4.438
480	2.7912	1.4737	2.0838	2.4984	3.385	4.005	4.386
960	2.7876	1.4737	2.0831	2.4953	3.376	3.986	4.325

amplitude of the transient component against r for Hycar-Thermax at 10 and 30 sec. after application of the voltage is shown as the lower two curves in Fig. 2; ordinate units for conductance are 10^{-10} amp./volt. A strong increase of this component with increasing concentration of the black appears. Therefore, while the steady state component for Thermax decreases with increasing concentration, the transient component increases. This change in the nature of the conductance process conforms to the adsorption theory. The bulk of the gum is depleted of ions and its resistivity increases; the ions attracted to the particles of the black probably form a somewhat diffuse and semiconducting layer on and around the latter. Their contribution manifests itself in a transient current of rather long relaxation time. The decrease of the steady state conductance and the increase of the transient conductance are thus seen to be two different aspects of a single mechanism, the redistribution of ions.

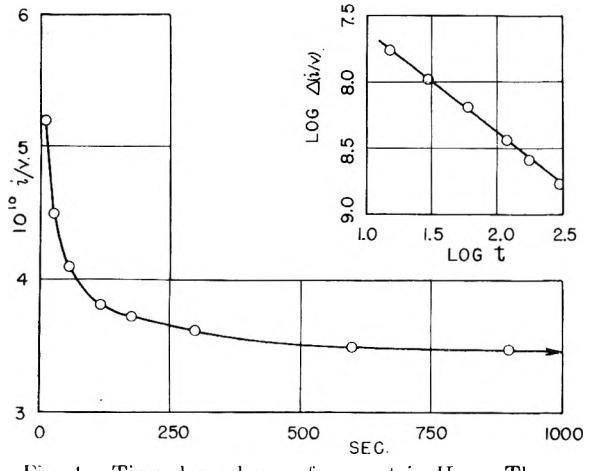

Fig. 4.—Time dependence of current in Hycar-Thermax (r = 0.96). Inset: verification of power law for transient component.

Dispersion of Dielectric Constant.—An abstract of our data on dispersion is contained in Table II, where the first column gives the frequency of the measurement, the second the dielectric constant ϵ_0 of the samples containing no carbon black (master batches), the next five the ratio ϵ/ϵ_0 for samples containing 100 r parts by weight of Thermax per 100 parts master batch and the last gives the ratio ϵ/ϵ_0 for samples containing 24 parts Vulcan SC per 100 of stock.

With Hycar, the relative increase of dielectric constant does not change significantly with frequency up to 64% Thermax. Therefore, up to this concentration, the simple mixture law is valid. With higher Thermax concentrations and with Vulcan SC, an increase in frequency from 100 c. to 0.5 Mc. decreases the capacitance ratio by 30% for 96% Thermax and by 25% for 24% Vulcan SC. It is significant that dispersion of the SC sample is less than that of the Thermax sample, although the low frequency dielectric constants are approximately the same. The general behavior of the systems based on GRS is the same as with Hycar; the total relative and absolute dispersion, however, is considerably smaller, as might be expected. Here the SC shows higher dispersion than the corresponding Thermax sample.

The central curves of Fig. 2 show the measured Hycar values for 0.5 Mc.; two GRS-values (not listed in the table) are also indicated. For comparison, the theoretical Hycar-Thermax curve from the top group of Fig. 2 is also shown (curve 1). While the observed low frequency points (upper curves of Fig. 2) lie above the theoretical curve, dispersion now has moved the new high frequency values below this curve. This seems at first surprising, because, according to Wiener's theory, the theoretical curve should represent a lower limit. But here the influence of the postulated semiconducting surface layer of the black appears. The calculated curve was based on densities

derived from size and weight; they were about 20% lower than the density of graphite. The "electrical" density, however, is not necessarily identical with the "geometrical" one. If the graphite core of the particles is surrounded by a layer whose relaxation times come into the frequency interval of the measurement, the nature of the current through these layers with increasing frequency gradually changes from conductive to capacitive and the layer eventually becomes transparent to the electric field. The high frequency end of the capacitance curve can, therefore, be calculated from the Bruggeman formula, if the density of the black is assumed to reach the value for graphite. Structure determinations of Rossman and Smith[13] indicate an average value of 2.2 for the blacks. Curve II of Fig. 2 is calculated with the latter value. Now the deviations are again positive. The SC value is higher than the Thermax value, as should be the case, if the increase with SC is mainly due to chain formation, that is, to non-uniformity of dispersion. The surface effect is not expected to play a role where chain formation is involved.

Dielectric Loss.—Figure 5 shows the dependence of dielectric loss on frequency for polar and non-polar samples. The data for Hycar (upper curves) show a characteristic dipole maximum. Curves for pure Hycar and Hycar with 64% Thermax are nearly indistinguishable but those for 96% Thermax and 24% Vulcan SC are systematically higher; the SC curve, while very much higher at low frequencies due to the ohmic component of the current, lies below the Thermax curve at high frequencies. As seen in Fig. 5, the loss factors for unfilled Hycar and Hycar with 96 parts Thermax are identical at about 30 c.; between this frequency and one kilocycle, the loss factors of the two samples begin to diverge, and then for still higher frequencies (up to our upper limit of 0.5 Mc.) the difference remains substantially constant, as shown by the fact that the corresponding curves in Fig. 5 become parallel at higher frequencies. This difference defines a conductance k.

All curves show a strong maximum at approximately 0.2–0.3 Mc. Addition of enough carbon to increase capacitance by about a factor of 4 is unable to bring about any significant shift in the position of the maximum. This maximum then must be the dipole mechanism proper of the C–CN group. The corresponding common component in the loss curve will be called tan δ_0. The ionic effect superposes on the dipole effect. According to what was shown before, it contains itself two components. The first represents the contribution of the steady state conductance and is given by $1/\omega RC$. The second one is associated with the slow transient that extends into the d.c. zone. A transient current proportional to t^{-n} $(n < 1)$ gives a loss tangent proportional to ω^{n-1}. The formula for the tangent of unfilled Hycar then reads

$$\tan \delta_1 = \tan \delta_0 + \beta_1 \omega^{n-1} + 1/\omega R_1 C_1 \qquad (3)$$

and that for the mixture with 96% Hycar

$$\tan \delta_2 = \tan \delta_0 + \beta_2 \omega^{n-1} + 1/\omega R_2 C_2 + \kappa_0 \qquad (4)$$

where the β's are constants. Since $R_2C_2 > R_1C_1$

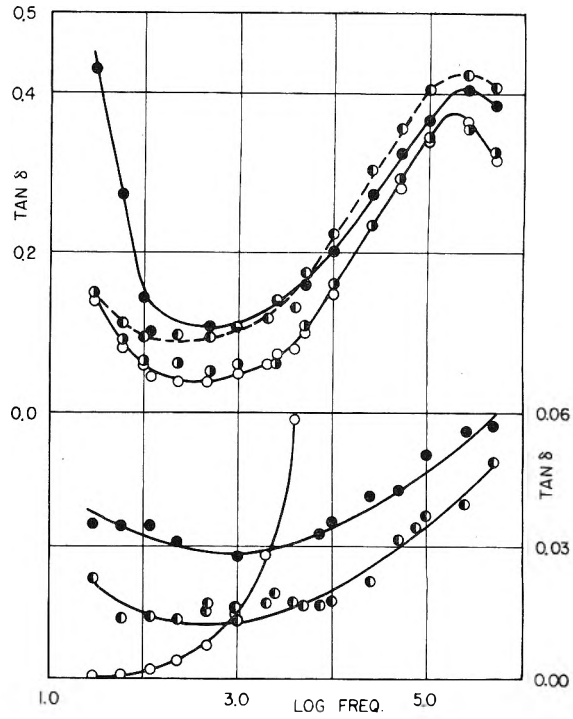

Fig. 5.—Dependence of dielectric loss on frequency and composition. Upper curves, Hycar. Open circles, $r = 0$; right-shaded circles, 64 parts Thermax; left-shaded circles, 96 parts Thermax; solid circles, 24 parts SC. Lower curves, GRS. Open circles, $r = 0$; solid circles, 24 parts SC; left-shaded circles, 96 parts Thermax.

(*cf.* Fig. 2), the contribution of the ohmic component at very low frequencies would be larger in Hycar than in the Hycar-Thermax samples. This is confirmed by the crossing of the curves in Fig. 5 at about 30 cycles. In the medium frequency interval $(100 < f < 1000)$, the higher amplitude of the transient in the mixture shows up in the difference of tangents; here the deviation of the difference curve from a constant value follows approximately a power law. Eventually the transient also dies out, and the constant difference k remains. Then if this analysis is correct, the contribution of the black to the power factor would be approximately constant and the corresponding power loss would increase proportional to frequency. Constant loss tangents are characteristic for many heterogeneous dielectrics. In the present case we attribute it to the semiconducting interface that may be considered similar to a heterogeneous dielectric with a widely distributed spectrum of relaxation times.

With GRS, the addition of the black produces a marked change in the course of the curve, as shown in Fig. 5 (lower curves). The curve for the pure gum starts with very low values at low frequencies, but the loss increases rapidly. The SC and Thermax curves, starting with considerably higher values, show much less variation and eventually fall below the first curve. We believe that the changes are due to the ion-adsorption action of the black. The fact that the addition of carbon black *reduces* the loss tangent at high frequencies can only be explained by a mechanism which is operative throughout the volume of the rubber

phase. The sole volume effect encountered was adsorption, which removes ions. Diffuse ionic atmospheres around the particles of the black would tend to give a constant loss tangent.

The general picture suggested by our results is the following: The particles of the black behave as if each contained a perfectly conducting graphite core inside a semi-conducting sheath of much lower density, surrounded by a diffuse ion atmosphere. These particles, together with their atmospheres, are distributed throughout the continuous elastomeric matrix. At high concentrations with coarse blacks and at low concentrations with fine blacks, chain formation appears which eventually leads to short circuiting of the samples and transforms them into conductors. Before this happens, a strong increase in capacitance is observed which can be quantitatively interpreted by Bruggeman's theory provided the dispersion remains uniform.

KINETICS OF THE REACTION OF CARBON DIOXIDE WITH CARBON

BY SABRI ERGUN

Contribution of the Branch of Coal-to-Oil Research, Bureau of Mines, Region V, Bruceton, Pa.

Received October 7, 1955

Kinetics of the reaction of carbon with CO_2 has been investigated in the temperature range 700–1400° at atmospheric pressures employing three carbons of different origin having different physical properties. The following reaction mechanism has been derived: Certain carbon atoms, reaction sites, can detach an oxygen atom from a gaseous CO_2 molecule, reducing CO_2 to CO and form an occupied site. Reversely, gaseous CO can remove the oxygen atom from occupied sites to form CO_2: $CO_2 + C_f \underset{k_1'}{\overset{k_1}{\rightleftharpoons}} CO + C_0$. These interactions constitute dynamic two-phase (solid-gas) oxidation–reduction and are termed "oxygen-exchange reactions." The carbon transfer from solid phase to gas phase originates from occupied sites: $C_0 \xrightarrow{k_3} CO$. This is the slowest step of the reactions and can be considered as unidirectional. The sorption of CO_2 is not a prerequisite step of the reaction. The reaction rate is proportional to the concentration of occupied sites. CO retards the rate by reducing the concentration of occupied sites. The rate constants k_1, k_1' and k_3 are functions of temperature only and are common to all carbons having trigonal (coplanar) bonds, regardless of origin, particle size, porosity and crystallinity. The differences in the reaction rates of carbons are due to specific number of reaction sites. In studying the validity of the above theory, data obtained in the present study have primarily been utilized. The theory has been found to be applicable to published data as well. For the first time it has been demonstrated that carbons of different origin, particle size, porosity and crystallinity can be treated on a common basis.

Introduction

Carbon dioxide is both a reactant and a product of the gasification, combustion and various other reactions of carbons. Its reactions with carbons play important roles in numerous industrial operations, such as generation of water and producer gases and smelting of ores. Carbon dioxide–carbon reactions, therefore, have been the subject of many investigations. As a result, both empirical and theoretical treatments have been developed, some useful but all limited in applicability.

Interest in the production of synthetic liquid fuels has stimulated research on gasification of coals. Synthesis gas constitutes a substantial fraction of the over-all cost of synthetic liquid fuels; therefore, reduction in the cost of its production is highly desirable. Work on improvement and development of processes has been intensified. However, basic solutions to the problem of gasification can be given on fundamental grounds only, that is kinetics of the reaction, dynamics of flow, diffusion and heat transfer.

The reaction of carbon dioxide with carbon is heterogeneous, and numerous problems are encountered in attempting to explain its mechanism. The stoichiometric equation, $CO_2 + C = 2CO$, does not reveal the mechanism of the reaction, which must be deduced from the over-all rates of reaction under varying experimental conditions. The deduction is generally difficult and becomes complicated when ancillary phenomena such as flow conditions, heat transfer and diffusion influence the over-all rates appreciably. An understanding of the possible influences of these phenomena on gasification rates was considered essential. Studies on flow conditions, diffusion and heat transfer were undertaken; some of these problems have been analyzed in previous papers.[1–3] These studies were integral with the present analysis of the interactions of carbon dioxide with carbon.

Theory

Studies of sorption[4] and surface reactions[5–10] with carbon–oxygen systems have demonstrated the ability of carbons to retain oxygen at certain sites on their surfaces by chemical bonding.

On an initially cleaned carbon surface, carbon dioxide is reduced to carbon monoxide at temperatures as low as 600°. The oxygen lost by dioxide remains on the carbon surface.[6,10–13] These studies

(1) S. Ergun, *Ind. Eng. Chem.*, **47**, 2075 (1955).
(2) S. Ergun, *Chem. Eng. Progress*, **48**, 227 (1952).
(3) S. Ergun, *Anal. Chem.*, **23**, 151 (1951).
(4) H. H. Lowry and G. A. Hulett, *J. Am. Chem. Soc.*, **42**, 1408 (1920).
(5) T. F. E. Rhead and R. V. Wheeler, *J. Chem. Soc.*, **101**, 831 (1912).
(6) I. Langmuir, *J. Am. Chem. Soc.*, **37**, 1139 (1915).
(7) A. Eucken, *Z. angew. Chem.*, **43**, 986 (1930).
(8) L. Meyer, *Z. physik. Chem.*, **B17**, 385 (1932).
(9) V. Sihvonen, *Z. Elektrochem.*, **40**, 456 (1934).
(10) W. E. J. Broom and M. W. Travers, *Proc. Roy. Soc. (London)*, **A135**, 512 (1932).
(11) H. Martin and L. Meyer, *Z. Elektrochem.*, **41**, 136 (1935).
(12) A. F. Semechkova and D. A. Frank-Kamenetsky, *Acta Physicochim., U.R.S.S.*, **12**, 899 (1940).
(13) J. Gadsby, F. J. Long, P. Sleightholm and K. W. Sykes, *Proc. Roy. Soc. (London)*, **A193**, 357 (1948).

demonstrate the ability of certain carbon atoms to detach an oxygen atom from a carbon dioxide molecule. In a reverse manner, oxygen retained on the surface can be removed by carbon monoxide.[12-16] These reactions may be expressed as

$$CO_2 + C_f \underset{k_1'}{\overset{k_1}{\rightleftharpoons}} CO + C_0 \qquad (1)$$

where C_f represents a free site capable of reaction and C_0 an occupied site, *i.e.*, a site possessing an oxygen atom. Equation 1 expresses the oxygen-exchange phenomenon, not the carbon transfer from solid to gas phase. Rate constants k_1 and k_1' are general rate constants, *i.e.*, probability factors, functions of temperature only. These constants have not been determined on an absolute basis; experimental evidence indicates that oxygen-exchange reactions are relatively fast.

The transfer of carbon from solid phase to gas phase originates from the occupied sites and may be expressed as

$$C_0 \xrightarrow{k_3} CO + nC_f \qquad (2)$$

where n is an integer having a value of 0, 1 or 2, when occupied sites are considered individually. When the reaction of a macroscopic carbon sample is considered, n can have any statistical value between 0 and 2; but the most likely value appears to be 1. The rate constant k_3 is a general rate constant function of temperature only. The reverse of the above reaction and the reactions shown in equation 1 would result in carbon transfer from gas to solid phase and to carbon deposition when the concentration of CO exceeds that required by thermodynamic equilibrium between CO_2 and CO. Experiments with C^{14} in the gas phase showed no detectable carbon transfer from gas to solid.[17] Moreover, carbon deposition on pure carbons at gasification temperatures has not been reported and could not be detected in the present studies. Reaction (2) can therefore be regarded as unidirectional.

The instantaneous rate of gasification of a carbon sample surrounded by a gas having uniform composition may be expressed as

$$dn/dt \equiv N_C = k_3(C_0)W \qquad (3)$$

where dn/dt or N_C is the rate of carbon transfer from solid phase to gas phase, atoms per second, (C_0) is the number of occupied sites per gram and W is the weight of the carbon, gram. In flow experiments the gas surrounding the solid generally is not uniform in composition. Equation 3 would therefore hold true for a differential amount of solid only

$$dN_C = k_3(C_0)\,dW \qquad (4)$$

Experimental evidence indicates that adsorption of CO_2 by carbon is negligible above 600°.[12] Some experiments have been reported in which CO_2 molecules were able to enter into the surface where they became fixed, leaving oxygen atoms to remove other carbon atoms;[18] however, such sites are believed to constitute not more than 1 or possibly 2% of the total number of reaction sites.[18] Sorption of CO in the presence of CO_2 and subsequent removal of the oxygen from the sorbed CO by gaseous CO would result in carbon transfer from the gas phase and in carbon deposition, which were not detectable in experiments with $C^{14}O_2$.[17] Temperature coefficients for sorption of inert gases, *e.g.*, He or N_2, on carbon rule out their sorption at gasification temperatures. Therefore, reaction sites can be regarded as either free or occupied by an atom oxygen

$$(C_t) = (C_f) + (C_0) \qquad (5)$$

where (C_t) is the total number of reaction sites per gram.

Under steady-state conditions the rate of formation of occupied sites would be equal to the rate of their disappearance

$$d(C_0)/dt = k_1(CO_2)(C_f) - k_1'(CO)(C_0) - k_3(C_0) = 0 \qquad (6)$$

where (CO_2) and (CO) represent the concentrations of CO_2 and CO in the gas phase, molecules per cubic centimeter. Solving for (C_0) from equations 5 and 6

$$(C_0) = k_1(CO_2)(C_t)/[k_1(CO_2) + k_1'(CO) + k_3)] \qquad (7)$$

Substitution of equation 7 in (4) yields

$$dN_C = k_1(CO_2)k_3(C_t)\,dW/[k_1(CO_2) + k_1'(CO) + k_3)] \qquad (8)$$

Equation 8 represents the rate of reaction of carbon by carbon dioxide in a general differential form.

At lower temperatures, oxygen-exchange reactions occur at temperatures approximately 200° lower than required for gasification at comparable rates; it follows that

$$k_1(CO_2) \gg k_3 \text{ and/or } k_1'(CO) \gg k_3 \qquad (9)$$

Since activation energies of oxygen-exchange reactions are reported to be 43 to 60 kcal.,[19] (compared to 59 kcal. for k_3 as determined in the present study) the inequalities (9) can be expected to be true over a wide range of gasification temperatures. The conditions of the inequalities (9) are identical with the attainment of a solid–gas heterogeneous equilibrium by the oxygen-exchange reactions

$$K_1 = k_1/k_1' = (CO)(C_f)/(CO_2)(C_f) \qquad (10)$$

Equilibrium constant K_1, defined above, does not involve any parameter that is a function of physical properties of carbon. K_1 can also be expected to be independent of pressure; it should be a function of temperature only.

From inequalities (9) it follows that k_3 in the denominators of equations 7 and 8 can be neglected. This simplification and substitution of K_1 in place of k_1/k_1' lead to

$$(C_0) = (C_t)/[1 + (CO)/K_1(CO_2)] \qquad (11)$$

and

$$dN_C = k_3(C_t)\,dW/[1 + (CO)/K_1(CO_2)] \qquad (12)$$

Equation 12 represents the differential reaction rate of carbon with CO_2. It can readily be applied to flow and closed systems. According to the equation the reaction rate is not determined by

(14) A. Key, "Gas Research Board Commun.," London, No. GRB 40 (1948).

(15) J. D. F. Marsh, "Inst. Gas Engrs. Commun.," London, No. 393 (1951).

(16) A. E. Reif, THIS JOURNAL, **56**, 785 (1952).

(17) F. Bonner and J. Turkevich, *J. Am. Chem. Soc.*, **73**, 561 (1951).

(18) F. Brown, *Trans. Faraday Soc.*, 1005 (1952).

(19) A. A. Orning and E. Sterling, THIS JOURNAL, **58**, 1044 (1954).

constant k_3 of the slowest step alone, however small the constant may be, but also by the equilibrium constant K_1 of the oxygen-exchange reactions as well as by the composition of the gas phase. At low concentrations of CO and CO_2 the inequalities (9) cannot be expected to be valid. In these instances equation 8 should be used in place of (12). Both equations represent instantaneous rates. Changes in concentrations of reaction sites, if any, as carbon reacts are determined by n of equation 2. Discussion of n will be made in a later study of reaction sites and their concentration as a function of burn-off.

The validity of the above development can be examined in several respects. According to equation 12 inert gas should have no influence on the reaction rates. This fact has been established experimentally in an earlier study.[1] It is well known that CO reduces the reaction rate of CO_2 with carbon. Some of the theories place the cause of retardation on the accumulation of chemisorbed O_2 on the surface,[12] or on the adsorption of CO on reaction sites,[13] while others explained it by equations similar to the reverse of equation 1.[14–16] The present study is in accord with the latter view; the equilibrium constant K_1 furnishes a quantitative explanation of the role of CO. The validity of equation 12 can be tested experimentally with respect to the influence of CO.

Probably the severest test for the above development lies in its treatment of all carbons with trigonal (coplanar) bonds on a common basis. For example, K_1 should be independent of origin, porosity, crystallinity, particle size, etc. Comparison of the experimental values of K_1 obtained with carbons of different origin and physical properties should serve as a severe test. Also, different carbons should yield the same values of k_3; however, the experimental procedure adopted in the present study permits determination of the product of k_3 with (C_t) rather than k_3 alone. Nevertheless, activation energies of $k_3(C_t)$ can be determined and the energy should be independent of the physical properties of carbon.

According to the present theory, the differences in the rates at which carbons react with CO_2 are due to the differences in the specific number of reaction sites (*cf.*, equation 8 or 12). Specific number should, therefore, serve as a direct and absolute measure of reactivity.

Application of Theory

The present experiments were conducted in isothermal fluidized beds. Integral equations therefore have been derived for isothermal flow systems under steady-state conditions. The integral equations can be used to test the validity of the above development and to determine the rate and equilibrium constants. Equation 12 can be applied directly to a differential section perpendicular to flow of an isothermal reactor. Substituting the ratio of the flow rate of CO to CO_2 in place of their respective concentrations and rearranging the equation

$$\int_0^{N_C} (K_1 + N_{CO}/N_{CO_2})\, dN_C = \int_0^W K_1 k_3(C_t)\, dW \quad (13)$$

where N_{CO} and N_{CO_2} represent the rates at which CO and CO_2 flow past the cross section considered, N_C the rate at which carbon is gasified between the inlet and the section and (C_t) the number of total reaction sites per gram. When no CO is admitted at the inlet, oxygen and carbon balances between the inlet and the differential section yields

$$N_C = N^0_{CO_2} - N_{CO_2} = (1/2)N_{CO} \quad (14)$$

where the superscript 0 denotes the conditions at the inlet. Substitution of equation 14 in 13 and $dN_C = -dN_{CO2}$ gives

$$\int_{N^0_{CO2}}^{N_{CO2}} (K_1 + 2N_{CO_2}/N_{CO_2} - 2)\, dN_{CO_2} = \int_0^W K_1 k_3(C_t)\, dW \quad (15)$$

Direct integration of the second term of equation 15 is permissible under two extreme flow conditions. Gas flow and reaction along the path of the flow establishes a concentration gradient; diffusion on the other hand opposes the gradient and mixes the gases. The two extreme conditions in the gas phase are "no mixing" and "complete mixing."[1] At fast flow rates back mixing is negligible; integration of equation 15 without placing restriction on the variation of N_{CO_2}, substitution of $X = N_{CO}/N_{CO_2} \equiv 2N^0_{CO_2}/N_{CO_2} - 2$, and proper rearrangement lead to

$$2(1 + 2/X)\ln(1 + X/2) - 2 = -K_1 + K_1 k_3(C_t)(1 + 2/X)(W/N^0_{CO_2}) \quad (16)$$

At low flow rates diffusion can mix the gases completely, *i.e.*, the composition gradient can disappear. Under these conditions N_{CO}/N_{CO_2} would be the same throughout the bed. Integration of equation 15 then yields

$$X = -K_1 + K_1 k_3(C_t)(1 + 2/X)(W/N^0_{CO_2}) \quad (17)$$

When gases are not mixed, experimental data can be represented graphically by plotting the left side of equation 16 *vs.* $(1 + 2/X)(W/N^0_{CO_2})$. The plots should result in straight lines as shown in Fig. 1a. The intercept on the abscissa corresponds to the value of $1/k_3(C_t)$ and the negative intercept on the ordinate to the value of K_1. For complete mixing of gases plots of the experimental data according to equation 17 should yield a straight line, the intercept of which on the abscissa should correspond to $1/k_3(C_t)$ and on the ordinate to $-K_1$. A typical set of experimental data for this condition is shown in Fig. 1b. Comparison of equations 16 and 17 shows that their right sides are identical. Because their left sides are not linear with each other over wide ranges of values of X, except for values of X as X approaches zero, experimental data that yield a straight line on one type of plot should not yield a straight line on the other. Accordingly, such plots could be used to ascertain which condition of flow prevailed. This test is illustrated in Fig. 2, where plot of equation 16 yielded a straight line and that of equation 17 a curve, indicating little back mixing. For partial mixing, plots of experimental data according to both equations should yield curves, as shown in Fig. 3. The values of $k_3(C_t)$ obtained from Figs. 1–3 should be multiplied by $6.02 \times 10^{23}/2.24 \times 10^4$ to convert them to site/g. sec.

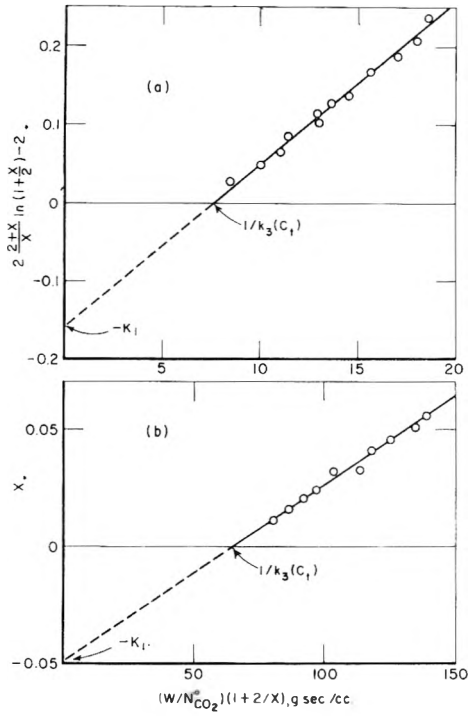

Fig. 1.—Reaction of CO_2 with an activated carbon: (a) at 850°; (b) at 750°.

Extrapolation of the lines to the point where they cross the abscissa is identical with the determination of the instantaneous rate at the inlet where the conversion is zero; when $(CO)/(CO_2) = 0$, equation 12 reduces to $dW/dN_C = 1/k_3(C_t)$ under all conditions of flow. On the other hand plots obtained by equations 16 and 17 lead to K_1 values that differ by a factor of 2. This factor can be calculated numerically as well as by comparing the limiting values of the ordinate function. As X approaches zero, the left side of equation 16 becomes

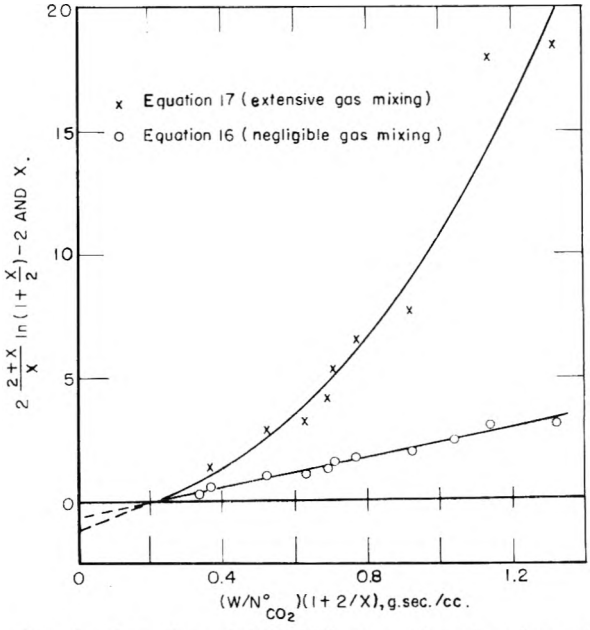

Fig. 2.—Reaction of CO_2 with an activated carbon at 1,025°. Data are plotted according to both equation 16 and 17.

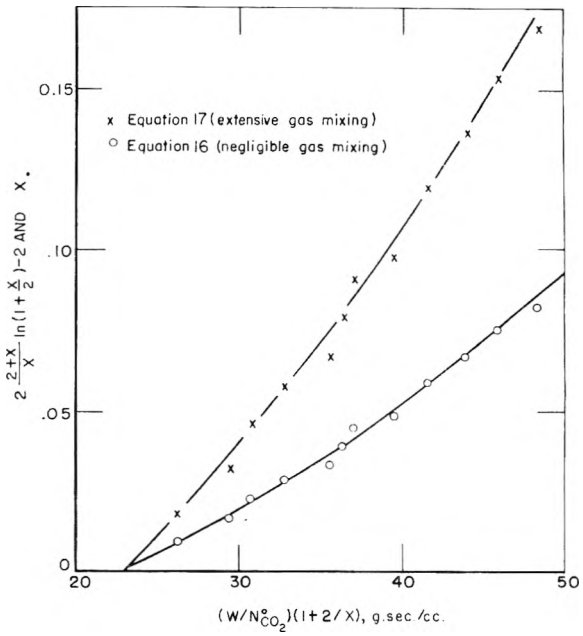

Fig. 3.—Reaction of CO_2 with an activated carbon at 800° (partial gas mixing).

equal to $X/2$. Therefore at low conversions plots of data according to both equations should yield straight lines, but the values of K_1 obtained would differ by a factor of 2. The analysis of kinetics is best accomplished from data obtained under one of the extreme flow conditions. The flow conditions prevailing at the gas velocities employed can be determined by preliminary experiments.[1]

When CO is admitted at the inlet, equations 16 and 17 take the forms

$$\frac{(2+X)(2+X^0)}{X-X_0}\ln\frac{2+X}{2+X^0}-2=-K_1-K_1k_3(C_t)\frac{(2+X)W}{(X-X^0)N^0_{CO_2}} \quad (18)$$

$$X=-K_1+K_1k_3(C_t)\frac{(2+X)W}{(X-X^0)N^0_{CO_2}} \quad (19)$$

The above equations can be used to account for the influence of inlet CO.

Experimental Procedure

The experiments were conducted in small fluidized beds under isothermal conditions to minimize the influence of rates of thermal-energy transfer upon the over-all rates. The reaction tube, 2.22 cm. inside diameter and 56 cm. long was made of a high temperature porcelain. The tube was held vertically in a furnace, the heated chamber of which was a prismatic cavity of 11.5 × 11.5 × 23.0 cm. The furnace was heated by four silicon carbide heating elements. Standard tapered Pyrex joints were fused to both ends of the reaction tube to eliminate high temperature seals and permit flexibility in operation. The temperature was measured with a Pt–Pt + 10% Rh thermocouple placed vertically in the tube from the top. The position of the thermocouple could be adjusted radially and vertically. A second thermocouple was inserted horizontally through a hole in the side of the furnace and placed against the outside wall of the reaction tube. The rates of flow of gas were measured by means of capillary flowmeters within a standard error of ±0.2%.

Closely screened and weighed amounts of carbons, ranging in size from 8–16 (1.8 mm.) to 170–200 mesh (0.081 mm.), U. S. Standard, were introduced from the top by removing the upper half of the tapered joint. Product gases were passed through a capillary flowmeter and sampling tubes. When the temperature of the bed and exit gas flow

rate assumed constant levels, *i.e.*, steady state, gas samples were taken for analysis. The loss in weight of the carbon sample, *i.e.*, burn-off, usually was kept below 5%; the loss was calculated from the rate and composition of the effluent gas and the time elapsed to reach steady state. Corrections were made in the weight of the sample for the amount of burn-off at the time of gas sampling. When a run was completed, the sample was removed by suction through a 6 mm. porcelain tube inserted into the reaction tube.

The aerodynamic surface area and density of the carbon samples were determined, as outlined previously,[3,20] in order to estimate rates necessary for fluidization.[1] Approximate rates of gasification were then obtained. Mixing in the gas phase was generally studied by conducting gasification experiments at successively increased rates of flow of carbon dioxide and with increased amounts of carbon while a constant ratio of weight of carbon to rate of flow of carbon dioxide was maintained. The most precise experimental values for the rate constants were obtained under conditions of either negligible mixing or thorough mixing; however, these conditions could not always be realized, owing to the fact that experiments in fluidized beds can be carried out only over a limited range of flow rates. This range lies between incidence of fluidization and bubble or slug formation and covers approximately a twofold flow rate.

Final gasification runs were conducted at constant rates of flow of carbon dioxide with successively increased amounts of carbon, for example, 1 to 12 g. Helium or nitrogen was used to flush the system and also to serve as a tracer in the experiments, that is, to check the material balance of the reaction. The rate of flow of inert gas was about one-tenth that of carbon dioxide.

To determine the influence of inert gases, they were introduced at increased rates while the flow rate of carbon dioxide remained the same. As seen in Fig. 4, helium had no effect on the reaction rates when its addition did not alter the flow pattern appreciably,[1] as expected from the present theory.

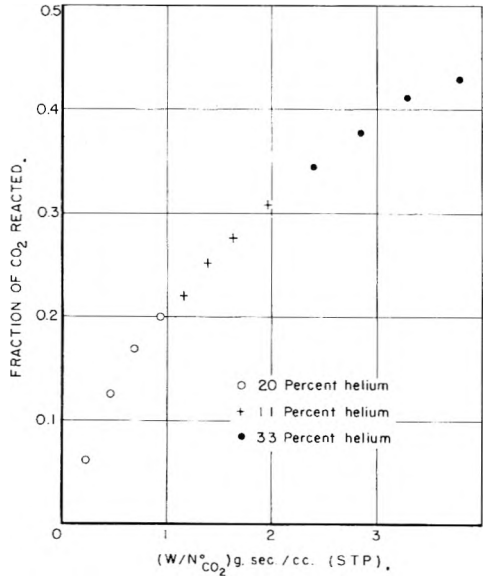

Fig. 4.—Reaction of CO_2 with an activated carbon at 900°. Introduction of helium had no marked influence on the reaction rate.

The effect of carbon monoxide was investigated also by introducing mixtures of carbon monoxide and carbon dioxide into the reactor. Data obtained were analyzed by equations 18 or 19. The same values of K_1 and $k_3(C_t)$ were obtained as in the absence of carbon monoxide at the inlet. The result was not surprising, because carbon monoxide is a product of the reaction and any theoretical equation that predicts the rates of gasification over wide ranges of carbon monoxide formation must account for the influence of carbon monoxide, whether it is introduced at the inlet or is formed as a reaction product.

Three carbons of different porosity and crystallinity were employed: Ceylon graphite, an activated carbon and activated graphite. The samples had little mineral content, ranging from traces up to 0.5%. More than 350 individual experiments were conducted at 50° intervals: At 700 to 1,050° with activated carbon, at 950 to 1,150° with activated graphite, and at 1,000 to 1,400° with Ceylon graphite. The precision of the experiments was estimated to be ±6%. The data used in the calculations involve the weight of carbon, the flow rate of carbon dioxide at the inlet and the ratio of carbon monoxide to carbon dioxide at the exit, equations 16 and 17. Since the constants K_1 and $k_3(C_t)$ are sufficient for a complete description of the results obtained, the results of individual experiments are not included here. The constants are listed in Table I.

TABLE I

EQUILIBRIUM AND RATE CONSTANTS OF THE REACTION OF CARBON DIOXIDE WITH CARBON

Carbon	Temp., °C.	K_1	$k_3(C_t)$, site/g. sec. $\times 10^{-18}$
Activated carbon	700	0.025	0.13
	750	.050	0.41
	800	.096	1.2
	850	.16	3.7
	900	.27	11
	950	.40	34
	1,000	.52	83
	1,025	.60	130
Activated graphite	900	.25	0.72
	950	.37	1.9
	1,000	.54	5.1
	1,050	.76	13
	1,100	1.0	27
	1,150	1.4	62
Ceylon graphite	1,000	0.23	0.93
	1,050	0.76	1.8
	1,100	1.0	4.6
	1,150	1.4	9.6
	1,200	1.8	19
	1,250	2.3	38
	1,300	2.4	77
	1,350	3.6	130
	1,400	4.5	230

Discussion of Results

The experimentally determined values of equilibrium constant K_1 of the oxygen-exchange reaction are plotted as a function of temperature in Fig. 5. All three carbons are included in the plot. The equilibrium constant was found to be a function of temperature alone—independent of source, particle size and other physical properties of the carbons. This conclusion accords with the present theory. The heat of reaction is 23 kcal. per mole in the temperature range of 800 to 1,400°. Because of its high temperature coefficient, the equilibrium has a pronounced effect on the rate of gasification. For example, the values of the constants are 0.022, 0.52 and 4.4 at 700, 1,000 and 1,400°, respectively. If, in the gas phase, the ratio of carbon monoxide to carbon dioxide is maintained at 1, the fraction of the reaction sites oxidized would be 0.0215, 0.34 and 0.81 at the respective temperatures; that is, when the reaction temperature is raised from 700 to 1,000°, the number of occupied sites would increase by a factor of 16 and when raised to 1,400°, by 38. If, on the other hand, the ratio of carbon monoxide to carbon dioxide is maintained at 0.1 the corresponding increases would be by factors

(20) S. Ergun, *Anal. Chem.*, **24**, 388 (1952).

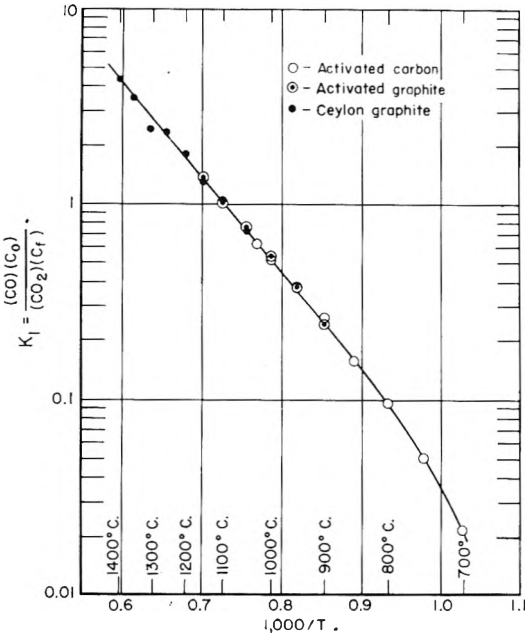

Fig. 5.—Equilibrium constant of the oxygen-exchange reaction as a function of temperature. (Average heat of reaction between 800 and 1,400° is 23 kcal./mole.)

of 22 and 140. The gasification rate is proportional to the number of occupied sites; thus, the effect of the equilibrium constant on the rates is through its influence on its concentration of occupied sites.

The experimentally determined values of the product $k_3(C_t)$ are plotted in Fig. 6 as a function of temperature. The energy of activation is 59 kcal. per mole for all three carbons, which is possible only if one of the following conditions is satisfied: (1) The number of reaction sites is independent of temperature; (2) the number of sites changes with temperature exponentially, and all carbons have the same temperature coefficient, regardless of the range of temperature in which they react. The first condition most likely is the case. Like K_1, k_3 therefore is a general rate constant for all carbons. The differences in the intercepts of the three lines on the ordinate correspond to the relative numbers of reaction sites per gram. If (C_t) is taken as unity for Ceylon graphite (80–100 mesh, U. S. Standard), it is 6 for the activated graphite and 100 for the charcoal. As the same values of K_1 and k_3 apply to all carbons, the only individual property affecting the rate of the reaction is the number of reaction sites per unit weight of carbon. The concentration of reaction sites is therefore a direct and absolute measure of reactivity. Although the relative numbers of sites for these

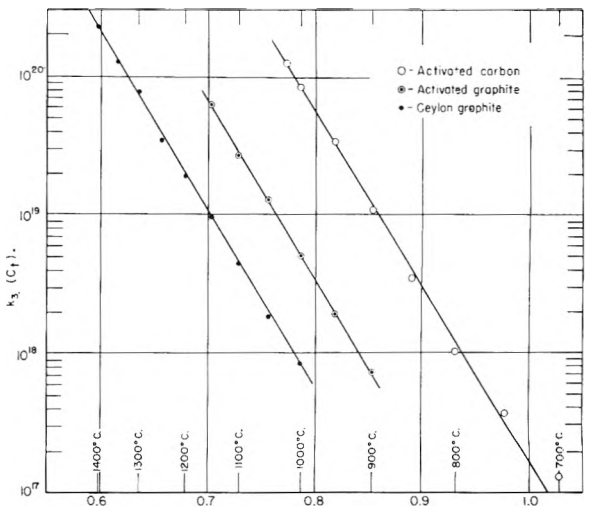

Fig. 6.—Constants of the gasification step as a function of temperature. (Energy of activation is 59 kcal./mole.)

greatly different carbons range from 1 to 100, they account for the differences in rates under conditions of temperature (700 to 1,400°) and pressure (atmospheric) that corresponds to actual gasification conditions. For charcoal and activated graphite, both of which are porous, the relative number of reaction sites per gram was found to be independent of particle size in the size range of 0.08 to 1.8 mm. With the non-porous Ceylon graphite, however, the number increased with decrease in size.

In the above analysis the reaction was studied in a statistical manner, that is, in terms of average properties during reaction and the constancy of k_3 and K_1 for a wide range of pure carbons has been demonstrated experimentally. The treatment does not preclude the possibility of the existence of more than one type of reaction site, for example, two, in which case K_1 and k_3, as determined, would be composite constants. The fact that these constants were the same for carbons of different crystallinity, porosity and particle size signifies that the distribution of the types of the sites was approximately the same. It signifies further an identity of the energy and chemical nature of the reaction sites.

Acknowledgment.—The author takes great pleasure in acknowledging the advice and constant encouragement given by H. H. Lowry, former director of the Coal Research Laboratory, Carnegie Institute of Technology, in the course of this study. This paper is based on a Doctor's Thesis submitted to Technische Hochschule, Vienna.

KINETICS OF THE STEAM–CARBON REACTION[1]

BY JESSE S. BINFORD, JR., AND HENRY EYRING

Contribution from the University of Utah, Department of Chemistry, Salt Lake City, Utah

Received October 8, 1955

A description is given of a more satisfactory type apparatus for the study of high temperature (1500°), low pressure (1 to 100 μ) heterogeneous processes in which one or more products is a gas. The water–gas reaction has been studied in the 900 to 1300° temperature range. This is the first kinetic study of this reaction at high temperatures in which the oxidizing gases have been carefully preheated to the reaction temperature. A zero-order reaction with an activation energy of 60.3 kcal./mole is found in the 900 to 1100°C. range, changing to a first-order process in the 1200 to 1300° range with a considerably lower value for the activation energy. Several possible mechanisms are discussed, including a surface rearrangement of adsorption sites and pre-dissociation of water vapor.

Introduction

There is a considerable amount of uncertainty in the literature regarding the mechanism of the water gas reaction, $C + H_2O \rightarrow CO + H_2$, above 900°. Most investigators agree that the primary products consist entirely of CO and H_2, but there is very little agreement on the magnitude of the rate, the activation energy and the order of the reaction.

The most reliable data come from experiments of two different types. The first type, historically, is one in which a graphite filament is heated electrically in the presence of the oxidizing gas. I. Langmuir[2] used this method for a study of the carbon–oxygen reaction. More recently Meyer[3] had studied the carbon–steam reaction by a similar method in which the water vapor flows continuously through the reaction chamber. R. F. Strickland-Constable[4] had modified this procedure by using a static system in which the products of the reaction were allowed to remain in the reaction chamber. V. Sihvonen[5,6] used both static and flow methods. These investigations were all conducted at extremely low pressures of water vapor (1–100 μ). At higher pressures the reaction became diffusion controlled and it was not possible to measure the activated process.[7] Meyer found the reaction rate too small to measure below 1700° and above this temperature to be zero order with an activation energy of approximately 90 kcal./mole. Strickland-Constable found in the 900 to 1300° range considerable hysteresis in his rate–temperature curves, but an activation energy (our calculation) of perhaps 35 kcal./mole. The order of the reaction was close to unity with respect to water pressure. None of the investigators found any evidence for the formation of products other than H_2 and CO.

At temperatures above 1300°, Strickland-Constable found the rate to pass through a maximum value and then to decrease. Sihvonen,[6] in an experiment designed to preheat the water molecules by passing them over an electrically heated platinum strip before they impinged on the carbon filament surface, observed a maximum in rate in the same temperature range. In another investigation,[8] in which no attempt was made to preheat the water, he reported the reaction around 1400° to be zero order and to have an activation energy of 88 kcal./mole.

Recently a second type method has been employed which is more satisfactory because the oxidizing gases are preheated. This is the method of Gulbransen and Andrew.[9,10] Gases and carbon were heated in a tube furnace and the weight change of the carbon was measured directly by means of a microbalance constructed inside the vacuum system. These workers have obtained excellent data for the low temperature (400 to 500°) carbon–oxygen reaction. They reported a limited amount of data for the carbon–carbon dioxide reaction at temperatures up to 900°. These data, however, are inconclusive, and the authors do not report a value for the activation energy.

In the present investigation the reaction between carbon and water has been studied in the temperature range 900 to 1300° and pressure range 1 to 40 μ. The sensitivity of the analysis was about 10^{-6} g. carbon (four liters of the product gases at 1 μ Hg and room temperature). The method had the same desirable feature of the Gulbransen–Andrew method, namely, the reactants were both brought to the same temperature before reaction occurs.

Description of Apparatus

The reaction chamber consists of a zirconium silicate furnace tube (30″ × 1.25″ × 1″) vertically mounted. The remainder of the vacuum system is Pyrex 7740, which fuses directly to the ceramic as shown by Gulbransen and Andrew.[11] The chamber is heated electrically by means of molybdenum coils wound on the tube. A long coil on the middle portion of the tube has shorter coils on either end overlapping it. Each coil has a separate power control and by a proper balance of power a constant temperature zone of about four inches is maintained in the hot region of the tube. The power input is controlled manually and temperature can be held to a constant value ±2°. The coils are surrounded by a steel jacket which is maintained at from 10^{-3} to 10^{-4} mm. by means of an oil diffusion pump. Radiation shielding is adequately provided by loosely packed "Fiberfrax" (Aluminum silicate) between the tube and steel jacket. Temperatures are measured with platinum–rhodium thermocouples. One thermocouple is placed in the center of the tube to measure the reaction temperature and three thermocouples are placed on the outside surface of the tube for temperature control.

The carbon sample is cut from a 1/4 inch diameter spectroscopic graphite electrode (National Carbon Company) to give a geometric surface area of 6.25 cm.^{2}. A small hole

(1) This research was supported by the United States Air Force through the Office of Scientific Research of the Air Research and Development Command.

(2) I. Langmuir, *J. Am. Chem. Soc.*, **37**, 1154 (1915).

(3) L. Meyer, *Trans. Faraday Soc.*, **34**, 1056 (1938).

(4) R. F. Strickland-Constable, *ibid.*, **43**, 769 (1947).

(5) V. Sihvonen, *Ann. Acad. Sci. Fennicae*, **A34**, No. 7 (1932).

(6) V. Sihvonen, *ibid.*, **A38**, No. 2 (1933).

(7) R. F. Strickland-Constable, *Trans. Faraday Soc.*, **40**, 333 (1944).

(8) V. Sihvonen, *Ann. Acad. Sci. Fennicae*, **A41**, No. 3 (1934).

(9) E. A. Gulbransen and K. F. Andrew, *Ind. Eng. Chem.*, **44**, 1034 (1952).

(10) E. A. Gulbransen and K. F. Andrew, *ibid.*, **44**, 1048 (1952).

(11) E. A. Gulbransen and K. F. Andrew, *ibid.*, **41**, 2762 (1949).

is drilled through one end of the sample and it is suspended on a platinum wire which may be raised and lowered magnetically. Ordinarily the sample is held above the furnace tube at room temperature until the furnace pressure and temperature have reached the desired values. It is then lowered rapidly into the high temperature zone to begin the run.

A round bottom flask serves as a reservoir for the water sample, the purity of which is such that any dissolved gases which are non-condensable at −80° are present in less than 1 part in 10,000. The water vapor is admitted to the vacuum system by means of a capillary and is preheated on alumina chips in the hot region of the furnace tube. Unreacted water and reaction product gases pass from the furnace through a mercury diffusion pump into a Dry Ice–acetone cold trap in which the water is deposited as ice. The reaction products (H_2 + CO) pass through the trap into a three-liter reservoir flask whose pressure is measured with a McLeod gage. The mercury diffusion pump has the characteristic feature of pumping at a constant speed for a given power input and intake pressure at various exhaust pressures up to 1 mm. The range of reservoir pressures (1–1000 μ) thus afforded is suitable for the reaction under study and is adequately measured by the McLeod gage. The low pressure side of the diffusion pump consists of from 95 to 100% water, depending on the extent of the reaction. This pressure is measured by a calibrated R.C.A. thermocouple gage. The calibration is obtained by using a gas mixture, 74% CH_4 and 26% dry air, having the same heat conductivity as water vapor after the equation of Knudsen.[12]

The water pressure is increased by increasing the flow rate into the furnace tube. Various flow rates of water vapor, as determined by the moisture condensed in the cold trap, are used, and the corresponding pressures in the reaction vessel are measured. The power input to the diffusion pump is kept at a constant value of 250 watts. The curve thus obtained is shown in Fig. 1. Thermostat settings vary from 31.6° for the slowest flow rate to 59.3° for the fastest. Pressure in the reaction tube remains at a constant value ±5% during a single run.

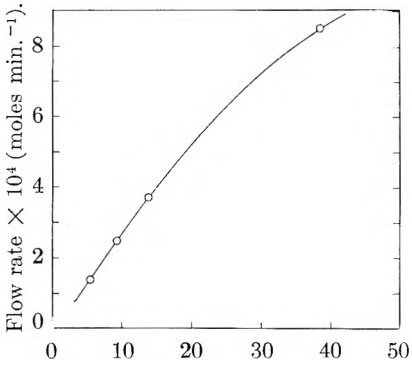

Fig. 1.—Pressure *vs.* flow relationship.

Many runs may be made on the same carbon sample at these low pressures. Once a sample is placed in the vacuum system it need not be exposed to the atmosphere during a long series of determinations at various temperatures and pressures. It is estimated that one sample weighing the order of a gram changed weight by less than 0.1 mg. during a series of twenty runs.

Experimental Results

The data taken from a typical run have been reproduced in Fig. 2. The slight initial increase in pressure before the admission of water vapor is attributed to outgassing of the furnace tube since for a cold furnace the closed vacuum system can maintain a pressure of 1 μ for several hours. In any event the rate of appearance of this gas is quite

(12) M. Knudsen, "The Kinetic Theory of Gases," 3rd Ed., John Wiley and Sons, Inc., New York, N. Y., 1950.

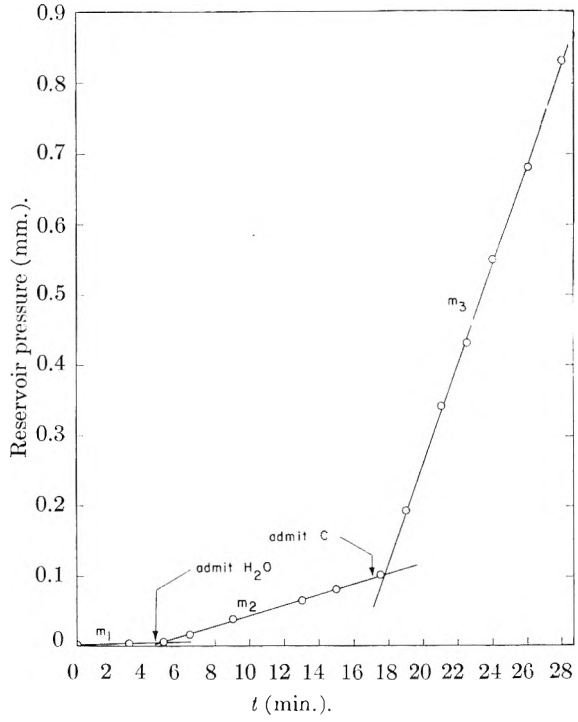

Fig. 2.—Run no. 37, 1303°, 10.3 μ.

negligible compared with the flow rates of water and the reaction rates observed. Outgassing rates, expressed in microns per minute, are found in column m_1 of Table I. The rapid increase in pressure upon admitting water to the system may be accounted for by the dissociation of water vapor into hydrogen and oxygen, $H_2O \rightarrow H_2 + {}^1/_2O_2$. The rate of pressure change in this part of the run is denoted by m_2 in Table I.

That m_2 does represent the rate of decomposition of water has been established by the following experiment. After passing water vapor through the furnace tube for a certain length of time the flow was discontinued and the permanent gases collected in the reservoir were exposed to an electrically heated platinum filament. The reservoir pressure dropped immediately to its original value indicating the recombination, $H_2 + {}^1/_2O_2 \rightarrow H_2O$, with subsequent condensation of the water in the Dry Ice–acetone trap. The amount of dissociation depended upon temperature, pressure and flow rate of the water vapor. The decomposition was probably catalytic, occurring mainly on the exposed platinum–rhodium thermocouple in the furnace tube.

This rate of formation of $H_2 + {}^1/_2O_2$, was increased by approximately 50% by lowering the platinum suspension wire into the hot region of the furnace without the carbon sample. The error thus introduced into the rate value, "v," of Table I, is seen to vary from 5 to 30%.

No analysis was made for O_2 with the carbon sample in the furnace tube. However one would expect the dissociation of H_2O on the carbon surface to lead always to the formation of H_2 + CO, and not free O_2.

The equilibrium amount of dissociation may be calculated from thermodynamic values published

TABLE I

EXPERIMENTAL DATA

Run	T, °C.	p, μ	m_1, μ/min.	m_2, μ/min.	m_3, μ/min.	x_{exp} × 10^3	x_{eq} × 10^3	$v \times 10^7$, moles/min. cm.^{2}
9	705	6.2	v. small	v. small	v. small	v. small	0.0095	v. small
10	804	6.6	0.003	0.014	0.092	0.0092	.051	0.0122
11	919	5.2	.013	.058	.155	.055	.33	.0152
12	1009	3.9	.033	.080	.39	.075	1.16	.049
13	1104	5.2	.078	.412	1.82	.42	3.0	.222
14	1222	6.6	.20	2.20	9.82	1.7	8.7	1.20
15	1298	6.2	.72	5.40	17.1	4.4	17.9	1.84
16	1204	3.0	.17	1.38	11.2	2.8	9.6	1.54
17	1106	2.8	.07	.56	4.0	1.2	3.7	0.53
18	1013	3.0	.050	.182	1.35	0.33	1.31	.184
19	912	4.3	.013	.040	0.178	0.042	0.31	.0216
20	809	2.8	v. small	v. small	0.035	v. small	...	.0055
21	1011	13.3	.06	.81	2.14	0.27	.76	.209
22	1015	26	.03	1.04	2.98	.22	.63	.34
23	1110	22.5	.08	1.90	8.47	.43	2.0	1.03
24	1110	17.5	.08	1.60	8.6	.45	2.1	1.10
25	1160	17	.12	2.43	16.9	.68	3.4	2.28
26	1205	17.5	.18	3.86	31.8	1.08	5.3	4.38
28	1114	9.0	.08	1.21	8.36	0.61	2.7	1.12
29	1114	15.5	.08	2.1	11.7	.66	2.3	1.51
30	1113	5.2	.08	0.78	6.82	.83	3.3	0.95
31	1009	5.7	.03	.20	1.62	.18	1.03	.223
32	1012	15	.03	.37	2.59	.11	0.73	.333
33	1009	8.5	.03	.37	1.67	.20	.90	.204
34	1009	5.7	.03	.26	1.55	.24	1.03	.202
35	1304	35	.3	19.6	157	3.2	10.0	21.5
36	1302	28	.6	15.4	129	3.0	11.0	17.9
37	1304	10.3	.2	7.7	70.6	3.5	15.2	9.86
38	1303	6.4	.3	4.8	50.1	4.1	17.7	7.11
39	1073	5.7	.06	0.38	3.80	0.33	2.1	0.536
40	1000	6.2	.1	.18	0.54	.09	0.85	.057
41	911	6.2	.03	.06	.27	.02	.27	.033
42	996	15.9	.03	.262	.678	.072	.61	.065
43	1116	14.8	.03	1.55	4.78	.94	2.3	.507
44	1113	27	.09	2.07	7.52	.40	1.9	.855
45	1111	38	.09	2.46	8.47	.37	1.6	.944
46	912	15.1	.07	0.12	0.32	.015	0.20	.031
47	1301	10.5	1.0	7.0	41.9	2.7	15.1	5.48
48	1301	29	0.3	16.8	88.2	3.1	10.6	11.2
49	906	10.8	.012	0.072	0.231	0.026	0.22	0.0250

by the U. S. National Bureau of Standards.[13] Values of K_f are reported at various temperatures in units of atm.$^{-1/2}$, where

$$K_f = \frac{(p_{H_2O})}{(p_{H_2})(p_{O_2})^{1/2}}$$

Let

x = degree of dissociation
p = total pressure in atm.

For $x << 1$ we obtain

$$K_f = \frac{1}{x\sqrt{px/2}}$$

and solving for x

$$x = \frac{(2)^{1/3}}{(K_f)^{2/3}(p)^{1/3}}$$

If p is expressed in μ, we have

$$x = \frac{0.115}{(K_f)^{2/3}(p)^{1/3}}$$

(13) U. S. Department of Commerce, National Bureau of Standards, Circular 500, Series III, 1947.

This quantity, denoted by x_{eq}, has been calculated for purposes of comparison with the experimental degree of dissociation, denoted by x_{exp}. Both values are shown in Table I.

The experimental degree of dissociation, $x_{exp.}$, is calculated in the following manner. Let

f = flow rate of water vapor in moles/min.

Then since

$m_2 - m_1$ = rate of formation of $H_2 + {}^1/_2O_2$ in μ/min.

we have

$$x_{exp} = \frac{{}^2/_3(m_2 - m_1)}{f} \times \frac{V}{RT}$$

where

V = vol. of reservoir, McLeod gage, and connecting system (3.7 l.)
T = room temp., (°K.)
R = gas constant (l. μ Hg °K.$^{-1}$ mole^{-1})
${}^2/_3$ = stoichiometric factor

When the water vapor had passed through the reaction chamber long enough to measure m_2, the

sample was introduced and the rate of pressure change in the gas reservoir increased sharply, as illustrated in Fig. 2. The slope of the pressure–time curve in this region is denoted by m_3 in Table I. The rate of reaction ($C + H_2O \rightarrow CO + H_2$) in moles carbon min.$^{-1}$ cm.$^{-2}$ is then given by

$$v = {}^1/_2(m_3 - m_2)\frac{V}{ART}$$

where A is the geometric surface area of carbon sample (6.25 cm.^{2}) and $^1/_2$ is the stoichiometric factor. The values thus calculated for v, are shown in Table I.

In order to determine the extent of the water-gas shift reaction, $CO + H_2O \rightarrow H_2 + CO_2$, an analysis was made for CO_2 in several runs at different temperatures. By lowering the cold trap temperature to that of liquid nitrogen, any CO_2 present would condense (v.p. = 10^{-2} μ at $-180°$), thus decreasing the gas reservoir pressure. No decrease was observed and it has been assumed in all runs that the products of reaction are CO and H_2.

Figure 3 shows the exponential variation of the reaction rate with reciprocal temperature, the pressure of water vapor varying from 3 to 38 μ. The activation energy calculated from this curve has the value 60.3 kcal./mole. The relatively small spread of the data in the 900 to 1100° range (8.43×10^{-4} to 7.28×10^{-4} °K.$^{-1}$, respectively), in spite of the wide variation in reaction pressures, indicates the reaction is zero order with respect to water vapor. The relationship between reaction rate and pressure is brought out more clearly in Fig. 4.

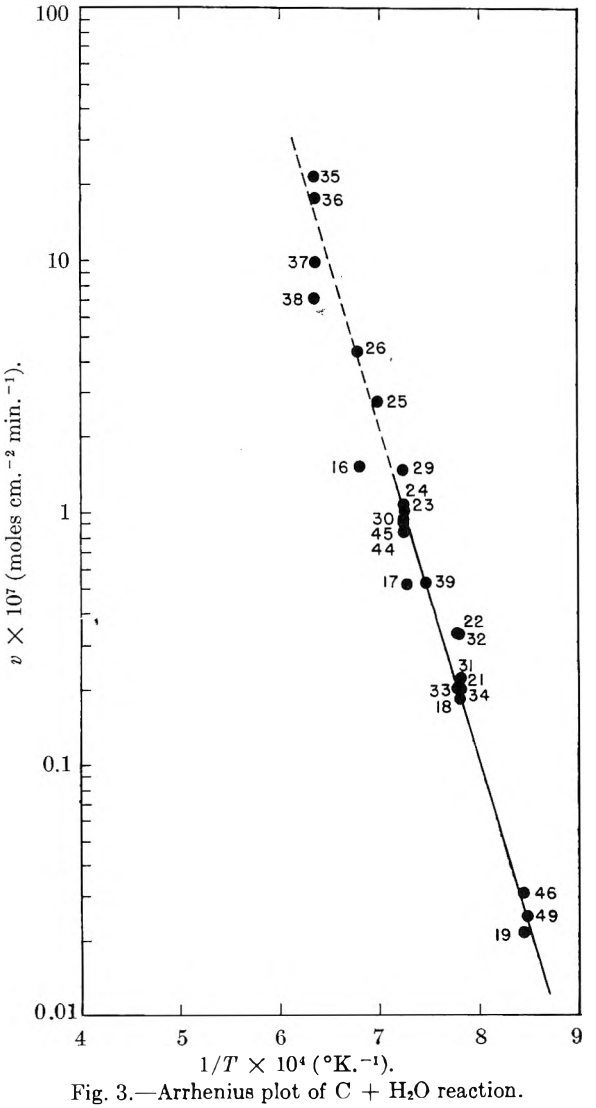

Fig. 3.—Arrhenius plot of C + H_2O reaction.

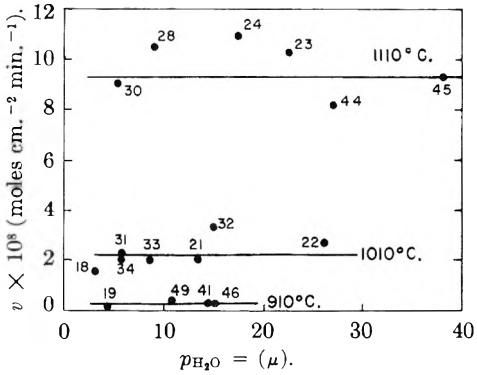

Fig. 4.—Reaction rate *vs.* steam pressure.

In the 1200 to 1300° range (6.79×10^{-4} to 6.35×10^{-4} °K.$^{-1}$, respectively), there is a definite increase in reaction rate with increasing pressure, which accounts for the wide spread in Fig. 3 of runs 16 and 26, at 1205°, and runs 35, 36, 37 and 38, at 1303°. The rate *vs.* pressure curves for 1205 and 1303° are given in Fig. 5. In equation form we have at 1303°

$$v = 4.86p + 44.2 \qquad (1)$$

where

$v \times 10^{-8}$ = moles C/min. cm.^{2}
p = mm. of water vapor

and similarly at 1205°

$$v = 1.96p + 8.0 \qquad (2)$$

The oxidation rate of a graphite sample was strongly dependent upon the oxidation history of that sample. One thing noticeable was that graphite having reacted for a while at a high temperature (1300°) had an abnormally rapid rate immediately afterwards at a low temperature (900°). The rate slowly decreased to a constant value as the reaction continued.

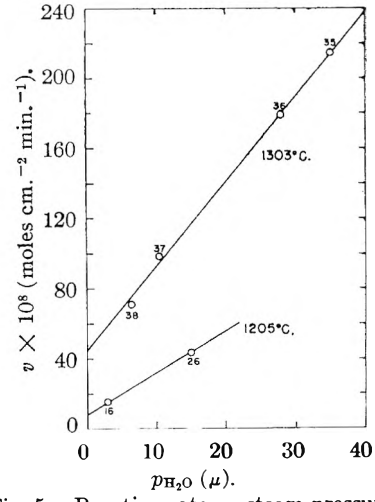

Fig. 5.—Reaction rate *vs.* steam pressure.

In run 49 (906°, 10.8 μ), we specifically investigated this effect to determine whether it was a result of some surface rearrangement of carbon atoms or whether the effect was merely a result of burning off a limited number of active carbon atoms remaining after the high temperature run. The sample was allowed to react with water for about an hour at 1300° and was then withdrawn from the furnace. The furnace temperature is then decreased to 906° and the sample is introduced and allowed to react with the water (reaction rate = 0.68×10^{-8} mole cm.$^{-2}$ min.$^{-1}$) for 20 minutes at which time the water was excluded. The sample was then allowed to remain at 906° for about five hours at which time water was readmitted (reaction rate = 0.63×10^{-8} mole cm.$^{-2}$ min.$^{-1}$). Within 40 to 50 minutes of reaction time this rate had decreased to 0.25×10^{-8} mole cm.$^{-2}$ min.$^{-1}$ and remained constant for ten hours. It was apparent that there were a small number of active carbon sites (*ca.* 10^{-7} mole/cm.^{2}) which were rapidly consumed. This corresponded to about a monolayer off the surface of the graphite using the roughness factor 300 reported by Gulbransen and Andrew.[10]

At all temperatures the rate of reaction was observed to increase gradually as oxidation proceeded. This may be the result of a slight increase in surface area as pitting occurred. For this reason we have not included some of the runs found in Table I in the Arrhenius plot of Fig. 3. Specifically, the first few runs of a fresh sample were omitted because the reaction rates were consistently low. Run 9 was a new sample and runs 9–15 were omitted. The only other sample used was introduced in run 40 and runs 40–43 were omitted for the same reason.

It was necessary to allow the reaction to continue long enough to establish steady-state conditions. One of the disadvantages of the heated carbon filament method discussed earlier was that it burned through rapidly and in some cases it was not possible to attain steady-state conditions.

Discussion of Results

From absolute rate theory[14] we have for the rate constant of any activated process

$$k' = \kappa \frac{kT}{h} e^{\Delta S/R^{\ddagger}} e^{-\Delta H^{\ddagger}/RT} \qquad (3)$$

in which the symbols have the usual meaning.

Since water at high temperatures probably does not undergo reversible adsorption on the surface of carbon we may use the rate of desorption and the reaction rate interchangeably. This rate is given by

$$v_d = k_{-1}\vartheta n_1 \qquad (4)$$

where k_{-1} is the rate constant for desorption, ϑ is the fraction of active sites covered and n_1 is the number of moles of active sites per cm.^{2}. Now if k_1 is the rate constant for adsorption and p is the pressure of water in the gas phase we have for the rate of adsorption

$$v_a = k_1 p(1 - \vartheta)n_1 \qquad (5)$$

Thus for the rate of disappearance of active sites, assuming that desorption of products leaves the same number of active sites as were occupied by them, we have

$$\frac{d\vartheta}{dt} = k_1 p(1 - \vartheta)n_1 - k_{-1}\vartheta n_1 \qquad (6)$$

Making the steady-state assumption that

$$\frac{d\vartheta}{dt} = 0 \qquad (7)$$

we obtain

$$k_{-1}\vartheta n_1 = k_1 p(1 - \vartheta)n_1 \qquad (8)$$

or

$$\vartheta = \frac{k_1 p}{k_{-1} + k_1 p} \qquad (9)$$

which is the Langmuir type isotherm. Substituting (9) in (4) and replacing v_d by v_1 we obtain for the rate of reaction

$$v_1 = \frac{k_{-1}k_1 p n_1}{k_{-1} + k_1 p} \qquad (10)$$

The zero-order kinetics observed in the 900–1100° range may be explained by assuming $k_{-1} << k_1 p$ which leads to $\vartheta = 1$ and

$$v_1 = k_{-1}n_1 \qquad (11)$$

If $\Delta H_1^{\ddagger}$ represents the activation energy for this process we have

$$\Delta H_{-1}^{\ddagger} = 60.3 \text{ kcal./mole.}$$

It is significant that the experiments of Strickland-Constable[4] indicate a first or fractional order kinetics in this same region of temperature and pressure. With a cold gas impinging on a hot surface, such as one has in the heated filament experiments, it may well be that the adsorption step is slower than the desorption step which would lead to first-order kinetics rather than zero order.

In order to calculate an activation energy in the 1200 to 1300° range let us consider the reaction rate–pressure relationships shown in Fig. 5. That these reaction rates do not extrapolate to zero for zero pressure indicates that there are two processes occurring simultaneously, one zero order with respect to water vapor pressure, and the other first order. The reaction rate may be expressed as

$$v = k_2 p n_2 + v_0 \qquad (12)$$

where k_2, n_2 are constants which will be identified below, p is the pressure of the water vapor, and v_0 is the zero-order reaction rate. One observes that the v_0 values in Fig. 5 are much lower than would be expected from the extrapolation of the low temperature zero-order reaction rate to the 1200 to 1300° range in Fig. 3.

It has been suggested[15] that there are two types of active sites in the imperfect graphite lattice which are important in oxidation processes. There is considerable evidence from kinetic studies of the carbon–oxygen reaction[4,7,16–21] that the relative num-

(14) S. Glasstone, K. J. Laidler and H. Eyring, "Theory of Rate Processes," McGraw-Hill Book Co., New York, N. Y., 1941.

(15) G. D. Blyholder, J. S. Binford and H. Eyring (to be published).
(16) V. Sihvonen, *Z. Elektrochem.*, **36**, 806 (1930).
(17) V. Sihvonen, *ibid.*, **40**, 456 (1934).
(18) X. Duval, *J. chim. phys.*, **47**, 339 (1950).
(19) A. Eucken, *Z. angew. Chem.*, **43**, 986 (1930).
(20) H. Martin and L. Meyer, *Z. Elektrochem.*, **41**, 136 (1935).
(21) L. Meyer, *Z. physik. Chem.*, **17B**, 385 (1932).

bers of the two types are different during oxidation at different temperatures.

We will refer to these two classes of sites as type 1 and type 2. Oxidation of type 1 and type 2 sites occurs simultaneously. The rate of oxidation of type 1 sites has already been expressed in equation 10. Similarly, the oxidation rate of type 2 sites is given by

$$v_2 = \frac{k_{-2}k_2pn_2}{k_{-2} + k_2p} \qquad (13)$$

where the constants have a completely analogous interpretation as for type 1 sites. For a first-order reaction in the 1200 to 1300° range we assume that $k_{-2} >> k_2p$ which gives

$$v_2 = k_2pn_2 \qquad (14)$$

which is the first term on the right hand side of (12). But $v_1 = v_0$ and on substituting (11) in (12) we obtain for the sum of rates

$$v = k_2pn_2 + k_{-1}n_1 \qquad (15)$$

In raising the reaction temperature from 1100 to 1200° we propose that the steady-state value of n_1 decreases to such an extent that the reaction proceeds mainly on the n_2 active sites which are type 2.

The high temperature activation energy which we have now identified with the activation energy for adsorption on type 2 site, $\Delta H^{\ddagger}_2$, may be calculated from the coefficients of p in equations 1 and 2. Here we assume the steady-state amounts of type 2 sites are the same at 1200° and 1300°. In this way we obtain

$$\Delta H^{\ddagger}_2 = 42.9 \text{ kcal./mole.}$$

This value is in better agreement with the value of 35 kcal./mole calculated from the data of Strickland-Constable.[4]

It is interesting to note that there is an almost linear dependence of the reaction rate at 1303° on the amount of oxygen formed by the dissociation of water. This relationship is shown in Fig. 6. Here we calculate the oxygen pressure from

$$p_{O_2} = (1/2)(x_{exp})(p_{H_2O})$$

where x_{exp} is the experimental degree of dissociation of water discussed earlier.

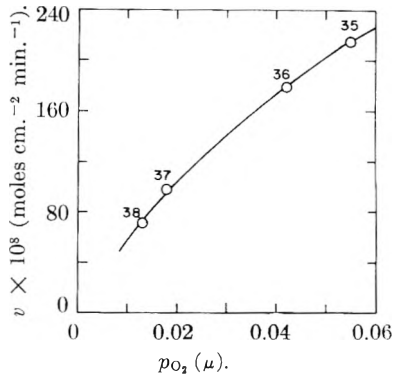

Fig. 6.—Reaction rate *vs.* oxygen pressure.

It may be that in the 1200 to 1300° range adsorbed oxygen acts as a catalyst for the carbon–steam reaction and that the slowest step in the series of processes leading to reaction is the adsorption of oxygen. The activation energy for the adsorption of oxygen on carbon has been obtained experimentally from the first-order carbon–oxygen reaction. Several of these values are tabulated below, and it is seen that they are all somewhat lower than our value of 42.9 kcal./mole.

TABLE II

CARBON–OXYGEN REACTION

Investigator	Temp. range (°C.)	$\Delta H^{\ddagger}$, kcal./mole
Gulbransen, Andrew[9]	425–575	36.7
Eucken[10]	800–1200	21
Meyer[3]	900–1250	20–30
Strickland-Constable[7]	800–1100	26
Sihvonen[16]	800–1400	28

Acknowledgment.—The furnace used in this study was designed by Dr. W. M. Fassell, Department of Metallurgy, University of Utah. We wish to express our great appreciation to Dr. George R. Hill, Jr., who worked with Dr. W. M. Tuddenham[22] on the water–gas reaction and generously advised us on various points.

(22) W. M. Tuddenham and G. R. Hill, *Ind. Eng. Chem.*, **47**, 2129 (1955).

REACTION HEATS OF ORGANIC COMPOUNDS. IV. A HIGH TEMPERATURE CALORIMETER AND THE HYDROGENATION OF METHYL, ETHYL AND VINYL CHLORIDES[1]

BY J. R. LACHER, E. EMERY, E. BOHMFALK AND J. D. PARK

Contribution of the University of Colorado, Boulder, Colorado

Received October 8, 1955

A calorimeter is described which permits one to measure vapor phase heats of reactions at about 248°. It uses condensing diphenyl ether as a constant temperature bath. At this temperature methyl, ethyl and vinyl chloride can be hydrogenated to give methane and ethane together with hydrogen chloride. The reaction heats have been measured.

In previous work[2] on the vapor phase heats of chemical reactions, an oil-bath was used as a thermostat. It had a maximum operating temperature of about 130°. Since many reactions of interest require a higher temperature to go to completion, two new calorimeters were constructed which use a condensing vapor[3] as a source of constant temperature. The present paper describes the construction and operation of one of these calorimeters which uses diphenyl ether as a condensing vapor. The heats of hydrogenation of methyl, ethyl and vinyl chloride are also presented.

Apparatus.—The calorimeter reaction chamber consists of a monel cylinder 7.5 inches long by $1^3/_8$ inches inside diameter. It is suspended from a circular brass plate. The catalyst is placed in the chamber through a $1^1/_8$ inch opening in the bottom. This is closed with a threaded monel plug and sealed with a lead gasket. The reactant gases enter the chamber through concentric monel tubes which extend to the bottom of the chamber. The product gases leave from the top and then pass through a monel heat exchanger which is coiled around the reaction chamber. This entire unit is enclosed by a quart dewar filled with tetra-2-ethylhexyl orthosilicate.[4] The latter is used as a volatile liquid and the heat of reaction is transferred to it. The dewar is supported on springs in a brass cylinder 14.5 inches long and 3.5 inches inside diameter, the top of which is bolted to the brass plate holding the reaction chamber. Hydrogen gas is bubbled through the volatile liquid by means of a monel frit located just below the reaction chamber. This serves to remove heat from the liquid. The spent gas passes out through a reflux condenser.

The calorimeter heater was constructed of four feet of nichrome wire and had a resistance of about 40 ohms. It was located just above the monel frit. The leads (one set for measuring voltage drop and the other for carrying current) were constructed of "Teflon" coated copper wire. The equipment for producing constant current and for measuring potential drops was similar to that previously described.[2] A six junction copper–constantan thermel was used to detect any difference in temperature between the liquid inside the dewar and the surrounding constant temperature bath. A "Teflon" suspension was used to insulate the junctions and the couple operated satisfactorily at the high temperature involved—248°.

The constant temperature bath was constructed from a cylindrical steel tank 13 inches in diameter and 30 inches in length. The brass cylinder containing the dewar and reaction chamber was suspended from the lid of this tank. All gases entering the dewar were passed through heat exchanger tubes made of $^1/_4$ inch monel and located in the condensing vapor. Evidence that the heat exchangers were adequate was obtained by running a single gas to the catalyst chamber and observing that it produced no cooling. Diphenyl ether was used as the boiling liquid and produced a temperature of 248°. A minimum of six liters were required to keep the liquid level above the wires of the heater. The latter were made of heavy nichrome and had a resistance of six ohms. The input voltage was regulated by means of a Sola constant voltage transformer and a variac.

The insulation for the condensing vapor tank consisted of a large cylindrical can filled with vermiculite and having a circular hole in the center into which the steel tank could be hoisted by means of a pulley. This insulating can was made from galvanized sheet steel and had an over-all dimension of 36 inches in diameter and 48 inches in height. It was fitted with four castors which made it easy to remove from a "walk-in-hood" for occasional repairs.

In order to maintain a constant temperature, the pressure of the condensing vapor was held constant. This was accomplished by connecting the reflux condenser on the vapor bath to a ballast tank filled with nitrogen. The tank was buried in the ground to minimize temperature fluctuations. A mercury leveling device run by a reversible Telechron motor was used to maintain a constant pressure. A 25-ohm platinum-resistance thermometer immersed in the condensing vapor served as the temperature sensing device. It formed one arm of a conventional Wheatstone bridge. Any unbalance of the bridge caused the galvanometer light to move on or off a photoelectric cell. The signal from the photoelectric cell was amplified and used to operate the reversible Telechron. The bath could be made to maintain a temperature within 0.001° during a run.

It is necessary to have three separate flow systems for the calorimeter: one for each of the reacting gases and a third for the hydrogen which bubbled through the volatile liquid in the dewar for cooling. The flow systems are basically the same and consist of a variable-level bubbler for maintaining a constant upstream pressure, a capillary flowmeter, a back pressure manometer, and in case of the reactant flow systems, a set of stopcocks for sending the gas to the calorimeter or to the hood. Precatalyst chambers are also included in the flow systems. Their purpose is to remove any poisons present in the reactants which might injure the catalyst in the calorimeter. In case of the hydrogen flow systems, palladium-on-carbon is used as a precatalyst to remove any oxygen present as water. The latter is removed by passing the gas through silica gel and phosphorus pentoxide-on-asbestos.

Experimental

Heat of Formation of Hydrogen Chloride.—When the construction of the high temperature calorimeter was completed, it was decided to measure the known heat of formation of hydrogen chloride.[5] The catalyst used was 5% palladium-on-activated carbon. The carbon, 6 to 20 mesh, was heated several hours with 10% nitric acid, washed with water, dried in an oven and finally evacuated several hours at 300°. 6.5 grams of palladium chloride was dissolved in 14 ml. of concentrated HCl and diluted to about 100 ml. The solution was poured over 65 g. of purified carbon and dried at 95°. The mixture was then placed in a chamber at 100° and hydrogen was passed over until the reduction of palladium chloride was complete. The catalyst was evacuated several hours at 248° before using. Chlorine from Matheson[6] was used without purification; commercial hydrogen 99.8% pure was treated to remove oxygen as previously described.

(1) This research was supported by the A.E.C. Contract No. AT(11-1)-168.

(2) J. R. Lacher, J. D. Park, *et al.*, *J. Am. Chem. Soc.*, **72**, 3231 (1950).

(3) We wish to thank Mr. E. J. Prosen, of the National Bureau of Standards, for suggesting this to us.

(4) This material was supplied by the Oronite Chemical Co. of San Francisco, California.

(5) F. D. Rossini, *Bur. Stand. J. Research*, **8**, 119 (1932).

(6) Matheson Co., Inc., Purity 99.5%.

In making a run, a high rate of flow of hydrogen through the volatile liquid in the dewar is set and maintained constant throughout the duration of the experiment. The cooling produced is balanced with electrical energy until isothermal conditions are obtained as measured by the 6-junction thermel and a photoelectric galvanometer. When this has been accomplished, the chemical reaction is started. The hydrogen is used in excess and chlorine is the limiting reactant. The chlorine flow rate is held constant and the electrical heat input is reduced until the heat evolution due to the reaction plus a small amount of electrical energy equals the cooling produced by the hydrogen in passing through the volatile liquid. The difference between the two electrical energy readings gives the rate of heat evolution due to the reaction. The rate of formation of the product, HCl, is determined by passing the product gases to an absorption tower for a definite period of time. The acid collected is diluted and aliquot portions are analyzed for HCl by titration with standard 0.03 *N* KOH solution using phenolphthalein indicator. The reaction between hydrogen and chlorine appeared to be quantitative under these conditions. The exit gases would not turn the color of starch iodide paper nor could chlorine be detected by its absorption at 330 mμ using a 10-cm. cell and a Beckman model DU spectrophotometer. The results obtained, shown in Table I, indicate that the calorimeter is working properly.

TABLE I

HEAT OF FORMATION OF HYDROGEN CHLORIDE AT 248°

H_2 flow, moles/min. $\times 10^4$	HCl formation, moles/min. $\times 10^4$	Energy rate, cal./min.	$-\Delta H$, cal./mole of HCl	% Dev. from $-22,225$[a]
5.4	4.577	10.151	22,180	−0.2
7.4	6.819	15.168	22,240	+0.1
10.2	9.657	21.511	22,280	+0.25

[a] Rossini's value corrected to 248°.

Hydrogenation of Methyl Chloride.—The methyl chloride used was obtained from Mathieson Co., purity 99+%. Since the infrared spectrum of material taken directly from the tank was identical to that of a fractionated sample, the material was used without further purification. The absorption spectrum is given in Fig. 1. It proved more difficult to hydrogenate methyl chloride than either vinyl or ethyl chloride. The catalyst was prepared by heating 70 g. of 10–20 mesh Columbia activated carbon for three hours in 20–25% hydrochloric acid. At the end of that time lead acetate paper showed the absence of H_2S vapor. The carbon was then washed free of acid and dried at 110° for 24 hours. Ten grams of palladium chloride was dissolved in 50 ml. of 10% hydrochloric acid and diluted to 100 ml. This solution was poured over 70 g. of carbon and the mixture dried on a steam-bath and finally in an oven at 110°. The material was transferred to a glass chamber and evacuated for two to three hours at 250°. Hydrogen was then passed over the catalyst until reduction was complete. Using this catalyst the conversion of methyl chloride was nearly quantitative.

The strong absorption peak at 13.45 μ shown by methyl chloride was used to follow the completeness of the reaction. A calibration curve was prepared giving the intensity of this band as a function of the pressure in mm. for methyl chloride. Using a flow rate of 4.1×10^{-4} mole/min. for methyl chloride and 9×10^{-4} mole/min. for hydrogen, the partial pressure of the unreacted methyl chloride in the exit gases was approximately one mm., indicating a conversion of 99.5%. During a run an excess of hydrogen was used and, since each molecule of methyl chloride which reacts yields one molecule of HCl, the rate of formation of HCl gives the rate of consumption of methyl chloride. This was determined by sending the exit gases to an absorption tower and titrating the collected HCl with KOH.

At the end of one of the runs, a sample of the exit gases was collected for infrared analyses. Since CH_4 absorbs weakly and was diluted with excess hydrogen, a meter cell was used. To protect the aluminized mirrors, the HCl was removed before the exit gases were passed into the cell. The spectrum obtained is presented in Fig. 1 together with that for CH_4. The latter was copied from the Catalog of Infrared Spectral Data of the NBS.[7] Except for a small amount of methyl chloride, the product spectra correspond to that of methane. The very slight amount of unreacted chloride is shown with a tenfold intensity due to the fact that the product sample was contained in a one-meter cell and the others in a ten-centimeter cell.

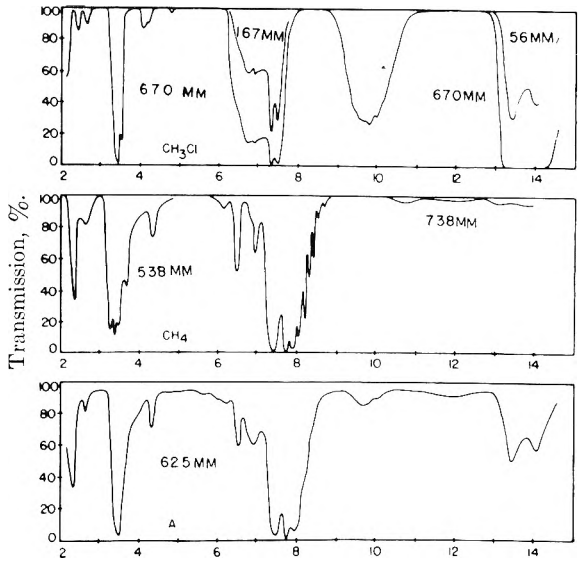

Fig. 1.—Infrared spectra of methyl chloride, methane and product gases from the hydrogenation of methyl chloride: A, product spectrum using meter cell; other spectra in 10 cm. cell.

Five runs were made, but one of these was discarded since difficulties occurred with the temperature controlling circuit. The results are shown in Table II.

TABLE II

HEAT OF HYDROGENATION OF METHYL CHLORIDE AT 248°

H_2 flow, moles/min. $\times 10^4$	HCl formation, moles/min. $\times 10^4$	Energy rate, cal./min.	$-\Delta H$,[a] cal./mole of CH_3Cl
8.5	3.548	6.974	19,660
9.3	3.993	7.836	19,620
9.1	4.132	8.129	19,670
8.8	4.224	8.326	19,710

[a] $-\Delta H$ (average) = 19,665 ± 45 cal./mole.

Hydrogenation of Ethyl Chloride.—The ethyl chloride was obtained from the Matheson Company and had a purity of 99.5%. The infrared spectrum of this material was the same as that distilled on a 100-plate Podbielniak Hypercal column, so it was judged that further purification was unnecessary. The spectrum is shown in Fig. 2. The catalyst used was seven per cent. palladium-on-carbon and the carbon was purified by a nitric acid treatment as previously described. It would hydrogenate ethyl chloride practically quantitatively at flow rates up to 5×10^{-4} moles/min. A sample of the product gases, treated to remove HCl, was collected in the meter cell and the spectrum obtained is shown in Fig. 2. It is identical to that of ethane[8] except for the slight absorption at 7.7 and 10.3 μ. This is due to about 0.1% of unreacted ethyl chloride. The rate of formation of ethane was taken to be equal to the rate of formation of HCl. Of the six runs made, four were completed without experimental difficulties and are given in Table III.

Hydrogenation of Vinyl Chloride.—Vinyl chloride of 99.8% purity from Matheson Co. was used without further purification. The infrared spectrum of this material is

(7) Catalog of Infrared Spectral Data, American Petroleum Institute Research Project No. 44, Serial No. 528.

(8) Copied from Catalog of Infrared Spectral Data, American Petroleum Institute Research Project No. 44, Serial No. 58 and 920.

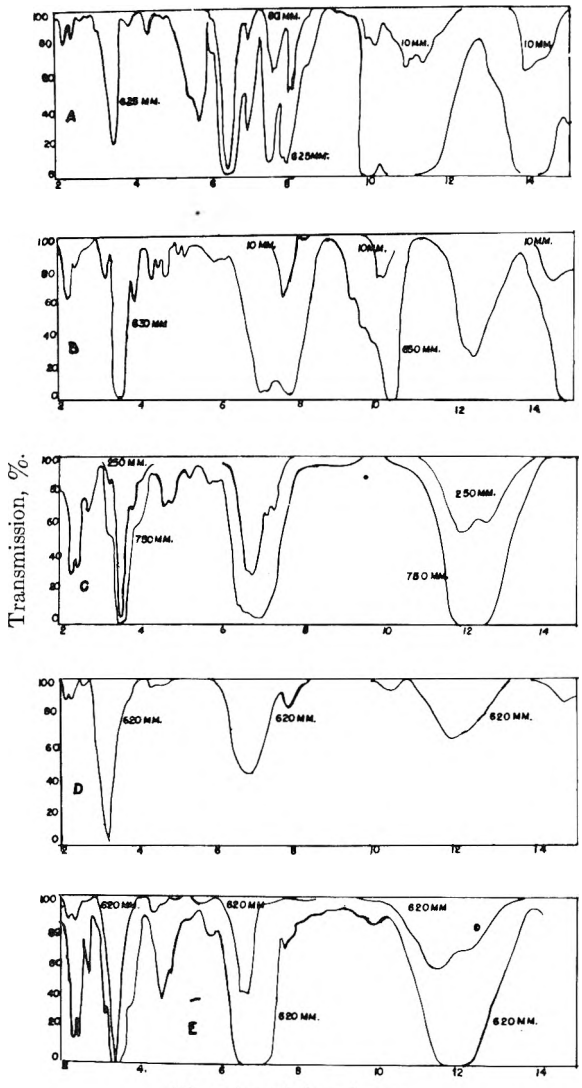

Fig. 2.—Infrared spectra of A, B and C; vinyl chloride, ethyl chloride, and ethane. Also the product gases from the hydrogenation of D and E. D, product gases from the hydrogenation of vinyl chloride; E, product gases from the hydrogenation of ethyl chloride.

given in Fig. 2 and is identical to that for the pure compound in the Catalog of Infrared Spectral Data of the NBS.[8] The reaction proceeded more readily than the hydrogenation of ethyl chloride using a similar catalyst. The infrared spectrum of the product gases, collected in a 10-cm. cell, is shown in Fig. 2. It is identical to that for ethane. A trace of ethyl chloride shows up in the slight absorption at 7.7, 10.3 and 14.7 μ. The strong band at 3.47 μ is due to an overlap of the strong band in ethane and absorption due to the hydrogen chloride. The rate of formation of ethane is taken to be equal to that of hydrogen chloride. Of the six runs made, four were completed without experimental difficulties and are given in Table IV.

TABLE III

HEAT OF HYDROGENATION OF ETHYL CHLORIDE AT 248°

H_2 flow, moles/min. $\times 10^4$	HCl formation, moles/min. $\times 10^4$	Energy rate, cal./min.	$-\Delta H$,[a] cal./mole of C_2H_5Cl
8.7	4.331	7.451	17,200
8.3	4.562	7.843	17,190
9.0	4.253	7.300	17,160
9.5	4.740	8.103	17,100

[a] $-\Delta H$ (average) = 17,160 ± 60 cal./mole.

TABLE IV

HEAT OF HYDROGENATION OF VINYL CHLORIDE AT 248°

H_2 flow, moles/min. $\times 10^4$	HCl formation, moles/min. $\times 10^4$	Energy rate, cal./min.	$-\Delta H$,[a] cal./mole of C_2H_3Cl
8.3	1.431	7.546	52,730
8.9	1.979	10.361	52,350
8.7	1.853	9.763	52,690
8.3	1.767	9.304	52,650

[a] $-\Delta H$ (average) = 52,610 ± 260 cal./mole.

Discussion of Results

In order to use these heats of hydrogenation to calculate the standard heats of formation of methyl, ethyl and vinyl chlorides, it is necessary to calculate the heat of reaction at 25°. This can be done by means of Kirchoff's equation, if the heat capacities of the reactants and products are known. Accurate values for the heat capacities of hydrogen, methane, ethane and hydrogen chloride over the necessary temperature range are given by the Bureau of Standards.[9] The heat capacity for methyl chloride has been calculated by Gelles and Pitzer.[10] The molar heat capacities at constant pressures for ethyl and vinyl chlorides were calculated by us and the results are shown in Table V.

TABLE V

GASEOUS HEAT CAPACITIES, CAL./MOLE/DEG.

Compound	Temperature, °K. 298	300	400	500	600
Ethyl chloride	14.80	14.88	18.44	21.64	24.35
Vinyl chloride	12.78	12.89	15.25	17.49	19.61

For ethyl chloride the vibrational assignments of Linnett[11] and of Gordon and Giauque[12] were used. Our heat capacities are about 0.1 cal. lower than those calculated by Daasch, Liang and Nielsen.[13] The assignment of Thompson and Torkington[14] was used for vinyl chloride. The corrected heats of hydrogenation at 25° are given as the first three entries in Table VI.

TABLE VI

HEATS OF REACTION AT 25°

Reaction	$-\Delta H$, cal./mole
$CH_3Cl + H_2 \longrightarrow CH_4 + HCl$	19,318
$C_2H_5Cl + H_2 \longrightarrow C_2H_6 + HCl$	16,559
$C_2H_3Cl + 2H_2 \longrightarrow C_2H_6 + HCl$	51,188
$C_{(gr)} + 3/2\ H_2 + 1/2\ Cl_2 \longrightarrow CH_3Cl$	20,634
$2C_{(gr)} + 5/2\ H_2 + 1/2\ Cl_2 \longrightarrow C_2H_5Cl$	25,740
$2C_{(gr)} + 3/2\ H_2 + 1/2\ Cl_2 \longrightarrow C_2H_3Cl$	−8,889
$CH_2{=}CH_2 + HCl \longrightarrow C_2H_5Cl$	16,173
$CH_2{=}CHCl + H_2 \longrightarrow C_2H_5Cl$	34,567

(9) "Selected Values of Properties of Hydrocarbons," A. P. I. Research Project No. 44, National Bureau of Standards.

(10) E. Gelles and K. S. Pitzer, *J. Am. Chem. Soc.*, **75**, 5259 (1953).

(11) J. W. Linnett, *Trans. Far. Soc.*, **36**, 527 (1940).

(12) J. Gordon and W. F. Giauque, *J. Am. Chem. Soc.*, **70**, 1506 (1948).

(13) L. W. Daasch, C. Y. Liang and J. Nielsen, *J. Chem. Phys.*, **22**, 1293 (1954).

(14) H. W. Thompson and P. Torkington, *Proc. Roy. Soc. (London)*, **A184**, 3 (1945).

The heats of formation of gaseous HCl, CH_4 and C_2H_6 are given as[9] −22,063, −17,889 and −20,236 cal. per mole, respectively. Using this information and the present data, we can calculate the heats of formation of methyl, ethyl and vinyl chlorides. The results are given in Table VI.

Bichowsky and Rossini[15] give 20.1 kcal. for the heat of formation of methyl chloride. For ethyl chloride they give 25.7 kcal. Recently Casey and Fordham[16] measured the heat of combustion of ethyl chloride and obtained a value of −341 ± 2.5 kcal. From this they calculate the heat of formation to be 24 kcal. The present method has an advantage over the combustion experiment in that the total heat effect is small. Bichowsky and Rossini[15] give −9 kcal. as the heat of formation of vinyl chloride. Using the present data, one can calculate the heat of addition of hydrogen chloride to ethylene to be −16,173 cal. and the heat of addition of hydrogen to vinyl chloride to be −34,567 cal. These are shown as the last two entries in Table VI. About 2000 cal. more heat is liberated when hydrogen is added to vinyl chloride than when it adds to ethylene.

(15) "Thermochemistry of Chemical Substances," F. R. Bichowsky and F. O. Rossini, Reinhold Publ. Co., New York, N. Y., 1936.

(16) D. W. H. Casey and S. Fordham, *J. Chem. Soc.*, 2513 (1951).

CARBON–OXYGEN AND CARBON–HYDROGEN SURFACE COMPLEXES[1]

By R. Nelson Smith, Jack Duffield, Robert A. Pierotti and John Mooi

Chemistry Department, Pomona College, Claremont, California

Received October 17, 1955

Experimental results show that hydrogen-treatment of carbon surfaces at 1000° is effective in removing carbon–oxygen complexes and that carbon–hydrogen complexes are not formed in their place. H_2-treatment *reduces* the hydrogen content of carbon samples, probably a result of the thermal treatment. The hydrogen content of a carbon sample is distributed throughout the sample and is not bound to the surface alone. Outgassing at 100° is effective in reducing the amount of carbon–oxygen complex on Graphon, a black, but it is not effective for a charcoal. H_2-treated surfaces rapidly pick up carbon–oxygen complexes on exposure to air at room temperature. The extent of carbon–oxygen complexes resulting from treatment of carbon surfaces with air, nitrous oxide, nitric oxide and water is given and related to previously published work.

In an effort to correlate some observed surface phenomena with the amount of carbon–oxygen complexes present on the surface, a microanalytical method was developed for the determination of these complexes. The method is published elsewhere,[2] but the results obtained with a few carbons are published and discussed here for the information of those who have used the same or similar carbons.

In addition, there is presented here some information about carbon–hydrogen surface complexes. There has been some question in the minds of the authors and others concerning the nature of carbon surfaces remaining after the hydrogen treatment used to remove carbon–oxygen complexes. H_2-treatment, as usually performed by the authors, consists of heating the sample *in vacuo* to 1000°, then adding an atmosphere of hydrogen. The hydrogen atmosphere is removed after 15 minutes and followed by a pumping period of about one-half hour. This addition of hydrogen followed by pumping is repeated two more times. After the third addition the sample is allowed to cool slowly from 1000° with continuous pumping by a high vacuum system. Pumping is usually continued for several hours or overnight. The question is: does removal of carbon–oxygen surface complexes by this treatment leave in their place a surface with carbon–hydrogen complexes?

(1) This is a progress report of work done under Contract N8onr 54700 with the Office of Naval Research. Reproduction in whole or in part is permitted for any purpose of the United States Government.

(2) R. N. Smith, J. Duffield, R. A. Pierotti and J. Mooi, *Anal. Chem.*, **28**, in press (1956).

Experimental

One black and two charcoals were used in this work. Their properties are as follows.

Graphon.—A partially graphitized carbon black (supplied through the courtesy of the Godfrey L. Cabot Co.) was made by heating Spheron Grade 6 (a medium processing channel black) to approximately 3000° in an electric furnace. The surface area is about 80 sq. m. per g. and its ash content is about 0.02%.

Su-60.—A sugar charcoal of extremely low ash content was prepared, starting with Confectioners AA sugar furnished through the courtesy of the California and Hawaiian Sugar Refining Corporation. This sugar was used because it had an ash content of 0.0008%. After activation[3] this charcoal had a BET area of 1020 sq. m. per g., using ethyl chloride, and its ash content was less than 0.005%.

B.—An activated commercial nut charcoal, de-ashed with HCl in a Soxhlet extractor, dried and heated to 1000° *in vacuo*. The BET surface area is 1050 sq. m. per g. and its ash content is about 0.2%.

Nitrous Oxide.—Obtained from the American Medical Gas Co. and used from the cylinder without further purification. Precautions were taken to prevent contamination on removal from the cylinder.

Nitric Oxide.—Obtained from the Matheson Co. and used from the cylinder without further purification. Precautions were taken to prevent contamination on removal from the cylinder.

Analytical Apparatus and Procedure.—The carbon–oxygen complexes were determined by a micro ter Meulen method.[2] The details concerning the treatment and handling of carbon samples are also included in this analytical article. Each analysis was alternated with a blank run, and a sample of pure benzoic acid (Parr Calorific Grade) was used occasionally as a check on catalyst performance. Each sample was outgassed *in vacuo* at 110° for 12 hours prior to analysis except where noted. After outgassing the samples were always stored, transferred and weighed in a nitrogen atmosphere.

The hydrogen contents were determined by burning samples in a stream of pure oxygen. The conventional

(3) R. N. Smith and J. Mooi, This Journal, **59**, 814 (1955).

method of Niederl and Niederl was not used because of the great length of time required for complete burning of samples. Instead the fast-flowrate and unpacked-tube method of Belcher and Spooner[4] was used with silver gauze as recommended by them for removal of sulfur. Only an Anhydrone absorption tube (in addition to a guard tube and mariotte bottle) was used after the train since water was the only product whose determination was desired. Nitrogen, sulfur and ash do not interfere with this determination and, in fact, sulfur could be determined simultaneously if desired. Technique and procedure were checked using pure benzoic acid (Parr Calorific Grade). The carbon samples were prepared for analysis as indicated in Table II.

Results

The results obtained with carbon–oxygen complexes are given in Table I and those for carbon–hydrogen complexes given in Table II. The sample treatments shown in Table I were chosen because of other work carried out in this Laboratory. For reasons previously published[2] it is believed that the results in Table I are not seriously in error because of the presence of sulfur, nitrogen or ash in the various samples. The nitrogen content was assumed to be negligibly small, though if it had not been, the same analytical method could have been used with Ascarite instead of Anhydrone in the

TABLE I

PER CENT. OXYGEN IN CARBON SAMPLES

Sample	Treatment before analysis	Sample wt., mg.	Oxygen, %	Oxygen av., %
Graphon	As supplied; not outgassed	504.3	0.0176	
		826.4	.0129	0.0153
	Outgassed only	623.2	.0043	
		553.9	.0032	.0038
	H_2-treated at 1000° for 15 min. No subsequent exposure to air	504.3	.000	
		826.4	.000	.000
	H_2-treated at 1000° for 15 min. Subsequent exposure to air at room temp. for 2 hr.	389.0	.0228	
		389.0	.0251	.0240
	Poured through air at 700°	390.4	.312	
		260.1	.342	
		316.1	.309	
		377.2	.358	.330
	Treated with N_2O at 500° for 3 hr. (3 exposures of 1 hr. each)	478.0	.0130	
		432.6	.0123	.0127
	Treated with NO at room temp. for 3 hr. (3 exposures of 1 hr. each)	566.5	.0235	
		542.7	.0294	
		578.7	.0292	
		458.8	.0291	.0278
Su-60	As made; not outgassed	189.8	.412	
		195.1	.428	
		197.1	.415	.415
	Outgassed only	221.8	.368	
		236.4	.402	.385
	H_2-treated at 1000° for 15 min. No subsequent exposure to air	170.9	.000	
		202.6	.000	.000
	H_2-treated at 1000° for 15 min. Subsequent exposure to air at room temp. for 24 hr.	170.9	.0676	
		202.6	.0570	
		193.8	.0687	.0644
	Treated with N_2O at 500° for 3 hr. (3 exposures of 1 hr. each)	178.2	1.19	
		146.0	1.22	1.21
	Treated with NO at room temp. for 3 hr. (3 exposures of 1 hr. each)	152.1	2.72	
		133.8	2.86	2.79
	Heated at 1000° for 2 weeks with continuous pumping. Then, at 100°, it was exposed to about 25 mm. H_2O vapor for 10 days. This was followed by 2 days of outgassing at 100°	274.1	0.434	
		182.0	.439	0.437
B	As supplied; not outgassed	60.7	4.46	
		50.6	4.23	
		57.1	4.25	
		68.5	4.15	4.27
	Outgassed only	114.4	4.41	
		90.1	4.20	
		164.1	4.38	
		168.5	4.55	4.39
	H_2-treated at 1000° for 15 min. No subsequent exposure to air	60.7	0.000	
		50.6	.000	.000
	H_2-treated at 1000° for 15 min. Subsequent exposure to air for 2 hr. at room temp.	153.7	.150	
		157.3	.141	.145
	H_2-treated at 1000° for 15 min. Subsequent exposure to air at room temp. for 7 days	156.8	.351	
		150.1	.297	
		155.2	.315	.321

TABLE II

PER CENT. HYDROGEN IN CARBON SAMPLES

Sample	Treatment prior to analysis	Sample wt., mg.	Hydrogen, %	Hydrogen av., %
Graphon	Outgassed at 450° for 4 hr.	499.1	0.038	
		557.0	.033	
		454.6	.033	0.035
	H_2-treated at 1000° for 1 hr. Pumped continuously while cooling	551.9	.026	
		542.4	.026	.026
Su-60	Outgassed at 450° for 4 hr.	116.0	.550	
		111.0	.510	
		102.9	.522	
		127.8	.525	.527
	H_2-treated at 1000° for 1 hr. Pumped continuously while cooling	129.8	.360	
		159.2	.350	
		128.2	.356	.355
	Outgassed at 1000° for 2 hr. Pumped continuously while cooling	118.4	.296	
		95.42	.304	
		91.75	.295	.298
	H_2-treated at 1250° for 8 hr. Cooled to room temp. in H_2 at 1 atm., then outgassed at 450° for 4 hr.	135.9	.167	
		117.0	.179	
		80.5	.175	.174

(4) R. Belcher and C. E. Spooner, *J. Chem. Soc.*, 313 (1943).

absorbent tube. The results in Tables I and II may be compared with the data given by Studebaker[5,6] for a variety of carbon blacks. His oxygen values were determined by the Unterzaucher method with suitable correction made for ash; his hydrogen values were determined by combustion analysis.

Discussion

Carbon–Oxygen Complexes.—Table I shows quantitatively the magnitude of some commonly-observed effects. Outgassing of the Graphon at 110° is effective in removing the majority of the oxygen, but in the case of the charcoals it has negligible effect. H_2-treatment of carbon surfaces at 1000° is very effective in removing carbon–oxygen complexes, at least as determined by a method which is itself a H_2-treatment. After H_2-treatment, carbon surfaces rapidly pick up oxygen from the air—Graphon an amount greater than that which it originally possessed, but the charcoals an amount which is only a fraction of what they originally possessed. Perhaps, in the case of the charcoals, much of the oxygen is associated with some of the hydrogen in a form related to the molecular structure of the material from which they were made (sugar or coconut shells). When this oxygen is removed and the sites destroyed by H_2-treatment molecular oxygen may not be able to be rebound to these sites again when the carbon is exposed to air. There is an additional slow uptake of oxygen over a period of time. It is interesting to note that the oxygen uptake per unit surface area is considerably greater on the hydrogen-treated Graphon than on the hydrogen-treated charcoals.

The extent of surface oxidation by N_2O at 500° is also given in Table I. At this temperature carbon surfaces rapidly catalyze the N_2O oxidation of CO. It has been demonstrated[3] that the carbon–oxygen complexes formed to the extent shown poison the surface for this reaction, but if CO is present in equal or larger quantity than N_2O this poisoning effect is essentially eliminated. The effect of these oxides on the reaction of N_2O with carbon surfaces will be published separately, but it may be said now that the rate of reaction is increased by their presence.

The extent of the room temperature oxidation of carbon surfaces by nitric oxide is about the same as by air on Graphon, but on Su-60 nitric oxide is about forty times more effective than air. The influence of this oxidation on the isotherms and heats of absorption of nitric oxide on carbon surfaces will be discussed in a separate paper.

It has been shown previously[7] that as water isotherms are determined the carbon surface is progressively oxidized, and as a result the adsorption of water is progressively increased. Air oxidation has the same effect.[8] This oxidation is no doubt the cause of the apparent negative net heat of adsorption observed by Coolidge[9] for the adsorption of water on charcoals. It is probably the cause also of the initial adsorption (the BET value of V_m) observed by Young, Chessick, Healey and Zettlemoyer,[10] for Millard, Caswell, Leger and Mills[11] have shown that H_2-treatment eliminates both the initial adsorption and the initial heat effect.

Carbon–Hydrogen Complexes.—As mentioned in the Introduction, there has been some question as to whether high-temperature hydrogen treatment actually cleans up the carbon surface or merely replaces the carbon–oxygen complexes by carbon–hydrogen complexes. The results in Table II indicate that H_2-treatment does not increase the amount of hydrogen held by the carbon. The hydrogen content actually decreases, but this is doubtless caused by the thermal treatment and not by the presence of hydrogen. In addition, a Graphon sample was burned stepwise, and the per cent. hydrogen calculated for the amount of carbon burned in each step. The results, using a 489.9-mg. sample, were as follows. Step 1: 86.6 mg. burned with 0.030% H. Step 2: 169.5 mg. burned with 0.026% H. Step 3: 186.2 mg. burned with 0.041% H. Step 4: 56.6 mg. burned with 0.078% H. If the whole sample had been burned at once it would have shown 0.035% H as indicated in Table II. These results show that the hydrogen which is present is not only on the surface but is distributed through the sample. This is reasonable since both blacks and charcoals are the pyrolyzed residues of organic compounds. It is also reasonable that the hydrogen content of Graphon should be so low since it is produced from Spheron Grade 6 (with 0.51% H) by heating to 3000° in an induction furnace. It is interesting to note that the hydrogen content of the interior of the Graphon particles is greater than the portion near the outside. It is also interesting to note that the ratio of the per cent. oxygen on the outgassed sample to that on the N_2O-treated sample to that on the NO-treated sample is 1.00:3.34:7.32 on Graphon and 1.00:3.15:7.25 on Su-60. At present no real significance can be attached to this observation.

(5) M. L. Studebaker, *India Rubber World*, **127**, 215 (1952).

(6) M. L. Studebaker, *Kautschuk und Gummi*, **6**, 193 (1953).

(7) C. Pierce, R. N. Smith, J. W. Wiley and H. Cordes, *J. Am. Chem. Soc.*, **73**, 4551 (1951).

(8) F. H. Healey, Y. Yu and J. J. Chessick, THIS JOURNAL, **59**, 399 (1955).

(9) A. S. Coolidge, *J. Am. Chem. Soc.*, **49**, 708 (1927).

(10) G. J. Young, J. J. Chessick, F. H. Healey and A. C. Zettlemoyer, THIS JOURNAL, **58**, 313 (1954).

(11) B. Millard, E. G. Caswell, E. E. Leger and D. R. Mills, *ibid.*, **59**, 976 (1955).

THE HEAT OF COMBUSTION OF CALCIUM[1,2]

BY ELMER J. HUBER, JR., AND CHARLES E. HOLLEY, JR.

Contribution from the University of California, Los Alamos Scientific Laboratory, Los Alamos, New Mexico

Received November 18, 1955

Calorimetric combustions of calcium metal were conducted at an initial temperature of 25° under an oxygen pressure of 50 atm. The energy of combustion under these conditions was found to be 15,806 joules/g. The corresponding standard heat of formation of the oxide, CaO, from the elements is calculated to be −635.09 ± 0.89 kjoules/mole. This value agrees with the presently accepted value.

Introduction.—The data in the literature on the heat of combustion of calcium are very limited. Muthman, Weiss and Metzger[3] found a value of −162.64 kcal./mole for the heat of formation of CaO based on combustion measurements. This differs significantly from the value of −151.9 kcal./mole selected by the National Bureau of Standards[4] from results of solution calorimetry. Guntz and Benoit[5] were unable to get consistent results for the heat of combustion of calcium. Since calcium metal of high purity has been prepared in connection with the research program of this Laboratory, it was thought desirable to attempt an accurate measurement of its heat of combustion. The heat of formation of CaO derived from this value serves as an independent check of the value obtained from solution calorimetry.

Three independent series of combustion measurements on calcium metal have been carried out at this Laboratory. The first series, the results of which have been reported,[2] used calcium metal which had not been analyzed for oxygen or hydrogen. The resulting value for the heat of formation of CaO, −150.67 ± 0.21 kcal./mole, is believed to be too low on the basis of the present work. In the second series an attempt was made to analyze the calcium for oxygen using a method based on dissolution of the metal in mercury to effect a separation from an insoluble residue. The residue was analyzed for calcium and, after correction for CaC_2 and Ca_3N_2, the oxygen was determined by difference. This method could probably be developed to give reliable results as no fundamental difficulties appear to be involved. However, after the work had been completed an unexplained trend was discovered in the data[6] and it was decided to repeat the work. The repetition was desirable also because the calcium used in the second series contained several tenths of a per cent of oxygen. In the third series, calcium of very high purity was available and a recently reported method was used for analyzing for oxygen which is believed to be reliable within the limit of its sensitivity. The results of the third series are given in this paper.

(1) This work was performed under the auspices of the A.E.C.

(2) Presented in part before the Section on Physical and Inorganic Chemistry, 123rd Meeting A.C.S., Los Angeles, Calif., March 16, 1953.

(3) W. Muthman, L. Weiss and J. Metzger, *Ann.*, **355**, 137 (1907).

(4) Selected Values of Chemical Thermodynamic Properties, N.B.S. Circular 500, 1952, p. 386.

(5) A. Guntz and F. Benoit, *Ann. Chim.*, **20**, 5 (1923).

(6) We are indebted to Dr. Guy Waddington, Bureau of Mines, Bartlesville, Oklahoma, for pointing out this trend.

Method.—The method involved the determination of the heat evolved from the burning of a weighed sample of the metal in a bomb calorimeter at a known initial pressure of oxygen. The energy equivalent of the calorimeter was determined from the heat of combustion of benzoic acid (NBS sample 39g). The completeness of combustion was determined by treating the combustion products with 8 *N* hydrochloric acid and measuring the amount of hydrogen evolved from any unburned metal present.

The uncertainties given are twice the corresponding standard deviations.

The units of energy used are the absolute joule and the defined calorie: 1 defined calorie = 4.1840 absolute joules.

The unit of mass is the gram mass *in vacuo*. The calcium metal was weighed to the nearest 0.0001 g. The water for the calorimeter was weighed to the nearest 0.01 g.

Apparatus.—The details of the construction and calibration of the calorimeter have been described.[7] The bomb used in this work is the same as there described. Its volume is approximately 360 ml. The calorimeter can is new so that a redetermination of the energy equivalent was necessary. The energy equivalent of the calorimeter with oxygen at 25 atm. pressure was 10,006.0 ± 3.8 joules/degree, based on 22 runs. When calcium was burned at 25 atm. pressure the amount of unburned metal was quite large (up to 7%) so runs were made at 50 atm. oxygen pressure. The energy equivalent was redetermined at this pressure and was found to be 10,009.8 ± 3.8 joules/degree for 20 runs. The calculated value from the energy equivalent at 25 atm. and the specific heat of the extra oxygen at 50 atm. is 10,013.9 ± 3.8 joules/degree (V_{gas} = 355 ml.). For this work the average value of 10,011.8 ± 2.7 joules/degree was used.

Calcium Metal.—The calcium metal was in the form of chunks. It was analyzed at this laboratory with the following results: Mg, 0.01%; C, 0.011%; H, 0.025%; O, 0.02%; N, <0.001%. No other metallic impurities were present in amounts greater than 0.01%. The metallic impurities were determined spectroscopically, the nitrogen by a Kjeldahl method and the carbon and hydrogen by combustion. The oxygen was determined by the method of Eberle, Lerner and Petretic.[8] The method was tested by running known amounts of CaO and the accuracy was found to be about ±1 mg. of oxygen. Runs were made on the pure calcium metal with various size samples ranging from approximately 1 to 5 g. There did not appear to be any trend with sample size. The average value, based on the larger sized samples, was found to be 0.02 ± 0.03% indicating that the amount of oxygen present was about at the limit of detection.

This method does not distinguish between oxygen as oxide and oxygen as hydroxide. The amount of oxygen is small enough so that the uncertainty thus introduced is small.

If it is assumed that the non-metallic impurities are combined with the calcium and not with the magnesium, the material is 99.42 mole per cent calcium metal.

An X-ray pattern of the metal showed only lines of metallic calcium.

The calcium metal showed a slight gain in weight when exposed to oxygen at 50 atm. pressure, the gain amounting to 0.9 mg. for 0.8 g. of metal in one hour. Correction was made for this gain on the assumption that a proportional gain was made by the calcium in the bomb prior to firing.

Combustion of Calcium.—The calcium was burned as chunks on sintered discs of CaO supported on a platinum

(7) C. E. Holley, Jr., and E. J. Huber, Jr., *J. Am. Chem. Soc.*, **73**, 5577 (1951).

(8) A. R. Eberle, M. W. Lerner and G. J. Petretic, *Anal. Chem.*, **27**, 1431 (1955).

TABLE I

THE HEAT OF COMBUSTION OF CALCIUM

Mass Ca burned, g.	Wt. CaO, g.	Wt. Mg, g.	Joules/deg. total	ΔT, °K.	Energy, total	Energy from Firing, j.	Energy from Mg, j.	Energy from Ca, j.	Ca, j./g.	Dev. from mean
0.8047	26.6	0.0082	10044.5	1.2886	12943.3	12.1	202.3	12728.9	15818.2	2.4
.8225	26.5	.0076	10044.5	1.3164	13222.6	15.9	187.5	13019.2	15828.8	13.0
.7409	27.3	.00845	10045.4	1.1875	11928.9	13.5	208.4	11707.0	15801.1	14.7
.7937	26.4	.0081	10044.5	1.2703	12759.5	14.9	199.8	12544.8	15805.5	10.3
.8036	26.6	.00875	10044.5	1.2906	12963.4	16.9	215.8	12730.7	15842.1	26.3
.8268	18.5	.00835	10038.7	1.3231	13282.2	13.4	206.0	13062.8	15799.2	16.6
									Av. 15815.8	13.9
									Standard dev. of mean	7.0

platform weighing 103.8 g. Two discs were used for each run. The discs were made by mixing 1.5% of beeswax in CCl_4 with the ignited powder and pressing at 10,000 p.s.i. in a hardened steel die. Ignition for one-half hour in air at 1,650° followed. The oxygen used contained no detectable nitrogen. Pure magnesium was used for the fuse wire. Its measured heat of combustion was 24,667 joules/g.[7] The amount varied from 0.0076 to 0.0087$_5$ g. Even if a double oxide was formed from the magnesium and calcium oxides the amount of magnesium is believed to be too small for this reaction to produce any significant heat change. Correction was made for the electrical energy used in igniting the wire. The total energy equivalent of the calorimeter and contents was used taking into account the discs, the platinum, and the difference in energy equivalent between the calcium oxide formed and the oxygen used. Combustion varied from 99.49 to 99.96% of completion. The initial temperature was 24.9° and the average final temperature was 26.1°. The results of the six runs are listed in Table I. This average value of 15,816 ± 14 must be corrected for the impurities present.

Correction for Impurities.—It is assumed that the oxygen is present as CaO, the carbon as CaC_2 which burns to CaO and CO_2 which react further to give $CaCO_3$, and the hydrogen as CaH_2 which forms CaO and H_2O which react further to give $Ca(OH)_2$. The percentage composition of the metal by weight on this assumption is Ca metal 99.37; CaC_2, 0.029; CaH_2, 0.52; CaO, 0.07; Mg, 0.01. The heat of combustion, Q, for pure calcium metal, per gram, is obtained from the equation: $0.9937Q + 0.00029 \times 26{,}970 + 0.0052 \times 18{,}880 + 0.00010 \times 24{,}670 = 15{,}816$ joules where the first term is the heat from the pure calcium metal, the second term from the CaC_2, the third term from the CaH_2, and the fourth term from the Mg. The sum of these terms is equated to the observed heat of combustion. Heats of solution and of alloy formation are ignored. Final products of combustion are considered to be CaO, $CaCO_3$, $Ca(OH)_2$ and MgO. The heat of combustion for calcium metal is calculated to be 15,806.5 joules/g. An alternative assumption can be made that the oxygen, with part of the hydrogen, exists as $Ca(OH)_2$ but this gives only a slightly different result. The correction due to impurities amounts to 0.06% of the uncorrected value.

Calculation of the Uncertainty.—The uncertainty to be attached to the corrected value includes the uncertainty in the determination of the energy equivalent which is 0.03%, the uncertainty in the calorimetric measurements which is 14.0 joules/g. or 0.09% and the uncertainty introduced in the correction for the impurities.

The main uncertainty introduced in the correction for the impurities is the accuracy of the analyses. The C and H are estimated to be correct to 2%, the O as discussed above, and the Mg to 50%. If the amounts of impurities are increased by the above percentages and the heat of combustion recalculated, the value 15,822 joules/g. is obtained. On this basis, the uncertainty introduced in the correction is the difference between 15,822 and 15,806 or 16 joules/g. which is 0.10%. There are additional small uncertainties which have been discussed above.

Combining these uncertainties, the over-all uncertainty = $\sqrt{0.03^2 + 0.09^2 + 0.10^2} = 0.14\%$ = 22 joules/g. The final corrected value is 15,806.5 ± 22 joules /g. for the heat of combustion of calcium metal in oxygen at 50 atm. pressure.

Composition of Calcium Oxide.—The CaO formed in some of the combustions was tested for the presence of CaO_2 by dissolving the combustion products in a solution containing 25 ml. of 12 N HCl, 2 g. of KI, 75 ml. of H_2O and 3 drops of 3% ammonium molybdate solution and titrating with standardized sodium thiosulfate solution to the starch end-point. The sensitivity of this method was estimated to be 0.0005 g. of CaO_2. No CaO_2 was found.

An X-ray examination of the combustion products showed only lines of CaO.

Heat of Formation of Calcium Oxide.—The heat of combustion reported above gives, for the reaction in the bomb, a value of $\Delta E_{24.9°} = -633.52 \pm 0.89$ absolute kjoules/mole. The correction of this value of 25° is less than the uncertainty in the result. To obtain the heat of formation it is necessary to correct for the deviation of oxygen from the perfect gas law and to convert from ΔE to ΔH. Using Rossini and Frandsen's[9] value of $(\partial \Delta E/\partial P)_{301°K.} = -6.51$ joules/atm./mole for oxygen, and taking $\Delta H = \Delta E + \Delta(PV)$, we have for the heat of formation of CaO, $\Delta H_{25°} = -635.09 \pm 0.89$ absolute kjoules/mole. In defined calories this is -151.79 ± 0.21 kcal./mole and agrees with the value, -151.9 kcal./mole, given in "Selected Values of Chemical Thermodynamic Properties."[4]

Acknowledgments.—The authors wish to express their thanks to W. J. McCreary for preparing the calcium metal. They also wish to acknowledge the valuable assistance of Jackson E. Harrar and Mary Repar Kline who did the analyses of the calcium metal for oxygen and E. L. Head, F. H. Ellinger, E. Van Kooten, E. Cramer and J. Pena in the other analytical work.

(9) F. D. Rossini and M. Frandsen, *J. Research Natl. Bur. Standards*, **9**, 733 (1932).

NOTES

CONCENTRATION EFFECTS ON SOLVENT EXTRACTION COEFFICIENTS OF SOME TRIVALENT METAL HALIDES[1a,b]

By Jerome Saldick[2]

Contribution from the Department of Chemistry, Brookhaven National Laboratory, Upton, N. Y.

Received August 17, 1955

The deviation from the Nernst distribution law shown by the hydrochloric acid: ferric chloride:isopropyl ether extraction system (*i.e.*, increase of extraction coefficient with increase of ferric concentration)[3] has been clearly explained[4,5] in terms of ion triplet formation in the organic phase. Conductivity phenomena observed in the organic phase and viewed in the light of the work of Fuoss and Kraus[6] form the basis for the ion association viewpoint.

Other trivalent metals whose halides extract together with one molecule of HCl or HBr, such as gold, gallium, thallium and indium, behave in a similar manner at high concentrations.[3]

The conductivity data of Campbell[4] also show that the $HFeCl_4$ species dissociates into ions in the organic phase in very *dilute* solution. This dissociation should produce an increase in the over-all metal extraction coefficient at very low ferric concentrations by decreasing the activity (per unit of total iron concentration) of the undissociated $HFeCl_4$ species in the organic phase, as shown below.

In the case of In(Br), Au(Cl), Tl(Cl) and Ga(Cl and Br), recent work by Irvine and co-workers[7] has shown that the extraction coefficients $E_{org/aq}$ of the metals in ether extraction from strong HCl and HBr solutions do increase as the metal concentrations in the aqueous phase decrease below approximately 10^{-3} M, approaching an upper limit at concentrations below 10^{-6} M. The addition of extractable acids (such as perchloric) to these systems suppresses this increase of $E_{org/aq}$ at low metal concentrations. If, as believed, these effects are due to ionic dissociation in the organic phase, the ferric system should behave in a similar fashion.

The Extraction Coefficient, $E_{org/aq}$.—Consider the organic phase to contain metal as undissociated HMX_4 species and as dissociated H^+ and MX_4^- ions (neglecting the details of hydration[4,5]). The chemical potentials of the HMX_4 species in the aqueous and organic phases are the same at equilibrium. For a given activity of HMX_4 species in the organic phase, the total metal concentration in that phase will be greater, the greater the extent of dissociation. For the sake of simplification, assume that the total concentration of HX in the aqueous phase is constant, and so large that changes in the metal concentration will not significantly affect the ionic strength. Under these conditions, the activity of the HMX_4 species in the aqueous phase is proportional to the sum of the concentrations of all metal-containing species present, $\Sigma(M)_w$, regardless of what they may be, provided only that each contains only one metal atom. Then

$$K_1\Sigma(M)_w = (HMX_4)_0 \qquad (1)$$

Parentheses refer to concentrations. The subscripts w and 0 refer to the aqueous and organic phases. K_1, defined as written, is not a true equilibrium constant; it is a product of thermodynamic equilibrium constants, appropriate activity coefficients, and, when necessary, also the activities of those species in the aqueous phase, such as H^+, X^- and HX, which are assumed to be *constant*. For example, K_1 includes the thermodynamic equilibrium constants of all the pertinent equilibria in the aqueous solution, the pertinent activity coefficients, the (constant) concentrations of H^+ and X^- in the aqueous phase, and also the activity coefficient of undissociated HMX_4 (which may be an ion pair) in the organic phase.

The effect of an extractable acid HY in the system (present in concentrations small enough that the ionic strength and acidity in the aqueous phase, fixed by the HX present, are not affected) comes into consideration when the important dissociations in the organic phase

$$HMX_4 \rightleftharpoons H^+ + MX_4^-$$
$$HX \rightleftharpoons H^+ + X^-$$
$$HY \rightleftharpoons H^+ + Y^-$$

are described by equilibrium equations

$$(HMX_4)_0 = K_2(H^+)_0(MX_4^-)_0 \qquad (2)$$
$$(HX)_0 = K_3(H^+)_0(X^-)_0 \qquad (3)$$
$$(HY)_0 = K_4(H^+)_0(Y^-)_0 \qquad (4)$$

The partition coefficient is

$$E_{0/w} = \frac{(MX_4^-)_0 + (HMX_4)_0}{\Sigma(M)_w} = \frac{K_1}{K_2(H^+)_0} + K_1 \qquad (5)$$

The relation

$$(H^+)_0 = (MX_4^-)_0 + (X^-)_0 + (Y^-)_0 \qquad (6)$$

is a statement of over-all electrical neutrality.

Then

$$(H^+)_0 = \frac{K_1\Sigma(M)_w}{K_2(H^+)_0} + \frac{(HX)_0}{K_3(H^+)_0} + \frac{(HY)_0}{K_4(H^+)_0} \qquad (7)$$

Assuming that $(HX)_0$ depends only on HX in the aqueous phase, and is constant, $K_3' = (HX)_0/K_3$.

(1) (a) Research performed under the auspices of the U. S. Atomic Energy Commission. (b) Presented before the Division of Physical and Inorganic Chemistry at the 126th National Meeting of the A.C.S., September, 1954.

(2) General Electric Co., ANPD, Cincinnati, Ohio.

(3) N. H. Nachtrieb and R. E. Fryxell, *J. Am. Chem. Soc.*, **74**, 897 (1952). This paper also contains references to earlier work in this field.

(4) D. E. Campbell, AECU 2313. Ph.D. thesis, Rensselaer Polytechnic Institute, Troy, N. Y., 1952.

(5) A. H. Laurene, AECU 2484. Ph.D. thesis, Rensselaer Polytechnic Institute, Troy, N. Y., 1952.

(6) R. M. Fuoss and C. A. Kraus, *J. Am. Chem. Soc.*, **55**, 21, 476, 1019, 2387, 3614 (1933).

(7) (a) R. H. Herber and J. W. Irvine, Jr., *ibid.*, **76**, 987 (1954); (b) R. H. Herber, W. E. Bennett, D. R. Bentz, L. C. Bogar, R. J. Dietz, Jr., G. S. Golden and J. W. Irvine, Jr., paper presented before the Division of Physical and Inorganic Chemistry at the 126th National Meeting of the A.C.S., September, 1954.

Similarly, since the partition equilibrium of HY is described by equation 8

$$K_5(H^+)_w(Y^-)_w = (HY)_0 \quad (8)$$

and since $(H^+)_w$ is controlled by the HX, we may write $K_5' = K_5(H^+)_w$. Solving for $(H^+)_0$

$$(H^+)_0 = \left(\frac{K_1\Sigma(M)_w}{K_2} + K_3' + \frac{K_5'(Y^-)_w}{K_4}\right)^{1/2} \quad (9)$$

and substituting in (5) gives

$$E_{0/w} = \frac{K_1}{K_2}\left(\frac{K_1\Sigma(M)_w}{K_2} + K_3' + \frac{K_5'(Y^-)_w}{K_4}\right)^{-1/2} + K_1 \quad (10)$$

which is of the form

$$E = A + \frac{B}{\sqrt{1 + C\Sigma(M)_w}} \quad (10a)$$

where

$$A = K_1,\ \frac{AC}{B^2} = K_2,\ B = \frac{K_1}{K_2}\left(K_3' + \frac{K_5'(Y^-)_w}{K_4}\right)^{-1/2}$$

$$C = \frac{K_1}{K_2}\left(K_3' + \frac{K_5'(Y^-)_w}{K_4}\right)^{-1}$$

$$\frac{B}{C} = \left(K_3' + \frac{K_5'(Y^-)_w}{K_4}\right)^{1/2}$$

Equation 10a shows that $E_{0/w}$ rises to a "high value" of $(K_1 + K_1/(K_2\sqrt{K_3'}))$ at low metal and Y^-_w concentrations, and decreases when these increase.

The point of inflection in the graph of E *vs.* log $\Sigma(M)_w$ occurs at

$$\Sigma(M)_w = \frac{2}{C} = \frac{2K_2}{K_1}\left(K_3' + \frac{K_5'(Y^-)_w}{K_4}\right) \quad (11)$$

At the point of inflection, in the absence of Y^-

$$\Sigma(M)_w = \frac{2K_2K_3'}{K_1} \propto \frac{(HMX_4)_w}{(H^+)_0(MX_4)_0} \Big/ \frac{(HX)_w}{(H^+)_0(X^-)_0} \quad (11a)$$

The numerator describes the partition of HMX_4, the denominator of HX. Both are moderately weak acids, hence the ratio and consequently the aqueous metal ion concentration at the point of inflection should not vary much with changes of the organic solvent. The experimental findings of Irvine, *et al.*, have shown that this is, indeed, descriptive of the behavior of these metals.[8]

K_3', K_4 and K_5' are independent of the metal present, and equation 10 contains only two parameters which depend on the metal species present. For a given solvent, the ratio B/C is a function of HX concentration only.

The ratio $K_5'/K_4 = (H^+)_0(Y^-)_0/(Y^-)_w$ which appears both in equation 10 describing the effect of $(Y^-)_w$ on E at constant $\Sigma(M)_w$ and in equation 11 describing the effect of $(Y^-)_w$ on $\Sigma(M)_w$ at the point of inflection may become accessible from data not involving metal extractions.[9]

Under certain conditions (*e.g.*, lower HX concentration) it may be also necessary to consider the equilibrium

$$(MX_3)_w \rightleftarrows (MX_3)_0$$

and

$$K_3'\Sigma(M)_w = (MX_3)_0$$

in addition to eq. 1. This seems to be true in the case of thallium,[10] for instance.

Activity coefficients of ions in the organic phase are factors in K_2, K_3 and K_4; these may not reasonably be expected to remain constant as the ionic strength of the organic phase changes. (The major contribution to the ionic strength in the organic phase comes from the H^+ and MX_4^- ions themselves in the absence of extractable HY). This effect may be expected to complicate quantitative application of equation 10, but is independent of solvent extraction processes and can in principle be understood.

The treatment above formally ascribes the variation in E to changes in the acidity in the organic phase. A thermodynamically similar development formally based on the equilibrium

$$(MX_4^-)_0 \rightleftarrows (MX_3)_0 + (X^-)_0$$

and formally stressing the effect of halide ions in the organic phase, leads to an equation identical with (10). However, other evidence[3,4] indicates that HMX_4 and MX_4^- are the significant species in the organic phase.

Acknowledgment.—The author wishes to thank Professor J. W. Irvine, Jr., for his coöperation in making the unpublished results of his group available and for helpful discussions, and Dr. R. W. Dodson for his encouragement and advice.

(8) J. W. Irvine, Jr., personal communication.

(9) Experiments performed by Dr. R. H. Herber show that the equivalent conductivity of $HClO_4$ extracted into ethers from aqueous solutions is distinctly higher than that of HCl.

(10) R. W. Dodson and R. D. Stoenner, private communication.

A NOTE ON THE OSMOTIC COEFFICIENTS OF AQUEOUS POTASSIUM CHLORIDE SOLUTIONS AT 25°

By R. A. Robinson

Department of Chemistry, University of Malaya, Singapore

Received October 10, 1955

Brown and Delaney[1] have recently described an ingenious method for measuring the vapor pressure lowering of an aqueous potassium chloride solution: the solution is maintained at 25° whilst the temperature of a sample of the solvent is progressively lowered until it registers the same vapor pressure, the equality of vapor pressure being judged by means of a sensitive interconnecting bellows pressure gage. Their experimental measurements were therefore temperature differences which were then converted into terms of vapor pressures by means of one of two relations between the temperature and the vapor pressure of pure water. Brown and Delaney expressed their results as osmotic coefficients, $\varphi = -(55.5062/2m)\ \ln P/P^0$, and gave a set of such coefficients over the range 0.025 to 2.38 M calculated by each method. Thus at 2.3783 M they found $\varphi = 0.9205$ or 0.9204 but at 0.02515 M, 0.9588 or 0.9659. This may suggest that the form of the relation between the vapor pressure of water and the temperature has great influence on the result. Nevertheless, because of the way in which the osmotic coefficient is defined, the effect of experimental error is considerably exaggerated for dilute solutions. Since an experi-

(1) O. L. I. Brown and C. M. Delaney, THIS JOURNAL, **58**, 255 (1954).

mental error in the measurement of the temperature difference is reflected in an almost directly proportional error in P/P^0, it is better to compare P/P^0 rather than φ as calculated by the two methods. I have therefore calculated P/P^0 from the φ values of Brown and Delaney and the results are given in Table I under the headings method I and method II. From an examination of the deviations of individual runs from the averages given in their Table II, it would seem that justice would be done to their work if we ascribed limits to their temperature measurements of $\pm 0.0002°$. This would correspond to approximately ± 0.00001 in P/P^0 whereas the average difference between Method I and Method II is 0.00004. Thus the method of calculation does introduce differences beyond the probable limits of experimental accuracy but not so very much greater.

It seemed worth while trying a third method of calculation based upon the equation of Keyes[2] for the vapor pressure of water

$$\log P^0 = -2892.3693/T - 2.892736 \log T - 4.9369728 \times 10^{-3}T + 5.606905 \times 10^{-6}T^2 - 4.645869 \times 10^{-9}T^3 + 3.7874 \times 10^{-12}T^4 + 19.3011421$$

In Table I the column headed method III gives the results calculated by this equation: it will be seen that they are in good agreement with the second method of Brown and Delaney. Under earlier data (a) I give some values of P/P^0 interpolated from the data of Gordon, *et al.*,[3] for concentrations below 0.1 M whilst those above 0.1 M are interpolated from a set of "best values" previously advanced.[4] The final column contains values calculated from some more recent computations of Guggenheim and Turgeon.[5] The maximum difference in P/P^0 is only 0.00006, the average is 0.00002, and it may be concluded that the measurements of Brown and Delaney are in excellent agreement with other data.

TABLE I

P/P^0 FOR POTASSIUM CHLORIDE SOLUTIONS AT 25°

m	Method I	Method II	Method III	Earlier data (a)	Earlier data (b)
0.02515	0.99913	0.99912	0.99912	0.99914	0.99913
.04445	.99848	.99847	.99847	.99849	.99847
.05621	.99810	.99808	.99808	.99810	.99807
.08020	.99732	.99730	.99730	.99731	.99727
.1210	.99602	.99598	.99598	.99600	
.1901	.99384	.99379	.99379	.99376	
.3180	.98977	.98970	.99969	.99968	
.4254	.98642	.98633	.98632	.98629	
.6025	.98081	.98072	.98070	.98070	
.7741	.97547	.97538	.97536	.97530	
1.8631	.94077	.94077	.94072	.94078	
2.3783	.92415	.92416	.92409	.92411	

(2) F. G. Keyes, *J. Chem. Phys.*, **8**, 602 (1947).

(3) W. J. Hornibrook, C. J. Janz and A. R. Gordon, *J. Am. Chem. Soc.*, **64**, 513 (1942).

(4) R. A. Robinson, *Trans. Roy. Soc. New Zealand*, **75**, 203 (1945); R. H. Stokes and B. J. Levien, *J. Am. Chem. Soc.*, **68**, 333 (1946); R. A. Robinson and R. H. Stokes, "Electrolyte Solutions," Butterworths Scientific Publications, London, 1955, p. 461.

(5) E. A. Guggenheim and J. C. Turgeon, *Trans. Faraday Soc.*, **51**, 747 (1955).

PRESSURE–COMPOSITION–TEMPERATURE RELATIONS IN THE PALLADIUM–HYDROGEN SYSTEM

BY KENNETH A. MOON

Contribution from Ordnance Materials Research Office, Watertown Arsenal, Watertown, Mass.

Received October 11, 1955

Passivity of palladium to hydrogen and hysteresis in the pressure–composition isotherms have been attributed by some[1] to the necessity of opening rifts in the metal in and along which dissolution of the hydrogen occurs. Others[2-4] have believed that the palladium–hydrogen alloys are normal homogeneous solutions and passivity has been attributed[5] to surface effects and hysteresis[6,7] to sluggishness of recrystallization. In view of the widespread current interest in metal–hydrogen systems and the continuing prevalence of the rift concept, it seems worthwhile to point out that the most reliable equilibrium pressure–composition–temperature measurements in the palladium–hydrogen system are consistent with the belief that the alloys are normal homogeneous solutions.

Figure 1 shows a projection of the pressure–composition–temperature surface constructed from data given in the literature.[8-11] There is a critical point at 295° and 20 atm., below which lies a univariant region where two phases are in equilibrium, both with face-centered cubic arrangement of the metal atoms. Lacher[2] has given a simple statistical mechanical interpretation of the equilibrium pressure–composition–temperature relationships, based on the assumptions that hydrogen atoms can be accommodated in the lattice up to a limiting concentration of 0.59 atoms per palladium atom; that each pair of nearest neighbor hydrogen atoms contributes a fixed amount of interaction energy regardless of the distribution of other hydrogen atoms; that the distribution of hydrogen atoms is random; and that the partition function of solute hydrogen atoms, relative to the lowest energy dissolved state, is independent of concentration. Rather good agreement between theory and experiment was obtained when the parameters in the theory were evaluated at the critical composition.

The success of Lacher's treatment is strong evidence against the rift concept, but this has been generally overlooked in the American literature. Lacher's approach can be supplemented with a phenomenological treatment of the data for the α alloys. The change of state is

$$\tfrac{1}{2}H_2(g) + 1/m\ Pd(s) = Pd_{1/m}H(s,\alpha), \qquad (1)$$

(1) D. P. Smith, *Phil. Mag.*, [7] **39**, 477 (1948).

(2) J. R. Lacher, *Proc. Roy. Soc. (London)*, **161A**, 525 (1937).

(3) C. Wagner, *Z. physik. Chem.*, **193**, 407 (1944).

(4) L. Pauling and F. J. Ewing, *J. Am. Chem. Soc.*, **70**, 1660 (1948).

(5) E. A. Gulbransen and K. F. Andrew, *J. Electrochem. Soc.*, **101**, 348 (1954).

(6) E. A. Owen, *Phil. Mag.*, [7] **35**, 50 (1944).

(7) C. Wagner, *Z. physik. Chem.*, **193**, 386 (1944).

(8) L. J. Gillespie and F. P. Hall, *J. Am. Chem. Soc.*, **48**, 1207 (1926).

(9) L. J. Gillespie and L. S. Galstaun, *ibid.*, **58**, 2565 (1936).

(10) A. Sieverts and G. Zapf, *Z. physik. Chem.*, **174A**, 359 (1935).

(11) P. S. Perminov, A. A. Orlov and A. N. Frumkin, *Doklady Akad. Nauk S.S.S.R.*, **84**, 749 (1952); *C. A.*, **46**, 10796c (1952).

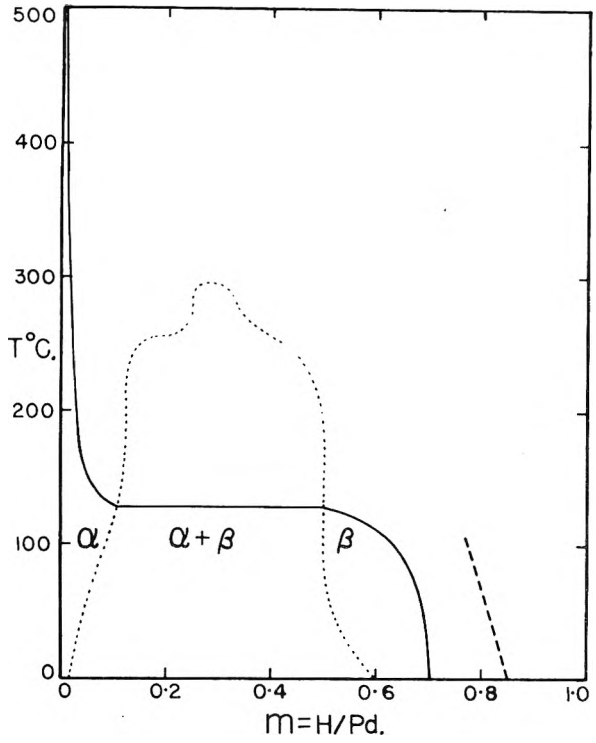

Fig. 1.—Phase relationships in the palladium–hydrogen system. The solid line is the one atmosphere isobar, constructed from data given by Gillespie, *et al.*, and Sieverts and Zapf. The dotted line, taken from Gillespie, *et al.*, is the locus of the univariant portions of the isobars from 0.004 to 20 atm. The dashed line is a portion of the 500 atm. isobar, estimated from the equations given by Perminov, *et al.*

and by definition

$$\log (p^{1/2}/m) = -\log K + \log(a/m) \qquad (2)$$

where K is the equilibrium constant for reaction 1, p is the equilibrium hydrogen pressure, m is the concentration of solute hydrogen in atom ratio H/Pd, and a is the corresponding activity. This assumes that hydrogen gas is ideal and that the activity of solvent palladium is unity. The logarithm of the activity coefficient of a dilute solute may usually be expressed as a power series in the concentration, so that equation 2 may be rewritten

$$\log(p^{1/2}/m) = -\log K + \beta m + \gamma m^2 + \ldots . \qquad (3)$$

The amenability of the p, m, T data to analysis in terms of this equation with satisfactory values of K, β, γ, etc., may be used as a test of the data as well as a criterion for normalcy of the solution. Accordingly, an attempt was made to fit all the data in the literature to equation 3, subject to the conditions that log K must be a linear function of reciprocal temperature and β, γ, etc., must be smooth functions of temperature. It was found that only the work of Gillespie and of Sieverts was amenable to this treatment. Figure 2 shows the results of Gillespie, *et al.*,[8,9] and of the one study by Sieverts[12] that fell in the same temperature range. It is seen that within the apparent experimental error, terms in powers of m beyond the first may be neglected. Careful smoothing of log K and β led to the relations

$$\log K = -4.200 + 521.9/T \qquad (4)$$

$$\beta = -926/(T - 215) \qquad (5)$$

For these equations pressure is in mm. of mercury and temperature is in degrees Kelvin. The parameter β was first smoothed graphically, and it was

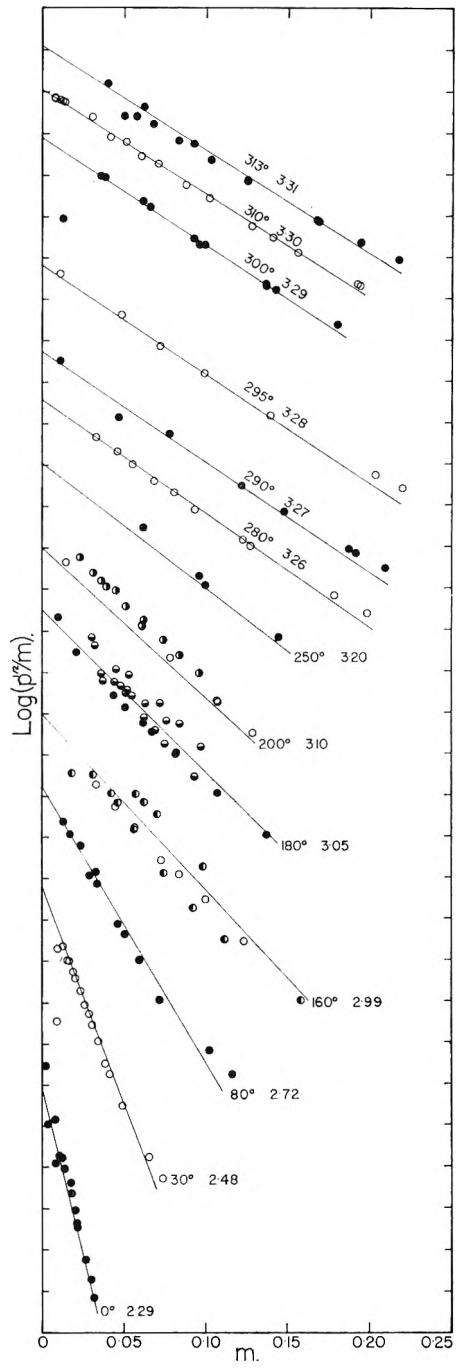

Fig. 2.—Isotherms for α palladium–hydrogen solutions. Open circles and filled circles are experimental results of Gillespie, *et al.* Half-filled circles are results of Bruning and Sieverts. The straight lines represent a smoothing of all the data in terms of four parameters as described in the text. Annotations give the temperature (°C.) and the numerical value of the intercept. One division on the vertical axis is 0.1 unit. Pressure p is in mm. of mercury and concentration m is in atom ratio H/Pd.

(12) H. Bruning and A. Sieverts, *Z. physik. Chem.*, **163A**, 409 (1933).

later discovered that a function of the form (5) could be fitted with only minor adjustments.

The straight lines in Fig. 2 were calculated from equations 4 and 5, and the good agreement between lines and points indicates that α palladium–hydrogen alloys are indeed true homogeneous solutions.[13] In rejecting the rift concept as a major feature of the palladium–hydrogen system, it is not intended to imply that segregation of solute atoms to disrupted areas of a solid (*i.e.*, "rifts") does not occur. On the contrary, interactions between solute atoms and dislocations, grain boundaries, etc., in a metal are of great metallurgical importance. However, the bulk extent of such effects is small and, from the physicochemical point of view, these effects are important only when the true solubility is very low.

(13) Recent neutron diffraction studies in this system conducted at Oak Ridge by C. G. Shull and co-workers have shown that the hydrogen atoms in the β solution occupy the octahedral interstitial sites in the metal structure. (J. Worsham, Thirteenth Annual Pittsburgh Diffraction Conference Meeting of the Joint American Crystallographic Association, Nov., 1955.)

VAPOR PRESSURES OF PERFLUOROPENTANES[1]

By Eugene John Barber and George H. Cady

Department of Chemistry, University of Washington, Seattle, Washington

Received October 14, 1955

The liquid–vapor equilibrium still described in an earlier report[2] has been used to measure the vapor pressures of pure perfluoropentanes which have also been described.[3,4] A sample of the fluorocarbon was boiled in the still under a constant pressure measured with a precision of 0.07 mm., and the temperature of the vapor escaping from the liquid was measured with a precision of 0.01°. To test the maximum error of the experimental method, the vapor pressure of water was measured over the range 155 to 2276 mm. Assuming the pressure readings to be correct, the probable error in the observed temperature reading was 0.04°. The greatest difference between an observed temperature and the corresponding temperature as interpolated from the table of precise vapor pressures in Lange's Handbook[5] was 0.12°. The vapor pressure of pure carbon tetrachloride was also measured and found to agree well with the vapor pressure equation of Scatchard, *et al.*,[6] as shown in Table I.

Observed vapor pressures of the fluorocarbons are given in Tables II to V.

Using these data and the method of least squares, equations have been established in the form

$$\log_{10} P_{mm} = A - \frac{B}{T} - \frac{C}{T^2}$$

Values for the constants A, B and C are given in Table VI. The absolute temperature, T, uses 273.16°K. as equivalent to 0°C.

Table I

Comparison of Observed Vapor Pressure of CCl_4 with Pressure Calculated from Scatchard's Equation

Temp., °C.	Obsd. pressure, mm.	Calcd. pressure, mm.
25.75	116.4	117.7
50.82	320.7	321.6
59.82	441.1	441.7
76.66	760.5	759.8

Table II

Vapor Pressure of Perfluoro-*n*-pentane (n-C_5F_{12})

Pressure, mm. at 0°	Temp., °C.	Pressure, mm. at 0°	Temp., °C.
347.56	9.67	1357.4	46.09
395.99	12.70	1574.5	50.80
447.94	15.68	1809.6	55.31
497.16	18.25	1801.0	54.94
547.68	20.69	1789.5	54.93
624.20	24.10	1976.2	58.28
743.95	28.74	2175.3	60.76
940.5	35.28	2391.5	64.79
1149.0	41.12		

Table III

Vapor Pressure of Perfluoroisopentane (iso-C_5F_{12})

Pressure, mm. at 0°	Temp., °C.	Pressure, mm. at 0°	Temp., °C.
458.41	16.96	1038.0	38.96
508.62	19.55	1162.3	42.35
558.09	21.92	1315.9	46.11
622.70	24.75	1473.2	49.64
675.71	26.97	1616.1	52.64
748.88	29.74	1755.8	55.39
771.30	30.54	1911.6	58.17
851.3	33.29	2087.5	61.23
927.5	35.73	2287.2	64.50

Table IV

Vapor Pressure of Perfluorocyclopentane (C_5F_{10})

Pressure, mm. at 0°	Temp., °C.	Pressure, mm. at 0°	Temp., °C.
618.29	17.06	1397.5	40.01
689.82	19.95	1531.7	42.82
761.55	22.57	1709.5	46.29
866.8	26.10	1883.6	49.42
967.3	29.12	2082.3	52.75
1079.9	32.25	2305.2	56.18
1224.7	35.96		

Table V

Vapor Pressure of Nonafluorocyclopentane (C_5F_9H)

Pressure, mm. at 0°	Temp., °C.	Pressure, mm. at 0°	Temp., °C.
322.87	17.00	1118.8	49.86
369.97	20.15	1243.0	53.05
424.50	23.49	1387.5	56.43
482.53	26.67	1526.4	59.48
544.98	29.73	1704.6	63.09
618.48	33.07	1919.5	67.05
695.36	36.18	2114.0	70.39
765.92	38.86	2308.3	73.50
858.6	42.08	2391.9	74.78
980.4	45.85		

(1) From the Ph.D. thesis of E. J. Barber, University of Washington, 1948.

(2) E. J. Barber and G. H. Cady, *J. Am. Chem. Soc.*, **73**, 4247 (1951).

(3) E. J. Barber, L. L. Burger and G. H. Cady, *ibid.*, **73**, 4241 (1951).

(4) L. L. Burger and G. H. Cady, *ibid.*, **73**, 4243 (1951).

(5) N. Lange, "Handbook of Chemistry," 2nd Ed., Handbook Publishers, Inc., Sandusky, Ohio, 1937.

(6) G. Scatchard, S. Wood and J. Mochel, *J. Am. Chem. Soc.*, **61**, 3206 (1939).

TABLE VI

CONSTANTS FOR VAPOR PRESSURE EQUATIONS

Compound	A	B	C	Range, mm.
n-C_5F_{12}	6.88375	961.192	75512.4	400–2400
iso-C_5F_{12}	6.77319	904.909	83581.8	450–2300
cyclo-C_5F_{10}	6.98522	1013.820	59041.9	600–2300
cyclo-C_5HF_9	6.77003	897.684	98217.8	300–2400

From the vapor pressures, the boiling points at one atmosphere have been obtained. The heats of vaporization also have been calculated using the Clapeyron equation

$$\Delta H_v^T = -\frac{2.303 \times 24.06}{760 \times 10^3} \times \frac{P(V_g - V_l)}{T} \times \frac{d \log_{10} P}{d \frac{1}{T}}$$

in which ΔH_v^T is the heat of vaporization in cal. per mole at temperature T, P is the pressure in mm. and V_g and V_l are the molar volumes of vapor and liquid in milliliters, respectively. The molar volumes of the liquids were calculated from their densities[4] and the molar volumes of the vapors were estimated from the best known behavior of fluorocarbon vapors. Details of the method of estimation are described in the thesis of one of the authors.[1] The "solubility parameter" at 25°, that is the square root of the energy of vaporization per cc. of liquid $(\Delta E_v/V)^{1/2}$ was also calculated. All of these quantities are recorded in Table VII.

TABLE VII

SOME PHYSICAL CONSTANTS OF FLUOROCARBONS

Substance	B.p. at 760 mm., °C.	ΔH_v at 25°, cal.	ΔH_v at 40°, cal.	ΔH_v at b.p., cal.	$\left(\frac{\Delta E_v}{V}\right)^{1/2}$ at 25° (cal./ml.)$^{1/2}$
n-C_5F_{12}	29.32	6565	6360	6510	5.77
iso-C_5F_{12}	30.12	6560	6345	6490	5.86
cyclo-C_5F_{10}	22.48	6275	6070	6305	6.09
cyclo-C_5HF_9	38.65	7015	6795	6815	6.59

Because of uncertainty about the magnitude of V_g, the error in ΔH_v^T may be as much at 100 cal. per mole. Since an error made for one substance would also be made for another, it is unlikely that differences between the above ΔH values are in error by more than about 10 to 20 cal. per mole.

Acknowledgment.—This work was performed under contract with the Office of Naval Research.

SOME PHYSICAL PROPERTIES OF TUNGSTEN HEXAFLUORIDE[1]

BY EUGENE JOHN BARBER AND GEORGE H. CADY

Department of Chemistry, University of Washington, Seattle, Washington

Received October 14, 1955

In order that liquid–vapor equilibria of systems of tungsten hexafluoride and fluorocarbons might be investigated[2,3] it was first necessary that tungsten hexafluoride be prepared and that some of its physical properties be studied. The fluoride was formed by treating pure tungsten with fluorine in a tube held at 350 to 400°. The product was then purified by three simple distillations over anhydrous potassium fluoride following the technique of Priest and Schumb.[4]

A time *vs.* temperature warming curve from −175 to 8° was run using the modified Skau[5] apparatus described by Burger.[6] Two "breaks" were found in the curve. One corresponded to the melting point at 2.0 ± 0.3° and the other to a transition point at −8.2 ± 0.1°. A melting point of 2.3° was found by Ruff and Ascher[7] but the transition point has not been reported previously. From the warming curve, the heats of transition and fusion are estimated to be approximately 1600 ± 300 cal. per mole and 500 ± 100 cal. per mole, respectively. Ruff and Ascher[7] gave a difference in heats of sublimation and vaporization of 2.4 kcal. per mole.

The vapor pressure of tungsten hexafluoride has been determined using the same method as that described in the note which immediately precedes this. Results are contained in Table I.

TABLE I

VAPOR PRESSURE OF TUNGSTEN HEXAFLUORIDE

Pressure, mm. at 0°	Temp., °C.	Pressure, mm. at 0°	Temp., °C.
619.64	11.83	1401.6	34.20
701.68	15.00	1542.7	37.11
762.29	17.15	1674.8	39.65
831.9	19.46	1799.1	41.90
929.7	22.42	1935.3	44.20
1029.2	25.24	2088.9	46.72
1134.1	27.99	2247.8	49.13
1244.9	30.74	2403.5	51.38

These data correspond to the equation

$$\log_{10} P_{mm} = 6.88699 - \frac{928.580}{T} - \frac{67942.9}{T^2}$$

From the vapor pressures, the boiling point at 760 mm. is found to be 17.06 ± 0.05° (lower than 17.5° reported by Ruff and Ascher). From the vapor pressures and the Clapeyron equation, together with reasonable assumptions about constants of the van der Waals equation of state for the vapor, the heat of vaporization per mole has been calculated to be 6150 cal. at 25°, 5930 cal. at 40° and 6245 cal. at the boiling point. The "solubility parameter," $(\Delta E_{vap}/V)^{1/2}$, was found to be 7.96 (cal. ml.$^{-1}$)$^{1/2}$ at 25°.

Ruff and Ascher[7] have measured the vapor pressure of solid tungsten hexafluoride and of the liquid up to a pressure of 700 mm. They considered only one solid phase to be present and were unaware of the transition point at −8.2°. If one uses their data to plot log P_{mm} *vs.* $1/T$, he finds evidence for a break in the curve at −8.2° as well as at 2.3° (their melting point). From their data for the solid the following equations for vapor pressures have been determined.

From −8.2° to 2.3°

$$\log_{10} P_{mm} = 8.1847 - \frac{1533.1}{T}$$

(1) From the Ph.D. thesis of E. J. Barber, University of Washington, 1948.

(2) E. J. Barber and G. H. Cady, *J. Am. Chem. Soc.*, **73**, 4247 (1951).

(3) Gilson H. Rohrback and G. H. Cady, *ibid.*, **73**, 4250 (1951).

(4) H. Priest and W. C. Schumb, *ibid.*, **70**, 2291 (1948).

(5) E. L. Skau, *Proc. Am. Acad. Sci.*, **67**, 551 (1932).

(6) L. L. Burger and G. H. Cady, *J. Am. Chem. Soc.*, **73**, 4243 (1951).

(7) O. Ruff and E. Ascher, *Z. anorg. allgem. Chem.*, **196**, 413 (1931)

Below −8.2°

$$\log_{10} P_{mm} = 10.0682 - \frac{2032.2}{T}$$

The slopes of these curves give a heat of transition of 2290 cal. per mole and a heat of fusion of 510 cal. per mole. These may be compared with the 1600 and 500 cal. per mole values given above.

Acknowledgment.—This work was done under contract with the Office of Naval Research.

VARIATION OF SEDIMENTATION CONSTANT WITH FIELD AND TEMPERATURE FOR NATURALLY OCCURRING POLYELECTROLYTES[1]

By D. A. I. Goring and Carol Chepeswick

Maritime Regional Laboratory, National Research Council, Halifax, N. S.

Received October 21, 1955

In the course of ultracentrifugal studies on sodium desoxyribonucleate (DNA), carrageenate[2,3] and alginate,[3,4] certain careful experiments were done to test the dependence of sedimentation rate on the centrifugal field and temperature. This is a brief report of the findings.

Experimental

Sodium carrageenate was extracted at 60° from the seaweed, *Chondrus crispus*, by the method reported previously.[2] Its intrinsic viscosity in acetate buffer (*p*H 5.5; $I = 0.05$) was 24 g.$^{-1}$ dl.

Sodium alginate was prepared by dialysis from a commercial sample previously described[4] as C-1. Its intrinsic viscosity in acetate–NaCl buffer (*p*H 5.5; $I = 0.15$) was 19.2 g.$^{-1}$ dl.

The preparation of the DNA has been given previously.[5] The sample was described as TNA-V.

Sedimentation was measured in a Spinco ultracentrifuge at room temperature or at 40–50° by warming the rotor and the cell.[2] At room temperature, the fixed couple readings increased 2–3° during the run. A similar decrease was noted at the higher temperatures. The mean of the fixed couple readings was corrected by the difference between the fixed and the free couple at the end of the run. Sedimentation constants were corrected to a solvent of pure water at 25° in the usual manner.

Polyelectrolytes were dissolved either in sodium acetate–NaCl buffer of ionic strength, $I = 0.15$ and *p*H 5.5 or a sodium phosphate buffer with $I = 0.002$ and *p*H 6.5.

In studying variation of field runs were carried out alternately at two speeds in series of 4 or 6 on samples of a single solution. The smallest concentration of solute consistent with sustained clarity of the diagrams was chosen by trial and error. Choice of conditions was particularly critical for measurements at low ionic strength. By use of a flat and a wedge cell, a solution and a control were co-sedimented. The ratio s/s_c was obtained where s_c was the sedimentation constant for the control. Errors due to rotor expansion, variation of speed or incorrect determination of temperature were thereby compensated. In the early runs edestin[6] (prepared in a monodisperse form from hemp seed) was used as the control. For this, almost spherical, molecule it was assumed that the rate of sedimentation was independent of the speed of centrifugation. With edestin as control, s was found independent of field for sodium carrageenate in the sodium acetate–NaCl buffer. Such solutions were therefore used as controls in the later runs at low ionic strength.

In studying the effect of temperature, measurements were made alternately at room temperature and 50° in series of four, with two at each temperature. The concentration of solute was 0.1%.

Results and Discussion

As shown in Table I, the ratios s/s_c are essentially constant for wide variations in field. The small differences observed could be due to experimental error. The invariance remains at low ionic strength when the molecule is considerably extended. These results suggest that no perceptible orientation of the molecule occurs as a result of the increase in the centrifugal field. Koenig and Perrings[7] have noted a similar invariance of s with field for DNA in 0.2 *M* NaCl. However, these authors claim a significant variation of s with field for bovine fibrinogen[8] and plasma albumin.[9]

Table I

Variation of s/s_c with Field

Polyelectrolyte	Concn., %	I	Field × 10^{-3} g	s/s_c	Mean dev., %
Carrageenate	0.03	0.15	44	0.525	0.6
			260	0.526	0.9
Carrageenate	0.03	0.002	63	0.614	0
			260	0.628	0.6
DNA	0.02	0.002	63	0.416	1.9
			260	0.434	0.9

An interesting effect was found with DNA. At high speeds the peak was sharp while at low speeds the peak appeared more diffuse. If, in a single run, the speed was reduced for a time and again increased the peak was alternately—sharp, diffuse and again sharp. This effect was observed and photographed in several experiments. The sedimentation constants corresponding to the three steps of the run agreed within ±5%. Evidently some property of the boundary varied reversibly with speed, although s remained unchanged.

Table II

Variation of Sedimentation Constant with Temperature

Polyelectrolyte	I	Temp., °C.	s°_{25}, S	Mean dev., %
Carrageenate	0.15	48.4	4.46	1.6
	0.15	28.6	4.59	2.4
	0.002	48.4	1.56	5.1
	0.002	28.6	1.27	4.7
Alginate	0.15	47.6	2.90	0.7
	0.15	28.0	2.67	1.9
	0.002	47.6	1.15	0.2
	0.002	28.0	0.96	3.6

The variation of s°_{25} with temperature is given in Table II. At $I = 0.15$ there was no significant change for carrageenate or alginate. At $I = 0.002$ there was a marked increase of s_{25} with temperature. Koenig and Perrings have found similar but smaller trends for DNA[7] and bovine

(1) Issued as N.R.C. No. 3884.

(2) D. A. I. Goring and E. G. Young, *Can. J. Chem.*, **33**, 480 (1955).

(3) D. A. I. Goring and Carol Chepeswick, *J. Colloid Sci.*, **10**, 440 (1955).

(4) D. L. Vincent, D. A. I. Goring and E. G. Young, *J. Appl. Sci.*, **5**, 374 (1955).

(5) A. M. Marko and G. C. Butler, *J. Biol. Chem.*, **190**, 165 (1951). The authors are indebted to Dr. Marko for providing the DNA.

(6) D. A. I. Goring and P. Johnson, *Arch. Biochem. Biophys.*, **56**, 448 (1955).

(7) V. L. Koenig and J. D. Perrings, *J. Colloid Sci.*, **8**, 452 (1953).

(8) V. L. Koenig and J. D. Perrings, *Arch. Biochem. Biophys.*, **40**, 218 (1952).

(9) V. L. Koenig and J. D. Perrings, *ibid.*, **41**, 367 (1952).

plasma albumin[9] in 0.2 *M* NaCl. The change in s°_{25} is possibly due to a decrease in the hydration of the polyelectrolyte at higher temperatures. With salt present, hydration would be less at all temperatures, and a difference in temperature might not produce a perceptible effect.

THE THERMODYNAMIC PROPERTIES OF CHLORAMINE, DICHLORAMINE AND NITROGEN TRICHLORIDE

By William L. Jolly

Department of Chemistry, University of California, Berkeley, Cal.

Received November 10, 1955

In both aqueous solutions[1] and in liquid ammonia solutions,[2] chloramine reacts with ammonia to form hydrazine. Therefore the thermodynamic properties of chloramine are of importance in discussing equilibria involved in the synthesis of hydrazine. In this note, the free energies of aqueous chloramine and related species are estimated from literature data. It is emphasized that some of the results are only rough approximations and are to be considered tentative until better experimental data are obtained.

The Acidities of Chloramine and Dichloramine.—For the following discussion, it will be convenient to define an aquo acid molecule as a water molecule in which one of the protons has been replaced by another group, R. The ionization of an aquo acid is thus represented by

$$HOR = H^+ + OR^- \qquad (1)$$

The corresponding ammono acid molecule is an ammonia molecule in which one of the protons has been replaced by the group R

$$H_2NR = H^+ + HNR^- \qquad (2)$$

The pK values for several ammono acids and the corresponding aquo acids are listed in Table I. It appears that most of the aquo acids tabulated are roughly 10^7 times stronger than the corresponding ammono acids.

Chloramine, NH_2Cl, may be looked upon as the ammono analog of hypochlorous acid, HOCl. Since the pK value for hypochlorous acid is about 7[3], one may estimate $pK = 14 \pm 2$ for chloramine. Hence in very alkaline solutions one should expect an appreciable concentration of chloramide ion, $NHCl^-$.

The acidity of dichloramine, $NHCl_2$, may be estimated from Table I and the acidities of several disubstituted ammonias. Phthalimide[3] (pK = 7.4) is about 10^7 times stronger as an acid than simple amides. Dicyanamide[3] ($pK \sim 1$) is about 10^{10} times stronger than cyanamide. The latter factor is greater because of the higher electronegativity of the cyano group and perhaps because of greater resonance stabilization in the anion. The acidity of N-cyanoacetamide[3] ($pK = 4$) lies between the acidities of phthalimide and dicyanamide. We estimate that the acidity of dichloramine is about 10^7 times stronger than that of chloramine, or $pK \sim 7 \pm 3$. It is possible, therefore, that in the pH range (pH 5 to pH 8) where one encounters dichloramine, an appreciable concentration of the dichloramide ion, NCl_2^-, exists. In our further calculations, however, we shall neglect the ionization of dichloramine.

TABLE I

pK VALUES FOR AMMONO AND AQUO ACIDS

Ammono acid	pK	Aquo acid	pK
Ammonia, HNH_2[3]	~33	Water, HOH[3]	16
Acetamide, CH_3CONH_2[4]	15	Acetic acid, CH_3COOH[3]	5 (5 + 6 = 11)[9]
Benzamide, $C_6H_3CONH_2$[4]	14.5	Benzoic acid, C_6H_6COOH[10]	4 (4 + 6 = 10)[9]
o-Nitroaniline, $(NO_2)C_6H_4NH_2$[5]	14	*o*-Nitrophenol, $(NO_2)C_6H_4OH$[5]	7
p-Nitroaniline, $(NO_2)C_6H_4NH_2$[5]	12	*p*-Nitrophenol, $(NO_2)C_6H_4OH$[5]	7
Sulfamide, $H_2NSO_2NH_2$[6]	~11	Sulfamic acid, H_2NSO_2OH[11]	1
Cyanamide, H_2NCN[3]	10.5	Cyanic acid, HOCN[12]	4
Benzenesulfonamide, $C_6H_5SO_2NH_2$[7]	~10	Benzenesulfonic acid, $C_6H_3SO_2OH$[13]	<1
Sulfanilamide, $(NH_2)C_6H_4SO_2NH_2$[8]	10	Sulfanilic acid, $(NH_2)C_6H_4SO_2OH$[14]	1.5
Nitramide, H_2NNO_2[3]	7	Nitric acid, $HONO_2$	<0

The methods of calculation are straightforward except for the estimation of the acid ionization constants of chloramine and dichloramine. A method for estimating the acidity of an ammono acid from the known acidity of the corresponding aquo acid (or *vice versa*) is outlined.

Equilibria between Chloramine, Dichloramine and Nitrogen Trichloride.—Chapin[15] states that dichloramine is produced by chlorination of excess ammonium ions at pH 4.4 to 8.5 and by acidification of chloramine solutions. He states that at higher pH values chloramine alone exists and that at lower pH values nitrogen trichloride is the prin-

(1) L. F. Audrieth and B. A. Ogg, "The Chemistry of Hydrazine," John Wiley and Sons, Inc., New York, N. Y., 1951.

(2) H. H. Sisler, F. T. Neth and F. R. Hurley, *J. Am. Chem. Soc.*, **76**, 3909 (1954).

(3) G. E. K. Branch and M. Calvin, "The Theory of Organic Chemistry," Prentice-Hall Inc., New York, N. Y., 1941.

(4) G. E. K. Branch and J. O. Clayton, *J. Am. Chem. Soc.*, **50**, 1680 (1928).

(5) A. I. Schattenstein, *Acta Physicochim. U.S.S.R.*, **10**, 121 (1939).

(6) Personal communication from Professor L. F. Audrieth.

(7) Determined by the author by pH titration.

(8) A. Albert and R. Goldacre, *Nature*, **149**, 245 (1942).

(9) Branch and Calvin[3] have estimated $\Delta pK = 6$ for the resonance energy of the carboxylate ion.

(10) W. M. Latimer, "Oxidation Potentials," 2nd ed., Prentice-Hall, Inc., New York, N. Y., 1952.

(11) Estimated from the data of M. E. Cupery, *Ind. Eng. Chem.*, **30**, 627 (1938).

(12) "International Critical Tables," Vol. VI, McGraw-Hill Book Co., Inc., New York, N. Y., 1929.

(13) R. S. Aird and M. P. Balfe, *Trans. Faraday Soc.*, **39**, 102 (1943).

(14) W. Carr and W. J. Schutt, *ibid.*, **35**, 579 (1939).

(15) R. M. Chapin, *J. Am. Chem. Soc.*, **51**, 2112 (1929).

cipal species. Metcalf and his co-workers,[16] studying more dilute solutions, found slightly different pH boundaries, but they are essentially in agreement with Chapin. From the experimental data of these investigators, we estimate $K = 10^6$ for the reaction

$$H^+ + 2NH_2Cl = NHCl_2 + NH_4^+ \qquad (3)$$

and $K = 10^4$ for

$$H^+ + 3NHCl_2 = 2NCl_3 + NH_4^+ \qquad (4)$$

Free Energy Calculations.—Metcalf and his co-workers[16] determined the equilibrium constant for the following reaction at 15°

$$NH_2Cl + OH^- = NH_3 + OCl^-$$
$$K_{15} = 1.6 \times 10^{-3}$$

By estimating the entropy of NH_2Cl as 30 e.u. and by using the known[10] entropy and free energy values for hydroxide, ammonia and hypochlorite, one calculates, for 25°, 18.6 kcal./mole for the free energy of formation of aqueous chloramine. Using this datum and the equilibrium constants for reactions (3) and (4), one calculates 48 and 79 kcal./mole for the free energies of formation, respectively, of aqueous dichloramine and aqueous nitrogen trichloride.

It is interesting to compare the above value for the free energy of formation of nitrogen trichloride with that calculated from the known thermal data. The heat of formation of NCl_3 (in CCl_4) is 55 kcal./mole.[17] Estimating the entropy as 45 e.u., we calculate 72 kcal./mole for the free energy of formation in CCl_4. Nitrogen trichloride is very much more soluble in CCl_4 than in water.[18] In order that the free energy of formation of NCl_3 be 79 kcal./mole, we must assume a partition coefficient of about 10^5, which is not an unreasonable value.

Oxidation Potentials for Aqueous Solutions.—There are two interesting points which arise when considering the oxidation potentials of chloramine and its derivatives: First, one observes from equations (3) and (4) that not only the pH, but also the ammonium ion (or ammonia) concentration is important in determining whether NH_2Cl, $NHCl_2$ or NCl_3 is the important species in solution. (It is unlikely that either NH_3Cl^+ or $NHCl^-$ would ever be encountered as the principal chlorine species in aqueous solution; these exist only in strongly acid[19] or strongly basic solutions, respectively.) Second, there can be ambiguity as to the oxidation states of nitrogen and chlorine in chloramine and its derivatives. It seems plausible to the author to assign chlorine to the +1 oxidation state and nitrogen to the −3 oxidation state in these compounds. The potential diagrams for solutions 1 molal in H^+ and 1 molal in NH_4^+ follow

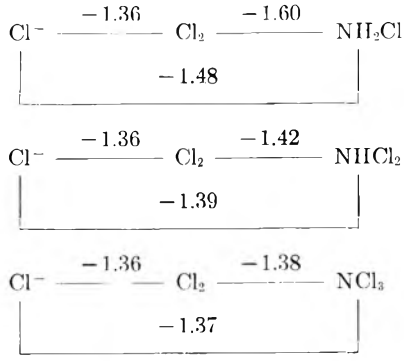

The Cl^-–NH_2Cl potential for alkaline solution (1 M OH^- and 1 M NH_3) is −0.81 v., and the Cl^-–$NHCl^-$ potential is approximately the same.

Oxidation Potentials for Liquid Ammonia Solutions.—Using methods of calculation outlined elsewhere,[20] one obtains the potential diagram for acid liquid ammonia solutions.

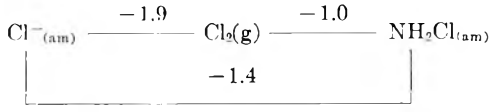

This potential diagram is significant in the anodic oxidation of chloride in liquid ammonia. The NH_4^+–N_2 potential is about zero volts and so nitrogen evolution is the thermodynamically favored anode reaction. However, at an anode with a high nitrogen overvoltage, it might be possible to form chloramine (and therefore hydrazine).

Acknowledgments.—The present work was carried out as one phase of a study of the synthesis of hydrazine sponsored by the Office of Ordnance Research, Contract DA-11-022-ORD-828. The author wishes to thank Professor L. F. Audrieth of the University of Illinois for his aid and encouragement.

(16) R. E. Corbett, W. S. Metcalf and F. G. Soper, *J. Chem. Soc.*, 1927 (1953).

(17) F. R. Bichowsky and F. D. Rossini, "The Thermochemistry of the Chemical Substances," Reinhold Publ. Corp., New York, N. Y., 1936.

(18) "Gmelins Handbuch der Anorganischen Chemie," "Chlor," Nr. 6, Verlag Chemie G.M.B.H., Berlin, 1927, p. 414.

(19) The basic dissociation constant of chloramine has been estimated as 10^{-15} by I. Weil and J. C. Morris, *J. Am. Chem. Soc.*, **71**, 3123 (1949).

(20) W. L. Jolly, THIS JOURNAL, **58**, 250 (1954).

THE QUESTION OF A PHASE TRANSITION IN SILICON

BY ELIZABETH A. WOOD

Bell Telephone Laboratories, Inc., Murray Hill, N. J.

Received November 4, 1955

The existence of a non-cubic (probably hexagonal) form of silicon was reported by Heyd, Khol and Kochanovská in 1947.[1] A report of this form appears in the Structure Reports[2] and in Wyckoff's "Crystal Structures."[3] The original report was of a preliminary nature, but no subsequent report was published. It therefore seemed desirable to determine whether the results could be repeated.

Heyd, *et al.*, looked for a non-cubic form of silicon because of the existence of the non-cubic forms

(1) F. Heyd, F. Khol and A. Kochanovská, *Collection Czechoslov. Chem. Communs.*, **12**, 502 (1947).

(2) Wilson, Barrett, Bijvoet and Robertson, "Structure Reports," Vol. 11, N.V.A. Oosthoek's Uitgevers, Utrecht, 1951.

(3) R. W. G. Wyckoff, "Crystal Structures," Vol. I, Interscience Publishers, New York, N. Y., 1951.

of carbon and tin. They tried to produce it in three different kinds of experiments: the first involved the addition of fluorides; the second, vacuum-evaporated silicon. The results of each of these were analyzed by X-ray diffraction at room temperature. In the third, Debye photographs were taken of pure silicon at 700°.

The first two experiments were, in the opinion of this writer, open to alternative explanation. The following attempts were made to repeat the last experiment.

Experiments

The first attempt to repeat this experiment was performed with powdered silicon ("Hyper pure" from du Pont) in a fused silica capillary at 700°. The Debye–Scherrer photograph, taken in a camera designed by W. L. Bond, of these laboratories, showed none of the lines listed by Heyd, Khol and Kochanovská.

A second attempt to repeat the experiment was made with silicon furnished by H. C. Theuerer of these laboratories which was prepared by decomposition of $SiCl_4$ with hydrogen. The resulting silicon was deposited from the vapor state onto a tantalum tape. A rod of this polycrystalline silicon was cut and fitted to the specimen holder of a commercially available high-temperature camera built by Central Research Laboratories, Inc., Red Wing, Minnesota. Debye–Scherrer photographs of this sample were taken at room temperature and at 700, 800 and 900°. No extra lines appeared at the higher temperatures, although the film was over-exposed to the point of halation.

Additional evidence for the non-existence of the high-temperature form was obtained by P. D. Garn of these laboratories who ran a differential thermal analysis of the "hyper-pure" silicon and found no evidence of a phase transition between room temperature and 1000°. This experiment was repeated three times.

Conclusions

X-Ray diffraction photographs taken at 700, 800 and 900° coupled with differential thermal analysis indicate no phase transition in pure silicon between room temperature and 1000°.

This evidence is contrary to the report by Heyd, Khol and Kochanovská that a non-cubic modification of silicon exists at 700°.

Acknowledgments.—The writer wishes to thank S. Geller for fruitful discussion, F. Barbieri for skillfully and carefully preparing the crystalline rod for the second experiment and V. Bala for taking the high temperature photographs.

THE STABILITY OF METAL CHELATES OF SUBSTITUTED ANTHRANILIC ACIDS

BY WILLIAM F. HARRIS[1] AND THOMAS R. SWEET

Department of Chemistry, the Ohio State University, Columbus, Ohio

Received October 29, 1955

The effect of a number of substituents on the chelating properties of anthranilic acid was studied. This was done by determination of the apparent formation constants of copper and cadmium with 3-methylanthranilic acid, N-methylanthranilic acid, anthranilic acid, 5-sulfoanthranilic acid, N-phenylanthranilic acid and 3,5-diiodoanthranilic acid in 50% dioxane solutions. The Bjerrum[2] titration method as modified by Calvin and Wilson[3] was adapted to the present work.

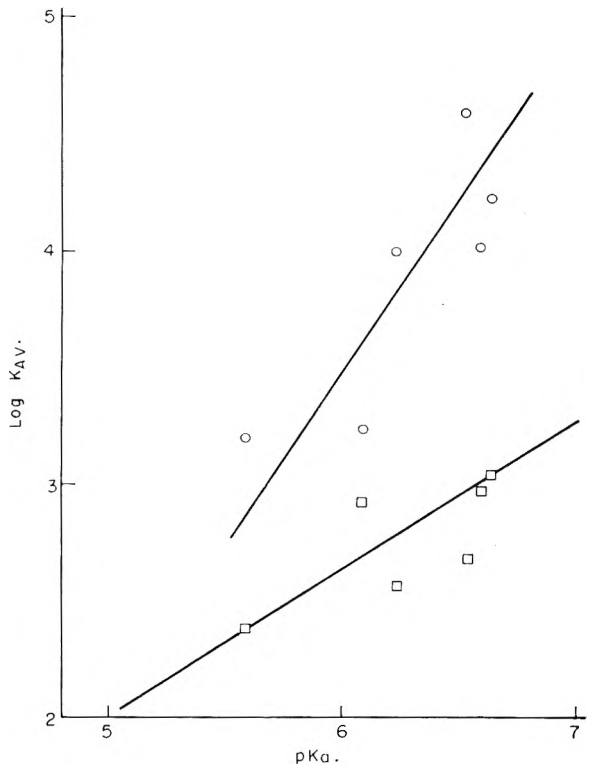

Fig. 1.—Correlation of log $K_{av.}$ with pK_a: ○, Cu chelates; □, Cd chelates.

Experimental

Materials.—The metal ion solutions were prepared and standardized by the method described in an earlier publication.[4] The dioxane was purified by the method suggested by Calvin and Wilson.[3] The anthranilic acid was obtained from Coleman and Bell Chemical Co. and was prepared for use by crystallizing several times from 50% acetic acid. The N-methyl, N-phenyl, and 3,5-diiodo derivatives were Eastman Kodak Co. white label reagents. The 3-methylanthranilic acid was obtained from Dr. H. Shechter of Ohio State University. It was prepared by reaction of 3-methylphthalic anhydride and hydrazoic acid in sulfuric acid.[5] 5-Sulfoanthranilic acid was prepared as described in an earlier publication.[4]

Procedure.—The weighed reagent was added as a solid to 50 ml. of purified dioxane. Water, nitric acid and metal ion were added in this order. The final volume was 100 ml. Nitric acid was not used with the 5-sulfoanthranilic acid. The titration procedure was the same as that described previously.[4]

Calculations.—The constants for the 5-sulfoanthranilic acid complexes were calculated by using the equations that the authors previously derived.[4]

TABLE I

pK_a VALUES OF ANTHRANILIC ACID AND SUBSTITUTED ANTHRANILIC ACIDS IN 50% DIOXANE

Reagent	pK_a
3,5-Diiodoanthranilic acid	5.59
N-Phenylanthranilic acid	6.09
5-Sulfoanthranilic acid	6.24
Anthranilic acid	6.53
N-Methylanthranilic acid	6.58
3-Methylanthranilic acid	6.64

(1) Abstracted from the doctoral dissertation of W. F. Harris presented to the Graduate School of the Ohio State University, August, 1955.

(2) J. Bjerrum, "Metal Amine Formation in Aqueous Solution," P. Haase and Son, Copenhagen, 1941.

(3) M. Calvin and K. W. Wilson, *J. Am. Chem. Soc.*, **67**, 2003 (1945).

(4) W. F. Harris and T. R. Sweet, *ibid.*, **77**, 2893 (1955).

(5) H. Barkemeyer, Master's Thesis, The Ohio State University, 1952.

TABLE II

CADMIUM AND COPPER CHELATES

Reagent	Metal	Metal concn. $\times 10^3$, M	Reagent concn. $\times 10^3$, M	$K_1 \times 10^{-4}$ (from graph)	$K_2 \times 10^{-2}$ (from graph)	$K_{av} \times 10^{-3}$ (from graph)	$K_2 \times 10^{-2}$ (calcd. from K_1 and $K_{av.}$)
3-Methylanthranilic acid	Cd	1.283	7.07	0.32	4.9	1.2	
	Cd	1.283	13.41	0.28	4.9	1.0	
3-Methylanthranilic acid	Cu	1.004	6.62	7.9	44	18	
	Cu	1.004	10.52	7.9	44	18	
N-Methylanthranilic acid	Cd	1.283	7.54	0.30	6.0	1.1	
	Cd	1.283	12.31	0.28	4.4	0.9	
N-Methylanthranilic acid	Cu	1.004	6.75	3.7	24	11	
	Cu	1.004	9.96	3.0	24	11	
Anthranilic acid	Cd	1.05	7.20	0.16		0.48	1.4
	Cd	1.05	10.91	0.16		0.48	1.4
Anthranilic acid	Cu	1.004	7.47	14		40	110
	Cu	0.502	7.39	14		40	110
5-Sulfoanthranilic acid	Cd	1.283	4.47	0.26		0.33	0.44
	Cd	1.283	6.66	0.26		0.33	0.44
5-Sulfoanthranilic acid	Cu	1.004	4.59	8.7		11	13
	Cu	1.004	6.86	6.0		10	16
N-Phenylanthranilic acid	Cd	1.283	5.34	0.21	5.8	0.98	
	Cd	1.283	8.86	0.19	4.4	0.73	
N-Phenylanthranilic acid	Cu	1.004	7.08	0.63		2.0	6.3
	Cu	0.502	7.11	0.54		1.6	4.7
3,5-Diiodoanthranilic acid	Cd	1.283	10.51	0.05	1.4	0.21	
	Cd	1.283	6.50	0.06		0.28	1.3
3,5-Diiodoanthranilic acid	Cu	1.004	5.38	0.45		1.6	5.6
	Cu	0.502	5.17	0.45		1.6	5.6

The equations used to calculate the formation constants for the metal chelates of anthranilic acid and the 3-methyl-N-methyl-, N-phenyl- and 3,5-diiodoanthranilic acid were

$$\bar{n} = \frac{Na^+ + H^+ - A - OH^- - \frac{K}{H^+}(T_{HR} + A + OH^- - Na^+ - H^+)}{T_M}$$

$$R^- = \frac{K}{H^+}(T_{HR} + A + OH^- - Na^+ - H^+)$$

HR represents the reagent
A represents the total added concentration of HNO_3
K represents the ionization constant of the carboxyl group
T_M represents the total added metal concentration
T_{HR} represents the total added reagent concentration

Since titrations of the reagents with NaOH showed that the pK value of the protonated nitrogen was less than 2 for all the reagents, this ionization constant was not considered in the calculations.

Results and Discussion

The negative logarithms of the ionization constants, obtained from the half equivalence points of titration curves made in 50% dioxane, are given in Table I.

The chelate formation constants are shown in Table II. The concentrations of metal ion and reagents in the table are the total added concentrations of each of these substances before the addition of sodium hydroxide.

No marked increase in the stability of the metal-anthranilic acid complexes was observed as a result of any of the ring or N-substitutions that were studied. In general, the stability constants follow the same trend as the ionization constants of the reagent. This correlation is shown graphically in Fig. 1. Some of the deviation in this graph may be attributed to the presence of the amino group, since changes in the availability of the N electrons for chelation are not necessarily indicated by the pK_a values. The stabilities of the copper chelates are considerably more dependent than the cadmium chelates on the pK_a of the reagents, as is shown by the greater slope of the copper curve in Fig. 1.

THE IONIC CHARACTER OF TRANSITION METAL HYDRIDES[1]

BY G. G. LIBOWITZ AND T. R. P. GIBB, JR.

Department of Chemistry, Tufts University, Medford, Mass.

Received December 8, 1955

The available literature[2-4] reveals that the radius of the hydrogen atom does not remain constant in different transition metal hydrides. Neither the assumption of covalent bonding nor of metallic bonding with the hydrogen situated in interstices of the metal structure, yield a consistent relation between the radii of the atoms and the observed internuclear distances. Values ranging from 0.27 to 0.80 Å. have been reported for the radius of the hydrogen atom in these compounds.

Because of the similarity between the heats of formation of rare earth hydrides and saline hy-

(1) This research was sponsored by the Atomic Energy Commission.

(2) G. Hagg, *Z. physik. Chem.*, **B11**, 433 (1930).

(3) R. E. Rundle, C. G. Shull and E. O. Wollan, *Acta Cryst.*, **5**, 22 (1952).

(4) R. E. Rundle, *J. Am. Chem. Soc.*, **73**, 4172 (1951).

drides, Dialer[5] suggested that the metal–hydrogen bonds in the rare earth hydrides of composition MH_2 are ionic. This assumption of ionic bonding can be extended to all hydrides of group IIIA and IVA metals, including the rare earth and actinide series, such that the radius of the hydride anion can be calculated from the observed internuclear distances and cation radii. This was done for all the transition metal hydrides for which sufficient data are available and as shown in Table I, the hydride anion radius remains reasonably constant at an average value of 1.29 Å. The deviation of ±0.05 Å. is better than can be expected in view of the uncertainty in cation radii and the variation in ionic character due to the different electronegativities of the metals. The cation radii and coördination number corrections used in this work were those of Zachariasen as given by Kittel.[11] The value 1.29 Å. seems reasonable when compared to the hydride anion radii calculated from the ionic alkali hydrides. From Table II, it can be seen that this radius decreases with increasing electronegativity of the cation. Therefore, a hydride radius somewhat less than 1.37 Å. would be expected for the transition metal hydrides.

TABLE I

HYDRIDE ANION RADII IN METALLIC HYDRIDES

Hydride	M–H distance, Å.	Cation radii, Å.	Oxidation state of cation	C.N. correction	H^- radius, Å.
TiH_2	1.93[2]	0.60	+4	0.08	1.25
ZrH_2	2.09[3]	0.77	+4	.08	1.24
LaH_2	2.45[6]	1.04	+3	.08	1.33
CeH_2	2.42[6]	1.02	+3	.08	1.32
PrH_2	2.39[6]	1.00	+3	.08	1.31
NdH_2	2.37[6]	0.99	+3	.08	1.30
SmH_2	2.33[6]	0.97	+3	.08	1.28
GdH_2	2.30[7]	0.95	+3	.08	1.27
AcH_2	2.46[8]	1.11	+3	.08	1.27
ThH_2	2.41[3]	0.99	+4	.08	1.34
PaH_3	2.32[9]	0.90	+5	.19	1.23
UH_3	2.32[4]	0.86	+6	.19	1.27
PuH_2	2.32[10]	0.90	+4	.08	1.34
				Av.	1.29 ± 0.05 Å.

TABLE II

HYDRIDE ANION RADII IN ALKALI METAL HYDRIDES

Hydride	M–H distance,[12] Å.	Cation radius, Å.	H^- radius, Å.
CsH	3.19	1.67	1.52
RbH	3.02	1.48	1.54
KH	2.85	1.33	1.52
NaH	2.44	0.98	1.46
LiH	2.05	0.68	1.37

With respect to the data in Table I, it should be pointed out that, regardless of the valence exhibited by the metal in the hydride, the radii used are for ions with the rare gas structure, except for the rare earths where the filling of the 4f shell was considered to have negligible influence on the xenon electronic structure, and plutonium where the more stable tetravalent state was used. Therefore, in every case, the charge of the cation exceeds its valence in the hydride. It is believed that the extra electrons which do not contribute to the formation of hydride anions, take part in residual weak metallic bonding, thus giving rise to the high electrical conductivity observed in these compounds.[13,14] Their ionic character on the other hand, accounts for their brittleness although in general the hydridic character is largely obscured by the residual metallic bonding. This discussion relates only to fully hydrided compounds (*i.e.*, the limiting-composition phase) and not to solutions of hydrogen in metals in which proton migration has been observed.[14]

(5) K. Dialer, *Monatsh.*, **79**, 311 (1948).

(6) C. E. Holley, R. N. R. Mulford, F. H. Ellinger, W. C. Koehler and W. H. Zachariasen, paper presented 127th meeting of ACS, April, 1955, Cincinnati, Ohio.

(7) A. Zalkin, Univ. Cal. Radiation Lab. Report No. 4519 (June 1955).

(8) J. D. Farr, A. L. Giorgi, M. G. Bowman and R. K. Money, Los Alamos Scientific Lab. Report No. LA 1545 (April 1953).

(9) P. A. Sellers, S. Fried, R. E. Elson and W. H. Zachariasen, *J. Am. Chem. Soc.*, **76**, 5935 (1954).

(10) R. N. R. Mulford and G. E. Sturdy, *ibid.*, **77**, 3449 (1955).

(11) C. Kittel, "Introduction to Solid State Physics," John Wiley and Sons, Inc., New York, N. Y. 1953, p. 40.

(12) E. Zintl and A. Harder, *Z. physik. Chem.*, **B14**, 265 (1931).

(13) F. H. Spedding, *et al.*, *Nucleonics*, **4**, 4 (1949).

(14) W. B. Hillig, Ph.D. Thesis, University of Michigan, 1953.

COMMUNICATION TO THE EDITOR

SECOND EXPLOSION LIMITS OF CARBON MONOXIDE–OXYGEN MIXTURES

Sir:

We wish to comment on the recent paper "Second Explosion Limits of Carbon Monoxide–Oxygen Mixtures" by Gordon and Knipe.[1]

In any system of reacting gases, the existence of an explosion peninsula in a pressure–temperature diagram bounded by a first explosion limit at lower pressures and by a second explosion limit at higher pressures, is evidence that a branched chain reaction occurs which competes with two chain breaking mechanisms, one predominating at lower and the other at higher pressures. The chain breaking mechanism predominating at lower pressures is the diffusion-controlled destruction of chain carriers at the surface of the vessel, whereas the chain breaking mechanism predominating at higher pressures is a gas phase reaction or a sequence of reactions controlled by a gas phase reaction, which is of higher order than the branched chain reaction. Both chain breaking mechanisms are, of course, operative at either limit. If the vessel surface is suitably treated so that it becomes strongly reflective to the chain carriers in question, or if the vessel diameter is made sufficiently large, surface chain breaking can be effectively suppressed. The second explosion limit is then solely determined by the competing gas phase chain branching and chain breaking reactions. Under these conditions, a study of the trend of the second explosion limit pressure with mixture composition at constant temperature provides a clue to the nature of the specific reactions occurring. On the other hand, if there is significant disturbance of the second limit data by surface chain breaking, the utility of such data for elucidating the specific reactions involved vanishes.

(1) A. S. Gordon and R. H. Knipe, This Journal, **59**, 1160 (1955).

It is by now common knowledge that the unravelling of the thermal reaction between hydrogen and oxygen rested on the ability to observe second explosion limits unmarred by surface chain breaking. In the case of the carbon monoxide–oxygen reaction, there is a surprisingly large number of imaginable reaction sequences for chain breaking and chain branching and the demand for second limit data free of surface chain breaking is even more urgent. No such data have been produced by Gordon and Knipe. On the contrary, their second limit data show a marked effect of the vessel surface. It is impossible to utilize such data for discerning the actual reactions occurring in the large catalogue of imaginable reactions. Hence, the specific mechanism proposed by these investigators is *ad hoc*.

The present authors have developed a procedure[2] which, over a wide range of mixture composition and temperature, effectively suppresses the surface chain breaking reaction. A very interesting dependence of the second limit on the mole fractions of oxygen and of diluent nitrogen was found. While we do not consider that the problem of the nature of the chain breaking and branching reactions is entirely solved, it is nevertheless noted that Gordon and Knipe's reaction scheme is inconsistent with the observed dependence of the second explosion limit on mixture composition.

Walter Roth[3]
Guenther von Elbe[4]
Bernard Lewis[4]

Received March 13, 1956

(2) G. von Elbe, B. Lewis and W. Roth, Fifth Symposium on Combustion, Reinhold Publishing Co., New York, Pg. 610, 1955. This work was done while all three authors were at the U. S. Bureau of Mines, Pittsburgh, Pa.

(3) General Electric Co., Research Laboratory, Schenectady, N. Y.
(4) Combustion and Explosives Research, Inc., Pittsburgh, Pennsylvania.

FIRE RETARDANT PAINTS

Number nine of the ADVANCES IN CHEMISTRY SERIES

A collection of papers comprising the Symposium on Fire Retardant Paints, presented before the Division of Paint, Plastics, and Printing Ink Chemistry at the 123rd meeting of the American Chemical Society, Los Angeles, Calif., March 1953

Edited by the staff of
Industrial and Engineering Chemistry

CONTENTS

94 pages

paper bound

$2.50 per copy

Published June 1954, by American Chemical Society 1155 Sixteenth St., N. W. Washington, D. C.

CHEMICAL NOMENCLATURE

Number eight of the
Advances in Chemistry Series
Edited by the staff of *Industrial and Engineering Chemistry*

A collection of papers comprising the Symposium on Chemical Nomenclature, presented before the Division of Chemical Literature at the 120th meeting—Diamond Jubilee—of the American Chemical Society, New York, N. Y., September 1951

INTRODUCTION

This symposium was a unique event. There have been conferences on chemical nomenclature, of which the outstanding one was the Congress of Geneva on organic nomenclature, held in 1892. But as far as my knowledge goes this series of papers presented in New York in 1951 constitutes the first symposium on chemical nomenclature held anywhere. The fortunate circumstance that the Diamond Jubilee of the AMERICAN CHEMICAL SOCIETY occurred immediately before the Sixteenth Conference of the International Union of Pure and Applied Chemistry made it possible to give the symposium a truly international character. Six different countries, Denmark, France, Germany, Great Britain, the Netherlands, and the United States, were represented among the eleven speakers. The three nomenclature commissions of the IUPAC were also represented, two by their presidents and one by its secretary. The letter of greeting from A. F. Holleman, former president of the Commission on the Nomenclature of Organic Chemistry, was written in his ninetieth year. W. P. Jorissen, former president of the Commission on the Nomenclature of Inorganic Chemistry, accepted an invitation to prepare a paper but was forced to withdraw for reasons of health. All the papers were read by their authors.

The symposium covered, in broad range and authoritative manner, the developments and problems of present-day chemical nomenclature. It is indeed gratifying that the papers can be published together as a number of the ADVANCES IN CHEMISTRY SERIES.

AUSTIN M. PATTERSON

112 pages

paper cover

$2.50

CONTENTS

Published August 15, 1953, by
AMERICAN CHEMICAL SOCIETY
1155 Sixteenth Street, N.W.
Washington, D. C.